ABSTRACT

SPIECKER, PAUL MATTHEW. The Impact of Asphaltene Chemistry and Solvation on Emulsion and Interfacial Film Formation. (Under the direction of Peter K. Kilpatrick)

Petroleum asphaltenes (*n*-heptane insolubles and toluene solubles) and fractions more and less soluble in mixtures of heptane and toluene (heptol) were analyzed chemically and by small angle neutron scattering (SANS). Asphaltene chemistry and their propensity to aggregate in solution were correlated to the stability of water-in-oil emulsions and the strength of adsorbed films at oil-water interfaces. Solubility profiles of the more soluble and less soluble fractions in heptol indicated strong cooperative asphaltene interactions. The less soluble asphaltene fractions had lower H/C ratios, higher N, V, Ni, and Fe contents than the more soluble or unfractionated asphaltenes. Neutron scattering studies at 25 and 80°C indicated asphaltenes near their solubility limit formed the largest aggregates. Highly aromatic solvents and the presence of petroleum resins disrupted intermolecular π and hydrogen bonding and reduced the degree of aggregation. Less soluble fractions formed aggregates considerably larger than the unfractionated asphaltenes (as high as 520 Å), while soluble asphaltenes formed the smallest aggregates (as low as 22 Å). Enhanced aromatic π-π bonding, dispersion forces and hydrogen bond interactions within the less soluble fraction likely caused large aggregate formation and low solubility.

Emulsion stability was gauged by the volume percentage of water resolved after centrifugation at high speed (15,000 rpm). Strong emulsion formers were characterized by intermediate to large aggregates with lower aromaticity and higher nitrogen polarity, Ni and V. Asphaltenes aggregating due primarily to H-bonding and by π-π interactions were

presumed to form a cohesive interfacial oil-water film and stable emulsions. At low aromaticities (≤ 30 % toluene), asphaltenes were poorly solvated without resins and did not form stable emulsions. Increasing the resin-asphaltene ratio to 5 or 10:1 of the less soluble asphaltene fractions significantly enhanced emulsion stability (< 20 vol % water resolved). Higher R/A (≥ 20) led to emulsions with partial stability (40-80 % water resolved).

A biconical bob interfacial shear rheometer was used to study the properties of asphaltene films at oil-water interfaces. The degree of film consolidation was determined from ratios of elasticity (G′)/film mass and yield stress/G′. Asphaltenes with higher concentrations of heavy metals (Ni: 330-360 ppm, V: 950-1000 ppm), lower aromaticity (H/C: 1.24-1.29), and higher polarity (N: 1.87-1.99) formed films of high elasticity, yield stress and consolidation.

THE IMPACT OF ASPHALTENE CHEMISTRY AND SOLVATION ON EMULSION AND INTERFACIAL FILM FORMATION

by

PAUL MATTHEW SPIECKER

A thesis submitted to the Graduate Faculty of
North Carolina State University
in partial fulfillment of the
requirements for the Degree of
Doctor of Philosophy

CHEMICAL ENGINEERING

Raleigh

2001

APPROVED BY:

Peter K. Kilpatrick Chair of Advisory Committee	Saad A. Khan
H. Henry Lamb	George W. Roberts

BIOGRAPHY

PAUL MATTHEW SPIECKER was born on September 20, 1973, in Severna Park, Maryland. He attended Severna Park High School. From 1991 to 1995, he attended Lafayette College in Easton, Pennsylvania, graduating with a Bachelor of Science degree in Chemical Engineering with Honors. From 1995 to 2001, he attended North Carolina State University in Raleigh, North Carolina, and graduated with a Ph.D. in Chemical Engineering. After completing his doctoral work, he accepted a position as a Research Engineer with ExxonMobil Upstream Research Company in Houston, Texas.

ACKNOWLEDGEMENTS

I wish to thank my advisor and mentor Dr. Peter Kilpatrick for providing the guidance through the research process. His positive attitude and patience are to be commended. While the road taken may have been circuitous, together we have learned much and have ultimately created a fine body of work.

I have enjoyed the opportunity of working with many fellow graduate students, postdoctoral associates and undergraduate assistants. Joe McLean, Andrew Sullivan and Keith Gawrys have all provided intellectual and experimental assistance during my stay at North Carolina State University. In addition, Jeff Yerian deserves recognition for providing an enjoyable working environment with many versions of hallway Olympics. I will always have an extra chair in my office just for you Jeff.

Kit Yeung has helped all of us so many times with work and personal related issues. Whether working in our lab or under my car he can always solve the tough problems. He is a truly selfless and considerate individual.

The most important influences in my life have come from my parents and my wife Sandra. My parents provided the best environment for growth as a boy and into adulthood. Throughout the years they have given complete support and guidance. Sandra has given me an amazing level of support and encouragement and deserves much credit for my happiness.

Finally I would like to acknowledge the Petroleum Environmental Research Forum through grants 95-02 and 97-07, the National Science Foundation through grant CTS-981727, and consortium funding from ExxonMobil, Texaco, Ondeo-Nalco Energy Systems, and Shell Oil Company for supporting this research.

TABLE OF CONTENTS

LIST OF TABLES

LIST OF FIGURES

CHAPTER 1
INTRODUCTION

1.1 Petroleum Production Challenges

Problems associated with well production, pipeline transfer, land and sea-based transportation and, ultimately, oil refining have all been linked to the presence of asphaltenic colloids.[1-13] During visbreaking and catalytic hydrocracking large amounts of sludge and sediment can form[14] ostensibly due to the flocculation of asphaltenes during processing.[15] Coke generation and asphaltene adsorption within catalytic cracking beds can reduce the effective catalyst surface area as well as the efficiency of coal hydropyrolysis.[16] Asphaltene deposition within reservoir rocks has been blamed for pronounced reductions in well productivity.[17] Asphaltenes have also been found to facilitate the formation of extremely stable water-in-crude oil emulsions.[5, 18-26] Understanding asphaltene chemistry and the fundamental mechanisms of colloid formation has been the driving force behind much petroleum research for the last half-century. The study of asphaltene colloidal properties has been motivated by their propensity to aggregate, flocculate, precipitate, and to adsorb onto interfaces.

1.2 Emulsion Formation

Crude oil is found in reservoirs along with water or brine and during oil removal, water is often coproduced. Water is also injected into the crude to remove salts or as steam to improve fractionation.[27] Petroleum emulsions (typically water-in-oil[5, 22, 28-30]) readily form with water in the highly turbulent nozzles and piping used for oil production. Petroleum recovery processes where emulsions often form are highlighted in Figure 1.1.

These emulsions can increase pumping and transportation expenses, corrosion of pipes, pumps, production equipment and distillation columns, and the poisoning of downstream refinery catalysts.[31]

Mixing immiscible liquids such as oil and water with a surface active agent will often yield an emulsion of oil droplets in water (o/w) or water droplets in oil (w/o) according to Bancroft's rule.[32] Examples of common emulsions types are shown in Figure 1.2. Bancroft's rule states that the liquid in which the surfactant is soluble becomes the continuous phase. Other factors such as oil-water volume fractions, surfactant concentration and hydrophile-lypophile balance will influence the type of emulsion formed. After droplets are completely dispersed within the continuous phase, surfactants migrate to the oil-water interface and can inhibit droplet rupture by steric, Marangoni-Gibbs, or rigid-film forming interactions. These stability mechanisms are outlined in Figures 1.3a-c.

1.2.1 Steric Stabilization

Surfactants containing a hydrophilic, polar head group and hydrophobic tail group will typically orient themselves at oil-water interfaces. The head group has a natural affinity for water while the tail group will preferentially remain in the oleic phase. Dispersed water droplets will thus be coated by surfactant material with hydrophobic tails protruding into the oil phase. When droplets approach each other, their adsorbed surfactant tails prevent droplet contact and coalescence.

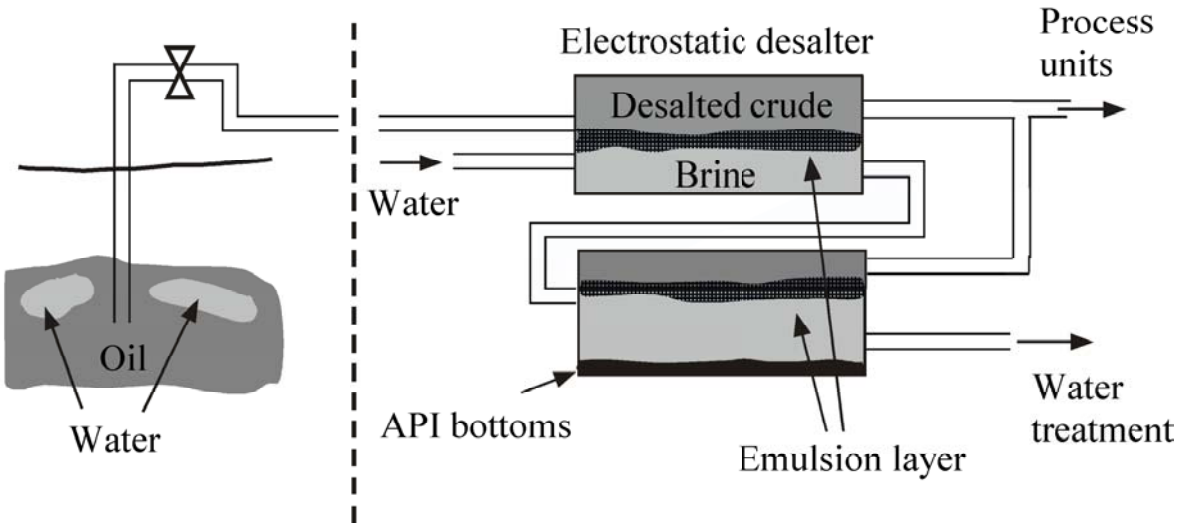

Figure 1.1 Petroleum recovery and process steps where water is introduced and emulsions form.

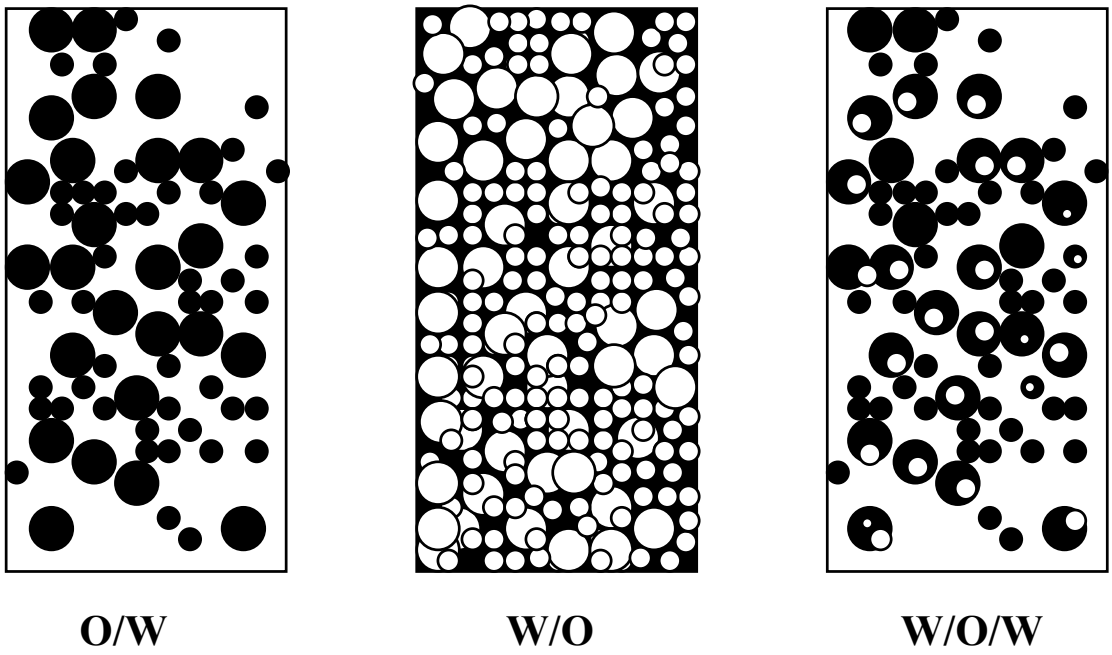

Figure 1.2 Common types of crude oil emulsions: oil-in-water (o/w), water-in-oil (w/o), and less common: water-in-oil-in-water (w/o/w).

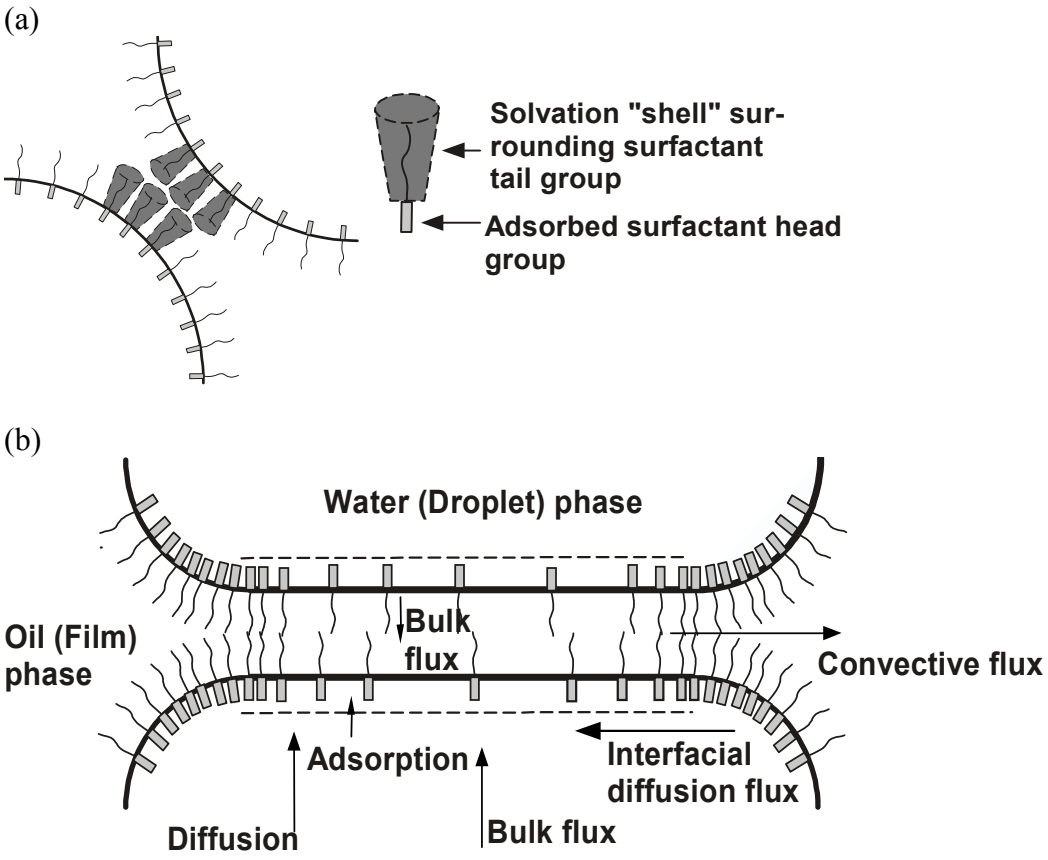

Figure 1.3 Depiction of surfactant stabilized emulsions: (a) steric repulsion, (b) Marangoni-Gibbs effect, and (c) rigid, elastic film surrounding water droplets in an oil continuum.

1.2.2 Marangoni-Gibbs Effect

The Marangoni-Gibbs effect can stabilize emulsions by preventing the drainage of continuous phase from between two opposing droplets. As droplets approach, their surfaces eventually become plane parallel (Figure 1.3c) and the film layer attempts to drain. This outward convection draws surfactants towards the droplet edges leaving a region of low surfactant concentration in the middle. This process sets up an unfavorable interfacial tension gradient along the interface. Surfactant diffusion thus proceeds in the direction opposing convection to eliminate the interfacial tension gradient. Stable emulsions can result from the balance of surface diffusion and film convection.

1.2.3 Rigid Film Formation

A third and most probable mechanism of petroleum emulsion stabilization comes from an adsorbed layer of material with high rigidity and elasticity. Asphaltenic aggregates in the oleic phase will adsorb to the oil-water interface and form a consolidated film or skin that resists droplet coalescence. This process can be quite complex and depends on asphaltene chemistry, solvency and the kinetics of diffusion and adsorption. Other factors leading to stable emulsions are high viscosity continuous phases, small-dispersed phase volume and droplet size, and low interfacial tensions.[31]

As early as 1948, Lawrence et al. tried to identify the agents responsible for the formation of sea water-Navy fuel oil emulsions.[33] They suggested that “soft asphalt” was the stabilizing agent and that as little as 0.75% in fuel oil created emulsions stable over several days. Blair linked the stability of petroleum emulsions to the formation of a

condensed and viscous film that acted as a barrier to droplet coalescence.[34] Many early studies were performed on the film forming and emulsifying behavior of crude oil-water systems.[3, 5, 19, 28, 35-40] These and later studies often held the asphaltenic constituents in crude oil responsible for film formation and stabilization.[19, 21, 28, 41]

1.3 Asphaltene Chemistry

Asphaltenes are defined as the portion of crude oil insoluble in *n*-alkanes such as *n*-heptane or *n*-pentane yet soluble in benzene or toluene.[42, 43] The "solubility class" definition of asphaltenes generates a broad distribution of molecular structures that can vary greatly from one crude oil to another. In general, asphaltenes are characterized by fused ring aromaticity, small aliphatic side chains, and polar heteroatom-containing functional groups. The most common techniques for determining the chemical constitution of asphaltenes include combustion elemental analysis (H/C, N, S)[44-48] inductively coupled plasma (V, Ni, Fe)[49-53], and Fourier transform infrared spectroscopy (polar functional group concentrations)[54-59]. A wealth of information can be drawn from these chemical analyses. H/C ratios between 1.0 and 1.2 and N, S, and O content of a few weight percent suggest that much of the asphaltene backbone consists of fused aromatic carbon interspersed with polar functional groups containing five to seven heteroatoms. FTIR analysis reveals many groups capable of forming hydrogen bonds. Many studies have indicated the presence of carboxylic acids, carbonyls, phenols, and pyrrolic and pyridinic nitrogen.[60-64] Based on these analyses, average asphaltene structures can be drawn (Figure 1.4).

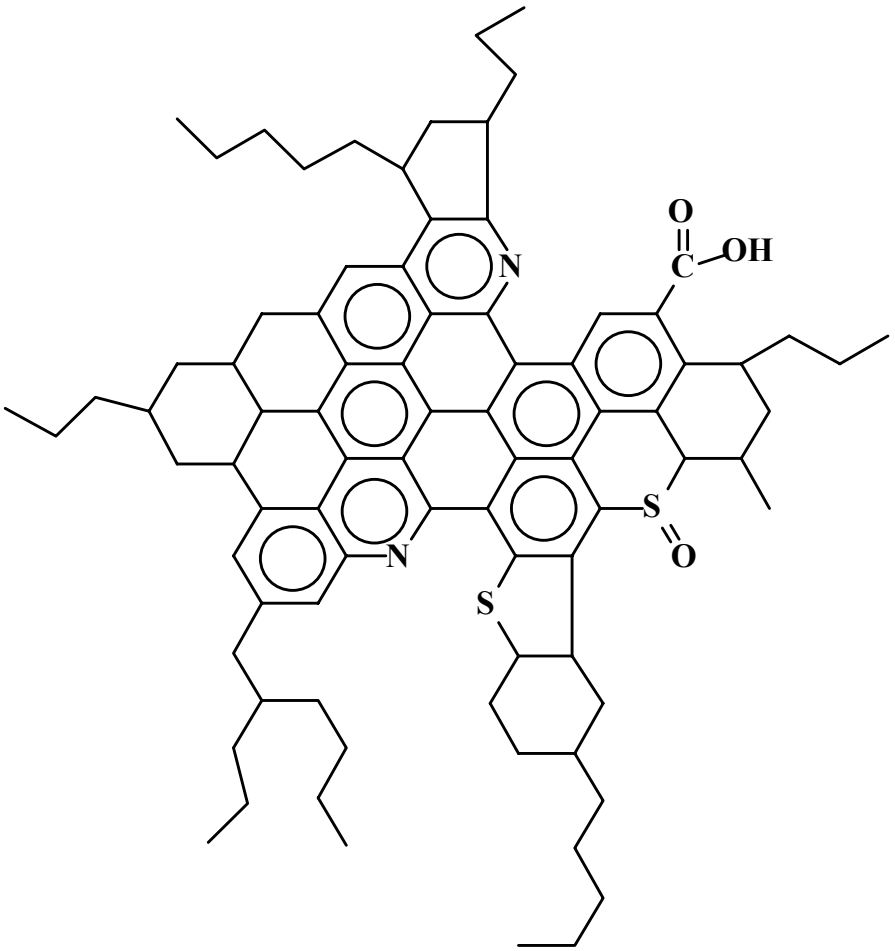

$C_{84}H_{100}N_2S_2O_3$ Mol. Wt. 1244

81.03 %C, 8.04 %H, 2.25 %N, 5.14 % S, 3.86 %O*

H/C = 1.19 (w/w), 40.4% Aromatic Carbon

*** All %'s are given as wt%**

Figure 1.4 Molecular structure of an average asphaltene.

1.4 Asphaltenes and Resins in Crude Oil

The notion of asphaltenes forming colloidal aggregates in crude oil was originally proposed by Nellensteyn [1] and later by Pfeiffer and Saal [2]. They proposed that "dispersions" of asphaltenic aggregates in heavy crudes are solvated by resins and other aromatic compounds. X-ray diffraction measurements by Yen et al. showed that dry asphaltenes contain a core of fused aromatic rings with an aliphatic periphery.[43] The flat aromatic core permits cofacial stacking of approximately four to five parallel sheets mediated by π-π bonding.[4] Polar functional groups are also capable of donating or accepting protons inter- and intra-molecularly. The most plausible mechanisms of asphaltene aggregation involve π-π overlap between aromatic sheets, hydrogen bonding between functional groups and other charge transfer interactions. The degree to which aggregate sizes vary is controlled by the polydispersity and chemistry of asphaltene monomers.

When characterizing crude oils we often refer to SARA fractionation where asphaltenes are removed by precipitation with a paraffinic solvent and the deasphalted oil (DAO or maltenes) is separated into saturates, aromatics and resins by chromatographic fractionation.[65-69] After asphaltenes, resins are the most polar and aromatic species in crude oil and, it has been suggested, contribute to the overall solubility of asphaltenes in crude oil by creating a strongly solvating layer on the polar and aromatic portions of the asphaltenic aggregates.[51, 70, 71] From chemical analyses, a proposed molecular structure of resins can be drawn (Figure 1.5). When resin solvated (Figure 1.6) asphaltene aggregates in crude oil encounter water droplets, the asphaltenes likely shed a portion of the resins and adsorb to the interface. This process is depicted in Figure 1.7. The solubility of asphaltenes in crude oil is mediated largely by resin solvation and thus resins play a critical role in

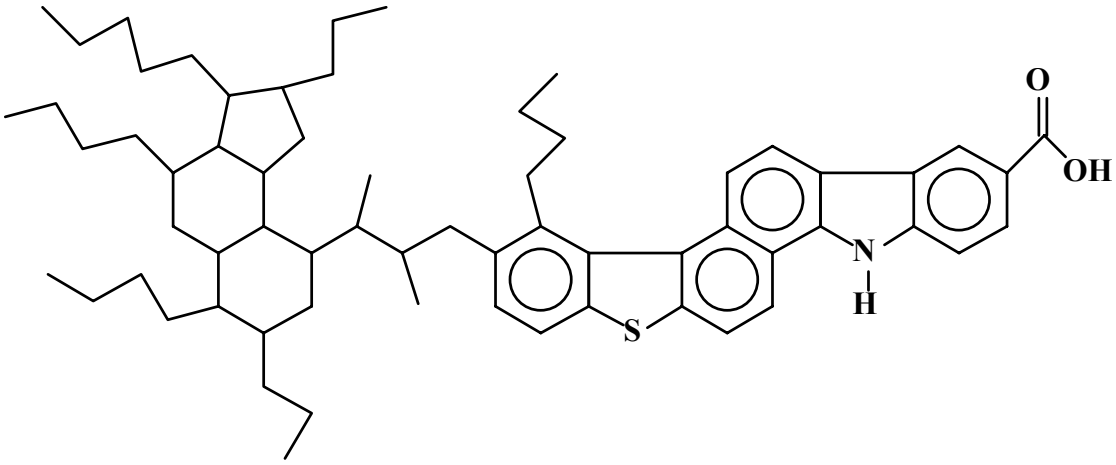

$C_{59}H_{78}NSO_2$ Mol. Wt. 865

81.9 %C, 9.1 %H, 1.6 %N, 3.7 % S, 3.7 %O*

H/C = 1.33 (w/w), 37% Aromatic Carbon

***** **All %'s are given as wt%**

Figure 1.5 Molecular structure of an average petroleum resin.

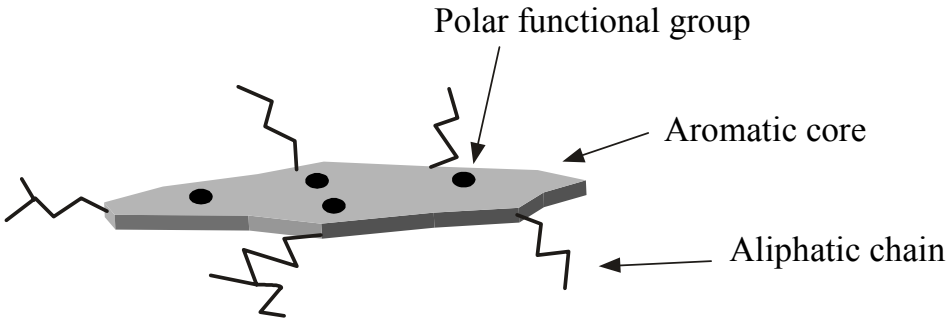

Asphaltene monomer

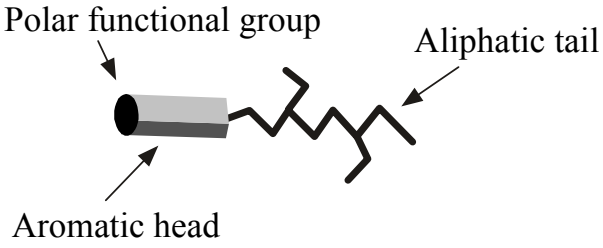

Resin molecule

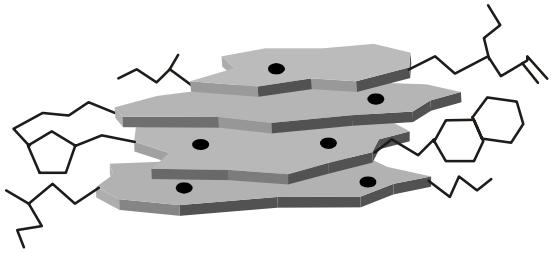

Asphaltene aggregate

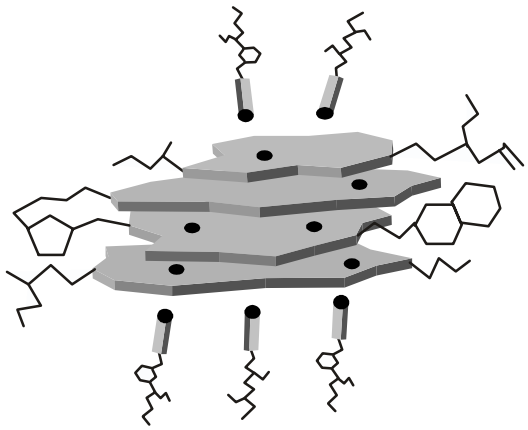

Resin solvated asphaltenic aggregate

Figure 1.6 Schematic of a resin solvated, asphaltenic aggregate: polydisperse asphaltene monomers stack cofacially with resins near the exposed top and bottom surfaces.

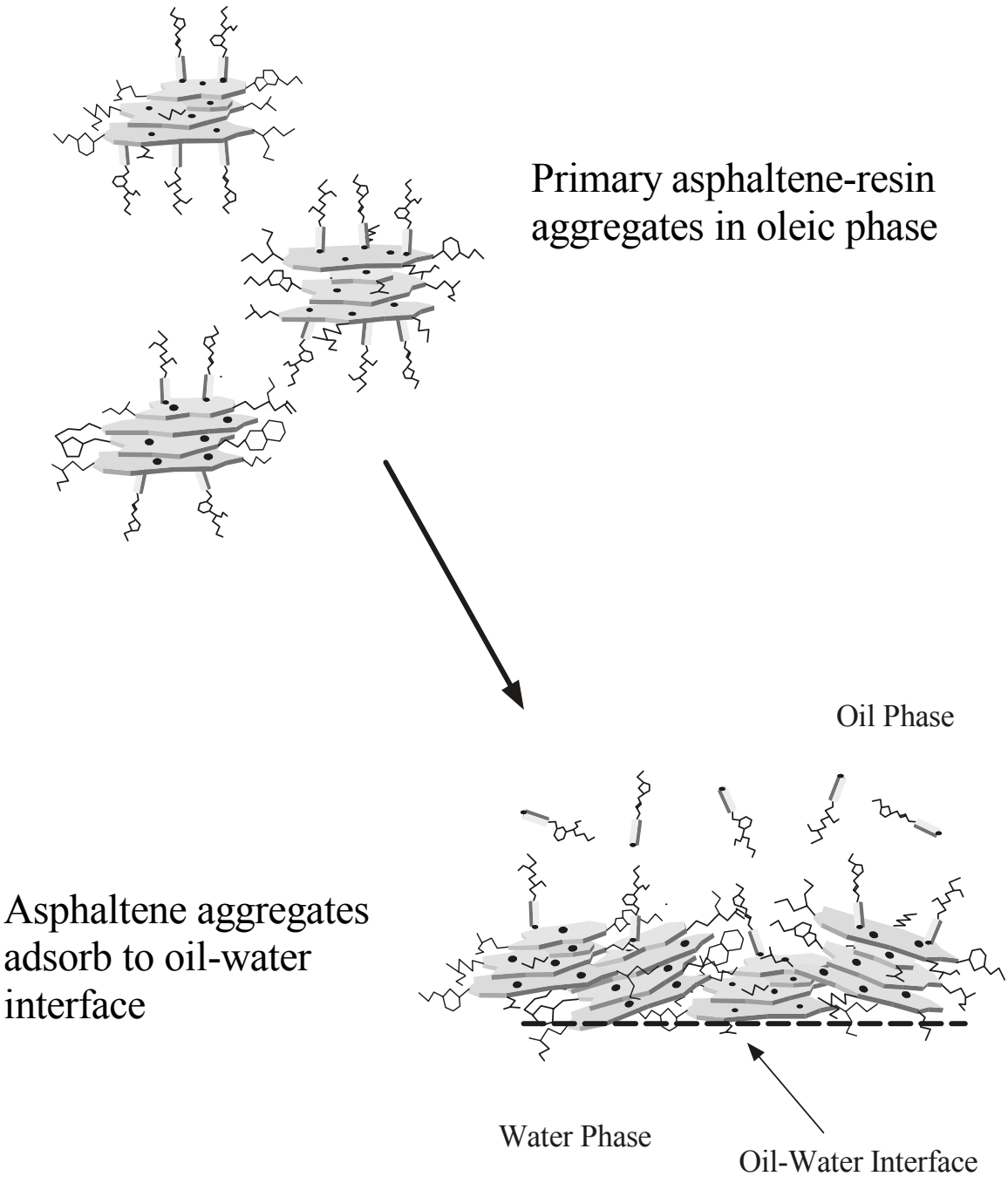

Figure 1.7 Primary asphaltene-resin aggregates at equilibrium in the oil phase. Asphaltene aggregates shed solvating resins and adsorb to oil-water interface through polar interactions and hydrogen bonding.

precipitation, and emulsion stabilization phenomena.[72-76] Resins, although quite surface-active, have not been found to stabilize water-in-oil emulsions by themselves in model systems.[18, 77] However, the presence of resins in solution can destabilize emulsions via asphaltene solvation and replacement at the oil-water interface.[18, 25, 78-80]

1.5 Quantifying Asphaltene Aggregation

1.5.1 Vapor Pressure Osmometry

The degree of asphaltene aggregation can be obtained from molar mass and neutron or x-ray scattering measurements. The most common technique for measuring number average molecular weights is vapor pressure osmometry in an aromatic and/or polar solvent (toluene, benzene, pyridine, or *o*-dichlorobenzene) at elevated temperature (50-130°C).[44, 70, 81-86] Typical molar masses range from about 800 to 3,000 g/mol in the best solvents. The dissociating power of the solvent is critical to obtaining the smallest number indicative of an asphaltene monomer. Molar mass variations with solvent and temperature suggest changes in aggregate size rather than conformational changes in asphaltene structure. Interaggregate π-π and hydrogen bonding is far weaker than covalent bonding between carbon atoms and can be broken down in the presence of a good solvent or at higher temperatures. Toluene, a weaker solvent, often results in molar masses of 3,000-6,000 g/mol. This size suggests that, under these solvent conditions, the asphaltenes are not large monomers, but rather oligomers of four to five monomers. A proposed schematic of asphaltene aggregation as a function of solvent strength is shown in Figure 1.8.

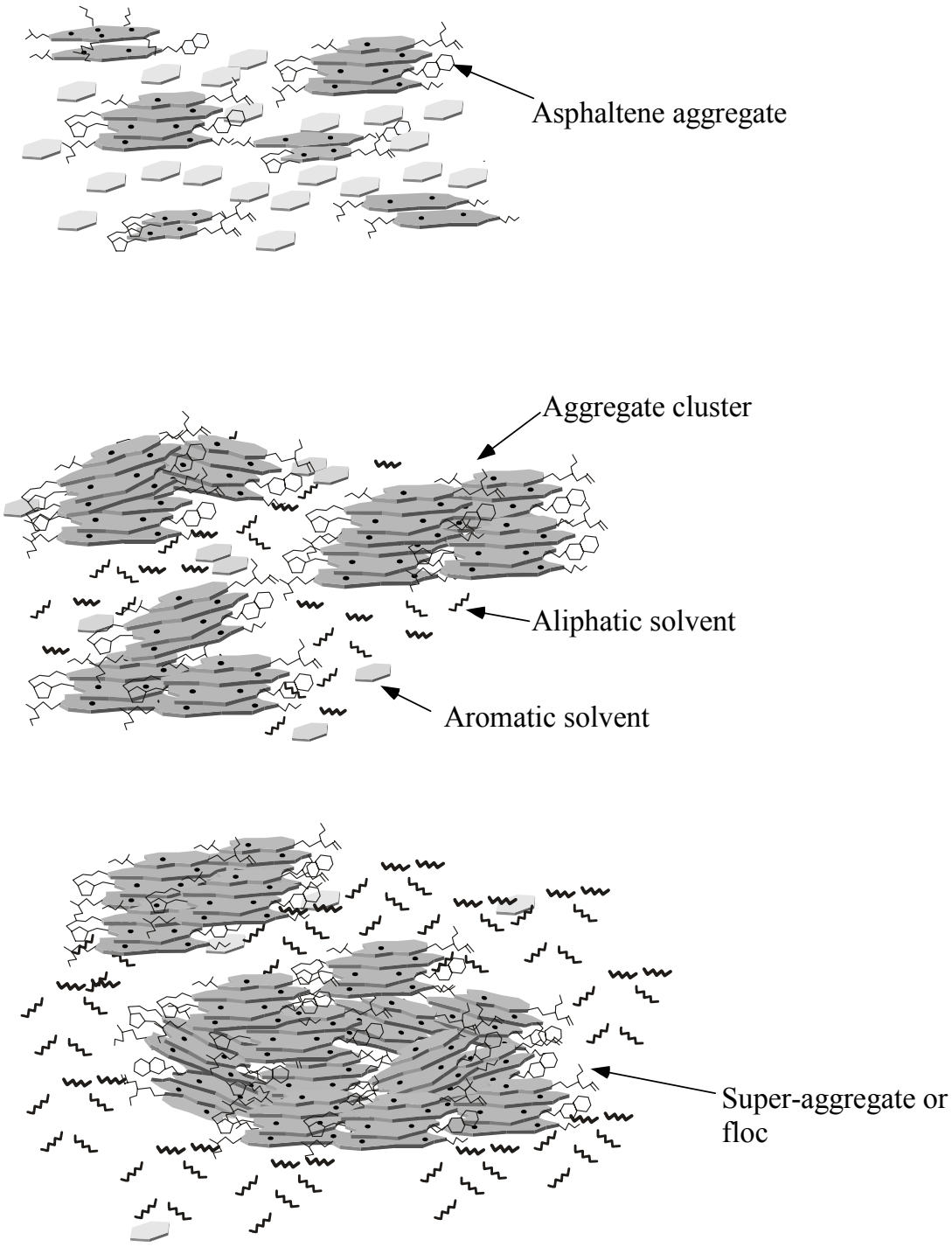

Figure 1.8 Schematic of asphaltene aggregate interactions in solvents of varying aromaticity:
Top – high aromaticity (>0.7 volume fraction toluene in heptane-toluene (heptol))
Middle – intermediate aromaticity (~ 0.5-0.7 volume fraction toluene in heptol)
Bottom – low aromaticity (< 0.5 volume fraction toluene).

1.5.2 Scattering Techniques

1.5.2.1 Asphaltene Aggregation

Neutron and x-ray scattering are very powerful tools to deduce sizes and morphologies of colloidal aggregates in solution. Numerous studies have been performed over the past decade or so to probe the effects of solvent, temperature and crude oil source on asphaltene aggregate size and polydispersity.[8, 11, 13, 73, 75, 87-100] While both x-ray and neutron scattering can provide colloid structure information, small angle neutron scattering (SANS) offers the advantage of solvent-solute contrast via deuteration SANS to decrease data collection times and probe the entire asphaltene aggregate. Small angle x-ray scattering (SAXS), on the other hand, can only discern the aromatic asphaltene core. Proper analysis of the scattering intensity curves can provide aggregate radius of gyration (R_g), shape and dimension.

1.5.2.2 Asphaltene-Resin Aggregation

While the effects of temperature, solvent aromaticity, and polarity have received much attention, the solvation of asphaltene aggregates by resins has not been fully explored. Espinat et al. measured the scattered intensity from asphaltenic aggregates in several solvents, at low and high temperatures and with resins.[73] In toluene, 2 wt % Boscan asphaltene solutions formed larger aggregates at room temperature (234 Å diameter) than at 76°C (175 Å). At room temperature, aggregates sizes were 2-4 times smaller in high polarity solvents such as pyridine and tetrahydrofuran than benzene. Bardon et al. explored the solvating effect of resins on Safaniya asphaltene aggregates by SANS and SAXS.[12]

Comparisons of scattering curves for asphaltene-resin systems to pure asphaltene and pure resin systems indicated solvation of asphaltenes by resins.

1.6 Asphaltene Film Formation at Oil-Water Interfaces

The knowledge gained by investigating interfacial properties is considerably more revealing than the information available from bulk emulsions. From interfacial studies, one can determine the fundamental mechanisms and kinetics of film formation, surfactant adsorption, and film rupture that ultimately govern emulsion behavior. The types of interfaces studied are typically air-water, where the surfactant resides in the aqueous phase or water-oil, where the surfactant resides in the aqueous or oleic phase. Various techniques exist for the study of adsorption of surface-active agents to air-water and oil-water interfaces.[101-105]

Researchers have linked interfacial film and emulsion forming behavior to petroleum asphaltenes and their interplay with resins as a solubilizing agent.[10, 19, 21, 22, 28, 29, 33, 38, 41, 106-115] One of the earliest investigations of a water-in-oil emulsion formed by asphaltenes dissolved in a model oil system was performed by van der Waarden.[22] His work pointed to many important film and emulsion forming behaviors of asphaltenes. He found that asphaltenes near their solubility limit in aliphatic-aromatic mixtures typically formed the most stable emulsions. Solvents of high aromaticity tended to prevent the flocculation of asphaltenes and formed weaker emulsions. In addition, the "rheological resistance" of the interface was measured using a torsion oscillation method where the oscillation amplitude of a glass disk suspended at the oil-water interface was monitored in the presence of asphaltenes. Results indicated that asphaltenes at or near the point of

flocculation developed a viscous film and that emulsion stability was facilitated by the adsorption of this coherent asphaltene layer.

Biconical bob rheometry has been applied to both crude oil-water and model oil-water interfaces.[37, 116-118] Cairns et al. employed a biconical bob rheometer to study the interfacial viscosities of crude oil-water films.[37] They found that viscosity increased with aging time of the interface several fold from 2 to 6 hours and suggested the presence of a viscous "interphase". Acevedo et al. examined the shear viscoelasticity and creep compliance of Cerro Negro crude oil and asphaltenes diluted in xylene using the biconical bob rheometer of Cairns.[117] High interfacial elasticities, rather than viscosities, were purported to correlate with strong emulsions. It was again suggested that mechanically strong films result from the adsorption of aggregated asphaltenes.

1.7 Overview of Dissertation

To help the petroleum industry improve the conversion of crude oil into useful product by reducing losses to sludge and emulsions, it is necessary to better understand the factors that affect their formation. Paramount to this understanding is an in-depth knowledge of the structures and interactions of the asphaltenic components responsible.

Chapter 2 examines the chemistry and solvency of asphaltenes from four crude oils. Asphaltenes were further separated into more and less soluble subfractions in mixtures of aliphatic and aromatic solvents. Solubility curves of asphaltenes in these solvent mixtures were generated to determine the limits of solubility. Small angle neutron scattering was performed on asphaltene solutions to probe the degree of aggregation in various solvent and

temperature regimes. The detailed study of the chemistry and aggregate-forming properties of asphaltene subfractions helped shed light on the mechanisms of aggregation.

In Chapter 3, we investigated the propensity of asphaltenes to form water-in-oil emulsions. Asphaltenes and their more and less soluble subfractions were dissolved in model oils of aliphatic and aromatic solvents and emulsified in the presence of water. It was our goal to relate the aggregation and solubility behavior of the asphaltenes and their subfractions to the corresponding strength of emulsions formed with these subfractions.

The solvating effects of resins on asphaltene aggregation and emulsion formation were investigated in Chapter 4. Neutron scattering of asphaltene aggregates and their more and less soluble fractions were compared to systems containing resins. Resins were also added to asphaltene solutions in mixtures of heptane and toluene to study their effect on water-in-oil emulsion stability.

Chapter 5 examines the elastic properties of asphaltene films at oil-water interfaces. A commercially available rheometer was modified with a serrated edge biconical bob for the study of rigid asphaltene films. Asphaltene solvency and chemistry were found to have a substantial impact on the kinetics of adsorption and degree of film consolidation. Factors were developed to compare the elasticity, yield stress and mass of films aged for different times and with different asphaltenes. Film strength and consolidation correlated well with the stability of emulsions formed under comparable conditions.

Chapter 6 summarizes the major findings in this study and contains suggestions for future work. This unified body of work examines the primary components responsible for emulsion formation and deposition in petroleum. In addition, a novel application of an accomplished technique for studying interfaces has been developed. The petroleum industry

can apply these findings to better characterize the asphaltenes responsible for aggregation and adsorption.

1.8 References

1. Nellensteyn, F.J., "The Constitution of Asphalt," *Journal of the Institute of Petroleum Technologists*, 1924, **10**: p. 311-325.

2. Pfeiffer, J.P. and R.N.J. Saal, "Asphaltic Bitumen as Colloid System," *Journal of Physical Chemistry*, 1940, **44**: p. 139-149.

3. Neumann, H., "Investigations Regarding the Separation of Crude Oil Emulsions," *Petrochemie*, 1965, **18**: p. 776-779.

4. Dickie, J.P. and T.F. Yen, "Macrostructures of the Asphaltic Fractions by Various Instrumental Methods," *Analytical Chemistry*, 1967, **39** (14): p. 1847-1852.

5. Berridge, S.A., M.T. Thew and A.G. Loriston-Clarke, "The Formation and Stability of Emulsions of Water in Crude Petroleum and Similar Stocks," *Journal of the Institute of Petroleum*, 1968, **54** (539): p. 333-357.

6. Speight, J.G., "Structural Analysis of Athabasca Asphaltenes by Proton Magnetic Resonance Spectroscopy," *Fuel*, 1971, **50**: p. 102-112.

7. Speight, J.G. and S.E. Moschopedis, "Some Observations on the Molecular "Nature" of Petroleum Asphaltenes," *Preprints -- ACS Division of Petroleum Chemistry*, 1979, **24** (4): p. 910-923.

8. Ravey, J.C., G. Ducouret and D. Espinat, "Asphaltene Macrostructure by Small Angle Neutron Scattering," *Fuel*, 1988, **67** (11): p. 1560-1567.

9. Sheu, E.Y., M.M.D. Tar and D.A. Storm, "Solution Properties of Colloids Formed by Petroleum Vacuum Residues," *Macromolecular Reports*, 1991, **A28**: p. 159-175.

10. Siffert, B., C. Bourgeois and E. Papirer, "Structure and Water-Oil Emulsifying Properties of Asphaltenes," *Fuel*, 1984, **63** (6): p. 834-837.

11. Herzog, P., D. Tchoubar and D. Espinat, "Macrostructure of Asphaltene Dispersions by Small-angle X-ray Scattering," *Fuel*, 1988, **67**: p. 245-250.

12. Bardon, C., et al., "The colloidal structure of crude oils and suspensions of asphaltenes and resins," *Fuel Science & Technology International*, 1996, **14** (1-2): p. 203-242.

13. Fenistein, D., et al., "Viscosimetric and neutron scattering study of asphaltene aggregates in mixed toluene/heptane solvents," *Langmuir*, 1998, **14** (5): p. 1013-1020.

14. Mushrush, G.W. and J.G. Speight, *Petroluem Products: Instability and Incompatibility*. Applied Energy Technology Series. 1995, Bristol, PA: Taylor and Francis.

15. Storm, D.A., S.J. DeCanio and E.Y. Sheu, *Sludge Formation During Heavy Oil Conversion*, in *Asphaltene Particles in Fossil Fuel Exploration, Recovery, Refining, and Production Processes*, M.K. Sharma and T.F. Yen, Editors. 1994, Plenum Press: New York. p. 81-90.

16. Lin, J.-R., J.-K. Park and T.F. Yen, *Upgrading From Petroleum and Coal-Derived Asphaltenes*, in *Asphaltene Particles in Fossil Fuel Exploration, Recovery, Refining, and Production Processes*, M.K. Sharma and T.F. Yen, Editors. 1994, Plenum Press: New York. p. 91-100.

17. Cimino, R., et al., *Solubility and Phase Behavior of Asphaltenes in Hydrocarbon Media*, in *Asphaltenes: Fundamentals and Applications*, E.Y. Sheu and O.C. Mullins, Editors. 1995, Plenum Press: New York. p. 97-130.

18. Fordedal, H., et al., "Crude Oil Emulsions in High Electric Fields as Studied by Dielectric Spectroscopy. Influence of Interaction Between Commercial and Indigenous Surfactants," *Colloids and Surfaces A: Physicochemical and Engineering Aspects*, 1996, **106**: p. 33-47.

19. Strassner, J.E., "Effect of pH on Interfacial Films and Stability of Crude Oil-Water Emulsions," *Journal of Petroleum Technology*, 1968, **20**: p. 303-312.

20. Sjöblom, J., et al., "Stabilization and Destabilization of Water-in-Crude Oil Emulsions from the Norwegian Continental Shelf. Correlation with Model Systems," *Advances in Colloid and Interface Science*, 1992, **41**: p. 241-271.

21. Taylor, S.E., "Resolving Crude Oil Emulsions," *Chemistry and Industry*, 1992, **20**: p. 770-773.

22. van der Waarden, M., "Stability of Emulsions of Water in Mineral Oils Containing Asphaltenes," *Kolloid Z. Z. Polymer*, 1958, **156** (2): p. 116-122.

23. Neumann, H.J. and B. Paczynska-Lahme, "Petroleum Emulsions--Properties, Stability and Demulsification," *Chemical Engineering Technology*, 1981, **53**: p. 911-916.

24. Sheu, E.Y. and M.B. Shields, "Asphaltene Surface Activity at Oil-Water Interfaces," *Society of Petroleum Engineers*, 1995, **28995**: p. 523-532.

25. McLean, J.D. and P.K. Kilpatrick, "Effects of Asphaltene Solvency on Stability of Water-in-Crude Oil Emulsions," *Journal of Colloid and Interface Science*, 1997, **189**: p. 242-253.

26. McLean, J.D., et al., *The Role of Petroleum Asphaltenes in the Stabilization of Water-in-Oil Emulsions*, in *Structures and Dynamics of Asphaltenes*, O.C. Mullins and E.Y. Sheu, Editors. 1998, Plenum Press: New York. p. 377-422.

27. Grace, R., *Commercial Emulsion Breaking*, in *Emulsions: Fundamentals and Applications in the Petroleum Industry*, L.L. Schramm, Editor. 1992, American Chemical Society: Washington, D.C. p. 313-339.

28. Mackay, G.D.M., et al., "The Formation of Water-in-Oil Emulsions Subsequent to an Oil Spill," *Journal of the Institute of Petroleum*, 1973, **59** (568): p. 164-172.

29. Johansen, E.J., et al., "Water-in-Crude Oil Emulsions from the Norwegian Continental Shelf Part I. Formation, Characterization and Stability Correlations," *Colloids and Surfaces*, 1989, **34**: p. 353-370.

30. Sjöblom, J., et al., "Water-in-Crude Oil Emulsions. Formation, Characterization, and Destabilization," *Progress in Colloid and Polymer Science*, 1990, **82**: p. 131-139.

31. Schramm, L.L., *Petroleum Emulsions: Basic Principles*, in *Emulsions: Fundamentals and Applications in the Petroleum Industry*. 1992, American Chemical Society: Washington, D.C. p. 1-49.

32. Bancroft, W.D., "Theory of Emulsification," *Journal of Physical Chemistry*, 1913, **17**: p. 501.

33. Lawrence, A.S.C. and W. Killner, "Emulsions of Seawater in Admiralty Fuel Oil with Special Reference to their Demulsification," *Journal of the Institute of Petroleum*, 1948, **34**: p. 281.

34. Blair, C.M., "Interfacial Films Affecting the Stability of Petroleum Emulsions," *Chemistry and Industry*, 1960: p. 538-544.

35. Dodd, C.G., "The Rheological Properties of Films at Crude Petroleum-Water Interfaces," *Journal of Physical Chemistry*, 1960, **64** (5): p. 544-550.

36. Kimbler, O.K., R.L. Reed and I.H. Silberberg, "Physical Characteristics of Natural Films Formed at Crude Oil-Water Interfaces," *Society of Petroleum Engineers Journal*, 1966 (6): p. 153-165.

37. Cairns, R.J.R., D.M. Grist and E.L. Neustadter. *The Effect of Crude Oil-Water Interfacial Properties on Water-Crude Oil Emulsion Stability*. in *Theory and Practice of Emulsion Technology*. 1974. Brunel University: Academic Press.

38. Oren, J.J. and G.D.M. MacKay, "Electrolyte and pH Effect on Emulsion Stability of Water-in-Petroleum Oils," *Fuel*, 1977, **56** (10): p. 382-384.

39. Jones, T.J., E.L. Neustadter and K.P. Whittingham, "Water-in-Crude Oil Emulsion Stability and Emulsion Destabilization by Chemical Demulsifiers," *Journal of Canadian Petroleum Technology*, 1978, **17** (2): p. 100-108.

40. Bridie, A.L., et al., "Formation, Prevention and Breaking of Sea Water in Crude Oil Emulsions 'Chocolate Mousses'," *Mar. Pollut. Bull.*, 1980, **11**: p. 343-348.

41. Shetty, C.S., A.D. Nikolov and D.T. Wasan, "Demulsification of Water in Oil Emulsions Using Water Soluble Demulsifiers," *Journal of Dispersion Science and Technology*, 1992, **13** (2): p. 121-133.

42. Mitchell, D.L. and J.G. Speight, "The Solubility of Asphaltenes in Hydrocarbon Solvents," *Fuel*, 1973, **52** (4): p. 149-152.

43. Yen, T.F., J.G. Erdman and S.S. Pollack, "Investigation of Structure of Petroleum Asphaltenes By X-Ray Diffraction," *Analytical Chemistry*, 1961, **33** (11): p. 1587-&.

44. Boduszynski, M.M., "Composition of Heavy Petroleums. 2. Molecular Characterization," *Energy & Fuels*, 1988, **2** (5): p. 597-613.

45. Bestougeff, M.A. and P. Gendrel. *Study on the Structure of Asphaltenic Constituents by Combined Physical and Chemical Methods*. in *147th American Chemical Society Meeting*. 1964. Philadelphia, PA: ACS, Division of Petroleum Chemistry.

46. McKay, J.F., D.R. Latham and W.E. Haines, "Composition of Petroleum Heavy Ends. 3. Comparison of the Composition of High-Boiling Petroleum Distillates and Petroleum > 675 C Residues," *Fuel*, 1981, **60** (1): p. 27-32.

47. Boduszynski, M.M., "Characterization of "Heavy" Crude Components," *Preprints ACS Division of Petroleum Chemistry*, 1985, **30**: p. 626-640.

48. Speight, J.G., "A Structural Investigation of the Constituents of Athabasca Bitumen by Proton Magnetic Resonance Spectroscopy," *Fuel*, 1970, **49**: p. 76-90.

49. Biggs, W.R., R.J. Brown and J.C. Fetzer, "Elemental Profiles of Hydrocarbon Materials by Size-Exclusion Chromatography/Inductively Coupled Plasma Atomic Emission Spectrometry," *Energy & Fuels*, 1987, **1** (3): p. 257-262.

50. Nalwaya, V., et al., "Studies on asphaltenes through analysis of polar fractions," *Industrial & Engineering Chemistry Research*, 1999, **38** (3): p. 964-972.

51. Reynolds, J.G. and W.R. Biggs, "Effects of Asphaltene Precipitation and a Modified D 2007 Separation on the Molecular Size of Vanadium- and Nickel-Containing Compounds in Heavy Residua," *Fuel Science and Technology International*, 1986, **4** (6): p. 749-777.

52. Reynolds, J.G. and W.R. Biggs, "Application of Size Exclusion Chromatography Coupled with Element-Specific Detection to the Study of Heavy Crude Oil and Residua Processing," *Accounts of Chemical Research*, 1988, **21** (9): p. 319-326.

53. Reynolds, J.G., et al., "Characterization of Nickel and Vanadium Compounds in Tar Sand Bitumen by Petroporphyrin Quantitation and Size Exclusion Chromatography Coupled with Element Specific Detection," *Preprints--ACS Division of Petroleum Chemistry*, 1988, **33** (2): p. 239-246.

54. Hasiba, H.H. and F.W. Jessen, "Film-Forming Compounds From Crude Oils, Interfacial Films and Paraffin Deposition," *The Journal of Canadian Petroleum Technology*, 1968, **7** (1): p. 1-12.

55. Petersen, J.C., "Quantitative Method Using Differential Infrared Spectrometry for the Determination of Compound Types Absorbing in the Carbonyl Region in Asphalts," *Analytical Chemistry*, 1975, **47** (1): p. 112-117.

56. Andersen, S.I., "Effect of Precipitation Temperature on the Composition of n-Heptane Asphaltenes," *Fuel Science and Technology International*, 1994, **12** (1): p. 51-74.

57. Chang, C.L. and H.S. Fogler, "Stabilization of Asphaltenes in Aliphatic Solvents Using Alkylbenzene-Derived Amphiphiles .1. Effect of the Chemical- Structure of Amphiphiles On Asphaltene Stabilization," *Langmuir*, 1994, **10** (6): p. 1749-1757.

58. Hasan, M.U., M.N. Siddiqui and M. Arab, "Separation and Characterization of Asphaltenes from Saudi Arabian Crudes," *Fuel*, 1988, **67** (8): p. 1131-1134.

59. Jacobson, J.M. and M.R. Gray, "Use of IR Spectroscopy and Nitrogen Titration Data in Structural Group Analysis of Bitumen," *Fuel*, 1987, **66** (6): p. 749-752.

60. Barbour, R.V. and J.C. Petersen, "Molecular Interactions of Asphalt: An Infrared Study of the Hydrogen-Bonding Basicity of Asphalt," *Analytical Chemistry*, 1974, **46** (2): p. 273-277.

61. Boduszynski, M.M., J.F. McKay and D.R. Latham, "Asphaltenes, Where Are You?," *Proceedings of the Association of Asphalt Paving Technologists*, 1980, **49**: p. 123-143.

62. Ignasiak, T., O.P. Strausz and D.S. Montgomery, "Oxygen Distribution and Hydrogen Bonding in Athabasca Asphaltene," *Fuel*, 1977, **56**: p. 359-365.

63. Moschopedis, S.E. and J.G. Speight, "Investigation of Hydrogen Bonding by Oxygen Functions in Athabasca Bitumen," *Fuel*, 1976, **55**: p. 187-192.

64. Petersen, J.C., "An Infra-red Study of Hydrogen Bonding in Asphalt," 1967: p. 295-305.

65. Miller, R., "Hydrocarbon Class Fractionation with Bonded-Phase Liquid Chromatography," *Analytical Chemistry*, 1982, **54** (11): p. 1742-1746.

66. Reynolds, J.G., "Characterization of Heavy Residua by Application of a Modified D 2007 and Asphaltene Separation: Effect of Solvents on Physical and Chemical Properties of Fractions Derived From Hondo 850^{O}F Residuum," *Fuel Science and Technology International*, 1987, **5** (5): p. 593-620.

67. Ali, M.F., A. Bukhari and M.U. Hasan, "Structural Characterization of Arabian Heavy Crude Oil Residue," *Fuel Science and Technology International*, 1989, **7** (8): p. 1179-1208.

68. Alula, M., et al., "Efficiency of Sequential Elution Solvent Chromatography-Extrography Technique for the Characterization of Hydroliquefaction and Pyrolysis Products," *Fuel*, 1989, **68** (10): p. 1330-1335.

69. Middleton, W.R., "Gradient Elution Chromatography Using Ultraviolet Monitors in the Analytical Fractionation of Heavy Petroleums," *Analytical Chemistry*, 1967, **39** (14): p. 1839-1846.

70. Al-Jarrah, M.M.H. and A.H. Al-Dujaili, "Characterization of Some Iraqi Asphalts II. New Findings on the Physical Nature of Asphaltenes," *Fuel Science and Technology International*, 1989, **7** (1): p. 69-88.

71. Nghiem, L.X., et al., "Efficient Modelling of Asphaltene Precipitation," *Society of Petroleum Engineers*, 1993, **5**: p. 375-384.

72. Andersen, S.I. and K.S. Birdi, "Aggregation of Asphaltenes as Determined by Calorimetry," *Journal of Colloid and Interface Science*, 1991, **142** (2): p. 497-502.

73. Espinat, D., et al., "Colloidal Macrostructure of Crude-Oil Studied By Neutron and X- Ray Small-Angle Scattering Techniques," *Journal De Physique Iv*, 1993, **3** (C8): p. 181-184.

74. Murgich, J., J.A. Abanero and O.P. Strausz, "Molecular recognition in aggregates formed by asphaltene and resin molecules from the Athabasca oil sand," *Energy & Fuels*, 1999, **13** (2): p. 278-286.

75. Barre, L., et al., "Colloidal structure of heavy crudes and asphaltene solutions," *Revue De L Institut Francais Du Petrole*, 1997, **52** (2): p. 161-175.

76. Murgich, J. and O.P. Strausz, "Molecular mechanics of aggregates of asphaltenes and resins of the Athabasca oil," *Petroleum Science and Technology*, 2001, **19** (1-2): p. 231-243.

77. McLean, J.D. and P.K. Kilpatrick, "Effects of asphaltene aggregation in model heptane-toluene mixtures on stability of water-in-oil emulsions," *Journal of Colloid and Interface Science*, 1997, **196** (1): p. 23-34.

78. Mohammed, R.A., et al., "Dewatering of Crude Oil Emulsions 2. Interfacial Properties of the Asphaltic Constituents of Crude Oil," *Colloids and Surfaces A: Physicochemical and Engineering Aspects*, 1993, **80**: p. 237-242.

79. Fordedal, H., et al., "A Multivariate Screening Analysis of W/O Emulsions in High External Electric Fields as Studied by Means of Dielectric Time Domain Spectroscopy, II," *Journal of Colloid and Interface Science*, 1996, **182**: p. 117-125.

80. Gafonova, O.V. and H.W. Yarranton, "The stabilization of water-in-hydrocarbon emulsions by asphaltenes and resins," *Journal of Colloid and Interface Science*, 2001, **241** (2): p. 469-478.

81. Acevedo, S., et al., "Asphaltenes and Resins From the Orinoco Basin," *Fuel*, 1985, **64**: p. 1741-1747.

82. Wiehe, I.A. and K.S. Liang, "Asphaltenes, Resins, and other petroleum macromolecules," *Fluid Phase Equilibria*, 1996, **117** (1-2): p. 201-210.

83. McKay, J.F., et al., "Petroleum Asphaltenes: Chemistry and Composition," *Analytical Chemistry of Liquid Fuel Sources, Advances in Chemistry Series*, 1978, **170**: p. 128-142.

84. Andersen, S.I., A. Keul and E. Stenby, "Variation in composition of subfractions of petroleum asphaltenes," *Petroleum Science and Technology*, 1997, **15** (7-8): p. 611-645.

85. Yarranton, H.W. and J.H. Masliyah, "Molar Mass Distribution and Solubility Modeling of Asphaltenes," *AICHE Journal*, 1996, **42** (12): p. 3533-3543.

86. Yarranton, H.W., H. Alboudwarej and R. Jakher, "Investigation of asphaltene association with vapor pressure osmometry and interfacial tension measurements," *Industrial & Engineering Chemistry Research*, 2000, **39** (8): p. 2916-2924.

87. Overfield, R.E., et al., "SANS Study of Asphaltene Aggregation," *Fuel Science & Technology International*, 1989, **7** (5-6): p. 611-624.

88. Ravey, J.C. and D. Espinat, "Macrostructure of Petroleum Asphaltenes by Small Angle Neutron Scattering," *Progress in Colloid and Polymer Science*, 1990, **81**: p. 127-130.

89. Sheu, E.Y., D.A. Storm and M.M.D. Tar, "Asphaltenes in Polar Solvents," *Journal of Non-Crystalline Solids*, 1991, **131-133**: p. 341-347.

90. Sheu, E.Y., M.M.D. Tar and D.A. Storm, "Colloidal Structure of Vacuum Residue in Solvents," *Preprints--ACS Division of Fuel Chemistry*, 1992, **37** (2): p. 844-848.

91. Storm, D.A., E.Y. Sheu and M.M. Detar, "Macrostructure of Asphaltenes in Vacuum Residue By Small-Angle X-Ray-Scattering," *Fuel*, 1993, **72** (7): p. 977-981.

92. Thiyagarajan, P., et al., "Temperature-Dependent Structural-Changes of Asphaltenes in 1- Methylnaphthalene," *Energy & Fuels*, 1995, **9** (5): p. 829-833.

93. Xu, Y.N., Y. Koga and O.P. Strausz, "Characterization of Athabasca Asphaltenes By Small-Angle X-Ray- Scattering," *Fuel*, 1995, **74** (7): p. 960-964.

94. Liu, Y.C., et al., "Fractal Structure of Asphaltenes in Toluene," *Fuel*, 1995, **74** (9): p. 1352-1356.

95. Rassamdana, H. and M. Sahimi, "Asphalt Flocculation and Deposition: II. Formation and Growth of Fractal Aggregates," *AICHE Journal*, 1996, **42** (12): p. 3318-3332.

96. Lin, M.Y., E.B. Sirota and H. Gang, "Neutron scattering characterization of asphaltene particles," *Abstracts of Papers of the American Chemical Society*, 1997, **213**: p. 66-FUEL.

97. Miller, J.T., et al., "Subfractionation and characterization of Mayan asphaltene," *Energy & Fuels*, 1998, **12** (6): p. 1290-1298.

98. Sirota, E.B., "Swelling of asphaltenes," *Petroleum Science and Technology*, 1998, **16** (3-4): p. 415-431.

99. Fenistein, D. and L. Barre, "Experimental measurement of the mass distribution of petroleum asphaltene aggregates using ultracentrifugation and small-angle X-ray scattering," *Fuel*, 2001, **80** (2): p. 283-287.

100. Savvidis, T.G., et al., "Aggregated structure of flocculated asphaltenes," *Aiche Journal*, 2001, **47** (1): p. 206-211.

101. Benjamins, J. and F.V. Vader, "The Determination of the Surface Shear Properties of Adsorbed Protein Layers," *Colloids and Surfaces*, 1992, **65** (2-3): p. 161-174.

102. Benjamins, J., A. Cagna and E.H. LucassenReynders, "Viscoelastic properties of triacylglycerol/water interfaces covered by proteins," *Colloids and Surfaces a-Physicochemical and Engineering Aspects*, 1996, **114**: p. 245-254.

103. Nino, M.R.R., et al., "Surface dilational properties of protein and lipid films at the air-water interface," *Langmuir*, 1998, **14** (8): p. 2160-2166.

104. Dufour, E., M. Dalgalarrondo and L. Adam, "Conformation of beta-lactoglobulin at an oil/water interface as determined from proteolysis and spectroscopic methods," *Journal of Colloid and Interface Science*, 1998, **207** (2): p. 264-272.

105. Ybert, C. and J.M. di Meglio, "Study of protein adsorption by dynamic surface tension measurements: Diffusive regime," *Langmuir*, 1998, **14** (2): p. 471-475.

106. Little, R.C., "Breaking Emulsions of Water in Navy Fuel Oils," *Fuel*, 1974, **53** (10): p. 246-252.

107. Cratin, P.D., "A Quantitative Characterization of pH-Dependent Systems," *Industrial and Engineering Chemistry*, 1969, **61** (2): p. 35-45.

108. Mansurov, I.R., E.Z. Il'yasova and V.P. Vygovskoi, "Shear Strength of Interfacial Films of Asphaltenes," *Chemistry and Technology of Fuels and Oils*, 1987, **23** (1-2): p. 96-98.

109. Menon, V.B. and D.T. Wasan, "Coalescence of Water-in-Shale Oil Emulsions," *Separation Science and Technology*, 1984, **19** (8 & 9): p. 555-574.

110. Mukherjee, S. and A.P. Kushnick. *Effect of Demulsifiers on Interfacial Properties Governing Crude Oil Demulsification*. in *Symposium On Advances in Oil Field*

Chemistry Presented Before the Division of Petroleum Chemistry, Inc. 1988. Toronto: American Chemical Society.

111. Isaacs, E.E., et al., "Electroacoustic Method for Monitoring the Coalescence of Water-in-Oil Emulsions," *Colloids and Surfaces*, 1990, **46**: p. 177-192.

112. Eley, D.D., et al., "Electron Micrography of Emulsions of Water in Crude Petroleum," *Journal of Colloid and Interface Science*, 1976, **54** (3): p. 462-466.

113. Hassander, H., B. Johansson and B. Tornell, "The Mechanism of Emulsion Stabilization by Small Silica (Ludox) Particles," *Colloids and Surfaces*, 1989, **40**: p. 93-105.

114. Papirer, E., et al., "Chemical Nature of Water/oil Emulsifying Properties of Asphaltenes," *Fuel*, 1982, **61**: p. 732-734.

115. Aveyard, R., et al., "The Resolution of Water-in-Crude Oil Emulsions by the Addition of Low Molar Mass Demulsifiers," *Journal of Colloid and Interface Science*, 1990, **139** (1): p. 128-138.

116. Neustadter, E.L., K.P. Whittingham and D.E. Graham, *Interfacial Rheological Properties of Crude Oil/Water Systems*, in *Surface Phenomena in Enhanced Oil Recovery*, D.O. Shah, Editor. 1981, Plenum Press: New York. p. 307-326.

117. Acevedo, S., et al., "Interfacial Rheological Studies of Extra-Heavy Crude Oils and Asphaltenes: Role of the Dispersion Effect of Resins in the Adsorption of Asphaltenes at the Interface of Water-in-Crude Oil Emulsions," *Colloids and Surfaces A: Physicochemical and Engineering Aspects*, 1993, **71**: p. 65-71.

118. Mohammed, R.A., et al., "Dewatering of Crude Oil Emulsions 1. Rheological Behavior of the Crude OIl-Water Interface," *Colloids and Surfaces A: Physicochemical and Engineering Aspects*, 1993, **80**: p. 223-235.

Aggregation and Solubility Behavior of Petroleum Asphaltenes and their Subfractions

P. Matthew Spiecker and Peter K. Kilpatrick

ABSTRACT

Petroleum asphaltenes (*n*-heptane insolubles) from Arab Heavy, B6, Canadon Seco and Hondo crude oils were fractionated in mixtures of heptane and toluene and analyzed chemically and by vapor pressure osmometry (VPO) and small angle neutron scattering (SANS). Solubility profiles of these asphaltenes were determined gravimetrically in mixtures of heptane and toluene and were completely soluble above a toluene volume fraction of 0.52. Solubility limits varied from a toluene volume fraction of 0.45 to 0.52. Preparative scale fractionations were performed on the four asphaltenes at toluene volume fractions between 0.3 and 0.4. Solubility profiles of the more soluble and less soluble fractions isolated preparatively in heptane-toluene mixtures indicated strong cooperative asphaltene interactions. The less soluble asphaltene fractions had lower H/C ratios, higher N, V, Ni, and Fe contents than the more soluble or unfractionated asphaltenes. Number average molar masses by VPO in toluene indicated that the less soluble fraction of B6 asphaltenes was highly aggregated (>10,000 g/mol) while the unfractionated and more soluble fractions approached monomer dimensions (~2,000 g/mol) at high dilution. Canadon Seco asphaltenes and their less soluble fraction had similar number average molar masses at high dilution (~3,000 g/mol). Neutron scattering studies at 25 and 80°C indicated Canadon Seco formed the largest aggregates in mixtures of heptane-toluene followed by B6, Hondo and Arab Heavy. At 25°C Canadon Seco formed asphaltene aggregates with correlation lengths ranging from 180 Å (highly aromatic solvent – $\varphi_{toluene}$=0.8) to 250 Å near its solubility limit ($\varphi_{toluene}$=0.52). The other asphaltenes formed aggregates with correlation lengths ranging

from 47 Å to 98 Å in pure toluene and near the solubility limit, respectively. Less soluble fractions formed aggregates considerably larger than the unfractionated asphaltenes (as high as 520 Å), while soluble asphaltenes formed the smallest aggregates (as low as 22 Å). Highly aggregated samples at 25°C were the most inclined to disaggregate upon heating and addition of 1-methylnaphthalene intensified this effect. The soluble fraction was near its minimum aggregate size at room temperature and was only marginally affected by the application of heat. Enhanced aromatic π-π bonding, dispersion forces and hydrogen bond interactions within the less soluble fraction likely caused large aggregate formation and low solubility.

CHAPTER 2

AGGREGATION AND SOLUBILITY BEHAVIOR OF PETROLEUM ASPHALTENES AND THEIR SUBFRACTIONS

2.1 Introduction

The study of asphaltene colloidal properties has been motivated by their propensity to aggregate, flocculate, precipitate, and to adsorb onto interfaces. The tendencies of asphaltenes to participate in colloidal and interfacial phenomena have posed great challenges for the petroleum industry. Problems associated with well production, pipeline transfer, land and sea-based transportation and, ultimately, oil refining have all been linked to the presence of asphaltenic colloids.[1-13] During visbreaking and catalytic hydrocracking large amounts of sludge and sediment can form [14] ostensibly due to the flocculation of asphaltenes during processing.[15] Coke generation and asphaltene adsorption within catalytic cracking beds can reduce the effective catalyst surface area as well as the efficiency of coal hydropyrolysis.[16] Asphaltene deposition within reservoir rocks has been blamed for pronounced reductions in well productivity.[17] Asphaltenes have also been found to facilitate the formation of extremely stable water-in-crude oil emulsions.[5, 18-26] Understanding asphaltene chemistry and the fundamental mechanisms of colloid formation has been the driving force behind much petroleum research for the last half-century.

Asphaltenes are defined as the portion of crude oil insoluble in *n*-alkanes such as *n*-heptane or n-pentane yet soluble in benzene or toluene.[27, 28] The "solubility class" definition of asphaltenes generates a broad distribution of molecular structures that can vary greatly from one crude oil to another. In general, asphaltenes are characterized by fused ring

aromaticity, small aliphatic side chains, and polar heteroatom-containing functional groups. It is common to characterize asphaltenes by their average properties (see Table 2.1). The most common techniques for determining the chemical constitution of asphaltenes include combustion elemental analysis (H/C, N, S),[29-33] inductively coupled plasma (V, Ni, Fe) [34-38], and Fourier transform infrared spectroscopy (polar functional group concentrations) [39-44]. A wealth of information can be drawn from these chemical analyses. H/C ratios between 1.0 and 1.2 and N, S, and O content of a few weight percent suggest that much of the asphaltene backbone consists of fused aromatic carbon interspersed with polar functional groups containing five to seven heteroatoms. FTIR analysis reveals many groups capable of forming hydrogen bonds. Many studies have indicated the presence of carboxylic acids, carbonyls, phenols, and pyrrolic and pyridinic nitrogen.[45-49] These groups are capable of donating or accepting protons inter- and intra-molecularly. The most plausible mechanisms of asphaltene aggregation involve π-π overlap between aromatic sheets, hydrogen bonding between functional groups and other charge transfer interactions. The degree to which aggregate sizes vary is controlled by the polydispersity and chemistry of asphaltene monomers. While these chemical analyses provide valuable information concerning asphaltene chemistry and offer possible mechanisms of interaction, they do not offer much insight into what governs the colloidal properties of asphaltenes.

The notion of asphaltenes forming colloidal aggregates in crude oil was originally proposed by Nellensteyn [1] and later by Pfeiffer and Saal [2]. They proposed that "dispersions" of asphaltenic aggregates in heavy crudes are solvated by resins and other aromatic compounds. X-ray diffraction measurements by Yen et al. showed that dry asphaltenes contain a core of fused aromatic rings with an aliphatic periphery.[28] The flat

aromatic core permits cofacial stacking of approximately four to five parallel sheets mediated by π-π bonding.[4] These early structural examinations were followed by more detailed and revealing investigations of the mechanisms of asphaltene aggregation and colloid formation.[8, 50-52]

The degree of asphaltene aggregation can be obtained from molar mass and neutron or x-ray scattering measurements. Asphaltene molecular weights have been probed by numerous techniques to yield values from one to several thousands of g/mol. The most common technique for measuring number average molecular weights is vapor pressure osmometry in an aromatic and/or polar solvent (toluene, benzene, pyridine, or *o*-dichlorobenzene) at elevated temperature (50-130°C).[29, 53-59] Typical molar masses range from about 800 to 3,000 g/mol in the best solvents. The dissociating power of the solvent is critical to obtaining the smallest number indicative of an asphaltene monomer. Molar mass variations with solvent and temperature suggest changes in aggregate size rather than conformational changes in asphaltene structure. Interaggregate π- and hydrogen bonding is far weaker than covalent bonding between carbon atoms and can be broken down in the presence of a good solvent or at higher temperatures. Toluene, a weaker solvent, often results in MW of 3,000-6,000 g/mol. This size suggests that, under these solvent conditions, the asphaltenes are not large monomers, but rather aggregates of four to five monomers.

Neutron and x-ray scattering are very powerful tools to deduce sizes and morphologies of colloidal aggregates in solution. Numerous studies have been performed over the past decade or so to probe the effects of solvent, temperature and crude oil source on asphaltene aggregate size and polydispersity.[8, 11, 13, 51, 52, 60-73] While both x-ray and neutron scattering can provide colloid structure information, SANS offers the advantage of

solvent-solute contrast via deuteration SANS to decrease data collection times and probe the entire asphaltene aggregate. SAXS, on the other hand, can only discern the aromatic asphaltene core. Proper analysis of the scattering intensity curves can provide aggregate radius of gyration (R_g), shape and dimension. However, careful consideration of the molecular picture presented earlier can help guide the analysis. The most logical shape to consider might be a flat disk with a large diameter to thickness ratio. In addition, asphaltene polydispersity should be accounted for. To date, mono- and polydisperse spheres[51, 74], flat disks[12, 60, 62], and prolate cylinders[64] have all been suggested as possible asphaltene structures. Sheu et al. suggested a polydisperse spheres model with a Schultz distribution best fit their scattering data.[74] Overfield et al. measured R_g of vacuum resid asphaltenes in deuterated toluene at several temperatures. R_g decreased from 116 Å at 25°C to 55 Å at 100°C and was explained by aggregate dissociation rather than an asphaltene conformational change. Aggregate size changes caused by temperature variation were, however, reversible.[60] Lin et al. fit $Q > 0.01$ $Å^{-1}$ data to a disk like model with average R_g around 40 Å.[69] At smaller Q values (i.e. larger length scales) the data suggest the presence of larger aggregates or particles too sizeable to probe by Guinier analysis. They suggested that these large particles had diameters of approximately 1,000 Å and often formed at high concentrations and/or low temperatures. Espinat et al. measured the scattered intensity from asphaltenes in several solvents and at low and high temperature.[62] In toluene, 2 wt % Boscan asphaltene solutions formed larger aggregates at room temperature (234 Å diameter) than at 76°C (175 Å). At room temperature, aggregates sizes were two to four times smaller in high polarity solvents such as pyridine and tetrahydrofuran than benzene. However, at elevated temperatures (up to 80°C), the solvent effect was less significant and aggregate size

approached a minimum. Increased heptane fraction in mixtures of heptane and toluene tend to enhance asphaltene aggregation and lead to higher R_g values.[13] A recent study by Fenistein and Barré on asphaltenes fractionated by ultracentrifugation found that R_g and molecular weight increased with fraction density/weight.[72] Molecular weights determined from neutron scattering of polydisperse asphaltene systems are weight averaged[13] and may be biased by the presence of a small number of high mass aggregates. As the aforementioned aggregate size data suggests, asphaltene solubility can vary appreciably in solvents containing different polarities and aromatic carbon content. Solvents that more closely resemble and interact with asphaltene microstructure can affect a greater state of dissolution than low polarity, aliphatic solvents. The application of heat can further disrupt the aggregation process and reduce the equilibrium aggregate size. Through asphaltene solubility and molecular dimension measurements in different solvents and temperature regimes we will begin to unravel the complex mechanisms of aggregation.

The detailed study of the chemistry and aggregate-forming properties of asphaltene subfractions will help shed light on the mechanisms of aggregation. By fractionating and concentrating the more polar and aromatic material, we should be able to enhance the degree of asphaltene aggregation. Several recent studies have probed the effects of asphaltene fractionation by differential solubility in terms of chemical composition.

Nalwaya et al.[35] and Kaminski et al.[75] have fractionated asphaltenes in mixtures of pentane and methylene chloride to analyze their chemistry and dissolution kinetics. Higher polarity fractions had lower rates of dissolution compared to lower polarity fractions. These authors linked the high polarity to heteroatom and metals content, particularly iron, nickel, and vanadium.

Yarranton and Masliyah employed solubility and precipitation methods to study the solution behavior of heptane precipitated Athabasca asphaltenes.[58] Asphaltenes were added to premixed hexane-toluene solutions and then filtered in the solubility method. The precipitation method involved complete dissolution in toluene followed by hexane addition and filtration. Except at low solute concentrations, both methods yielded identical mass fractions of insoluble asphaltenes. At a toluene volume fraction equal to 0.5, less than 10 % (w/w) of the asphaltenes were insoluble. Presumably, the insolubles mass fraction was negligible in solvents that were more aromatic. Of greater significance, molar masses were inversely proportional to the extent of precipitation. In solvents very close to the solubility limit (slightly below 50 % (v/v) toluene), where only a small fraction precipitated, asphaltene insolubles had the highest molar mass. As the solvent blends became less aromatic, the fraction precipitated increased and molar mass decreased. These results suggest that the asphaltenes most prone to precipitation have the largest monomer or unit sheets and/or aggregate to the greatest extent.

Andersen et al. studied the precipitation of asphaltenes in mixtures of heptane and toluene from undiluted Boscan crude oil and from the heptane insoluble portion of Boscan crude.[57] They found that asphaltenes remained soluble to a greater extent in crude oil (presumably due to resins and other aromatics) than in heptane-toluene at identical heptane-toluene ratios. Enhanced solubility reduced the yield of insolubles and concentrated more polar and aromatic structures as evidenced from fluorescence measurements. Of greatest consequence was the large difference between soluble and insoluble asphaltene molar masses by VPO. The soluble asphaltenes formed aggregates nearly five times smaller than corresponding insolubles.

In this work, we have determined the solubility profiles of four asphaltenes in mixtures of heptane and toluene at fixed concentration. At solvent conditions where asphaltenes precipitate (high ratios of heptane to toluene), we have isolated the soluble and insoluble material for further study. Additional solubility profiles were prepared for the soluble and insoluble fractions in mixtures of heptane and toluene. Detailed chemical analyses were performed to measure the degree of polarity and aromaticity in the insoluble fraction. Intermolecular interactions were probed with SANS in various heptane-toluene mixtures at room and at high temperatures. This study has been undertaken to correlate the concentration of polar and aromatic material in asphaltene subfractions to their solubility and aggregation behavior.

2.2 Experimental

2.2.1 Asphaltene Source

Asphaltenes were precipitated from four crude oils: B6 and Hondo (off-shore California), Arab Heavy (Safaniya), and Canadon Seco (Argentina). These crude oils are asphaltene rich and vary in viscosity, resin content and asphaltene H/C ratio. Basic crude oil and asphaltene properties are summarized in Table 2.2.

2.2.2 Asphaltene Precipitation

All crude oils were stored near 0°C in sealed containers under an argon blanket to minimize possible oxidation. The crude oil was warmed and shaken vigorously to ensure homogeneity before sampling. In a 1 L flask (typically 6-8 flasks were used), 15-20 g of crude oil were diluted with *n*-heptane 40:1 by volume. All solvents were obtained from

Fisher Scientific and were HPLC grade. Since the oils were both quite viscous and only partially soluble in heptane, the flasks were initially hand shaken to completely disperse all material. After 24 hours of continuous shaking, the precipitated asphaltenes were removed by vacuum filtration through 15 cm diameter, 1.5 μm Whatman 934-AH glass microfiber filter paper. The filter paper was supported on a ceramic Büchner funnel placed on a 1 L vacuum flask. The asphaltenes were rinsed with heptane (~250 mL/flask) to remove remaining soluble material (maltenes). The Büchner funnel was then transferred to a new vacuum flask. Methylene chloride was used to redissolve the asphaltenes under partial vacuum. (Methylene chloride has a high vapor pressure and low boiling point, which causes it to evaporate rapidly and reduce the local temperature. Atmospheric moisture would often condense and freeze on the filter paper hindering the flow of the organic phase.) The methylene chloride-asphaltene solution was rotary evaporated under partial vacuum at 40°C. After evaporating a substantial volume of solvent, the remaining solution was transferred to glass jars and placed under an argon stream for further drying. Once nearly dry, the samples were moved into a nitrogen flushed vacuum oven at 50°C for 24-36 hours.

2.2.3 Asphaltene Solubility Determination

The solubility of all asphaltenes was determined gravimetrically in mixtures of heptane and toluene. Asphaltenes were added to 20 mL glass vials and dissolved in 15 mL of a heptane-toluene (heptol) mixture bringing the concentration to 0.75 % (w/v) (mass solute/volume solvent). This corresponds to a mass concentration of approximately 1 % (w/w). Asphaltenes were first dissolved in toluene for several hours followed by heptane addition and equilibration over night. The solutions were then vacuum filtered through 5.5

cm diameter, 1.5 μm Whatman 934-AH glass microfiber filter paper. A rinse solvent (7.5 mL) equivalent in heptol composition to the asphaltene solution was poured immediately onto the filter paper to remove any remaining soluble material. The Büchner funnel was then transferred to a new vacuum flask and rinsed with methylene chloride to dissolve the precipitate; warm solvent was used if necessary to effect dissolution.

Upon asphaltene fractionation two solutions were generated: one containing the more soluble or "Soluble" asphaltenes in heptol and the other containing the less soluble or "Precipitated" asphaltenes in methylene chloride. Each solution was rotary evaporated, transferred to 15 mL vials and dried in a nitrogen flushed, 50°C vacuum oven for 24 hours. The solubility of asphaltenes in heptol was subsequently gauged by the percentage of material that precipitated in a particular solvent mixture.

In addition to determining the solubility profiles of the unfractionated or "Whole" asphaltenes, profiles of the fractions were generated over the full spectrum of heptol mixtures. To probe the chemical differences between the asphaltenes that precipitated and those that remained soluble, each asphaltene was separated into Precipitate and Soluble fractions at the preparative scale. The heptol mixture was asphaltene specific and was chosen to generate a 1/3:2/3 mass fraction split into Precipitate/Soluble. This split generated fractions with distinguishable chemical and physical behavior as well as sufficient material for subsequent analysis.

2.2.4 Chemical Characterization

Metals content was determined by ICP with a Jerrel Ash 9000 after ashing the samples at 600°C and dissolving in HCl and deionized water. All analyses were performed

at Nalco/Exxon in Sugar Land, TX. Number average molecular weights of selected asphaltenes were determined in toluene at 53°C with a Corona Wescan Vapor Pressure Osmometer. Solutions were prepared at concentrations ranging from 1 to 20 mg/mL.

2.2.5 Small Angle Neutron Scattering: 25°C

Neutron scattering is an important technique for determining solute aggregate sizes on the Å to nm scale. A broad Q range, high neutron flux and large number of scatterers are the ideal conditions to probe the scattering behavior of aggregates. These conditions resulted in a scattering time of 10-20 minutes per sample and the ability to probe aggregates of a wide size range. Measurements were performed on the 30 m, NG7 small angle spectrometer at the National Institute of Standards and Technology in Gaithersburg, MD. Neutrons of 6 Å and 0.22 spread ($\Delta\lambda/\lambda$) were scattered from the sample and collected on a two dimensional detector (65 cm by 65 cm, 1 cm by 1 cm resolution). The instrument geometry and neutron wavelength values bound the operating Q range following the equation:

$$Q = 4\pi\lambda^{-1}\sin\theta \qquad (1)$$

where θ is half the scattering angle and λ is the neutron wavelength. The available Q range extended from 0.0015 to 0.6 $Å^{-1}$ but an intermediate range of 0.0022 to 0.3 $Å^{-1}$ was adequate for most asphaltene solutions.

The sample holder was thermally equilibrated to 25°C and accommodated 8 cells. The cylindrical quartz sample cells (NSG Precision Cells #37-H-5) had a path length of 5 mm and held 2 mL of solution. Asphaltene samples (1 % (w/w)) were dissolved in

perdeuterated solvents -- toluene and heptane or 1-methylnaphthalene -- to enhance scattering contrast. Solvents obtained from CDN Isotopes were of greater than 99.9 % chemical purity and 99.5 % perdeuteration. Dissolution was performed first in perdeuterated toluene followed by heptane addition followed by equilibration over several days. All solutions were transferred from glass vials to the quartz cells without filtration, even in the cases where some precipitation was evident (a low temperature phenomenon).

During beam operation, all eight samples were run at high Q with the detector positioned close to the sample (large θ). After each sample had been run, the detector was repositioned to allow for low Q scanning (small θ). The data was reduced through background and transmission correction followed by low Q-high Q splicing.

2.2.6 Small Angle Neutron Scattering: 80°C

High temperature neutron scattering of the asphaltene samples was performed on both NG1 (8 m) and NG7 (30 m) beamlines. Both instruments had multisample holders, with attached circulating water-glycol baths, capable of maintaining 80°C. All samples underwent a temperature cycle (80°C, 1 hour) in our laboratory prior to heptane addition to ensure complete dissolution. On site (NIST), asphaltene solutions were transferred to 5 mm path length quartz cells and placed in an 80°C bath for 1 hour. This time allowed the solutions to reach thermodynamic equilibrium prior to testing.

2.2.7 Data Handling

Several analysis techniques were used to determine aggregate size and morphology. These included fitting Lorentzian line shapes (using non-linear least squares regression) to

calculate asphaltene correlation lengths (ξ) and Guinier analysis of the low Q portion to determine R_g. Following Ornstein-Zernicke formalism the scattering intensity, *I*, can be related to the scattering vector, *Q*, by:

$$I(Q) = \frac{I_0}{1+(Q\xi)^2} + A \tag{2}$$

where ξ is the correlation length and *A* is a background correction factor.[71, 76] This Lorentzian line shape form was applied to systems with characteristic scattering curves that plateaued at low Q. In the other systems scattering intensity increased monotonically with decreasing Q. A power law term was necessary to account for these large agglomerates in solution. Also, the natural logarithm of the scattering intensity expression was taken to reduce the bias towards the Q regions containing a high density of data points. The functional form of this equation is:

$$\ln\left[I(Q)\right] = \ln\left[\frac{I_1}{Q^4} + \frac{I_0}{1+(Q\xi)^2} + A\right] \tag{3}$$

The scattering intensity function I(Q) may also be expressed as[77]

$$I(Q) = N_p V_p (\Delta\rho)^2 P(Q) S(Q) \tag{4}$$

where N_p is the number of particles, V_p is the particle volume, $\Delta\rho$ is the scattering contrast between solute and solvent, *P(Q)* is the particle form factor and *S(Q)* is the interparticle structure factor. In dilute solutions *S(Q)* can be neglected.

In dilute solutions with no scattering contributions from very large particles the Guinier approximation can be used to determine R_g[78] where

$$I(Q) = I(0)e^{\left(-Q^2 R_g^2/3\right)} \tag{5}$$

and

$$I(0) = N_p V_p (\Delta\rho)^2 \quad (6)$$

R_g can be obtained from the slope of the line fit from ln $I(Q)$ vs Q^2 in the region where QR_g is less than 1.

2.3 Results and Discussion

2.3.1 Asphaltene Solubility

Solubility profiles of each asphaltene determined gravimetrically are shown in Figure 2.1. The asphaltenes were found to be completely soluble in pure toluene and in heptol mixtures of high aromaticity (>52 % (v/v) toluene). At a critical heptane-toluene ratio, the first signs of precipitation were evident. The critical heptol concentration for initial formation of precipitates ranged from 45-52 % (v/v) toluene. After the onset of precipitation, decreased toluene concentration led to increased precipitate formation.

The process of precipitation was controlled by asphaltene-asphaltene and asphaltene-solvent interactions. In heptol solutions containing more than 50 % (v/v) toluene, asphaltene aggregates were sufficiently well solvated to remain in solution. As the solvent became more aliphatic, inter-aggregate forces exceeded the solvating "strength" of the heptol mixture. Component solubility parameters can provide a measure of this "strength". Hildebrand developed the initial solubility parameter formalism for non-polar and non-interacting systems.[79] Later, Hansen extended the Hildebrand solubility parameter to include polar and hydrogen bonding interactions.[80] The parameters of the solvents used in this study are shown in Table 2.3. Replacing toluene with heptane caused a reduction in all three parameter components and a corresponding decrease in asphaltene solubility. As mentioned

before, asphaltenes are characterized by their high aromaticity, the presence of polar heteroatoms and their ability to form hydrogen bonds. Based on solubility parameter arguments, the less soluble fraction of asphaltenes likely contained the highest percentage of fused aromatic rings and polar heteroatoms. Further decreasing the toluene volume fraction created a solvent less capable of dissolving the aromatic and polar asphaltenic species. As a result, the percentage of insoluble asphaltenes increased.

Andersen performed a series of precipitation and redissolution experiments in heptol on Boscan asphaltenes.[57] Direct addition of heptol containing 30 % (v/v) toluene to the crude oil precipitated 20 % (w/w) of the asphaltenes. As the toluene fraction was reduced to 0.2, half of the asphaltenes precipitated. Resins and other aromatic components present in the crude clearly enhanced asphaltene solubility. After precipitating asphaltenes in heptane and redissolving in heptol, the results obtained compare well with our results. At a toluene fraction of 0.5, 13 % (w/w) of the asphaltenes became insoluble. Precipitation climbed to 46 % (w/w) at a toluene fraction of 0.4 and to 60 % at a toluene fraction of 0.3. Boscan asphaltenes are apparently slightly less soluble than the least soluble asphaltene in our study (CS).

The shape of the solubility curve reveals some information on the distribution of aromatic and polar (low solubility) constituents in the asphaltenes. AH asphaltenes were the most soluble and remained completely soluble until the toluene volume fraction reached 0.45. At a given heptol ratio they had the least fraction of precipitated material compared to the other asphaltenes investigated. The other three asphaltenes were closer in terms of their respective solubilities. Any slope changes from one heptol ratio to the next may be partly attributed to experimental scattering but can also be explained by asphaltene heterodispersity.

2.3.2 Asphaltene Fractionation

As described above, reducing the toluene fraction will likely concentrate the more aromatic and polar asphaltenes, due to lower solvent dispersion, polar, hydrogen bonding parameters. The heptol ratios used and fractionation results are shown in Table 2.4. Due to its high solubility, AH was precipitated at the highest ratio of heptane to toluene. The other three asphaltenes underwent fractionation at heptol ratios close or equal to 40 % toluene. Throughout the course of the study, AH and B6 were fractionated three times each, with reasonable reproducibility (see Table 2.4).

There were several differences observed between the Precipitate and Whole asphaltenes. After the initial filtration and heptol rinse steps, the Precipitate fraction remaining on the filter paper was significantly less soluble in methylene chloride than the Whole. B6, CS, and HO were the least soluble and required submerging in warm to hot solvent for five to ten minutes to completely redissolve. This behavior indicates the Precipitate had an enhanced degree of interaggregate bonding compared to the Whole and Soluble. In solution, the Soluble fraction cooperatively solvates the Precipitate to retain the system's solubility.

Solubility curves of the Soluble and Precipitate asphaltenes are shown in Figures 2.2a-d. The Precipitate solubility curves provided the most convincing support for cooperative aggregate interaction. At concentrations in excess of 80 % (v/v) toluene all of the Precipitate fractions were completely soluble within experimental uncertainty. In the case of B6 and HO Precipitate, dropping the toluene fraction to 0.7 precipitated between 20 and 40 % (w/w) of the asphaltenes. CS Precipitate accumulated a significant fraction of

insolubles at 60 % toluene and the most soluble of the four, AH Precipitate, began to precipitate at 55 % toluene. Cooperative solvation is evident between the Precipitate and Soluble fractions. When both are present in solution, the solubility curve generated is equivalent to the Whole asphaltenes. However, removing the Soluble fraction causes the Precipitate to become insoluble at a much higher toluene fraction, particularly with B6 and HO. If the Precipitate were non-interacting, it would begin to precipitate at the same heptol ratio as the Whole and then proceed at a much steeper slope.

Also noteworthy was the solubility behavior of the Soluble asphaltenes at the same heptol ratios used for their preparation. At 30 % toluene, one would expect AH Soluble to be completely soluble, however, about 15 % of the asphaltenes precipitated. Both B6 and HO Soluble demonstrated this "early" precipitation behavior to a lesser degree while CS Soluble behaved "ideally". In these cases, it is likely that the Solubles may benefit from some portion of the Precipitate to help them retain solubility.

In all cases, the Soluble fraction was far more soluble than either the Whole or Precipitate. Removing the Soluble from the Precipitate dramatically decreased the kinetics of dissolution and ultimate solubility of the Precipitate. In this sense, the Soluble fraction acted cooperatively to keep the more aromatic and polar material in solution.

2.3.3 Asphaltene Fraction Chemistry

Reducing the toluene volume fraction decreased the solvent aromaticity and to some extent, its polarity. In heptol, asphaltenes containing a greater fraction of aromatic carbon or higher polarity were driven from solution first as toluene concentration decreased. H/C ratio and nitrogen contents of all asphaltenes and their fractions are shown in Figures 2.3a-b. H/C

correlates well with aromaticity; a lower H/C ratio implies a greater number of fused aromatic rings. In all cases, the Precipitate fraction was enriched in aromatic carbon while the Soluble aromaticity was diminished. As the aromaticity of the fractions increased from Soluble to Whole to Precipitate, the trend in nitrogen content was the opposite. More nitrogen present within an asphaltene ring structure increases its basicity and polarity. Nitrogen can be found in several functional forms including amines, amides (carbonyl amides), pyrroles, and pyridines. Functional groups like pyridine are basic and can accept hydrogen bonds. Hydrogen bonding can lead to some of the strongest intermolecular forces, shy of covalent bonding, and are greater than the influences of dispersion forces between aromatic asphaltenic cores. The remaining elemental analysis results appear in Tables 2.5 and 2.6. Sulfur is typically found in thiophenic rings, sulfides, and, to a smaller extent, in sulfoxide groups. Sulfoxides may be present because of asphaltene oxidation during handling. As stated before, asphaltenes were handled under argon atmosphere to minimize oxidation. Both AH and HO are sulfur rich followed by B6, while CS contains very little sulfur. There does not appear to be a correlation between asphaltene fraction or solubility behavior and sulfur content. Again, the variations from Soluble to Precipitate are subtle, but both increased polarity and aromaticity contribute to the macroscopic solubility behavior. Many of our observations were supported by Andersen's chemical analyses of Boscan asphaltene fractions.

Ni and V are often bound within porphyrin rings in asphaltenes. These metals have been associated with difficulties during hydrocatalytic upgrading of crude oils.[81] In general, the Precipitate samples were enriched with Fe, Ni, V and Na. B6 and HO fractions contained very similar amounts of Ni and V and were both higher than AH and CS. CS,

however, had the highest concentration of Fe in all fractions. Kaminski et al. fractionated asphaltenes in mixtures of methylene chloride and pentane and found that the most polar fraction contained the highest concentrations of Fe, Ni, and V and also had the lowest dissolution rates in dodecyl benzene sulfonic acid-heptane mixtures.[75]

The high concentration of Na (K and Ca also) in B6 fractions may be due in part to its offshore source. At 25,000 ppm, Na accounts for nearly 3 wt % of the Precipitate fraction. Metal chlorides or hydroxides could account for these high values. It would be surprising, however, to suggest that they were soluble in non-aqueous solvents such as heptane, toluene, and methylene chloride. Water with dissolved salts may have been dispersed in the crude oil during asphaltene precipitation. This material may have either co-precipitated or not passed through the filtering medium after excess heptane addition. Subsequent methylene chloride-asphaltene dissolution must have carried the salts through the filter. Vacuum filtration of methylene chloride typically induces solvent evaporation and condensation of atmospheric moisture. Excess water from the air may have aided the dissolution of the metal chlorides or hydroxides. This same process likely occurred during the Soluble-Precipitate fractionation of the Whole asphaltene.

In order to test for the presence of water-soluble salts, B6 crude oil was dissolved in methylene chloride and extracted with deionized water in a separatory funnel. The Na content of the asphaltenes precipitated from the water-extracted crude oil was reduced to 35 ppm. Ca and K were reduced to nearly the same value. Ni, V and Fe remained unchanged after water extraction. This suggests that the high alkali and alkaline earth metals content in B6 was attributable to either water-soluble salts or short chain soaps of corresponding carboxylic acids.

Based on the relative aromaticity and nitrogen content of the four Whole asphaltenes, some plausible explanations of precipitation can be offered. AH Whole had the least nitrogen but the second lowest H/C ratio, therefore the precipitation mechanism was likely controlled by dispersion forces or differences between asphaltene and solvent aromaticity. B6 and HO Whole had the highest H/C ratios but were rich in nitrogen. It is likely that precipitation occurred predominantly because of inter-aggregate polar interactions not just aromaticity. CS Whole asphaltenes were the most aromatic and had low nitrogen content. Dispersion forces and aromatic π-bonding likely controlled the formation of precipitates in this case. We believe that intra- and inter-aggregate forces control the degree to which each asphaltene fraction aggregates. As we will demonstrate in the next section, variations in the chemistries of the asphaltene fractions are linked to the size of aggregates formed in solution. In subsequent papers, we will demonstrate the impact of aggregate formation on the stability of asphaltene stabilized water-in-oil emulsions and the properties of asphaltene films at oil-water interfaces.

2.3.4 Vapor Pressure Osmometry of Asphaltenes and their Fractions

Apparent number average molecular weights of several asphaltenes and their more and less soluble fractions were measured over a range of concentrations (Figures 2.4 and 2.5). The values of ΔV/C at each concentration were converted to an apparent molar mass using the calibration factor determined for a standard solute (Benzil). Yarranton found that heptane precipitated asphaltene molar masses increased with bulk concentration to a limiting value beyond approximately 20 g/L (~ 2 wt %).[59] The molar mass of Athabasca asphaltenes at 50°C approached 2,000 g/mol at low concentration and was considered a good

approximation of the monomer mass. At high concentration, the molar mass limiting value approached 10,000 g/mol, a value indicative of an aggregate with four to five monomers. ΔV measurements at very low concentrations (<1 g/L) can be challenging due to low sensitivity and are often subject to scatter. The degree of asphaltene association clearly increased with decreased temperature and solvent polarity. However, low concentration extrapolation revealed molar masses approximately 1,000-2,000 g/mol.

VPO molar masses of B6 Soluble, Whole and Precipitate in toluene appear in Figure 2.4. As expected B6 Soluble had the lowest molecular weight at all concentrations probed. It seemed to reach a limiting molar mass just under 3,000 g/mol. Assuming a trend at low concentration similar to Yarranton, the minimum molar mass would approach a value somewhat less than 2,000 g/mol. B6 Whole was slightly more aromatic, polar and less soluble than the Soluble fraction. Accordingly, its molar masses were approximately 500 g/mol higher than the Soluble fraction between 3 and 10 g/L. The zero concentration molar mass was likely slightly greater as well. B6 Precipitate molar masses were substantially higher than the more soluble asphaltenes by almost an order of magnitude. Even at high dilution, the apparent molar mass exceeded 10,000 g/mol and approached 14,000 at 10 g/L (~ 1 wt %). B6 Precipitate asphaltenes were quite difficult to dissolve even at elevated temperatures. SANS data presented in the coming sections were measured at room temperature and 80°C in an effort to fully dissociate large aggregates. These less soluble asphaltenes may not be fully dissociated at intermediate temperature (53°C) and formed very large aggregates suggesting strong intermolecular interactions. Presumably, higher temperatures or stronger solvents (*o*-dichlorobenzene at 120°C) would facilitate aggregate dissolution.

HO Precipitate asphaltenes possessed similar aromaticity, polarity, and solubility characteristics to B6 Precipitate. VPO molar masses in toluene at 53°C indicated that HO Precipitate formed smaller aggregates than those of B6. Intermolecular forces between monomers and aggregates were likely weaker than B6 resulting in smaller aggregates. In contrast to B6 Whole and its less soluble fraction, CS Whole and Precipitate had nearly identical molar masses at each concentration examined. Zero concentration extrapolation indicated minimum sized aggregate molar masses of approximately 3,000 g/mol. The inability to reach molar masses of 1,000-2,000 g/mol, often referred to as the theoretical asphaltene monomer molar mass, with B6 and HO Precipitate suggests we have not achieved complete dissociation. B6 Whole and Soluble asphaltenes were the most highly solvated and may be highly dissociated at low concentrations. Zero concentration extrapolated molar masses around 2,000 g/mol suggest solvation has formed monomers. As we will show in the following sections the molar mass similarities between CS Whole and Precipitate may be a result of number averaging the molar mass rather than weight averaging (SANS).

2.3.5 Small Angle Neutron Scattering: 25°C

Several key trends were demonstrated by the neutron scattering behavior of asphaltene-heptol systems:

- Asphaltenes in solution are readily distinguished from partially insoluble systems from the shapes of scattering curves.
- The most soluble asphaltenes could be fit with simple Lorentzian line shapes while less soluble (more aggregated) asphaltenes required an additional term to account for low Q scattering.

- CS formed the largest aggregates followed by B6, HO and AH. This held for Whole, Soluble, and Precipitate fractions.
- Precipitate asphaltenes formed the largest aggregates while Solubles formed the smallest.
- Aggregate dimension grew as asphaltenes approached their solubility limit (decreasing toluene content).

Neutron scattering curves of intensity (I) versus scattering vector (Q) of B6 Whole in several mixtures of deuterated heptol are shown in Figure 2.6. Toluene percentages from 55 to 80 % (v/v) were within the soluble regime while 40% fell in the precipitated regime (from Figure 2.1). In all cases, the intensity curves have a significant negative slope at low values of Q. This is indicative of large aggregates (on the order of 1/Qmin or $\geq$ 500 Å) present in solution. These aggregates were smaller than 1.5 μm, however, since above 55% toluene all systems were soluble to filtration. At intermediate Q, the relative ordering of the intensities suggests aggregates in 55% toluene were the largest followed by 60% toluene and so on. The least intense scattering measured in the soluble regime was at 80 % toluene. After crossing the solubility limit, however, precipitation occurred causing some material to settle at the bottom of the quartz cell. These insolubles had size scales greater than 1,500 Å (according to solubility behavior) and were just beyond the lower Q limit range accessible by SANS. The scattering intensity in the intermediate Q range decreased because of aggregates forming flocs and becoming much larger. The remaining soluble aggregates were much smaller than those at 55 % toluene resulting in reduced scattering intensity. As will be shown in the following section this reduction in scattering intensity corresponds a two fold decrease in aggregate size.

I(Q) versus Q scattering curves were fit with Lorentzian line shapes to determine solute correlation lengths. Data showing a plateau in scattering at low Q were fit with a Lorentzian plus constant term as shown in Figure 2.7a. The correlation length (ξ) of AH Soluble asphaltenes was determined to be 24 Å in a 50:50 heptol mixture. An example of a system exhibiting significant low Q scattering is shown in Figure 2.7b. Here ξ of B6 Whole asphaltenes in 40:60 heptol is 77 Å, considerably larger than AH Soluble. Correlation lengths presented in the following sections were determined by one of these two fitting techniques.

Correlation lengths deduced from SANS scattering curves of the Whole asphaltenes dissolved in solutions of varying heptol ratio appear in Figure 2.8. While the solubility behavior of these asphaltenes appear to be similar, the neutron scattering data indicate that CS forms the largest aggregates in heptol. These aggregates are likely dominated by aromatic ring, π-bond interactions due to their low H/C ratio and low nitrogen content. Another trend seen is the increase in correlation length with decreased toluene content. This increase suggests that inter-aggregate associations increase as the solvating power of heptol decreases. A maximum in correlation length lies very close to the solubility limit of the Whole asphaltenes. The aggregates continued to grow because of the reduced aromaticity until precipitation occurred. Crossing the solubility limit caused agglomeration and precipitation of the largest aggregates. The resulting correlation length in the precipitated regime is only a measure of the material remaining in solution and is hence lower than the correlation lengths of the asphaltenes at the solubility limit. Aggregate ξ tended to plateau above 70 % toluene where additional solvent aromaticity was insufficient to further disrupt inter-aggregate bonds. Very similar behavior was seen using Cold Lake asphaltenes in

mixtures of 1-methylnaphthaltene and dodecane.[71] At low to moderate asphaltene concentrations correlation lengths increased to a maximum as the aliphatic solvent volume fraction increased. Upon reaching a critical dodecane volume fraction, the correlation length dropped because of phase separation.

In summary, Whole asphaltenes, when completely dissolved, were shown to form minimum sized aggregates in the most aromatic solvents. Reducing solvent aromaticity caused aggregate dimensions to increase in response to a less favorable solvent environment. At the solubility limit, aggregation reached a maximum. In the insoluble regime, flocs formed and the most polar, aromatic asphaltenes precipitated. As a result, the inventory of aggregated asphaltenes probed in the intermediate Q region decreased. Differences between Soluble and Precipitate solubility chemistry and solubility behavior suggested the more soluble asphaltenes would form smaller aggregates while the less soluble material would be more prone to aggregation. As seen in Figures 2.9a and 2.9b, the Soluble asphaltenes formed smaller aggregates than both the Whole or Precipitate. Except for AH, the Soluble aggregates reached a maximum dimension at a toluene volume fraction near their solubility limits (just above 50 % (v/v) toluene). AH Soluble may have required a more aliphatic solvent to cause a substantial reduction in the intermediate Q intensity. AH, B6 and HO Soluble formed the smallest aggregates (20-35 Å in pure toluene), while CS Soluble formed much larger aggregates (70 Å in pure toluene).(Figure 2.9a) A solvent window extending from about 45 to 70% toluene bracketed the region of largest to smallest aggregates (in the soluble regime). Above 70 % toluene, the aggregates reached a minimum size and additional solvent aromaticity was unable the further disrupt inter-aggregate bonds.

Guinier analysis was only performed on Soluble asphaltenes on the toluene rich side of their solubility limits. These asphaltenes did not exhibit significant low Q scattering. This approximation is only valid in the low Q regime where $QR_g<1$ and assumes negligible inter-aggregate interactions. CS Soluble had considerable low Q scattering even in pure toluene and was not included in the analysis. The Rg values of AH, B6 and HO Soluble asphaltenes appear in Table 2.7. Not surprisingly, both ξ and R_g increased as the solvents became more aliphatic. Comparing the form of the Guinier approximation and Lorentzian equations we see that R_g is proportional to $\xi \times \sqrt{3}$. Greater uncertainty in the low Q data may explain the slight deviation from this relation where R_g/ξ was between 1.4 and 1.6 rather than 1.73 ($\sqrt{3}$).

The scattering curves of Precipitated asphaltenes were nearly featureless and thus had considerable overlap between large agglomerate scattering and smaller aggregate Guinier behavior. As mentioned before, B6, CS and HO proved to be difficult to dissolve. Not surprisingly, their tendency to aggregate was much higher than the Whole asphaltenes. Once in solution, the Precipitates formed very large aggregates with correlation lengths from 100 Å (AH) to nearly 500 Å (CS).(Figure 2.9b) The uncertainty of CS Precipitate correlation lengths was higher than the other asphaltenes due to substantial overlap in intermediate and low Q regions and nearly featureless scattering curves. It is clear that enhanced aromatic and polar inter-aggregate forces created very large and sparingly soluble aggregates in heptol, at 25°C.

2.3.6 Small Angle Neutron Scattering: 80°C

To probe the effects of temperature on aggregation, neutron scattering experiments were performed at 80°C. During sample preparation, all solutions were heated to 80°C for

one hour then returned to room temperature. This step was added to fully dissolve the largest aggregates in solution. After running a few temperature-cycled samples at 25°C, it was clear that the large aggregates were still present. Scattering curves of CS Precipitate in 100% toluene at 25°C with and without preheating and at 80°C are shown in Figure 2.10. Similarities between the temperature cycled and non-temperature cycled samples examined at room temperature strongly suggests that both systems were at equilibrium when the neutron scattering experiments were performed. Given the very large aggregates present in the CS Precipitate solutions, the addition of heat should have its greatest impact in breaking interaggregate bonds.

Comparing the scattering curves and correlation lengths of the asphaltenes at 25 and 80°C revealed dramatic but predictable heat effects. A series of comparative scattering plots for B6 Soluble, Whole and Precipitate at low and high temperatures is shown in Figures 2.11a-c. B6 Soluble did not show intense low Q scattering at 25°C and the effect of heating was minimal; correlation lengths were reduced modestly from 48 to 40 Å. Unlike B6 Soluble, B6 Whole and Precipitate at 25°C had intense low Q scattering. In these two cases, scattering intensities were reduced more than 10-fold as a result of raising the temperature and correlation lengths dropped from 77 Å (Whole) and 230 Å (Precipitate) to 57 Å and 70 Å respectively. Figures 2.12a-d present correlation lengths of asphaltene fractions at similar heptol ratios at room temperature and at 80°C.

The relative ordering between asphaltenes of the same fraction is unchanged from 25 to 80°C. AH Soluble formed aggregates nearly the same size as HO Soluble, although at a lower toluene concentration. These two were followed closely in aggregate size by B6 Soluble. Again, CS Soluble was much larger at all heptol ratios, although in pure toluene its

minimum aggregates were just 42 Å. These trends were seen in the Whole asphaltenes where CS Whole was considerably larger at intermediate heptol. In general, the Precipitate fraction was the most responsive to heat where aggregate ξ fell below 100 Å. In addition, the scattering curves had sufficient shape to reduce the uncertainty in ξ. The intense temperature response of the Precipitate fraction compared to the Soluble indicates a high degree of intra-aggregate bonding. The process of fractionation enriched the least soluble asphaltenes with these intermolecular associating groups causing them to aggregate and precipitate from solution. Discrepancies arose, however, between the aggregate sizes of CS Whole and Precipitate determined by VPO and SANS. VPO molar masses are number averaged and both asphaltene fractions had nearly identical masses. If a small fraction of the less soluble fraction were poorly dissolved and formed large aggregates the number average molecular would change little. In contrast, SANS provides weight average properties of aggregate size, so a small fraction of large, flocculated asphaltenes will skew the measured aggregate size. The polydisperse nature of asphaltenes and the aggregates they form almost necessitates determining weight and number average properties to fully characterize them.

The temperature differences between VPO and SANS measurements may also explain the discrepancy between B6 and CS Whole and Precipitate aggregate sizes. On a percentage basis, the reduction in correlation length of CS Precipitate from 25 to 80°C was greater than that of B6 Precipitate. CS Precipitate asphaltenes presumably are more receptive to heating and suggests a weaker degree of intermolecular bonding than B6 Precipitate. At 53°C, B6 Precipitate was still highly aggregated and required additional heating to dissolve.

An attempt was made to find the dimensions of minimum sized aggregates by dissolving the asphaltenes in deuterated 1-methylnaphthalene. This solvent has a higher

aromaticity than toluene and is considerably larger in molecular dimension. Hansen solubility parameters indicate 1-methylnaphthalene has a higher degree of dispersion and hydrogen bonding capacity than toluene (Table 2.3). These properties make it more chemically similar to asphaltenes and thus may help better dissolve aggregates. The correlation lengths determined from scattering curves are shown in Table 2.8. Depending on data availability, the corresponding correlation length in pure toluene at 80°C appears to the right of the 1-methylnaphthalene results. In all cases, 1-methylnaphthalene was a better asphaltene solvent than pure toluene. Specifically, CS Soluble, B6 Whole and Precipitate, and HO Precipitate had the most favorable response to the new solvent. The most soluble asphaltene tested thus far tested had an R_g of 16.9 Å followed by B6 and HO Soluble. It would be quite difficult to further reduce aggregate sizes except by addition of a somewhat more polar solvent (possibly chlorinated) or solvating agent (such as resins).

In all cases, Soluble asphaltenes were affected the least and Precipitates were affected the most by the temperature increase. This evidence suggests the Precipitate fraction was enriched with temperature-sensitive intermolecular bonds. The most plausible intermolecular bonding mechanism is hydrogen bonding. These bonds are quite sensitive to temperature and can be broken down upon heating. Morphological changes such as disruption of crystallinity are not likely since this long-range order is not present at any temperature. Bragg scattering peaks indicative of crystallinity are not evident in the scattering curves. Most waxes have melting points above 60-70°C and could explain a transformation from wax crystals at 25°C. Wax particles could contribute to low Q scattering if present and then disappear upon heating to 80°C. To rule out the possibility of wax contamination, high temperature simulated distillation (HTSimDist) was performed on B6 and CS Whole.

Normal paraffins from C_5 to C_{120} can be detected in a petroleum sample by GC. Waxes appear as distinct peaks as a function of elution time (inset Figure 2.13). Neither B6 nor CS asphaltenes contain any discernable wax peaks. The lower intensity broad humps are a result of the asphaltene hydrocarbon structure. These findings rule out the possibility of neutron scattering from non-asphaltenic structures that may be present in crude oil. Each of the aggregation phenomena seen resulted from the propensity of asphaltenes to form aggregates mediated by intermolecular bonding.

2.4 Conclusions

The solubility behaviors, chemical properties and aggregation extents of four asphaltenes and their soluble and insoluble fractions were examined. Whole, unfractionated asphaltenes were soluble to filtration in heptol containing greater than 52 % (v/v) toluene. Decreasing the volume fraction of toluene drove asphaltenes out of solution because of lower solvent aromaticity, polarity and hydrogen bonding capacity. The tendency of asphaltenes to aggregate increased as the solubility limit was approached. After crossing into the insoluble regime, asphaltenes precipitated and the correlation length decreased. The more soluble fractions had a solubility limit approximately 10 % (v/v) lower in toluene than the Whole asphaltenes. The solubility limits of the less soluble fractions were shifted higher in toluene by up to 30 % (v/v). This indicates the cooperative nature of the more and less soluble material present in the heterodisperse asphaltenes. The more soluble asphaltenes must aid the dissolution of the higher aromaticity and polarity material.

Number average molar masses determined by VPO in toluene at 53°C indicated that B6 Precipitate asphaltenes were highly aggregated while CS Precipitate asphaltenes appeared

to be dissociated. The molar masses of B6 and HO Precipitate compared to CS Precipitate suggest higher degrees of intermolecular associations in light of SANS aggregation behavior.

SANS indicated that most of the asphaltene systems contained a portion of highly aggregated material approximately 1,000 Å. Heating the samples broke down some of the aggregate structure and reduced the intensity of the low Q scattering. Aggregate dimensions of the less soluble asphaltenes were reduced to the greatest extent with heat suggesting temperature sensitive inter-aggregate bonds were broken. In 1-methylnaphthalene (a better asphaltene solvent) at high temperatures, aggregate sizes were further reduced compared to those in heptol mixtures. These results point to the presence of aromatic π-π bonding, polar heteroatom interactions and H-bonding that hold individual asphaltenes and their aggregates together. The less soluble asphaltenes contribute the majority of species responsible for aggregation and are likely the agents that cause many petroleum production problems such as deposition and water-in-oil emulsion stabilization.

2.6 Acknowledgements

This research has been supported by PERF contract #97-07, the National Science Foundation (grant CTS-981727) and shared consortium funding from ExxonMobil, Texaco, Ondeo-Nalco Energy Systems, and Shell Oil Company. Eric Sirota of ExxonMobil Corporate Research provided the SANS beam time and Min Lin at NIST assisted with the SANS experimental procedure and the initial data reduction. We also want to thank Paul Lindemuth of Ondeo-Nalco Energy Systems for facilitating the ICP metals analyses.

2.6 References

1. Nellensteyn, F.J., "The Constitution of Asphalt," *Journal of the Institute of Petroleum Technologists*, 1924, **10**: p. 311-325.

2. Pfeiffer, J.P. and R.N.J. Saal, "Asphaltic Bitumen as Colloid System," *Journal of Physical Chemistry*, 1940, **44**: p. 139-149.

3. Neumann, H., "Investigations Regarding the Separation of Crude Oil Emulsions," *Petrochemie*, 1965, **18**: p. 776-779.

4. Dickie, J.P. and T.F. Yen, "Macrostructures of the Asphaltic Fractions by Various Instrumental Methods," *Analytical Chemistry*, 1967, **39** (14): p. 1847-1852.

5. Berridge, S.A., M.T. Thew and A.G. Loriston-Clarke, "The Formation and Stability of Emulsions of Water in Crude Petroleum and Similar Stocks," *Journal of the Institute of Petroleum*, 1968, **54** (539): p. 333-357.

6. Speight, J.G., "Structural Analysis of Athabasca Asphaltenes by Proton Magnetic Resonance Spectroscopy," *Fuel*, 1971, **50**: p. 102-112.

7. Speight, J.G. and S.E. Moschopedis, "Some Observations on the Molecular "Nature" of Petroleum Asphaltenes," *Preprints -- ACS Division of Petroleum Chemistry*, 1979, **24** (4): p. 910-923.

8. Ravey, J.C., G. Ducouret and D. Espinat, "Asphaltene Macrostructure by Small Angle Neutron Scattering," *Fuel*, 1988, **67** (11): p. 1560-1567.

9. Sheu, E.Y., M.M.D. Tar and D.A. Storm, "Solution Properties of Colloids Formed by Petroleum Vacuum Residues," *Macromolecular Reports*, 1991, **A28**: p. 159-175.

10. Siffert, B., C. Bourgeois and E. Papirer, "Structure and Water-Oil Emulsifying Properties of Asphaltenes," *Fuel*, 1984, **63** (6): p. 834-837.

11. Herzog, P., D. Tchoubar and D. Espinat, "Macrostructure of Asphaltene Dispersions by Small-angle X-ray Scattering," *Fuel*, 1988, **67**: p. 245-250.

12. Bardon, C., et al., "The colloidal structure of crude oils and suspensions of asphaltenes and resins," *Fuel Science & Technology International*, 1996, **14** (1-2): p. 203-242.

13. Fenistein, D., et al., "Viscosimetric and neutron scattering study of asphaltene aggregates in mixed toluene/heptane solvents," *Langmuir*, 1998, **14** (5): p. 1013-1020.

14. Mushrush, G.W. and J.G. Speight, *Petroluem Products: Instability and Incompatibility*. Applied Energy Technology Series. 1995, Bristol, PA: Taylor and Francis.

15. Storm, D.A., S.J. DeCanio and E.Y. Sheu, *Sludge Formation During Heavy Oil Conversion*, in *Asphaltene Particles in Fossil Fuel Exploration, Recovery, Refining, and Production Processes*, M.K. Sharma and T.F. Yen, Editors. 1994, Plenum Press: New York. p. 81-90.

16. Lin, J.-R., J.-K. Park and T.F. Yen, *Upgrading From Petroleum and Coal-Derived Asphaltenes*, in *Asphaltene Particles in Fossil Fuel Exploration, Recovery, Refining, and Production Processes*, M.K. Sharma and T.F. Yen, Editors. 1994, Plenum Press: New York. p. 91-100.

17. Cimino, R., et al., *Solubility and Phase Behavior of Asphaltenes in Hydrocarbon Media*, in *Asphaltenes: Fundamentals and Applications*, E.Y. Sheu and O.C. Mullins, Editors. 1995, Plenum Press: New York. p. 97-130.

18. Fordedal, H., et al., "Crude Oil Emulsions in High Electric Fields as Studied by Dielectric Spectroscopy. Influence of Interaction Between Commercial and Indigenous Surfactants," *Colloids and Surfaces A: Physicochemical and Engineering Aspects*, 1996, **106**: p. 33-47.

19. Strassner, J.E., "Effect of pH on Interfacial Films and Stability of Crude Oil-Water Emulsions," *Journal of Petroleum Technology*, 1968, **20**: p. 303-312.

20. Sjöblom, J., et al., "Stabilization and Destabilization of Water-in-Crude Oil Emulsions from the Norwegian Continental Shelf. Correlation with Model Systems," *Advances in Colloid and Interface Science*, 1992, **41**: p. 241-271.

21. Taylor, S.E., "Resolving Crude Oil Emulsions," *Chemistry and Industry*, 1992, **20**: p. 770-773.

22. van der Waarden, M., "Stability of Emulsions of Water in Mineral Oils Containing Asphaltenes," *Kolloid Z. Z. Polymer*, 1958, **156** (2): p. 116-122.

23. Neumann, H.J. and B. Paczynska-Lahme, "Petroleum Emulsions--Properties, Stability and Demulsification," *Chemical Engineering Technology*, 1981, **53**: p. 911-916.

24. Sheu, E.Y. and M.B. Shields, "Asphaltene Surface Activity at Oil-Water Interfaces," *Society of Petroleum Engineers*, 1995, **28995**: p. 523-532.

25. McLean, J.D. and P.K. Kilpatrick, "Effects of Asphaltene Solvency on Stability of Water-in-Crude Oil Emulsions," *Journal of Colloid and Interface Science*, 1997, **189**: p. 242-253.

26. McLean, J.D., et al., *The Role of Petroleum Asphaltenes in the Stabilization of Water-in-Oil Emulsions*, in *Structures and Dynamics of Asphaltenes*, O.C. Mullins and E.Y. Sheu, Editors. 1998, Plenum Press: New York. p. 377-422.

27. Mitchell, D.L. and J.G. Speight, "The Solubility of Asphaltenes in Hydrocarbon Solvents," *Fuel*, 1973, **52** (4): p. 149-152.

28. Yen, T.F., J.G. Erdman and S.S. Pollack, "Investigation of Structure of Petroleum Asphaltenes By X-Ray Diffraction," *Analytical Chemistry*, 1961, **33** (11): p. 1587-&.

29. Boduszynski, M.M., "Composition of Heavy Petroleums. 2. Molecular Characterization," *Energy & Fuels*, 1988, **2** (5): p. 597-613.

30. Bestougeff, M.A. and P. Gendrel. *Study on the Structure of Asphaltenic Constituents by Combined Physical and Chemical Methods*. in *147th American Chemical Society Meeting*. 1964. Philadelphia, PA: ACS, Division of Petroleum Chemistry.

31. McKay, J.F., D.R. Latham and W.E. Haines, "Composition of Petroleum Heavy Ends. 3. Comparison of the Composition of High-Boiling Petroleum Distillates and Petroleum > 675 C Residues," *Fuel*, 1981, **60** (1): p. 27-32.

32. Boduszynski, M.M., "Characterization of "Heavy" Crude Components," *Preprints ACS Division of Petroleum Chemistry*, 1985, **30**: p. 626-640.

33. Speight, J.G., "A Structural Investigation of the Constituents of Athabasca Bitumen by Proton Magnetic Resonance Spectroscopy," *Fuel*, 1970, **49**: p. 76-90.

34. Biggs, W.R., R.J. Brown and J.C. Fetzer, "Elemental Profiles of Hydrocarbon Materials by Size-Exclusion Chromatography/Inductively Coupled Plasma Atomic Emission Spectrometry," *Energy & Fuels*, 1987, **1** (3): p. 257-262.

35. Nalwaya, V., et al., "Studies on asphaltenes through analysis of polar fractions," *Industrial & Engineering Chemistry Research*, 1999, **38** (3): p. 964-972.

36. Reynolds, J.G. and W.R. Biggs, "Effects of Asphaltene Precipitation and a Modified D 2007 Separation on the Molecular Size of Vanadium- and Nickel-Containing Compounds in Heavy Residua," *Fuel Science and Technology International*, 1986, **4** (6): p. 749-777.

37. Reynolds, J.G. and W.R. Biggs, "Application of Size Exclusion Chromatography Coupled with Element-Specific Detection to the Study of Heavy Crude Oil and Residua Processing," *Accounts of Chemical Research*, 1988, **21** (9): p. 319-326.

38. Reynolds, J.G., et al., "Characterization of Nickel and Vanadium Compounds in Tar Sand Bitumen by Petroporphyrin Quantitation and Size Exclusion Chromatography Coupled with Element Specific Detection," *Preprints--ACS Division of Petroleum Chemistry*, 1988, **33** (2): p. 239-246.

39. Hasiba, H.H. and F.W. Jessen, "Film-Forming Compounds From Crude Oils, Interfacial Films and Paraffin Deposition," *The Journal of Canadian Petroleum Technology*, 1968, **7** (1): p. 1-12.

40. Petersen, J.C., "Quantitative Method Using Differential Infrared Spectrometry for the Determination of Compound Types Absorbing in the Carbonyl Region in Asphalts," *Analytical Chemistry*, 1975, **47** (1): p. 112-117.

41. Andersen, S.I., "Effect of Precipitation Temperature on the Composition of n-Heptane Asphaltenes," *Fuel Science and Technology International*, 1994, **12** (1): p. 51-74.

42. Chang, C.L. and H.S. Fogler, "Stabilization of Asphaltenes in Aliphatic Solvents Using Alkylbenzene-Derived Amphiphiles .1. Effect of the Chemical- Structure of Amphiphiles On Asphaltene Stabilization," *Langmuir*, 1994, **10** (6): p. 1749-1757.

43. Hasan, M.U., M.N. Siddiqui and M. Arab, "Separation and Characterization of Asphaltenes from Saudi Arabian Crudes," *Fuel*, 1988, **67** (8): p. 1131-1134.

44. Jacobson, J.M. and M.R. Gray, "Use of IR Spectroscopy and Nitrogen Titration Data in Structural Group Analysis of Bitumen," *Fuel*, 1987, **66** (6): p. 749-752.

45. Barbour, R.V. and J.C. Petersen, "Molecular Interactions of Asphalt: An Infrared Study of the Hydrogen-Bonding Basicity of Asphalt," *Analytical Chemistry*, 1974, **46** (2): p. 273-277.

46. Boduszynski, M.M., J.F. McKay and D.R. Latham, "Asphaltenes, Where Are You?," *Proceedings of the Association of Asphalt Paving Technologists*, 1980, **49**: p. 123-143.

47. Ignasiak, T., O.P. Strausz and D.S. Montgomery, "Oxygen Distribution and Hydrogen Bonding in Athabasca Asphaltene," *Fuel*, 1977, **56**: p. 359-365.

48. Moschopedis, S.E. and J.G. Speight, "Investigation of Hydrogen Bonding by Oxygen Functions in Athabasca Bitumen," *Fuel*, 1976, **55**: p. 187-192.

49. Petersen, J.C., "An Infra-red Study of Hydrogen Bonding in Asphalt," 1967: p. 295-305.

50. Maruska, H.P. and M.L. Rao, "The Role of Polar Species in the Aggregation of Asphaltenes," *Fuel Science and Technology International*, 1987, **5** (2): p. 119-168.

51. Overfield, R.E., et al., "SANS Study of Asphaltene Aggregation," *Fuel Science & Technology International*, 1989, **7** (5-6): p. 611-624.

52. Sheu, E.Y., D.A. Storm and M.M.D. Tar, "Asphaltenes in Polar Solvents," *Journal of Non-Crystalline Solids*, 1991, **131-133**: p. 341-347.

53. Al-Jarrah, M.M.H. and A.H. Al-Dujaili, "Characterization of Some Iraqi Asphalts II. New Findings on the Physical Nature of Asphaltenes," *Fuel Science and Technology International*, 1989, **7** (1): p. 69-88.

54. Acevedo, S., et al., "Asphaltenes and Resins From the Orinoco Basin," *Fuel*, 1985, **64**: p. 1741-1747.

55. Wiehe, I.A. and K.S. Liang, "Asphaltenes, Resins, and other petroleum macromolecules," *Fluid Phase Equilibria*, 1996, **117** (1-2): p. 201-210.

56. McKay, J.F., et al., "Petroleum Asphaltenes: Chemistry and Composition," *Analytical Chemistry of Liquid Fuel Sources, Advances in Chemistry Series*, 1978, **170**: p. 128-142.

57. Andersen, S.I., A. Keul and E. Stenby, "Variation in composition of subfractions of petroleum asphaltenes," *Petroleum Science and Technology*, 1997, **15** (7-8): p. 611-645.

58. Yarranton, H.W. and J.H. Masliyah, "Molar Mass Distribution and Solubility Modeling of Asphaltenes," *AICHE Journal*, 1996, **42** (12): p. 3533-3543.

59. Yarranton, H.W., H. Alboudwarej and R. Jakher, "Investigation of asphaltene association with vapor pressure osmometry and interfacial tension measurements," *Industrial & Engineering Chemistry Research*, 2000, **39** (8): p. 2916-2924.

60. Ravey, J.C. and D. Espinat, "Macrostructure of Petroleum Asphaltenes by Small Angle Neutron Scattering," *Progress in Colloid and Polymer Science*, 1990, **81**: p. 127-130.

61. Sheu, E.Y., M.M.D. Tar and D.A. Storm, "Colloidal Structure of Vacuum Residue in Solvents," *Preprints--ACS Division of Fuel Chemistry*, 1992, **37** (2): p. 844-848.

62. Espinat, D., et al., "Colloidal Macrostructure of Crude-Oil Studied By Neutron and X- Ray Small-Angle Scattering Techniques," *Journal De Physique Iv*, 1993, **3** (C8): p. 181-184.

63. Storm, D.A., E.Y. Sheu and M.M. Detar, "Macrostructure of Asphaltenes in Vacuum Residue By Small-Angle X-Ray-Scattering," *Fuel*, 1993, **72** (7): p. 977-981.

64. Thiyagarajan, P., et al., "Temperature-Dependent Structural-Changes of Asphaltenes in 1- Methylnaphthalene," *Energy & Fuels*, 1995, **9** (5): p. 829-833.

65. Xu, Y.N., Y. Koga and O.P. Strausz, "Characterization of Athabasca Asphaltenes By Small-Angle X-Ray- Scattering," *Fuel*, 1995, **74** (7): p. 960-964.

66. Liu, Y.C., et al., "Fractal Structure of Asphaltenes in Toluene," *Fuel*, 1995, **74** (9): p. 1352-1356.

67. Rassamdana, H. and M. Sahimi, "Asphalt Flocculation and Deposition: II. Formation and Growth of Fractal Aggregates," *AICHE Journal*, 1996, **42** (12): p. 3318-3332.

68. Barre, L., et al., "Colloidal structure of heavy crudes and asphaltene solutions," *Revue De L Institut Francais Du Petrole*, 1997, **52** (2): p. 161-175.

69. Lin, M.Y., E.B. Sirota and H. Gang, "Neutron scattering characterization of asphaltene particles," *Abstracts of Papers of the American Chemical Society*, 1997, **213**: p. 66-FUEL.

70. Miller, J.T., et al., "Subfractionation and characterization of Mayan asphaltene," *Energy & Fuels*, 1998, **12** (6): p. 1290-1298.

71. Sirota, E.B., "Swelling of asphaltenes," *Petroleum Science and Technology*, 1998, **16** (3-4): p. 415-431.

72. Fenistein, D. and L. Barre, "Experimental measurement of the mass distribution of petroleum asphaltene aggregates using ultracentrifugation and small-angle X-ray scattering," *Fuel*, 2001, **80** (2): p. 283-287.

73. Savvidis, T.G., et al., "Aggregated structure of flocculated asphaltenes," *Aiche Journal*, 2001, **47** (1): p. 206-211.

74. Sheu, E.Y., et al., "Polydispersity Analysis of Asphaltene Solutions in Toluene," *Journal of Colloid and Interface Science*, 1992, **153** (2): p. 399-410.

75. Kaminski, T.J., et al., "Classification of asphaltenes via fractionation and the effect of heteroatom content on dissolution kinetics," *Energy & Fuels*, 2000, **14** (1): p. 25-30.

76. de Gennes, P.-G., *Scaling Concepts in Polymer Physics*. 1979, Ithaca, NY: Cornell University Press.

77. Feigin, L.A. and D.I. Svergun, *Structure Analysis by Small Angle X-ray and Neutron Scattering*. 1987, New York: Plenum.

78. Guinier, A. and G. Fournet, *Small Angle Scattering of X-rays*. 1955, New York: Jorn Wiley and Sons, Inc.

79. Hildebrand, J.H. and R.L. Scott, *Regular Solutions*. 1962, New York.

80. Hansen, C.M., "Universality of Solubility Parameter," *Industrial & Engineering Chemistry Product Research and Development*, 1969, **8** (1): p. 2-&.

81. Ali, M.F., et al., "Nickel and Vanadyl Porphyrins in Saudi Arabian Crude Oils," *Energy & Fuels*, 1993, **7** (2): p. 179-184.

82. Barton, A.F.M., *CRC Handbook of Solubility Parameters and other Cohesion Parameters*. 1983, Boca Raton, Fl: CRC Press.

Table 2.1 Typical Values of Elemental Compositions in Asphaltenes

Element (wt%)	
H/C	1.0-1.2
Nitrogen	1.0-1.2
Sulfur	2.0-6.0
Oxygen	0.8-2.0
Vanadium (ppm)	100-300

Table 2.2 Crude Oil Properties

Crude	Wt % Asph	R/A Ratio	H/C Asph	Viscosity (cP) 100°F
AH	6.7	1.12	1.14	33.8
B6	13.1	0.92	1.22	2030
CS	7.5	1.19	1.11	70
HO	14.8	1.39	1.29	363

Table 2.3 Hansen Solubility Parameters[82]

Solvent	Hansen $(mJ\ m^{-3})^{1/2}$			
	δ_d	δ_p	δ_h	δ_t
n-Heptane	15.3	0.0	0.0	15.3
Toluene	18.0	1.4	2.0	18.2
1-Methylnaphthalene	20.7	0.8	4.7	21.2

Table 2.4 Asphaltene Fractionation Results (wt %)

Asphaltene	*n*-Heptane-Toluene Ratio	Precipitate	Soluble
AH	70:30	38.4	61.6
		34.4	65.6
		32.2	67.8
	Average	35.0.±3.1	65.0±3.1
B6	60:40	33.2	66.8
		31.6	68.4
		32.4	67.6
	Average	32.4±0.8	67.6±0.8
CS	60:40	35.7	64.3
HO	61:39	28.2	71.8
		33.1	66.9
	Average	30.7	69.3

Table 2.5 Elemental Analysis (wt %)

	Sulfur			Oxygen		
Asphaltene	Soluble	Whole	Precipitate	Soluble	Whole	Precipitate
AH	8.06	8.32	7.66	1.92	1.64	2.52
B6	7.25	6.68	6.33	2.67	2.90	2.81
CS	0.52	0.52	0.48	2.11	1.73	2.27
HO	8.42	8.53	8.48	2.51	2.10	2.66

Table 2.6 Metals Analysis (ppm)

	Iron			Nickel			Vanadium			Sodium		
Asphaltene	Sol	W	Ppt	Sol	W	Ppt	Sol	W	Ppt	Sol	W	Ppt
AH	14	26	50	84	160	160	350	490	540	31	31	31
B6	7.9	35	47	350	330	410	1000	1000	1200	27	9300	25000
CS	51	77	150	19	21	28	42	48	48	43	130	180
HO	6.3	16	12	340	360	410	930	950	1100	11.9	550	1800

Table 2.7 Rg (Å) of Soluble Asphaltenes from Guinier Analysis (25°C)

% Toluene	AH Soluble	B6 Soluble	HO Soluble
100	35		47
70		56	46
60	38	57	49
50	38	77	65
45			82
40	46		

Table 2.8 Correlation length (Å) of Asphaltenes in 1-Methylnaphthalene and Toluene (80°C)

Asphaltene	Soluble		Whole		Precipitate	
	MN	Tol	MN	Tol	MN	Tol
AH	17		24	27	31	37
B6	24		36	42	52	70
CS	32	42	40		48	
HO	23		32	33	46	55

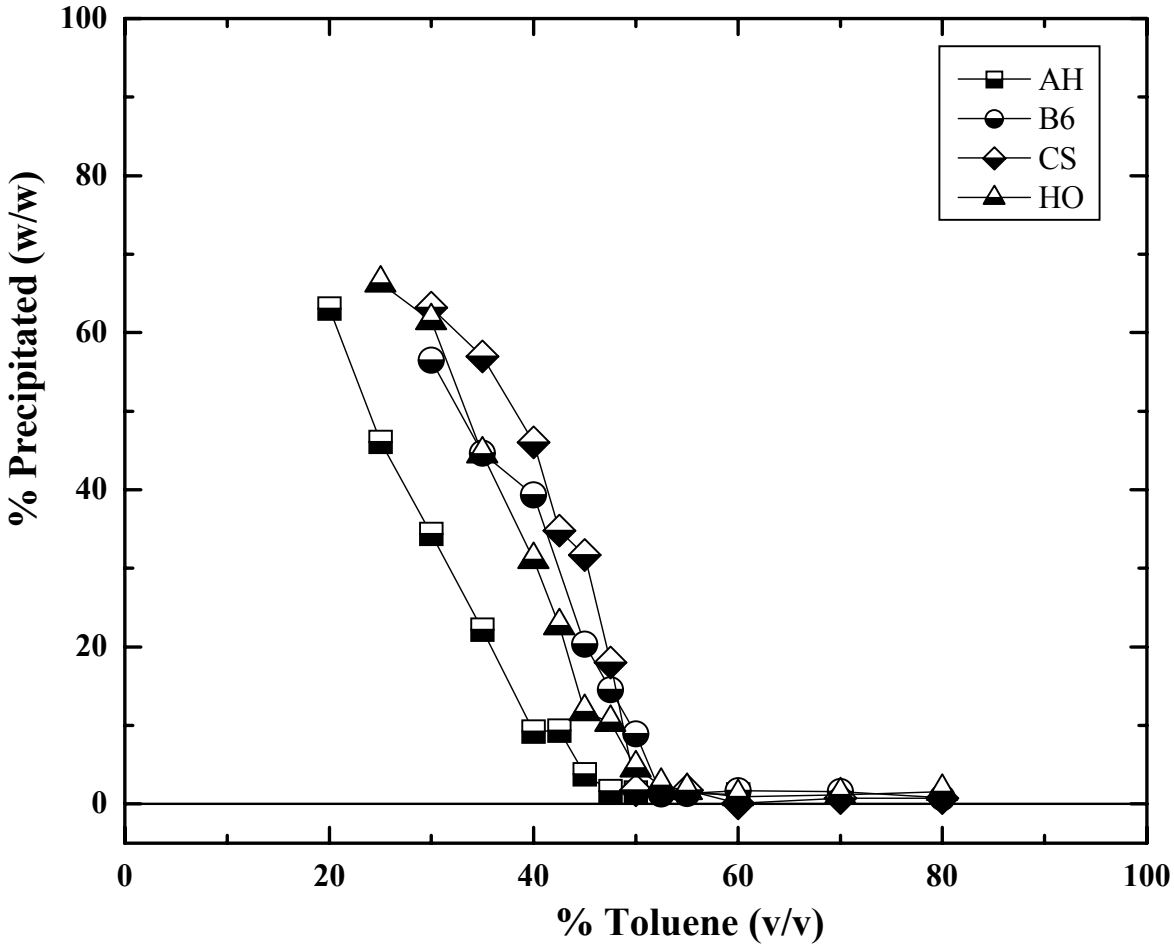

Figure 2.1 Solubility profiles of Whole asphaltenes in heptol.

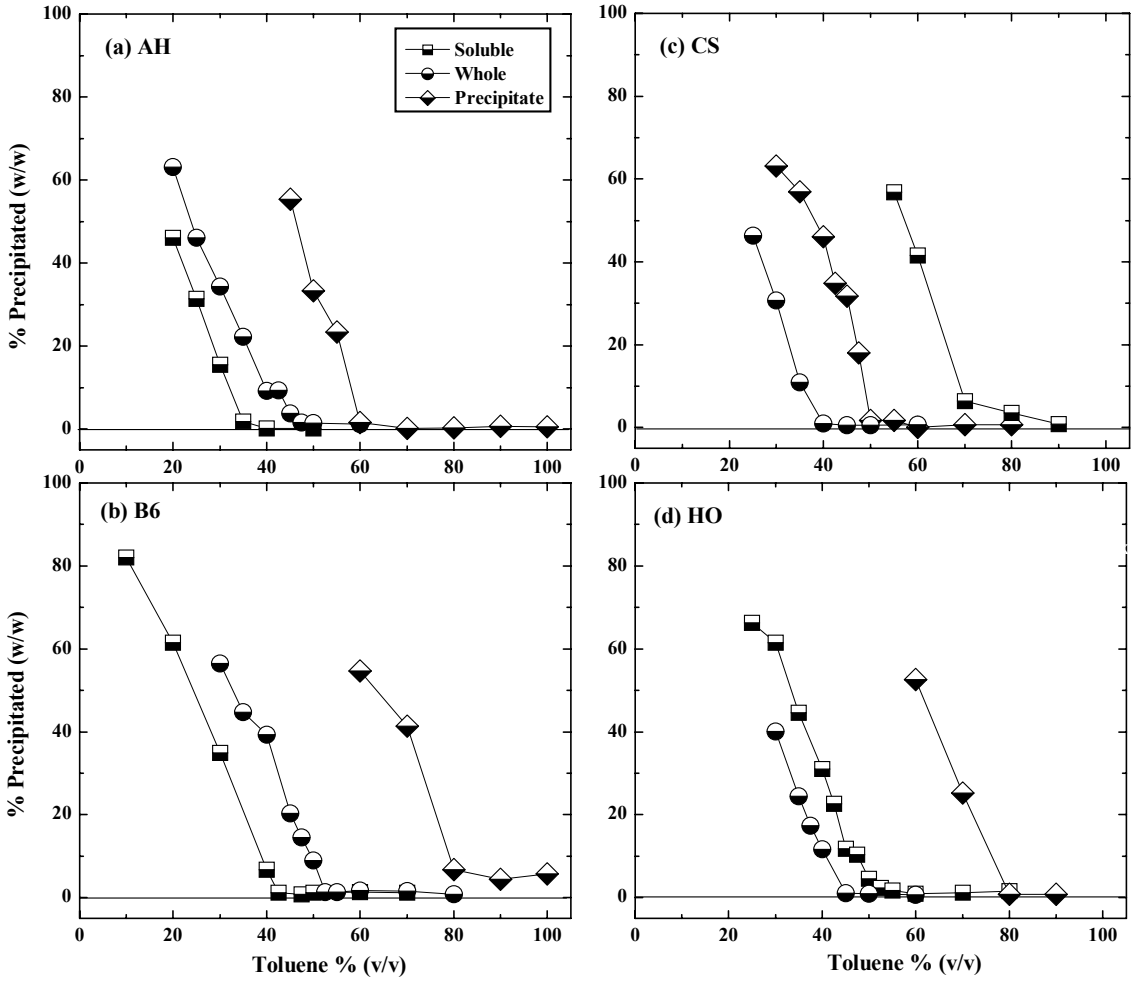

Figure 2.2 Solubility profiles of Whole, Soluble and Precipitate asphaltenes in heptol.

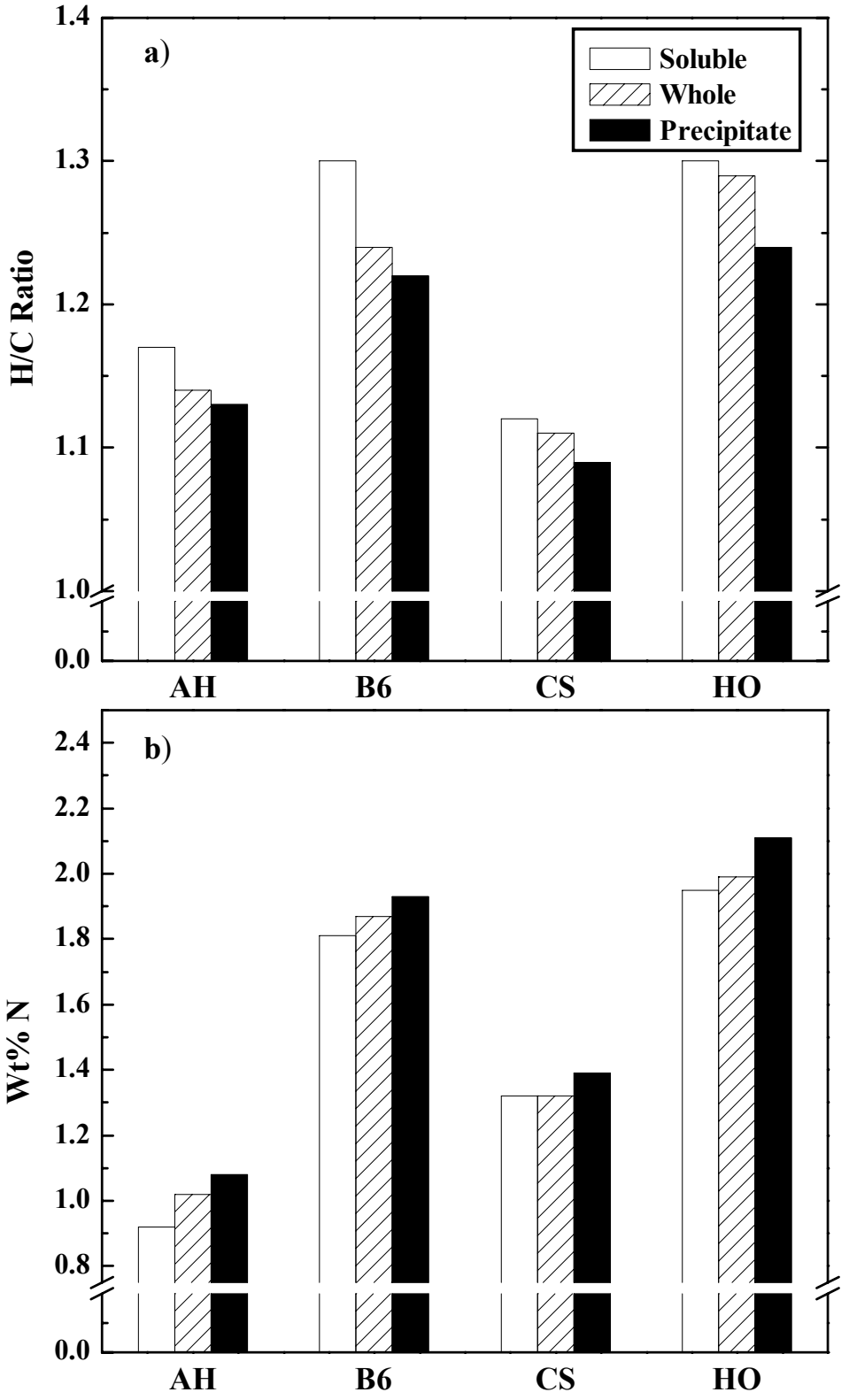

Figure 2.3 Elemental analysis results of Soluble, Whole and Precipitated asphaltenes.

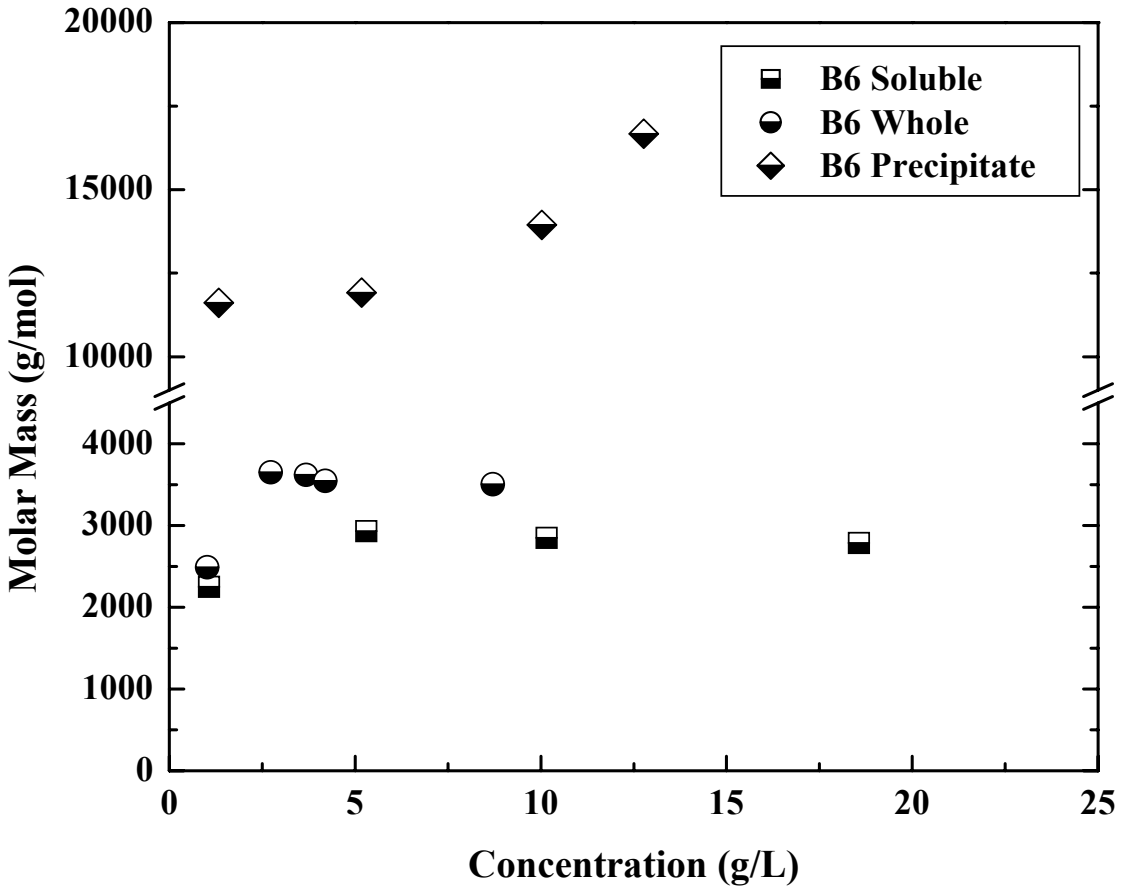

Figure 2.4 VPO molar masses of B6 asphaltenes (Soluble, Whole and Precipitate) in toluene at 53°C.

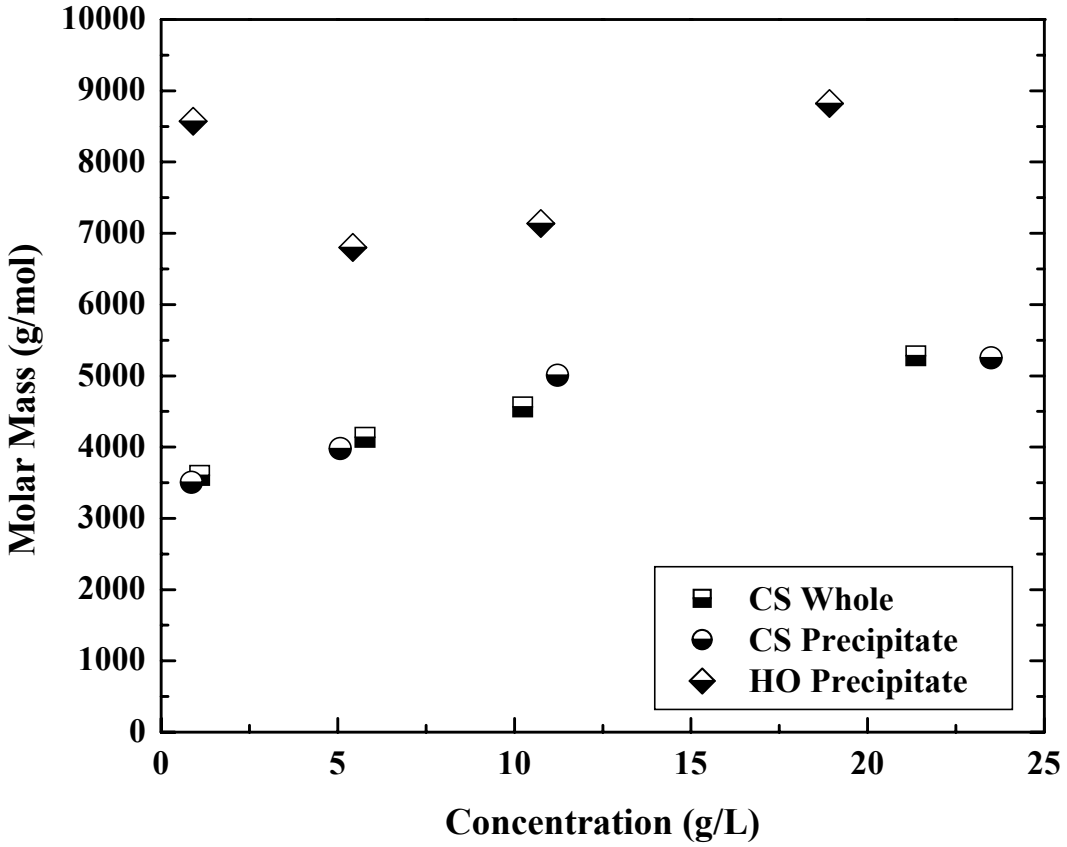

Figure 2.5 VPO molar masses of CS (Whole and Precipitate) and HO (Precipitate) asphaltenes in toluene at 53°C.

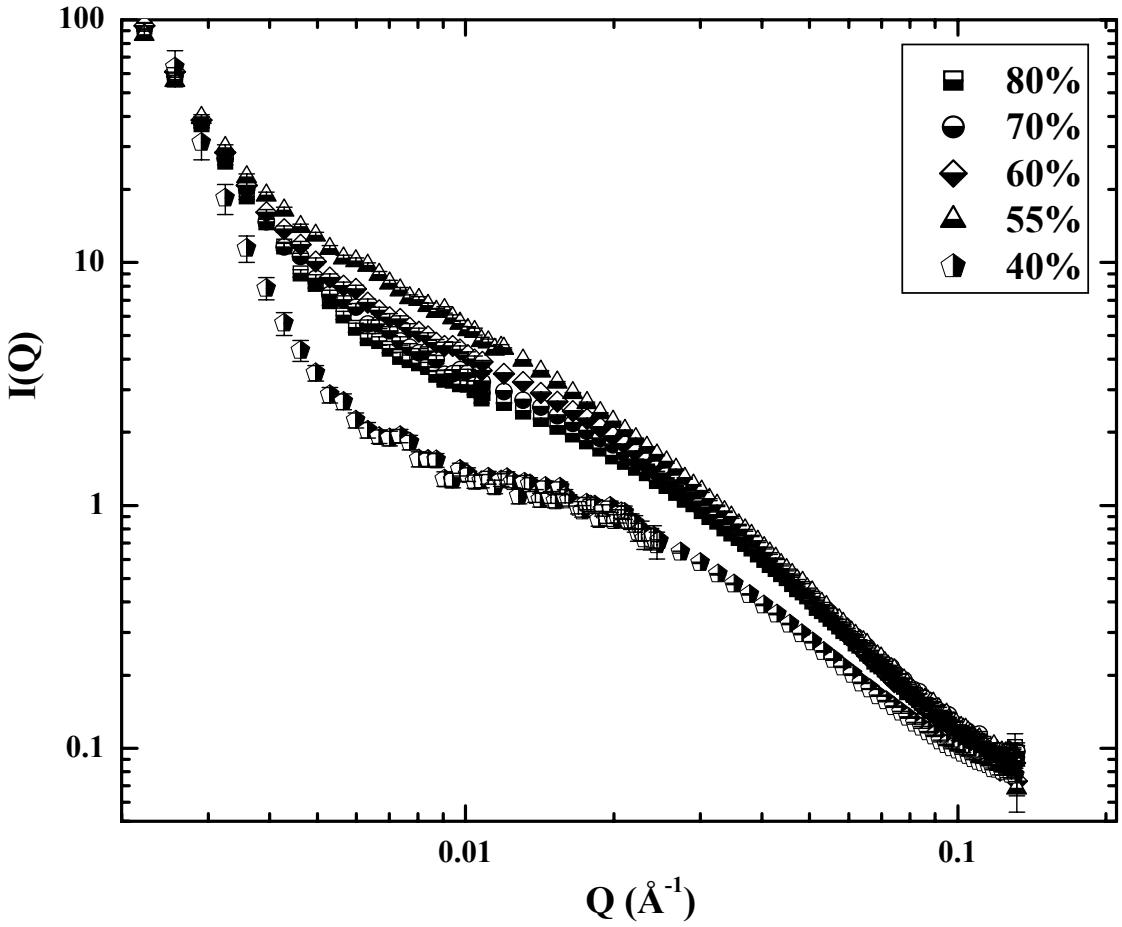

Figure 2.6 SANS curves of B6 Whole asphaltenes in d-heptane, d-toluene at 1 wt%, 25°C.

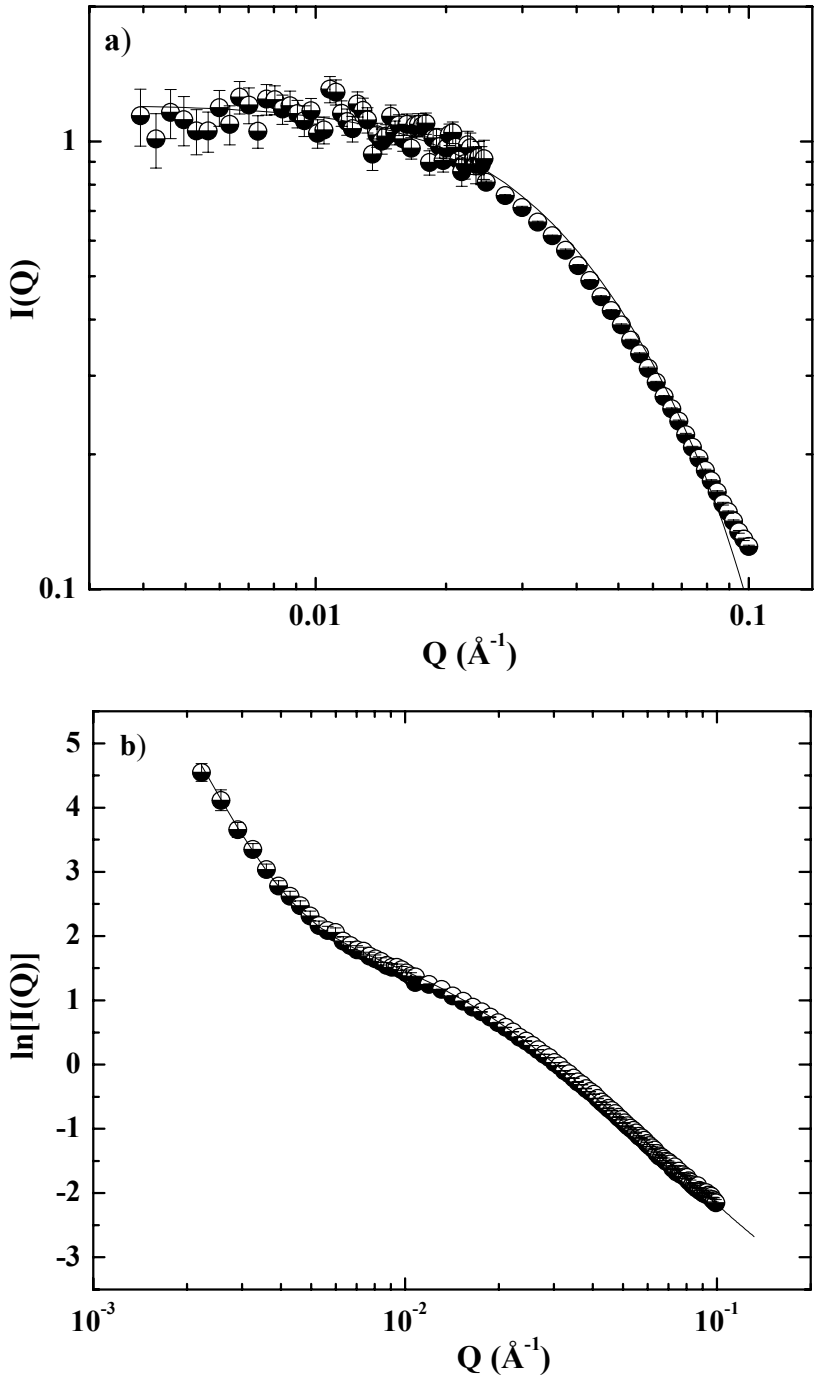

Figure 2.7 SANS fits using Lorentzian line shapes.

a) AH Soluble asphaltenes: 1 wt %, 50 % (v/v) toluene in heptol, 25°C
Background: -0.097 ± 0.037, I_0: 1.31 ± 0.03
ξ: 24.4 ± 1.2

b) B6 Whole asphaltenes: 1 wt %, 60 % (v/v) toluene in heptol, 25°C
Background: 0.0068 ± 0.0015, I_0: 6.44 ± 0.08, I_1: 2.42E-9 ± 3.49E-11
ξ: 77.2 ± 0.7

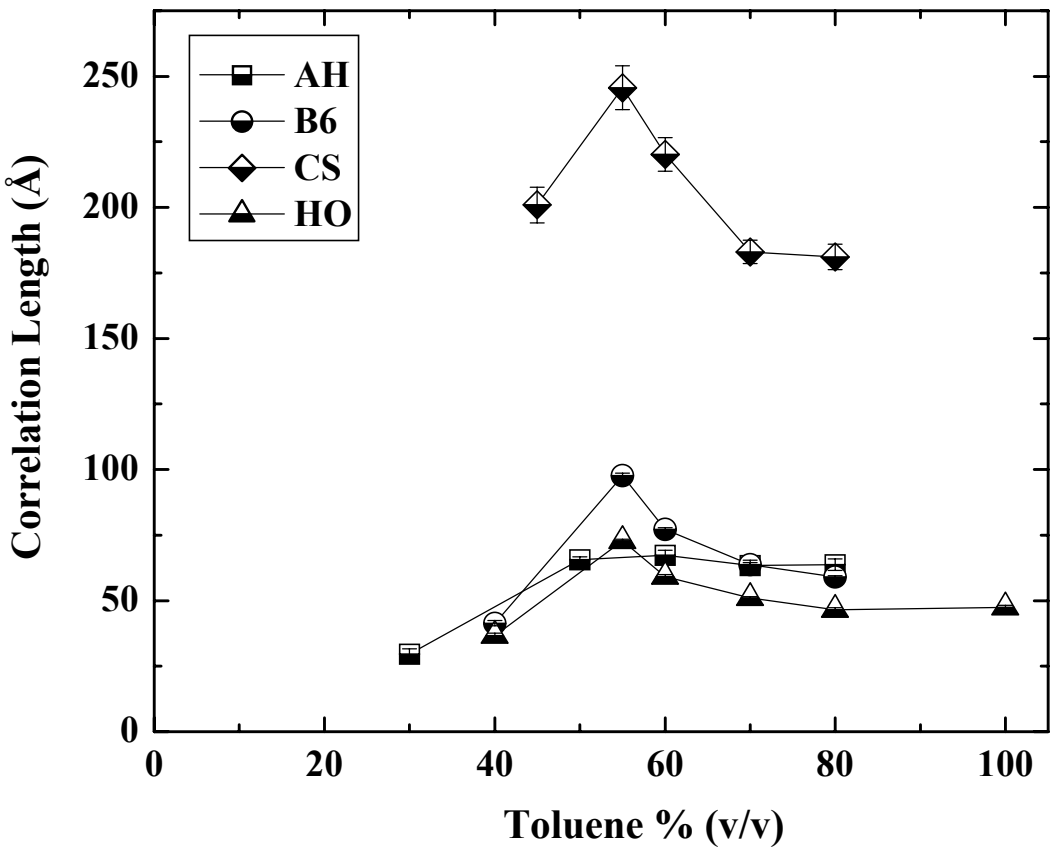

Figure 2.8 Correlation lengths of Whole asphaltenes in heptol determined by SANS: 1 wt %, 25°C.

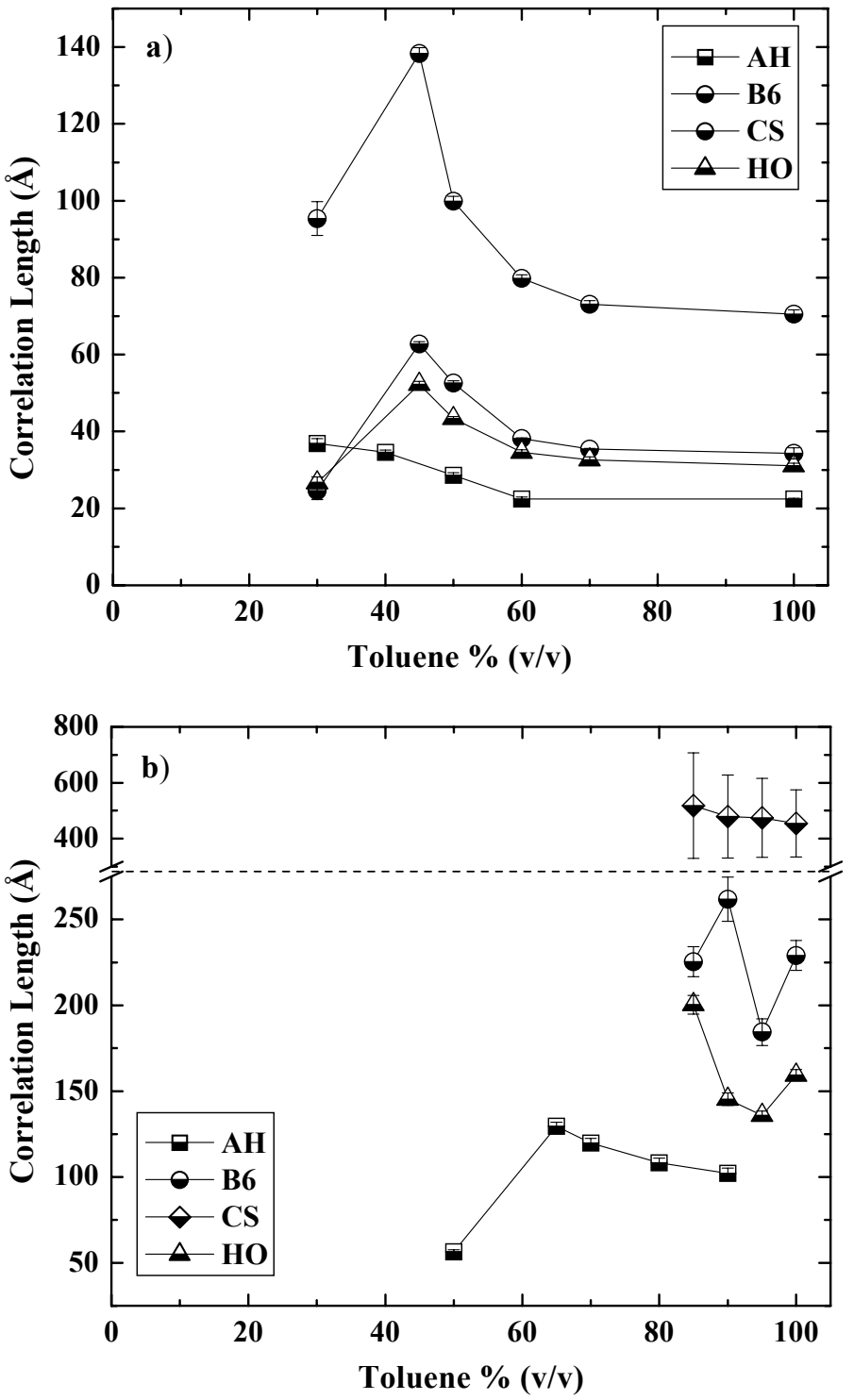

Figure 2.9 a,b. Correlation lengths of Soluble (a) and Precipitate (b) asphaltenes in heptol by SANS: 1 wt %, 25°C.

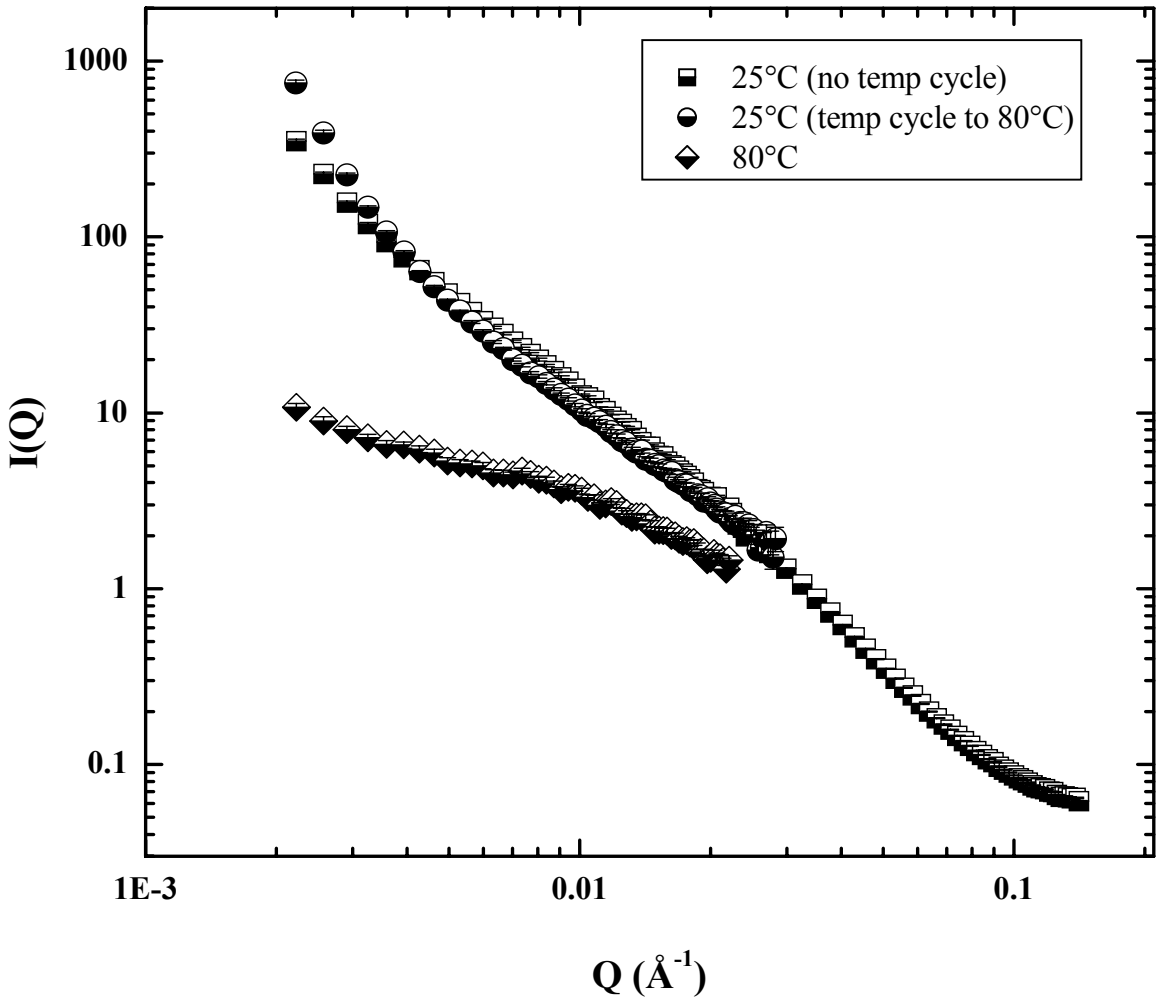

Figure 2.10 SANS curves of CS Precipitate asphaltenes in toluene at 25 and 80°C: 1 wt %. Temperature cycled solution was raised to 80°C for 1 hour and then cooled before running.

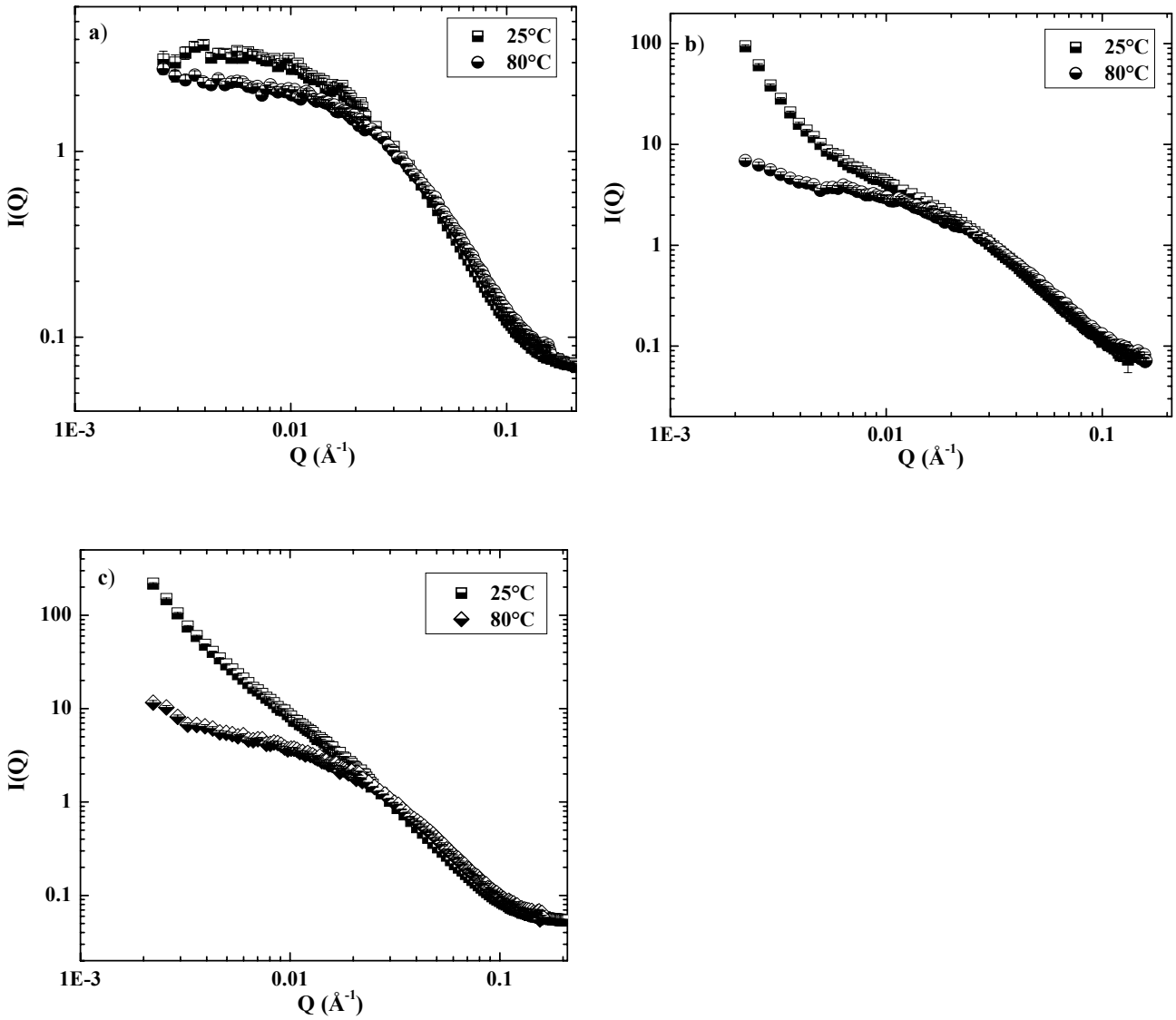

Figure 2.11 a-c SANS curves of asphaltenes in heptol: 1 wt%.

a) B6 Soluble in 50 % toluene
b) B6 Whole in 60 % toluene
c) B6 Precipitate in 100 % toluene

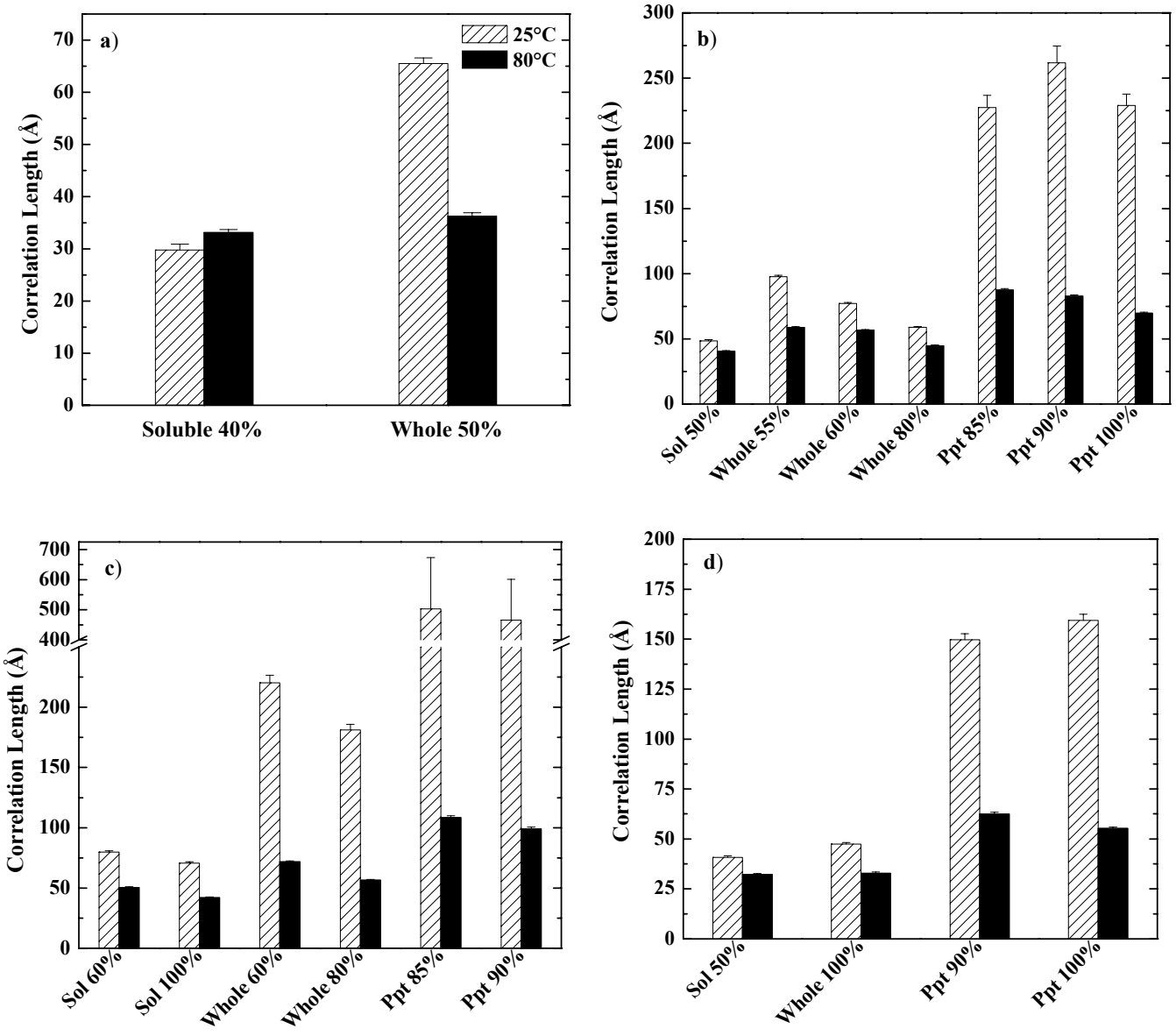

Figure 2.12 a-d Correlation lengths of Whole, Soluble and Precipitate asphaltenes in heptol at 25 and 80°C: 1 wt %.

a) AH
b) B6
c) CS
d) HO

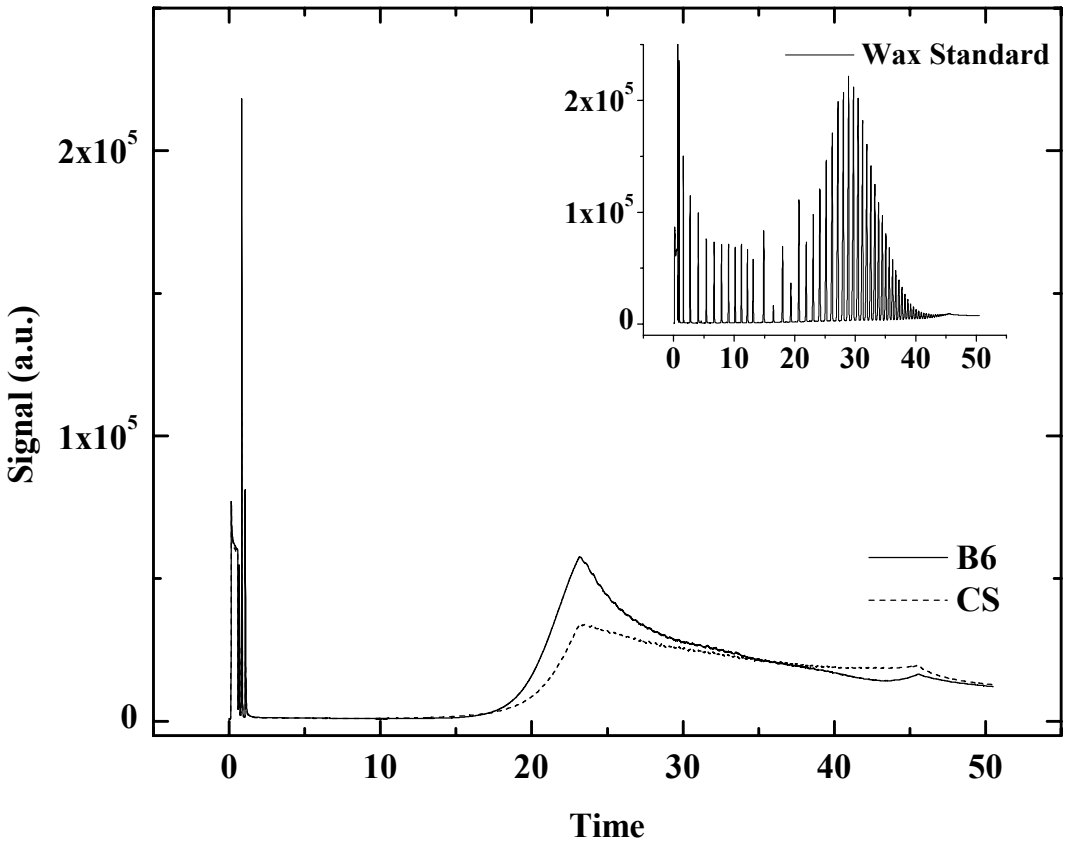

Figure 2.13 HTSimDist GC scan of B6 Whole, CS Whole and wax standard (inset).

The Role of Asphaltene Solubility and Chemistry on the Stability of Water-in-Oil Emulsions

P. Matthew Spiecker and Peter K. Kilpatrick

ABSTRACT

Water-in-oil emulsions were prepared by homogenizing water and mixtures of heptane and toluene (heptol) containing asphaltenes (*n*-heptane insolubles and toluene solubles) from four crude oils (Arab Heavy, B6, Canadon Seco, and Hondo). Emulsion stability was gauged by the volume percentage of water resolved after centrifugation at high speed (15,000 rpm). B6 and Hondo asphaltenes formed emulsions considerably more stable over a broad range of toluene volume fractions than Arab Heavy and Canadon Seco. Sauter mean droplet diameters determined from optical microscopy ranged from 7.1 to 11.1 μm immediately following homogenization. Preparative scale fractionations were performed on the four asphaltenes at toluene volume fractions between 0.3 and 0.4 via vacuum filtration. Solubility profiles of the more soluble and less soluble fractions isolated in heptol mixtures indicated strong cooperative asphaltene interactions. The less soluble asphaltene fractions had lower H/C ratios, higher nitrogen content, and formed much larger aggregates than the more soluble or unfractionated asphaltenes, suggesting that aggregation may be governed by the degree of aromatic π-π bonding and polar interactions between heteroatoms.

The relative stabilities of emulsions indicated that asphaltenes fell into several classes. The defining characteristics of each category were asphaltene aggregate size, H/C ratio, and N, Ni, and V content. Class 1 emulsions were the weakest and formed by high aromaticity asphaltenes (H/C 1.12-1.17) with small aggregate sizes (34.5-138 Å), containing lower concentrations of N (<1.32%) and heavy metals. Class 2 and 3 emulsions were very

stable and formed by intermediate to large aggregates (53.2-262 Å) with lower aromaticity but higher concentration of N, Ni and V. Class 4 emulsions were also quite weak and formed by highly aggregated asphaltenes (246-520 Å) with higher aromaticity (H/C 1.09-1.11) and lower N, Ni, and V content. Asphaltenes aggregating due primarily to H-bonding and by π-π interactions were presumed to form a cohesive interfacial oil-water film and stable emulsions. Weaker emulsions were likely caused by less interfacially active π-π dominated asphaltene aggregates.

CHAPTER 3

THE ROLE OF ASPHALTENE SOLUBILITY AND CHEMISTRY ON THE STABILITY OF WATER-IN-OIL EMULSIONS

3.1 Introduction

Through the course of petroleum recovery from underground oil wells, to transportation and refining, production challenges are often encountered. Many of these problems can be traced to high molecular weight, colloid-forming components found in the heavier crude fractions[1-6]. These compounds can lead to the formation of catalyst and equipment fouling emulsions, sludge, and coke. Crude oil is found in reservoirs along with water or brine and during oil removal, water is often coproduced. Water is also injected into the crude to remove salts or as steam to improve fractionation.[7] Petroleum emulsions (typically water-in-oil[1, 8-11]) readily form with water in the highly turbulent nozzles and piping used for oil production. These emulsions can increase pumping and transportation expenses, corrosion of pipes, pumps, production equipment and distillation columns, and the poisoning of downstream refinery catalysts. [12]

Mixing immiscible liquids such as oil and water with a surface active agent will often yield an emulsion of oil droplets in water (o/w) or water droplets in oil (w/o) according to Bancroft's rule.[13]. Bancroft's rule states that the liquid in which the surfactant is soluble becomes the continuous phase. Other factors such as oil-water volume fractions, surfactant concentration and hydrophile-lypophile balance will also influence the type of emulsion formed. After droplets are completely dispersed within the continuous phase, surfactants migrate to the oil-water interface and can inhibit droplet rupture by steric, electrostatic,

Marangoni-Gibbs, or rigid-film forming interactions. Other factors leading to stable emulsions are high viscosity continuous phases, small dispersed phase volume and droplet size, and low interfacial tensions.[12]

As early as 1948, Lawrence et al. tried to identify the agents responsible for the formation of sea water-Navy fuel oil emulsions.[5] They suggested that "soft asphalt" was the stabilizing agent and that as little as 0.75% in fuel oil created emulsions stable over several days. Blair linked the stability of petroleum emulsions to the formation of a condensed and viscous film that acted as a barrier to droplet coalescence.[2] Many early studies were performed on the film forming and emulsifying behavior of crude oil-water systems.[1, 9, 14-21] These and later studies often held the asphaltenic constituents in crude oil responsible for film formation and stabilization.[9, 17, 22, 23]

Asphaltenes are defined as the portion of crude oil insoluble in *n*-alkanes such as *n*-heptane or *n*-pentane yet soluble in benzene or toluene.[24, 25] The "solubility class" definition of asphaltenes generates a broad distribution of molecular structures that can vary greatly from one crude oil to another. In general, asphaltenes are characterized by fused ring aromaticity, small aliphatic side chains, and polar heteroatom-containing functional groups. H/C ratios between 1.0 and 1.2 and N, S, and O content of a few weight percent suggest that much of the asphaltene backbone contains fused aromatic carbon interspersed with a handful of polar functional groups. Depending on the solvent chosen, number average molecular weights by vapor pressure osmometry can range from ca. 800 to 3000 g/mol.[26-33] Many studies have indicated the presence of carboxylic acids, carbonyl, phenol, pyrroles, and pyridine functionality.[34-38] These groups are capable of donating or accepting protons inter- and intra-molecularly. The most plausible mechanisms of asphaltene aggregation

involve π-π overlap between aromatic sheets, hydrogen bonding between functional groups and other charge transfer interactions. The degree of aggregation is controlled by the polydispersity and chemistry of asphaltene monomers.

One of the earliest investigations of a water-in-oil emulsion formed by asphaltenes dissolved in a model oil system was performed by van der Waarden.[8] His work pointed to many important film and emulsion forming behaviors of asphaltenes. He found that asphaltenes near their solubility limit in aliphatic-aromatic mixtures typically formed the most stable emulsions. Solvents of high aromaticity tended to prevent the flocculation of asphaltenes and formed weaker emulsions. In addition, the "rheological resistance" of the interface was measured using a torsion oscillation method where the oscillation amplitude of a glass disk suspended at the oil-water interface was monitored in the presence of asphaltenes. Results indicated that asphaltenes at or near the point of flocculation developed a viscous film and that emulsion stability was facilitated by the adsorption of this coherent asphaltene layer. Subsequent research in the field has focused primarily on the film forming and emulsion properties of asphaltene aggregates.[39-50]

While the study of asphaltene containing oil-water systems has been a fruitful area of research lately, there are just a handful of investigations on asphaltene subfractions and even fewer relating emulsion behavior to asphaltene chemistry. Andersen has recently fractionated asphaltenes in mixtures of aliphatic and aromatic solvents by solubility and characterized their different chemistries.[31] Others have used ion exchange chromatography to separate asphaltenes into acidic, basic and neutral groups for subsequent determination of chemical properties.[30, 51-53] However, none of these studies involved studying interfacial or emulsion forming properties. Clearly, the scientific community lacks

an in-depth understanding of asphaltene subfraction chemistry and behavior at the oil-water interface. It is now well recognized that asphaltenes from different crude oil sources can have vastly different properties. At the same time, asphaltenes are comprised of a polydisperse collection of molecular chemistries that determine their overall chemical and physical properties. Certainly, this polydispersity will reveal fractions highly prone to aggregation and interfacial adsorption and others that are quite soluble.

To help improve the conversion of crude oil into useful product by reducing losses to sludge and emulsions, it is necessary to better understand the factors that affect their formation. Paramount to this understanding is an in-depth knowledge of the structures and interactions of the asphaltenic components responsible. In this study, we investigate the propensity of asphaltenes to form water-in-oil emulsions. Asphaltenes and their more and less soluble subfractions were dissolved in model oils of aliphatic and aromatic solvents and emulsified in the presence of water. It was our goal to relate the aggregation and solubility behavior of the asphaltenes and their subfractions to the corresponding strength of emulsions formed with these subfractions.

3.2 Experimental

3.2.1 Asphaltene Source

Asphaltenes were precipitated from four crude oils: B6 and Hondo (off-shore California), Arab Heavy (Safaniya), and Canadon Seco (Argentina). These crude oils are asphaltene rich and vary in viscosity, resin content and asphaltene H/C ratio. Basic crude oil and asphaltene properties are summarized in Table 3.1.

3.2.2 Asphaltene Precipitation and Fractionation

Asphaltenes were precipitated from each crude oil with a 40:1 excess of n-heptane, vacuum filtered, dried in a nitrogen flushed oven. The crude oil asphaltenes were labeled "Whole". These asphaltenes were separated into more and less soluble fractions by redissolving in toluene and then inducing partial precipitation through heptane addition. The asphaltene concentration in heptol (heptane-toluene) was 0.75 % (w/v) (~1 % (w/w)). Above a toluene volume fraction of approximately 0.5, the Whole asphaltenes from all crude oils were completely soluble. The volume fraction of toluene chosen to induce precipitation ranged from 0.3 to 0.4 depending on asphaltene solubility. Each Whole asphaltene was separated into a soluble fraction, or "Soluble" (~67 % by mass) and an insoluble fraction, or "Precipitate" (~33 % by mass). Solubility curves of the Whole, Soluble and Precipitate were generated by filtering asphaltene-heptol solutions and weighing the amounts of soluble and insoluble material. Details of the precipitation and fractionation procedures can be found in a previous publication.[54]

3.2.3 Small Angle Neutron Scattering

Neutron scattering of asphaltenes was performed at NIST in Gaithersburg, MD on the NG7 (30 m) beam line. Asphaltene solutions (1 wt %) were prepared in perdeuterated heptane and toluene solutions and studied at 25°C. Scattering intensity versus scattering angle (I(Q) vs. Q) data were fit to Lorentzian line shapes using a non-linear least squares regression to determine the aggregate correlation lengths. Further operational details can be found in a previous publication.[54]

3.2.4 Emulsification and Stability Measurements

Asphaltenes were weighed into 20 mL jars and dissolved in toluene for 24 hours. B6, CS and HO Precipitate asphaltene solutions in toluene were placed in a 70°C water bath to ensure complete dissolution before heptane addition. These solutions equilibrated for an additional 24 hours. Once dissolved, heptane was added to adjust the state of asphaltene solvency. The final solute concentration in 4 mL of heptol was 0.37 % (w/v), or equivalently, 0.5 % (w/w). Before emulsification, this model oil was transferred to a 15 mL jar followed by 6 mL of pH 6 deionized water. A 750-watt Virtis Cyclone I.Q. Homogenizer with 6 mm rotor-stator mixing head was used to emulsify the oil-water system. This unit can control rotor speed from 5000 to 30,000 rpm and maintain speed regardless of applied load. The mixer reached its operating speed of 15,000 rpm after 10-15 seconds. During the acceleration period, most of the water was brought from the bottom of the jar and blended with oil. Three minutes of homogenization was sufficient to create minimum sized droplets (<1-10 μm) of water dispersed in oil.

Droplet size distributions and Sauter mean diameters were determined for selected emulsions. Immediately following emulsification, 0.2-0.3 mL of the emulsion were removed with a pipette and diluted in ~3 mL of mineral oil. Dilution in a viscous liquid significantly reduced the speed of water droplet settling, droplet coalescence and facilitated optical microscopy. A small drop of diluted emulsion was placed on a glass slide followed by a cover slide. Droplet images were captured with an Olympus BH-2 microscope and Olympus PM-10AD 35 mm camera system. Photographs were taken of two regions in each emulsion samples and 500-800 droplets were analyzed on regions of both images. The Sauter mean droplet diameter, or d_{32}, can be calculated from:

$$d_{32} = \frac{\sum n_i d_i^3}{\sum n_i d_i^2} \tag{1.1}$$

where n_i is the frequency of droplets with a diameter d_i.[55] Also, the third moment of the distribution, or the skewness, was determined about the origin following:

$$skewness = \frac{\sum n_i (d_i)^3}{\sum n_i} \tag{1.2}$$

After homogenization, the viscous emulsions were transferred into 10 mL polypropylene centrifuge tubes (Nalgene). Following a 24 hr period of aging, the emulsions were centrifuged for 1 hour at 15,000 rpm in a Sorvall RC5C centrifuge equipped with an SS-34 rotor. Three distinct layers were evident following centrifugation corresponding to creamed oil, dense emulsion and coalesced water. Creamed oil was discarded and a glass pipette was used to transfer resolved water to a small graduated cylinder. Three to six replicates were performed and the error reported as the standard deviation of the emulsion stability values. Emulsion stabilities were calculated from the volume of water resolved:

$$\%\ Water\ resolved = \frac{Volume\ resolved}{6\ ml}\ X\ 100$$

Initial testing indicated that emulsions containing high asphaltene concentrations (≥ 0.5 % w/v) and oil volume fractions were completely stable even after centrifugation, while low asphaltene concentration, high water content systems were generally resolved completely by centrifugation. An oil volume fraction of 0.4 and asphaltene concentration

equal to 0.37 % w/v were sufficient to form gravity stable emulsions with sufficient dynamic range following centrifugation. At these conditions, each of the four asphaltene systems and their more and less soluble subfractions were completely emulsified in all mixtures of heptol. The most stable systems resolved just a small fraction of the dispersed water emulsified while the least stable systems were completely resolved after centrifugation.

3.3 Results and Discussion

3.3.1 Whole Asphaltene Emulsion Stability

The stability of emulsions formed with Whole asphaltenes in heptol is shown in Figure 3.1. Most emulsion stability measurements were precise to within ± 5 % water resolved. Error bars have been removed for clarity. Higher amounts of water resolved indicate weaker emulsions because of increased droplet coalescence. Lower values indicate reduced droplet coalescence and more stable emulsions. The results of the Whole asphaltene tests indicate that emulsion stability was dominated by two primary factors: asphaltene type and solubility in heptol.

The Whole asphaltenes fell into two categories of emulsion stability: strong emulsion formers (B6 and HO) and weak emulsion formers (AH and CS). B6 and HO Whole formed very stable emulsions over a wide range of toluene volume fractions and were considerably more stable than AH and CS Whole. The water resolved curves were generally U-shaped, indicating maximum emulsion stability at intermediate toluene volume fractions and minimum stability at the extremes (consistent with earlier work[42]). In the first part, we will present the emulsion stability, asphaltene solubility and aggregate size of weak and strong Whole asphaltenes followed by their Soluble and Precipitate fractions. The stability

trends of Whole asphaltenes and their more and less soluble subfractions can be understood in light of recent studies on asphaltene solubility, chemistry, and aggregate sizes.[54]

To help elucidate the mechanisms of emulsion formation and stability, the results of Whole, Soluble, and Precipitate asphaltene systems will then be divided into four classes. Each class comprises a more narrow set of asphaltene properties and emulsion behaviors. Due to the polydisperse nature of asphaltenes and occasional crossover of emulsion behavior and chemical properties, some of the Whole or fractionated asphaltenes may bridge two classes. However, from the results we will see an emerging picture of the role of asphaltene chemistry and aggregation behavior in governing emulsion stability.

3.3.2 Weak Emulsion Formers: AH and CS Whole

Emulsion stability curves of AH and CS Whole are replotted in Figures 3.2a-b, in addition to asphaltene solubility (% precipitated (w/w)) and aggregate correlation lengths by SANS. Nearly all heptol ratios produced emulsions with more than 50% water resolved. Maximum stability fell in a narrow range of toluene volume fractions from 0.4 to 0.6. Outside this range, more than 70% of the original water had resolved after centrifugation, indicating particularly weak emulsions.

In the asphaltene soluble regime (greater than about 50 % (v/v) toluene or to the right of the vertical line), asphaltenes formed as aggregates of several nanometer size. Neutron scattering allowed the determination of average aggregate sizes (correlation lengths) in mixtures of heptane and toluene. Heptane and toluene can be characterized by three-component Hansen solubility parameters, which include terms for dispersion, polar and hydrogen bonding interactions (Table 3.2).[56] Highly aromatic solvents (toluene-rich),

possessing a higher dispersion parameter and modest polar and H-bonding parameters (> 1), presumably minimized aggregation by solvating polar aromatic asphaltene cores and disrupting intermolecular π and hydrogen bonding. As the intermolecular forces holding the aggregates together were weakened, resolved water approached a maximum and emulsions were weak and unstable.

By reducing the toluene volume fraction, asphaltenes aggregated to a greater extent and were more prone to adsorb at the oil-water interface. Small, well solvated aggregates will naturally remain in solution more so than large aggregates near the asphaltene solubility limit. Larger aggregates are driven to the oil-water interface and adsorb in an attempt to reduce the interfacial tension and thus minimize free energy. These effects were more apparent in CS Whole than AH where correlation lengths climbed from 183 Å at 70 % (v/v) toluene to 246 Å just above the solubility limit and water resolved fell. Further decreasing solvent aromaticity brought both systems to their threshold limit of asphaltene solubility (between 45 and 50% toluene). As a result, asphaltenes began to precipitate with size scales exceeding 1.5 μm. The correlation lengths determined by SANS in the precipitated regime could not account for these very large aggregates whose Q range fell below the limit of detection ($Q < 0.001$ $Å^{-1}$). However, even in this intermediate solvent regime, systems containing up to 30% precipitate were still capable of partial emulsion stabilization. This stability can be attributed to the highly surface active nature of the remaining soluble asphaltenes.

Emulsions were largely unstable at very low toluene volume fraction (<0.3). Large, bulky precipitates formed in these highly aliphatic solvents were not able to knit themselves into a cohesive film around the finely dispersed water droplets. The oil-water interfaces

seemed to act as deposition sites for the precipitated asphaltenes since the post-emulsification creamed oil was nearly transparent and evidently devoid of solute. Even with all the asphaltenes adsorbing to the interface, the bulky nature of the asphaltenes prevented stable emulsion formation. In addition, the large flocculated aggregates did not provide an adequate inventory for droplet coverage. To illustrate, 1 μm diameter spherical asphaltene flocs can form monolayer coverage over 1.85×10^{10} μm^2 of oil-water interface. However, 6 mL of 10 μm diameter water droplets create 3.6×10^{12} μm^2 of interface. In this case, the system is asphaltene aggregate limited and complete emulsification of the water is not possible. Compared to 1 μm flocs, 50 Å spherical aggregates can provide monolayer coverage over 3.7×10^{12} μm^2 of oil-water interface and thus ensure complete emulsification.

3.3.3 Strong Emulsion Formers: B6 and HO Whole Asphaltenes

B6 and HO Whole asphaltenes formed stable emulsions over a considerably wider heptol range than AH and CS (Figure 3.3a-b). B6 emulsions had less than 20 % (v/v) water resolved over a spread in heptol ratios from 30 % to 90 % (v/v) toluene. HO emulsions were comparably stable between 45 % and 60 % toluene but destabilized outside of this range. Not surprisingly, the two asphaltenes had very similar solubility curves. In aromatic solvents the asphaltenes were well solvated and formed minimum sized aggregates that grew to a maximum at the solubility limit. Between 80 % and 55 % toluene, B6 aggregates grew from 59 to 98 Å while HO grew from 46 to 73 Å. Emulsions prepared in pure toluene, however, were still quite stable indicating high interfacial activity and propensity to form strong films. B6 and HO asphaltenes are enriched in polar functionality and have higher H/C ratios than AH and CS Whole (Table 3.1). The increased emulsion stability of B6 and HO may be

attributed to enhanced hydrogen bond interactions between individual asphaltene aggregates and between these aggregates and water droplets.

Maximum emulsion stability was located near the solubility limit and the point of largest aggregate dimension. In this region, asphaltenes were at a maximum state of combined interfacial activity and film formation, a phenomenon seen by others.[8, 42] Upon crossing the solubility limit at 50 % toluene, both asphaltenes began to precipitate. As the precipitated material initially accumulated, the emulsion stability remained high for a short period then rapidly fell. In highly aliphatic solvents, the insoluble asphaltenes were simply not capable of effectively stabilizing an oil-water interface due to their size and inability to form a cohesive film. B6 Whole, however, formed very stable emulsions at 30% toluene where a large portion of its asphaltenes had precipitated. Apparently, the remaining soluble material was still quite surface active and able to stabilize 80% of the homogenized water.

3.3.4 Asphaltene Fractions

The connection between water-in-oil emulsion stability and the solubility and aggregate formation behavior of asphaltenes is evident in the Whole asphaltene studies. Average chemical properties and polydispersity within each asphaltene help shape the aforementioned physical behaviors over a range of aliphatic, intermediate and aromatic solvent regimes. There are fractions within asphaltenes enriched with polar functional groups and fused aromatic rings making them less soluble and more prone to aggregation. A class of complementary asphaltenes is less polar and more soluble. In a previous work, we have demonstrated the existence of these two classes characterized by very different solubilities and aggregate sizes in heptol. We will show in the following sections that these

more soluble and less soluble asphaltene fractions not only differ in solubility but also in their propensity to form stable water-in-oil emulsions.

3.3.4.1 Weak Emulsion Formers: AH and CS

3.3.4.2.1 AH Soluble and Precipitate

AH Whole asphaltenes were fractionated into Soluble and Precipitate in heptol containing 30 % (v/v) toluene. On average this heptol ratio yielded 65 % (w/w) Soluble and 35 % (w/w) Precipitate. AH Whole was the most soluble of the four Whole asphaltenes studied and required the highest ratio of heptane to toluene to generate sufficient Precipitate material. In a previous work, we found that the Soluble and Precipitate fractions from each asphaltene behaved cooperatively. In fact, the Soluble asphaltenes cooperatively interacted with the Precipitate to enhance the system solubility. Once separated, the Precipitate fraction displayed a shift in solubility towards higher aromaticity. This less soluble fraction was somewhat enriched in polar nitrogen functionality and aromatic carbon (Table 3.1). Because of concentrated aromaticity and polarity, larger aggregates were formed in solution (110-130 Å in highly aromatic heptol) (Figure 3.4b). On the other hand, AH Soluble asphaltenes were more soluble than the Whole asphaltenes and formed very small aggregates by neutron scattering in the soluble regime (22-35 Å) (Figure 3.4a, note scale change between a and b). These more soluble asphaltenes also had lower aromaticity (higher H/C ratio) and nitrogen polarity (Table 3.1).

The solubility and aggregation properties of the two fractions influenced their emulsion stability behavior. The stability maximum of AH Soluble was located at a lower toluene fraction (0.4) than the Whole (0.55) or Precipitate (0.5-0.6). Maximum stability was

reached very near the solubility limit where the largest aggregates were formed. These aggregates approached their limit of solubility and were prone to interfacial adsorption. At low aromaticity, AH Soluble formed stronger emulsions than the Whole or Precipitate fraction. This stability shift was caused by the greater availability of material still soluble to adsorb and stabilize oil-water interfaces. As toluene concentration was lowered and more precipitates formed the emulsion stability fell. AH Soluble formed stable emulsions over a very narrow heptol range, while increased solubility from 40 to 45 % (v/v) toluene led to slightly smaller aggregates (less than 35 Å) and a dramatic drop in stability. AH Precipitate asphaltenes formed the weakest emulsions due to large aggregate formation and low surface activity. Both AH Soluble and Whole form smaller aggregates and have a lower % toluene solubility limit than the other asphaltenes investigated here. In addition, the emulsions formed appear to be quite weak due to high asphaltene solubility and low polarity. Even though AH Precipitate asphaltenes are slightly enriched with aromatic carbon and polar nitrogen resulting in slightly larger aggregates, the degree of interfacial film formation and cohesion is still low.

3.3.4.2.1 CS Soluble and Precipitate

Unlike AH Soluble, CS Soluble formed stronger emulsions than CS Whole did at higher solvent aromaticity (Figure 3.5a). Both asphaltenes behaved in a similar fashion below 40 % (v/v) toluene where they reached their solubility limit and began to precipitate. Each emulsion was less stabile as the solvent became aliphatic and drove asphaltenes from solution. At higher solvent aromaticity, the Soluble fraction formed aggregates approximately 100 Å smaller than the Whole. This size reduction may have increased the

lability of the aggregates enough to adsorb and form a stabilizing film. Because of reduced aggregate size, CS Soluble contained a greater number of surface-active species capable of film formation. Again, a delicate balance existed between aggregate solubility and surface activity.

CS Precipitate asphaltenes formed the largest aggregates in the absence of the Soluble fraction (Figure 3.5b). These large, bulky aggregates were ineffective at stabilizing emulsions to an appreciable extent. Slightly stronger emulsions were found in the insoluble regime below 70 % toluene. After removing the largest aggregates, the remaining smaller asphaltenes were possibly more capable film formers and became more surface-active at these conditions.

The process of fractionation generated two asphaltenes classes that differed in solubility and chemistry. These differences translated into new emulsion stability behaviors. Aggregate size appears to play a defining role in emulsion stability with AH and CS asphaltenes. AH Whole asphaltenes were the most stable at their solubility limit with an aggregate correlation length of 67 Å. The same was true for AH Soluble when the correlation length was between 35 and 37 Å. AH Precipitate asphaltenes formed the most stable emulsions in the precipitated regime where aggregate size fell to 56.4 Å. CS Soluble asphaltenes formed more stable emulsions than Whole or Precipitate when in the soluble regime with aggregate sizes from 73 to 100 Å. Both CS Whole and Precipitate asphaltenes formed their strongest emulsions in the insoluble regime where the remaining soluble aggregates were presumably around 200 Å.

3.3.4.2 Strong Emulsion Formers: B6 and HO

While AH and CS fractionated asphaltenes formed relatively weak emulsions, their B6 and HO counterparts stabilized water-in-oil emulsions to a greater extent. B6 Soluble asphaltenes generated stable emulsions over between 20 and 80 % toluene (Figure 3.6a). Due to their enhanced solubility relative to Whole asphaltenes, emulsion stability fell markedly at the highest solvent aromaticity. The Soluble fraction was also more stable at 20 % toluene (v/v) than the Whole. At this heptol condition, the Whole asphaltenes had a higher percentage of precipitated material that was not surface active. Even though close to 60 % (w/w) of the B6 Soluble asphaltenes precipitated at a toluene volume fraction of 0.2, the remaining material was still capable of interfacial adsorption and emulsion stabilization. Presumably, the asphaltenic aggregates in solution were quite small (~20 Å). The growth of aggregate sizes near the solubility limit had no perceptible effect on emulsion stability. Within a 20 % toluene spread around the point of maximum sized aggregates, the emulsions were almost completely stable with just a small fraction of resolved water. The inventory of surface-active aggregates was sufficient to effect stabilization. Above 60 % toluene, the Soluble asphaltene aggregate size did not vary appreciably, however, the emulsion stability decreased substantially between 80 and 90 % toluene. The solvating power of additional toluene was not sufficient to break down the forces holding the asphaltenic sheets together. At this point, the presence of hydrogen bonds and other electron donor-acceptor interactions kept the small aggregates from coming apart. Reduction in emulsion stability was likely caused by increased solubility and diminished surface activity of the minimum sized aggregates.

B6 Precipitate formed very large aggregates in highly aromatic solvents suggesting a high degree of intermolecular association (Figure 3.6b). Clearly, the presence of these large aggregates did not hinder the emulsion stability of the system. This fraction was quite insoluble at most heptol ratios and as such, lost its ability to stabilize emulsions below 50 % toluene. As the asphaltenes became insoluble, they became too large to adsorb and form a cohesive film at the oil-water interface. Their presence may have also hindered the adsorption of smaller, more labile aggregates to the interface. Precipitates likely found themselves at the interface due to the high ratio of dispersed water to oil. They may have remained at the interface in order to lower the interfacial tension and overall free energy. However, their size may have restricted the adsorption of the more soluble aggregates and prevented them from forming an interconnecting film.

HO Soluble and Precipitate behaved very similarly to the B6 fractions (Figures 3.7a-b). Above its solubility limit HO Soluble was not effective at stabilizing emulsions. Beyond 60 % toluene the aggregate size reached a minimum of approximately 30 Å while water resolved approached 90 %. Minimum sized aggregates could not be dissociated above 60% toluene, but their interfacial activity was reduced in solvents of higher aromaticity. HO Soluble formed highly stable emulsions between 35 and 50% toluene. When the aggregate sizes fell below 40 Å, the systems were no longer stable. For comparison, B6 Soluble aggregates reached a minimum of 40 Å and were able to form stable emulsions up to 80 % toluene.

With a 10 % toluene shift in solubility and % water resolved curves, HO Precipitate asphaltenes would appear to mirror their B6 counterparts. HO Precipitate asphaltenes were slightly more soluble than B6 Precipitate and formed aggregates 50 to 100 Å smaller.

Enhanced solubility pushed the transition from strong to weak emulsion formation below 50% toluene. Both HO and B6 Precipitate contained an abundant supply of interfacially active asphaltenes capable of film formation.

The neutron scattering curves of all four Precipitate asphaltenes had high intensity scattering at low Q (< 0.01 $Å^{-1}$). This suggested the presence of very large flocs with sizes greater than the correlation lengths reported. For the most part, the Whole asphaltenes from each crude oil also had the same types of large particles. On the other hand, the Soluble asphaltenes were free of low Q scattering in their soluble regimes except for CS Soluble. From this investigation, we can infer that the presence or lack of particles over 200 to 300 Å are not necessary for the stabilization of asphaltene emulsions. B6 and HO Soluble asphaltenes formed very stable emulsions with aggregates slightly greater than 40 Å. Precipitated B6 and HO asphaltenes formed 150 to 250 Å aggregates in aromatic solvents but were still able to stabilize emulsions.

3.3.5 Emulsion Stability Classes:

3.3.5.1 Class 1: AH Soluble-Whole-Precipitate, CS Soluble

The first class of behavior is characterized by weakly formed emulsions resulting from asphaltenes of high solubility, small aggregate sizes and low interfacial film cohesion (Figure 3.8). Error bars have been removed to improve clarity. In addition, vertical lines representing the solubility limits of each asphaltene in heptol have replaced the solubility curves (see Table 3.3 for the toluene concentration and aggregate size (ξ) at the solubility limit as well as asphaltene chemistry). Correlation lengths of the aggregates determined from SANS are available in the previous figures but, in summary, aggregate sizes reach their

maximum in the soluble regime close to the solubility limit and decrease as the solvent becomes more aromatic. In the precipitated regime, correlation lengths of the remaining soluble material are smaller than the maximum values.

Each of the AH asphaltenes had the lowest solubility limit in relation to the other Whole, Soluble, and Precipitate asphaltenes. As a result, their emulsion stability maxima were located in the least aromatic solvents. In general, however, overall emulsion stability was quite low and only three samples (AH Soluble in 35% and 40% toluene and CS Soluble in 50 % toluene) had less than 40 % water resolved.

While the low H/C ratios indicate higher aromaticities than B6 and HO asphaltenes, low nitrogen content suggests lower polarity and decreased H-bonding capacity. Aggregates tend to be small in this class of asphaltenes most notably AH Soluble and Whole (34.5 Å and 67 Å respectively) at their point of maximum emulsion stability. Aggregation is likely driven in these systems by π-π interactions between asphaltene monomers and much less by H-bonding interactions. The reduction in H-bond potential may contribute to low surface activity, weak oil-water interface adsorption, cohesion, and correspondingly low emulsion stability.

A photomicrograph and emulsion droplet size histogram of CS Soluble asphaltenes at 50 % toluene appears in Figure 3.9. A small volume of emulsion was diluted in mineral oil before placement on a glass slide. Undiluted emulsion droplets contained a high density of droplets that made size analysis difficult also Class 1 emulsions often rapidly coalesced when placed on the glass slide. Diluting the emulsions retained the droplet sizes formed after blending long enough to analyze their distributions. As the histogram indicates, the majority of droplets were less than 5 μm in diameter; however, the Sauter mean diameter (d_{32}) was

11.1 μm. The droplet distribution was skewed the farthest away from the origin of all emulsions examined by microscopy. Representing the volume to surface area ratio of the emulsion, d_{32} is heavily weighted by the presence of larger droplets with high volume to area ratios. While CS Soluble formed its most stable emulsion at 50 % toluene, it was much less stable than Class 2 or 3 emulsions. Direct comparisons between droplet diameters measured immediately after homogenization and emulsion stability measured after 24 hours reveal that strong emulsions often form when small droplets are generated (Table 3.4). Of all the emulsions analyzed by photomicrography, CS Soluble had the largest Sauter mean diameter and intermediate stability.

3.3.5.2 Class 2: B6 Soluble, HO Soluble-Whole

From the small soluble and weakly emulsifying aggregates of AH and CS Soluble, we step to larger, polar asphaltenes that form stable emulsions over an intermediate range of heptol (Figure 3.10). This class is characterized by very high emulsion stability at intermediate heptol ratios and low stability at the extremes (U-shaped stability curves described earlier). The solubility limits of these asphaltenes fall between 42 (B6 Soluble) and 52 % (HO Whole) toluene. Aggregate sizes at the solubility limits range from 52 to 73 Å and result in asphaltenes with sufficient lability to diffuse and adsorb to oil-water interfaces. While higher H/C ratios suggest lower asphaltene aromaticities, the nitrogen content of these asphaltenes is greater than Class 1 asphaltenes. It is likely that H-bonding between monomers dominates the forces governing aggregate structure and gives rise to a greater affinity for the oil-water interface. These medium sized aggregates provide a

sufficient inventory of material while their H-bonding capacity likely enhances the degree of interfacial adsorption and cohesion.

Differences are apparent between B6 Soluble and the HO asphaltenes where the range of emulsion stability of B6 is noticeably wider. It has the capacity to generate stable emulsions down to 20 % toluene and as high as 80 % toluene. However, its level of solubility is too high above 80 % toluene for interfacially active aggregates to form emulsion stabilizing films.

Below the solubility limit, the quantity of precipitated material grew to point where the quantity of surface-active aggregates was not sufficient for interfacial coverage. The most surface-active compounds likely aggregate the strongest and precipitate in heptol mixtures slightly less aromatic than the solubility limit. This process of aggregation and precipitation reduces the quantity and quality of asphaltenes capable of cohesive interfacial film formation, and as a result, weak emulsions are formed.

The Sauter mean diameters after homogenization of B6 Soluble asphaltene emulsions are shown in Table 3.4 and Figure 3.11 (60 % toluene). Solvency conditions that generated stable emulsions at 24 hours also created emulsions stable to microscopy without dilution. B6 Soluble asphaltene emulsions in pure toluene, however, coalesced when placed on the glass slide without dilution. At 20 % toluene, the solubility of B6 Soluble asphaltenes is limited and the average emulsion stability was high (Figure 3.10) but on the verge of instability. These conditions generated a Sauter mean diameter of 10.9 μm and a skewness of 317. At 60 % toluene, the emulsions were more stable, the asphaltenes were completely soluble and the mean diameter decreased to 8.2 μm and skewness decreased to 191. While sufficient mixing energy and asphaltene coverage generated small droplets, the degree of

film consolidation and strength at 24 hours was not adequate to create stable emulsions in pure toluene.

3.3.5.3 Class 3: B6 Whole-Precipitate, HO Precipitate

Figure 3.12 shows the emulsion stability and solubility limits of the most strongly surface active asphaltenes. What differentiates Class 3 from Class 2 asphaltenes is their strong emulsion forming behavior in highly aromatic solvents. These three fractions have the highest aromaticities of B6 and HO asphaltenes and the highest nitrogen contents of all asphaltenes. Their respective solubility limits are located at higher toluene volume fractions than the other asphaltenes. The intermolecular interactions between asphaltene monomers and aggregates are very strong because of enhanced aromaticity and polarity. While aggregates sizes are quite large (particularly HO and B6 Precipitate) and the asphaltenes may not be very labile, their propensity to adsorb dominates. In addition to aromaticity and polarity, both Class 2 and 3 asphaltenes have much higher levels of Ni and V. These two metals can be found in porphyrin rings within the asphaltene core structure and are often present in the petroleum fraction forming the stabilizing film at oil-water interfaces.[57, 58]

Asphaltenes of this type do not form stable emulsions in solvents of low aromaticity since solubility is quite low. These low solubility asphaltenes can precipitate in solvents with less than 80 % toluene (B6 Precipitate) and thus do not have an adequate inventory of surface-active soluble material. As precipitates accumulate, they become too large and deposit in mass quantities onto oil-water interfaces rather than adsorbing into a cohesive film.

B6 Whole and Precipitate asphaltene mean diameters are shown in Table 3.4. The histogram and photomicrograph of B6 Precipitate in toluene is shown in Figure 3.13. Class 3

emulsions were found to have high emulsion stability in aromatic solvents that became weaker when asphaltene solubility decreased. At the highest solvent aromaticity, both B6 Whole and Precipitate formed the smallest mean droplet diameters. These conditions also promoted strong emulsion formation. B6 Whole asphaltenes formed more stable emulsions near their solubility limit at 60 % toluene with a slightly larger mean droplet diameter. In poor solvents, mean droplet diameters and the distribution skewness increased more significantly while emulsion stabilities decreased.

3.3.5.4 Class 4: CS Whole-Precipitate

The fourth class of emulsion behavior is characterized by low stability because of large aggregate formation rather than high solubility (Figure 3.14). CS Precipitate and Whole asphaltenes form the largest aggregates in heptol. Aggregation is governed by π-π interactions between highly aromatic (low H/C) asphaltene cores. The nitrogen content of these asphaltenes is considerably lower than B6 and HO and may not H-bond well at the oil-water surface. In addition, the Ni and V contents of CS asphaltenes are significantly lower than B6 and HO implying diminished interactions between heavy metal ions and electron pairs in pyrrolic or porphyrin functional groups.

These very large aggregates also present an inventory challenge to interfacial formation. Large aggregate formation implies a reduced number of total surface-active species available in solution. The reduced number and surface activity of the CS Whole and Precipitate asphaltenes leads to the formation of weak emulsions.

Class 4 emulsions were quite weak and had mean droplet diameters larger than the most stable emulsions formed by B6 and HO asphaltenes (Figure 3.15, Table 3.4). While

mean diameters exceeded those of the most stable emulsions, the differences were subtle. Stability after a day of aging, however, varied considerably. The process of droplet coalescence after the initial homogenization ultimately determines emulsion stability. Asphaltene film consolidation and strength are the most important factors in emulsion stability and clearly, CS asphaltenes are poor film formers compared to B6 and HO.

3.4 Conclusions

Asphaltenes from four crude oils were isolated and separated into more and less soluble subfractions in mixtures of heptane and toluene. Emulsions were prepared by high-energy homogenization of asphaltenes dissolved in heptol with water. The chemical differences between an asphaltene and its fractions were often subtle while solubility and emulsion behavior were significant. AH and CS asphaltenes had the lowest H/C ratios, nitrogen concentrations and heavy metal contents. However, AH formed aggregates considerably smaller than CS. It is possible that the monomer molecular weight of CS was greater than that of AH and contributed to the aggregate size discrepancy. B6 and HO asphaltenes were slightly less aromatic but had higher nitrogen and heavy metal contents. They also formed aggregates with correlation lengths intermediate to AH and CS. The Soluble fractions of each asphaltene were characterized by lower H/C ratios, lower polar N content and smaller aggregates compared to the Whole and Precipitate fractions.

Asphaltenes were divided into four classes according to their emulsion stability behavior and exhibited trends in aggregate size, H/C ratio, and N, Ni, and V content. Asphaltenes in Class 1 were quite soluble, aromatic (H/C ratios from 1.12-1.17), and had the lowest N (0.92-1.32%), Ni (19-160 ppm), and V (42-540 ppm) contents. Asphaltene

aggregation was presumed to occur predominantly through π-π interactions between delocalized electrons on adjacent aromatic rings. Low polarity suggested a low degree of hydrogen bonding. These asphaltenes were not capable of forming stable emulsions.

The next class of asphaltenes (B6 Soluble and Whole and Hondo Soluble) formed maximum sized aggregates between 52.3 and 73.8 Å, were less aromatic (higher H/C ratios) and were enriched in N, Ni, and V. These asphaltenes formed very stable emulsions at intermediate heptane-toluene ratios likely because of enhanced polar interactions, such as H-bonding, between asphaltene monomers. A third class of asphaltenes (B6 Whole, Precipitate and HO Precipitate) formed very stable emulsions at the highest solvent aromaticities. Aggregates sizes often exceeded 200 Å and asphaltenes were enriched in N, Ni, and V. Interfacial activity was dominated by the same interaggregate mechanisms as the second class but lower asphaltene solubility shifted the emulsion behavior towards higher aromaticity.

The final class of asphaltenes (Canadon Seco Whole and Precipitate) was the most aromatic with very little N, Ni, and V. Aggregate sizes approached 500 Å and emulsion stability was very low. Large aggregates and low polarity resulted in poor interfacial activity and reduced supply of asphaltenes capable of forming cohesive, H-bond mediated oil-water films.

These asphaltene class distinctions highlight several components necessary or suggested for stable emulsion formation. Moderate aggregate sizes approximately ~60-250 Å spanned the range of stable emulsion formers. However, aggregate size alone was not sufficient to determine emulsion stability. The solubility of an asphaltene or its fractions also played a critical role in the location of maximum emulsion stability. Soluble asphaltenes

tended to form stable emulsions at lower aromaticity than the Whole or Precipitate asphaltenes. Nitrogen, nickel and vanadium concentrations appeared to coincide with emulsions of high stability. These elements likely indicate higher levels of intermolecular bonding or attractive interactions necessary for oil-water film formation particularly H-bonding and electron donor acceptor. While the study of emulsion behavior helps us better understand the role of the various chemistries present in asphaltenes, it is merely one step towards understanding the behaviors of crude oil in its natural state.

3.5 Acknowledgements

This study was funded by grants from the National Science Foundation (CTS-981727), PERF (97-07) and a shared consortium including ExxonMobil, Ondeo-Nalco Energy Systems, Shell Oil Company, and Texaco.

3.6 References

1. Berridge, S.A., M.T. Thew and A.G. Loriston-Clarke, "The Formation and Stability of Emulsions of Water in Crude Petroleum and Similar Stocks," *Journal of the Institute of Petroleum*, 1968, **54** (539): p. 333-357.

2. Blair, C.M., "Interfacial Films Affecting the Stability of Petroleum Emulsions," *Chemistry and Industry*, 1960: p. 538-544.

3. Nellensteyn, F.J., "The Constitution of Asphalt," *Journal of the Institute of Petroleum Technologists*, 1924, **10**: p. 311-325.

4. Pfeiffer, J.P. and R.N.J. Saal, "Asphaltic Bitumen as Colloid System," *Journal of Physical Chemistry*, 1940, **44**: p. 139-149.

5. Lawrence, A.S.C. and W. Killner, "Emulsions of Seawater in Admiralty Fuel Oil with Special Reference to their Demulsification," *Journal of the Institute of Petroleum*, 1948, **34**: p. 281.

6. Denekas, M.O., et al., "Material Adsorbed at Crude Petroleum-Water Interfaces," *Ind. and Eng. Chem.*, 1951, **43** (5): p. 1165-1169.

7. Grace, R., *Commercial Emulsion Breaking*, in *Emulsions: Fundamentals and Applications in the Petroleum Industry*, L.L. Schramm, Editor. 1992, American Chemical Society: Washington, D.C. p. 313-339.

8. van der Waarden, M., "Stability of Emulsions of Water in Mineral Oils Containing Asphaltenes," *Kolloid Z. Z. Polymer*, 1958, **156** (2): p. 116-122.

9. Mackay, G.D.M., et al., "The Formation of Water-in-Oil Emulsions Subsequent to an Oil Spill," *Journal of the Institute of Petroleum*, 1973, **59** (568): p. 164-172.

10. Johansen, E.J., et al., "Water-in-Crude Oil Emulsions from the Norwegian Continental Shelf Part I. Formation, Characterization and Stability Correlations," *Colloids and Surfaces*, 1989, **34**: p. 353-370.

11. Sjöblom, J., et al., "Water-in-Crude Oil Emulsions. Formation, Characterization, and Destabilization," *Progress in Colloid and Polymer Science*, 1990, **82**: p. 131-139.

12. Schramm, L.L., *Petroleum Emulsions: Basic Principles*, in *Emulsions: Fundamentals and Applications in the Petroleum Industry*. 1992, American Chemical Society: Washington, D.C. p. 1-49.

13. Bancroft, W.D., "Theory of Emulsification," *Journal of Physical Chemistry*, 1913, **17**: p. 501.

14. Dodd, C.G., "The Rheological Properties of Films at Crude Petroleum-Water Interfaces," *Journal of Physical Chemistry*, 1960, **64** (5): p. 544-550.

15. Neumann, H., "Investigations Regarding the Separation of Crude Oil Emulsions," *Petrochemie*, 1965, **18**: p. 776-779.

16. Kimbler, O.K., R.L. Reed and I.H. Silberberg, "Physical Characteristics of Natural Films Formed at Crude Oil-Water Interfaces," *Society of Petroleum Engineers Journal*, 1966 (6): p. 153-165.

17. Strassner, J.E., "Effect of pH on Interfacial Films and Stability of Crude Oil-Water Emulsions," *Journal of Petroleum Technology*, 1968, **20**: p. 303-312.

18. Cairns, R.J.R., D.M. Grist and E.L. Neustadter. *The Effect of Crude Oil-Water Interfacial Properties on Water-Crude Oil Emulsion Stability*. in *Theory and Practice of Emulsion Technology*. 1974. Brunel University: Academic Press.

19. Oren, J.J. and G.D.M. MacKay, "Electrolyte and pH Effect on Emulsion Stability of Water-in-Petroleum Oils," *Fuel*, 1977, **56** (10): p. 382-384.

20. Jones, T.J., E.L. Neustadter and K.P. Whittingham, "Water-in-Crude Oil Emulsion Stability and Emulsion Destabilization by Chemical Demulsifiers," *Journal of Canadian Petroleum Technology*, 1978, **17** (2): p. 100-108.

21. Bridie, A.L., et al., "Formation, Prevention and Breaking of Sea Water in Crude Oil Emulsions 'Chocolate Mousses'," *Mar. Pollut. Bull.*, 1980, **11**: p. 343-348.

22. Taylor, S.E., "Resolving Crude Oil Emulsions," *Chemistry and Industry*, 1992, **20**: p. 770-773.

23. Shetty, C.S., A.D. Nikolov and D.T. Wasan, "Demulsification of Water in Oil Emulsions Using Water Soluble Demulsifiers," *Journal of Dispersion Science and Technology*, 1992, **13** (2): p. 121-133.

24. Mitchell, D.L. and J.G. Speight, "The Solubility of Asphaltenes in Hydrocarbon Solvents," *Fuel*, 1973, **52** (4): p. 149-152.

25. Yen, T.F., J.G. Erdman and S.S. Pollack, "Investigation of Structure of Petroleum Asphaltenes By X-Ray Diffraction," *Analytical Chemistry*, 1961, **33** (11): p. 1587-&.

26. Al-Jarrah, M.M.H. and A.H. Al-Dujaili, "Characterization of Some Iraqi Asphalts II. New Findings on the Physical Nature of Asphaltenes," *Fuel Science and Technology International*, 1989, **7** (1): p. 69-88.

27. Acevedo, S., et al., "Asphaltenes and Resins From the Orinoco Basin," *Fuel*, 1985, **64**: p. 1741-1747.

28. Boduszynski, M.M., "Composition of Heavy Petroleums. 2. Molecular Characterization," *Energy & Fuels*, 1988, **2** (5): p. 597-613.

29. Wiehe, I.A. and K.S. Liang, "Asphaltenes, Resins, and other petroleum macromolecules," *Fluid Phase Equilibria*, 1996, **117** (1-2): p. 201-210.

30. McKay, J.F., et al., "Petroleum Asphaltenes: Chemistry and Composition," *Analytical Chemistry of Liquid Fuel Sources, Advances in Chemistry Series*, 1978, **170**: p. 128-142.

31. Andersen, S.I., A. Keul and E. Stenby, "Variation in composition of subfractions of petroleum asphaltenes," *Petroleum Science and Technology*, 1997, **15** (7-8): p. 611-645.

32. Yarranton, H.W. and J.H. Masliyah, "Molar Mass Distribution and Solubility Modeling of Asphaltenes," *AICHE Journal*, 1996, **42** (12): p. 3533-3543.

33. Yarranton, H.W., H. Alboudwarej and R. Jakher, "Investigation of asphaltene association with vapor pressure osmometry and interfacial tension measurements," *Industrial & Engineering Chemistry Research*, 2000, **39** (8): p. 2916-2924.

34. Barbour, R.V. and J.C. Petersen, "Molecular Interactions of Asphalt: An Infrared Study of the Hydrogen-Bonding Basicity of Asphalt," *Analytical Chemistry*, 1974, **46** (2): p. 273-277.

35. Boduszynski, M.M., J.F. McKay and D.R. Latham, "Asphaltenes, Where Are You?," *Proceedings of the Association of Asphalt Paving Technologists*, 1980, **49**: p. 123-143.

36. Ignasiak, T., O.P. Strausz and D.S. Montgomery, "Oxygen Distribution and Hydrogen Bonding in Athabasca Asphaltene," *Fuel*, 1977, **56**: p. 359-365.

37. Moschopedis, S.E. and J.G. Speight, "Investigation of Hydrogen Bonding by Oxygen Functions in Athabasca Bitumen," *Fuel*, 1976, **55**: p. 187-192.

38. Petersen, J.C., "An Infra-red Study of Hydrogen Bonding in Asphalt," 1967: p. 295-305.

39. Sjöblom, J., et al., "Stabilization and Destabilization of Water-in-Crude Oil Emulsions from the Norwegian Continental Shelf. Correlation with Model Systems," *Advances in Colloid and Interface Science*, 1992, **41**: p. 241-271.

40. Fordedal, H., et al., "Crude Oil Emulsions in High Electric Fields as Studied by Dielectric Spectroscopy. Influence of Interaction Between Commercial and Indigenous Surfactants," *Colloids and Surfaces A: Physicochemical and Engineering Aspects*, 1996, **106**: p. 33-47.

41. Mouraille, O., et al., "Stability of Water-in-Crude Oil Emulsions: Role Played by the State of Solvation of Asphaltenes and by Waxes," *J. Dispersion Science and Technology*, 1998, **19** (2&3): p. 339-367.

42. McLean, J.D. and P.K. Kilpatrick, "Effects of asphaltene aggregation in model heptane-toluene mixtures on stability of water-in-oil emulsions," *Journal of Colloid and Interface Science*, 1997, **196** (1): p. 23-34.

43. Acevedo, S., et al., "Isolation and Characterization of Natural Surfactants from Extra Heavy Crude Oils, Asphaltenes, and Maltenes. Interpretation of Their Interfacial Tension-pH Behaviour in Terms of Ion Pair Formation," *Fuel*, 1992, **71** (6): p. 619-623.

44. Acevedo, S., et al., "Interfacial Rheological Studies of Extra-Heavy Crude Oils and Asphaltenes: Role of the Dispersion Effect of Resins in the Adsorption of Asphaltenes at the Interface of Water-in-Crude Oil Emulsions," *Colloids and Surfaces A: Physicochemical and Engineering Aspects*, 1993, **71**: p. 65-71.

45. Mohammed, R.A., et al., "Dewatering of Crude Oil Emulsions 2. Interfacial Properties of the Asphaltic Constituents of Crude Oil," *Colloids and Surfaces A: Physicochemical and Engineering Aspects*, 1993, **80**: p. 237-242.

46. Sheu, E.Y. and M.B. Shields, "Asphaltene Surface Activity at Oil-Water Interfaces," *Society of Petroleum Engineers*, 1995, **28995**: p. 523-532.

47. McLean, J.D., et al., *The Role of Petroleum Asphaltenes in the Stabilization of Water-in-Oil Emulsions*, in *Structures and Dynamics of Asphaltenes*, O.C. Mullins and E.Y. Sheu, Editors. 1998, Plenum Press: New York. p. 377-422.

48. Ovalles, C., et al., "Structure/interfacial activity relationships and thermal stability studies of Cerro Negro crude oil and its acid, basic and neutral fractions," *Fuel*, 1998, **77** (3): p. 121-126.

49. Singh, S., J.D. McLean and P.K. Kilpatrick, "Fused Ring Aromatic Solvency in Destabilizing Water-in-Asphaltene-Heptane-Toluene Emulsions," *Journal of Dispersion Science and Technology*, 1999, **20** (1-2): p. 279-293.

50. Yarranton, H.W., H. Hussein and J.H. Masliyah, "Water-in-hydrocarbon emulsions stabilized by asphaltenes at low concentrations," *Journal of Colloid and Interface Science*, 2000, **228** (1): p. 52-63.

51. Siffert, B., C. Bourgeois and E. Papirer, "Structure and Water-Oil Emulsifying Properties of Asphaltenes," *Fuel*, 1984, **63** (6): p. 834-837.

52. Selucky, M.L., et al., *Structure-Related Properties of Athabasca Asphaltenes and Resins as Indicated by Chromatographic Separation*, in *Chemistry of Asphaltenes*, J.W. Bunger and N.C. Li, Editors. 1981, American Chemical Society: Washington D C. p. 83-118.

53. Hasan, M., M.N. Siddiqui and M. Arab, "Chromatographic Separation and Characterization of Asphaltene Subfractions from Saudi Arabian Crudes," *Fuel*, 1988, **67** (9): p. 1307-1309.

54. Spiecker, P.M. and P.K. Kilpatrick, "Aggregation and solubility behavior of petroleum asphaltenes and their subfractions," *Langmuir, to be submitted*, 2001.

55. Eley, D.D., M.J. Hey and J.D. Symonds, "Emulsions of Water in Asphaltene-Containing Oils .1. Droplet Size Distribution and Emulsification Rates," *Colloids and Surfaces*, 1988, **32** (1-2): p. 87-101.

56. Hansen, C.M., "The Three Dimensional Solubility Parameter - Key to Paint Component Affinities: I. Solvents Plasticizers, Polymers, and Resins," *Journal of Paint Technology*, 1967, **39** (505): p. 104-117.

57. Dodd, C.G., J.W. Moore and M.O. Denekas, "Metalliferous Substances Adsorbed at Crude Petroleum-Water Interfaces," *Industrial and Engineering Chemistry*, 1952, **44** (11): p. 2585-2590.

58. Dunning, H.N., J.W. Moore and M.O. Denekas, "Interfacial Activities and Porphyrin Contents of Petroleum Extracts," *Industrial and Engineering Chemistry*, 1953, **45** (August): p. 1759-1765.

59. Barton, A.F.M., *CRC Handbook of Solubility Parameters and other Cohesion Parameters*. 1983, Boca Raton, Fl: CRC Press.

Table 3.1 Elemental Analysis of Asphaltenes and their Fractions

	H/C			N (wt %)		
Asphaltene	Soluble	Whole	Precipitate	Soluble	Whole	Precipitate
AH	1.17	1.14	1.13	0.92	1.02	1.08
B6	1.30	1.24	1.22	1.81	1.87	1.93
CS	1.12	1.11	1.09	1.32	1.32	1.39
HO	1.30	1.29	1.24	1.95	1.99	2.11

Table 3.2 Hansen Solubility Parameters[59]

Solvent	Hansen $(mJ\ m^{-3})^{½}$			
	δ_d	δ_p	δ_h	δ_t
n-Heptane	15.3	0.0	0.0	15.3
Toluene	18.0	1.4	2.0	18.2

Table 3.3 Emulsion Stability Classes and Asphaltene Characteristics

Class	Asph	Fraction	Solubility Limit (% Toluene)	ξ (Å)	H/C	N (wt%)	Ni (ppm)	V (ppm)
1	AH	Sol	38	34.5	1.17	0.92	84	350
		Whole	48	67.3	1.14	1.02	160	490
		Ppt	60	130	1.13	1.08	160	540
	CS	Sol	40	138	1.12	1.32	19	42
2	HO	Sol	45	52.3	1.30	1.95	340	930
		Whole	52	72.8	1.29	1.99	360	950
	B6	Sol	42	62.7	1.30	1.81	350	1000
3	B6	Whole	52	97.6	1.24	1.87	330	1000
		Ppt	90	262	1.22	1.93	410	1200
	HO	Ppt	80	200	1.24	2.11	410	1100
4	CS	Whole	50	246	1.11	1.32	21	48
		Ppt	70	520	1.09	1.39	28	48

Table 3.4 Emulsion Stability Classes and Sauter Mean Droplet Diameters (d_{32}). d_{32} determined from photomicrography immediately following homogenization. Volume % water resolved measured only on emulsion examined by optical microscopy.

Class	Asph	Fraction	(% Toluene)	d_{32} (μm) (0 hrs)	Skewness about origin	% Water Resolved (24 hrs)
1	CS	Sol	50	11.1	406	73
2	B6	Sol	20	10.9	317	62
			60	8.2	191	40
			100	9.0	249	80
	HO	Whole	60	7.8	183	18
			100	5.7	74.5	50
3	B6	Whole	20	10.2	280	68
			60	7.4	166	25
			100	7.1	81.3	27
		Ppt	50	9.2	224	33
			70	7.9	129	25
			100	7.5	136	18
	HO	Ppt	90	5.4	62.7	33
4	CS	Whole	45	8.0	218	45
			60	9.6	202	80
		Ppt	50	9.0	235	43
			70	8.1	157	52

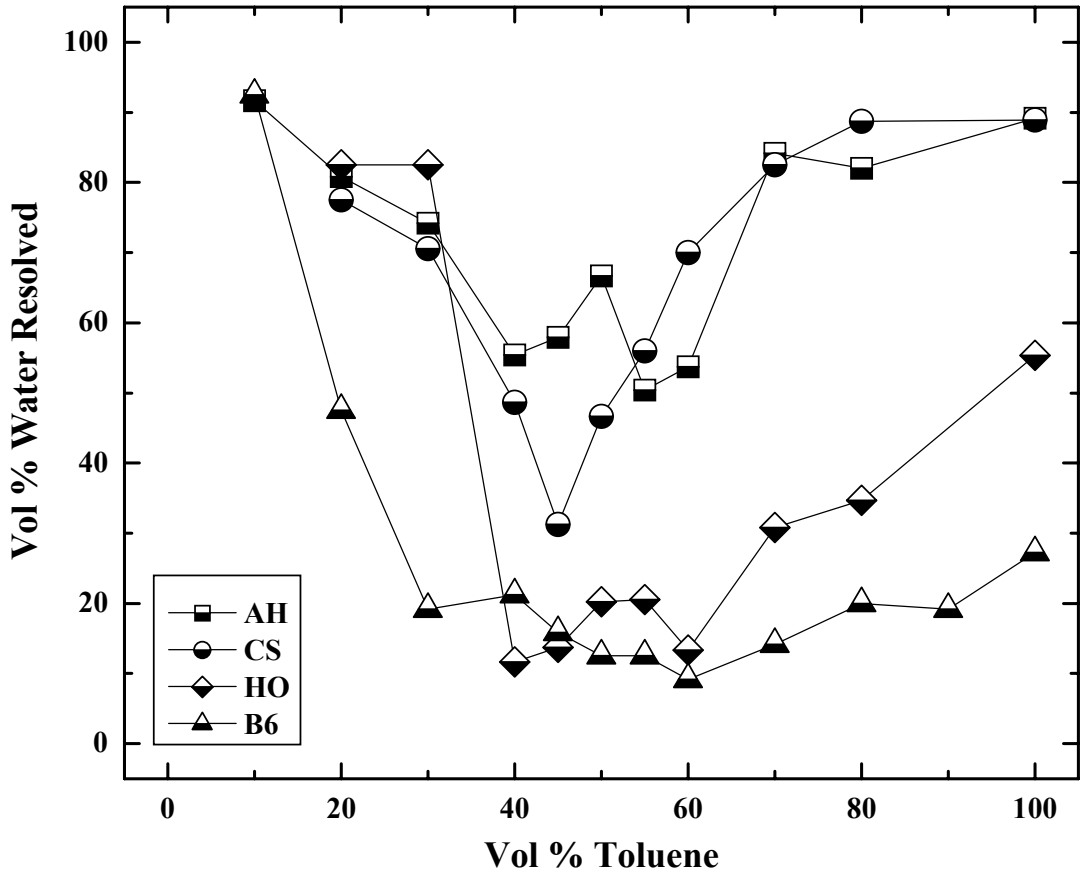

Figure 3.1 Emulsion stability of Whole asphaltenes in heptol at 0.37 % (w/v). Emulsion systems contain 40 % (v/v) water and 60 % (v/v) model oil. Error bars removed for clarity.

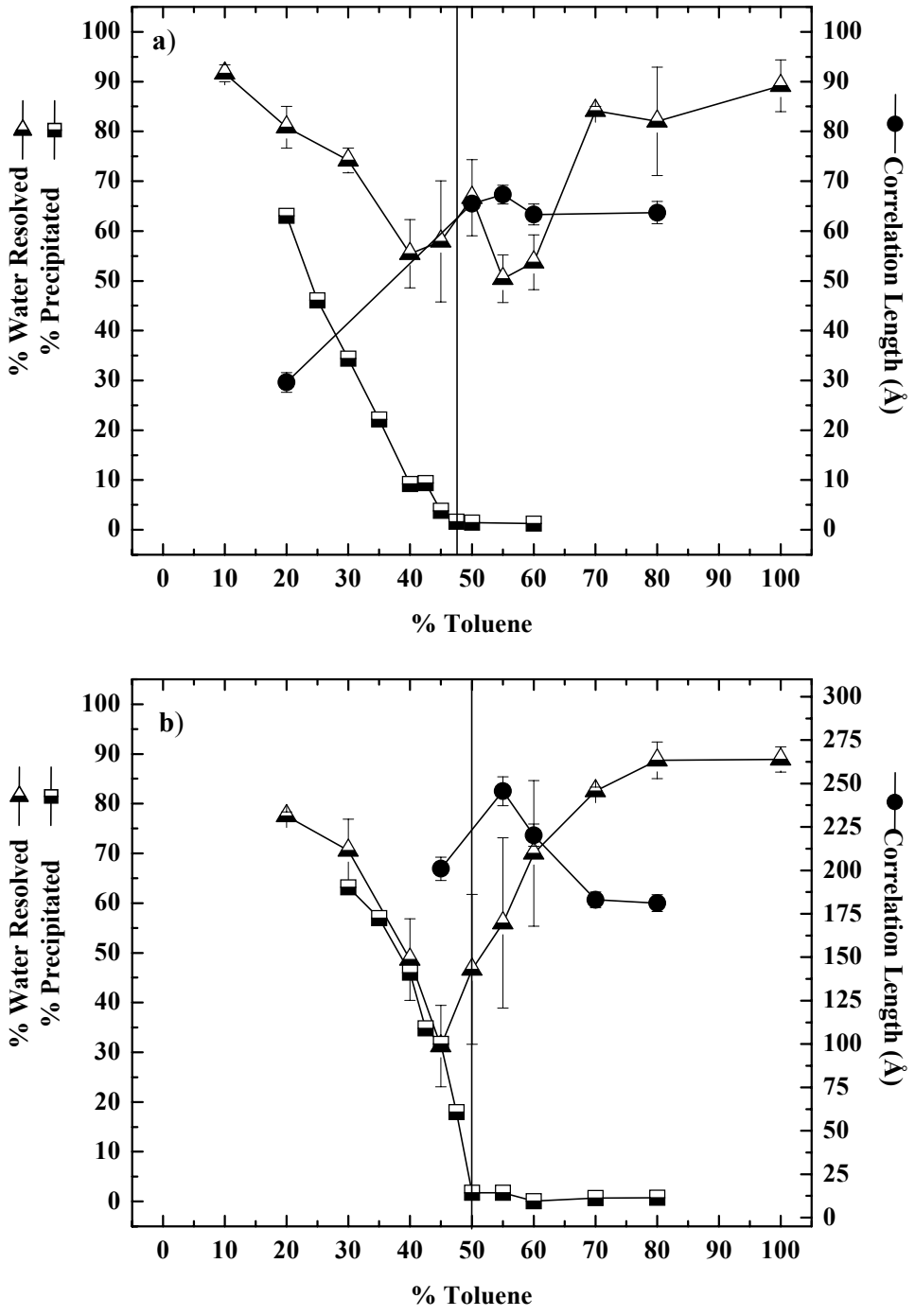

Figure 3.2 Emulsion stability of Whole asphaltenes in heptol at 0.5 % (w/w) determined as % Water Resolved (v/v). Solubility measured by filtration of 1.0 % (w/w) asphaltenes in heptol as % Precipitated (w/w). Aggregate sizes from SANS of 1.0 % (w/w) in deuterated heptol at 25°C as determined by non-linear least squares regression.

a) AH
b) CS

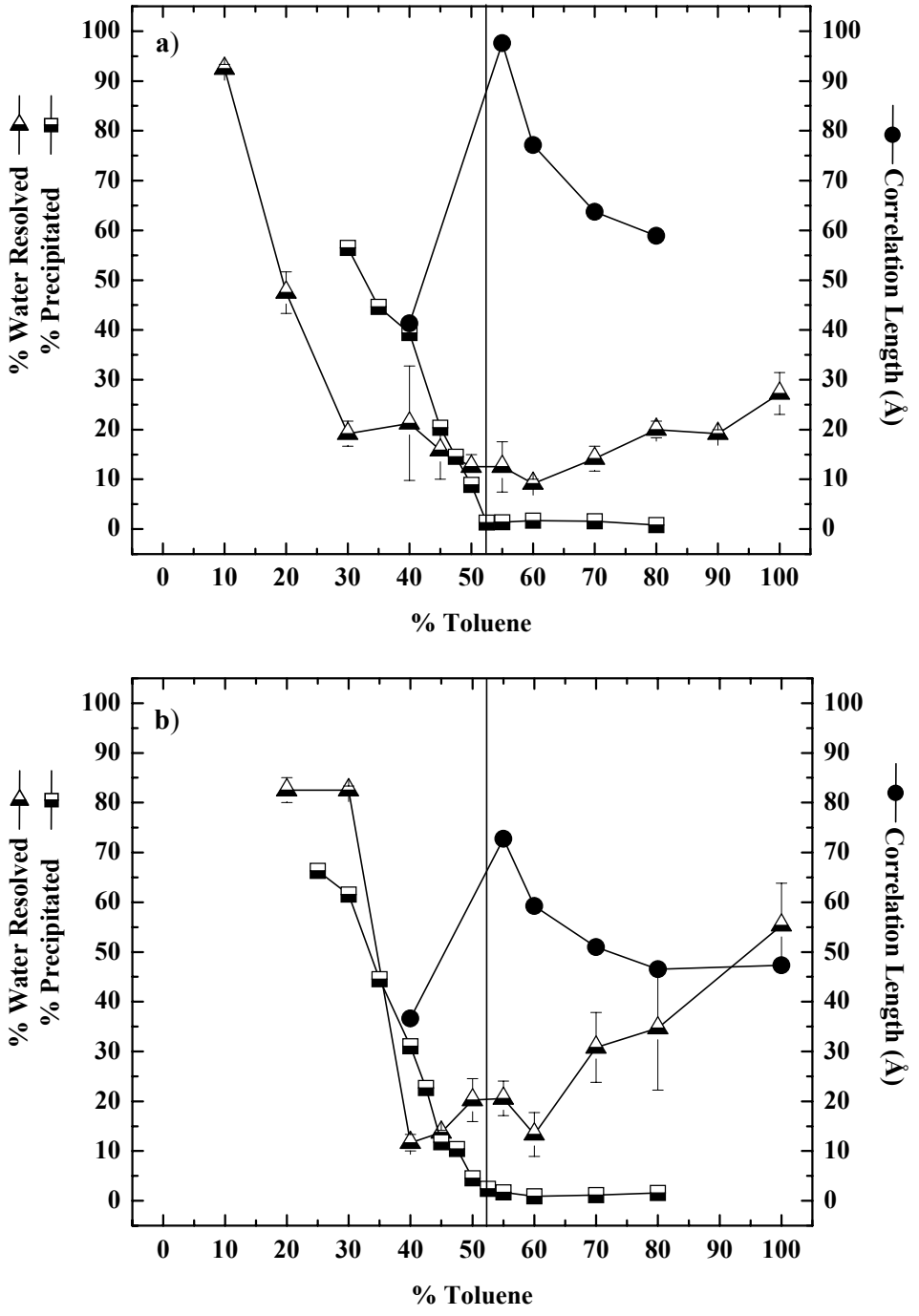

Figure 3.3 Emulsion stability of Whole asphaltenes in heptol at 0.5 % (w/w) determined as % Water Resolved (v/v). Solubility measured by filtration of 1.0 % (w/w) asphaltenes in heptol as % Precipitated (w/w). Aggregate sizes from SANS of 1.0 % (w/w) in deuterated heptol at 25°C as determined by non-linear least squares regression.

a) B6
b) HO

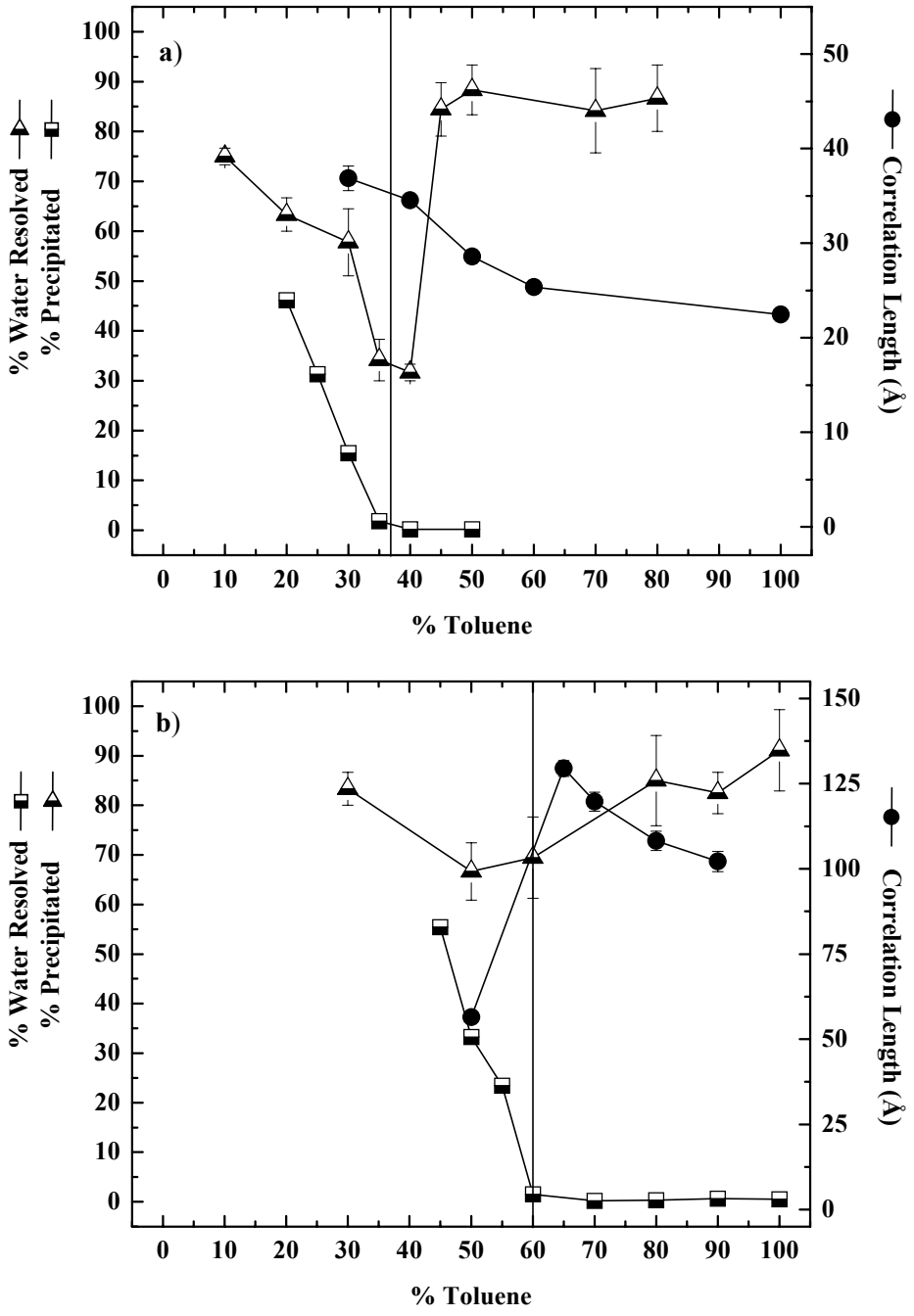

Figure 3.4 Emulsion stability of AH asphaltenes in heptol at 0.5 % (w/w) determined as % Water Resolved (v/v). Solubility measured by filtration of 1.0 % (w/w) asphaltenes in heptol as % Precipitated (w/w). Aggregate sizes from SANS of 1.0 % (w/w) in deuterated heptol at 25°C as determined by non-linear least squares regression.

a) Soluble
b) Precipitate

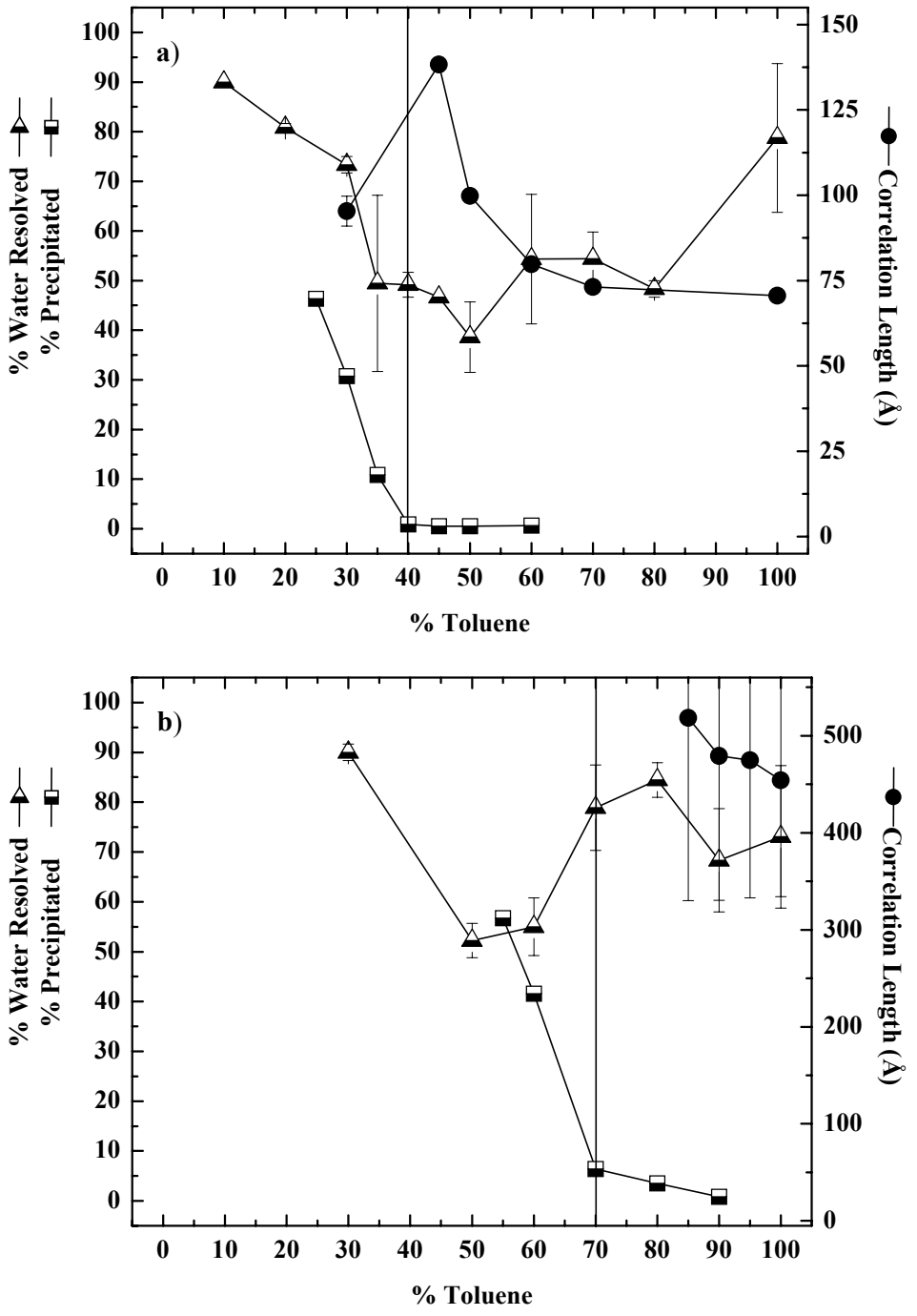

Figure 3.5 Emulsion stability of CS asphaltenes in heptol at 0.5 % (w/w) determined as % Water Resolved (v/v). Solubility measured by filtration of 1.0 % (w/w) asphaltenes in heptol as % Precipitated (w/w). Aggregate sizes from SANS of 1.0 % (w/w) in deuterated heptol at 25°C as determined by non-linear least squares regression.

a) Soluble
b) Precipitate

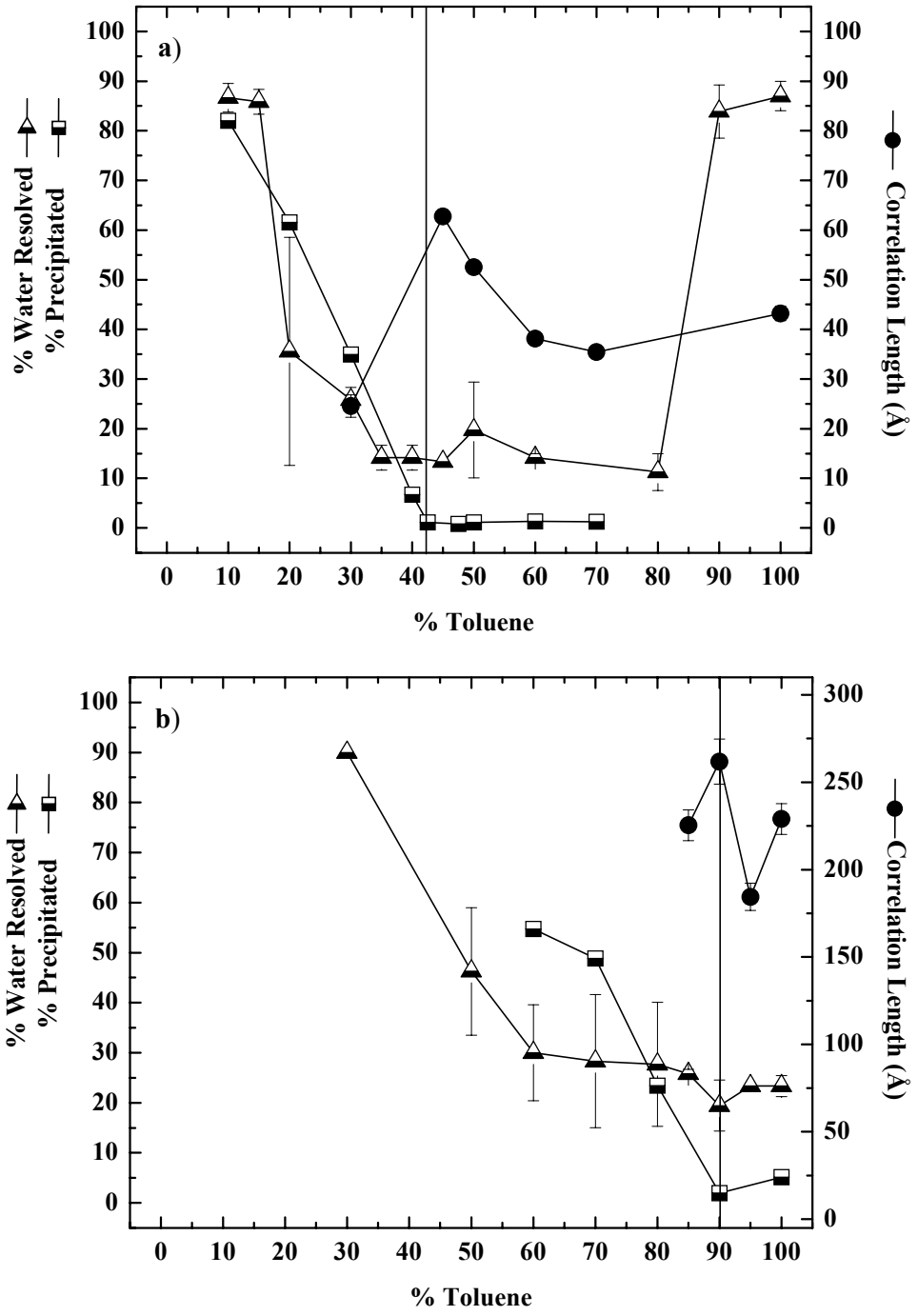

Figure 3.6 Emulsion stability of B6 asphaltenes in heptol at 0.5 % (w/w) determined as % Water Resolved (v/v). Solubility measured by filtration of 1.0 % (w/w) asphaltenes in heptol as % Precipitated (w/w). Aggregate sizes from SANS of 1.0 % (w/w) in deuterated heptol at 25°C as determined by non-linear least squares regression.

a) Soluble
b) Precipitate

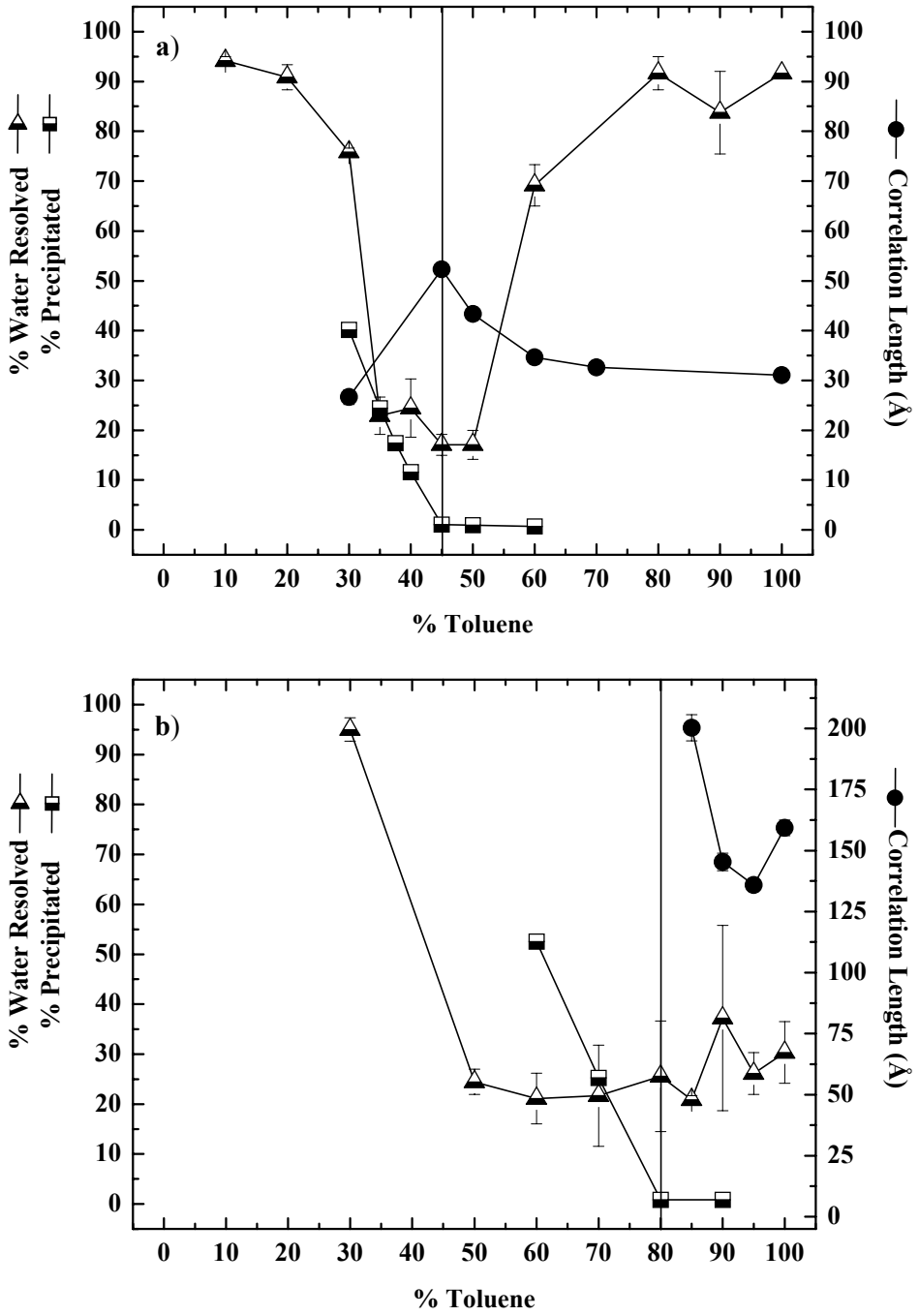

Figure 3.7 Emulsion stability of HO asphaltenes in heptol at 0.5 % (w/w) determined as % Water Resolved (v/v). Solubility measured by filtration of 1.0 % (w/w) asphaltenes in heptol as % Precipitated (w/w). Aggregate sizes from SANS of 1.0 % (w/w) in deuterated heptol at 25°C as determined by non-linear least squares regression.

a) Soluble
b) Precipitate

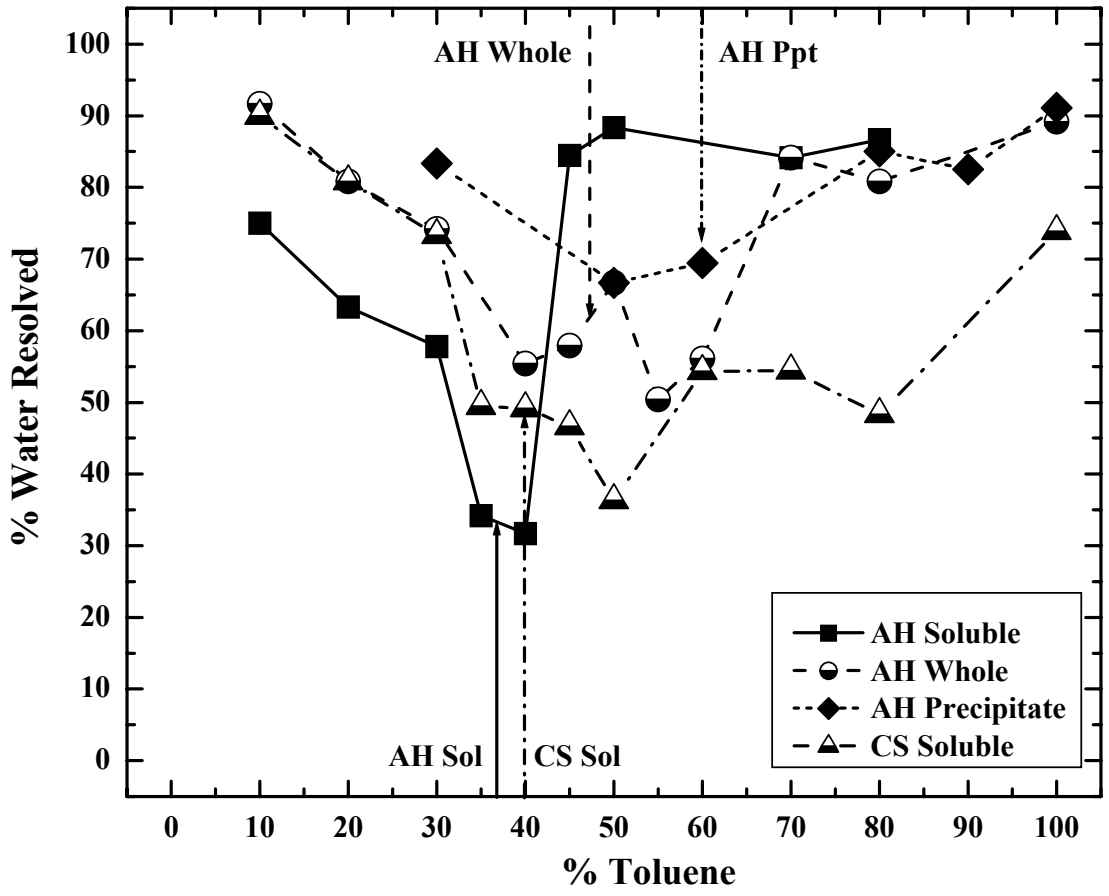

Figure 3.8 Class 1 emulsion behavior. Emulsion conditions identical to previous figures. Vertical lines represent solubility limits of asphaltenes to which they point.

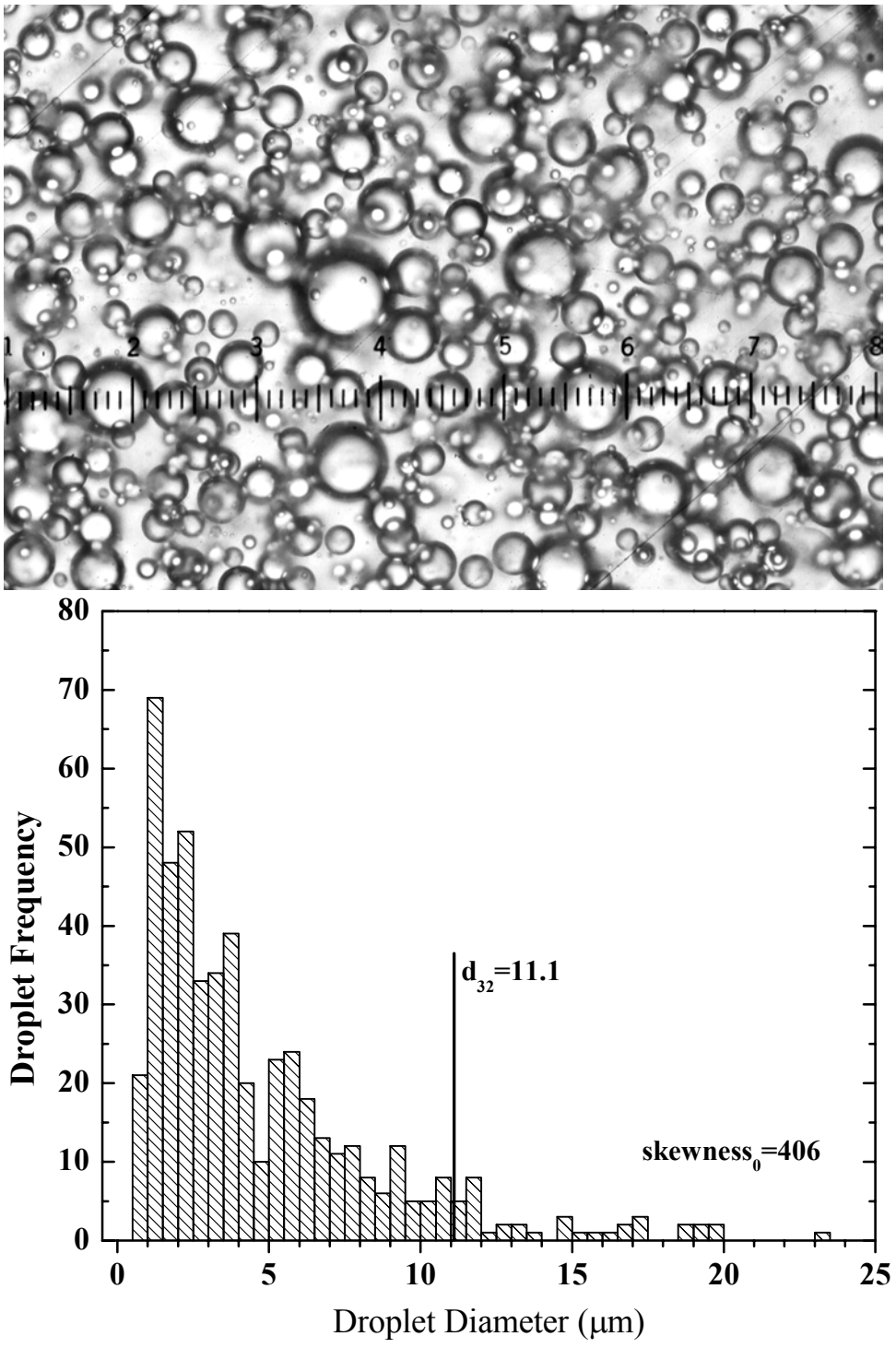

Figure 3.9 Class 1 emulsion former CS Soluble in heptol (50 % toluene). Emulsion resolved 73 % of water after 24 hours following centrifugation. Frequency distributions are the sum of two distributions from two different photographs. Emulsion diluted in five parts mineral oil. *skewness*$_0$ is skewness about the origin. Each minor division on photomicrograph is equal to 3.57 μm.

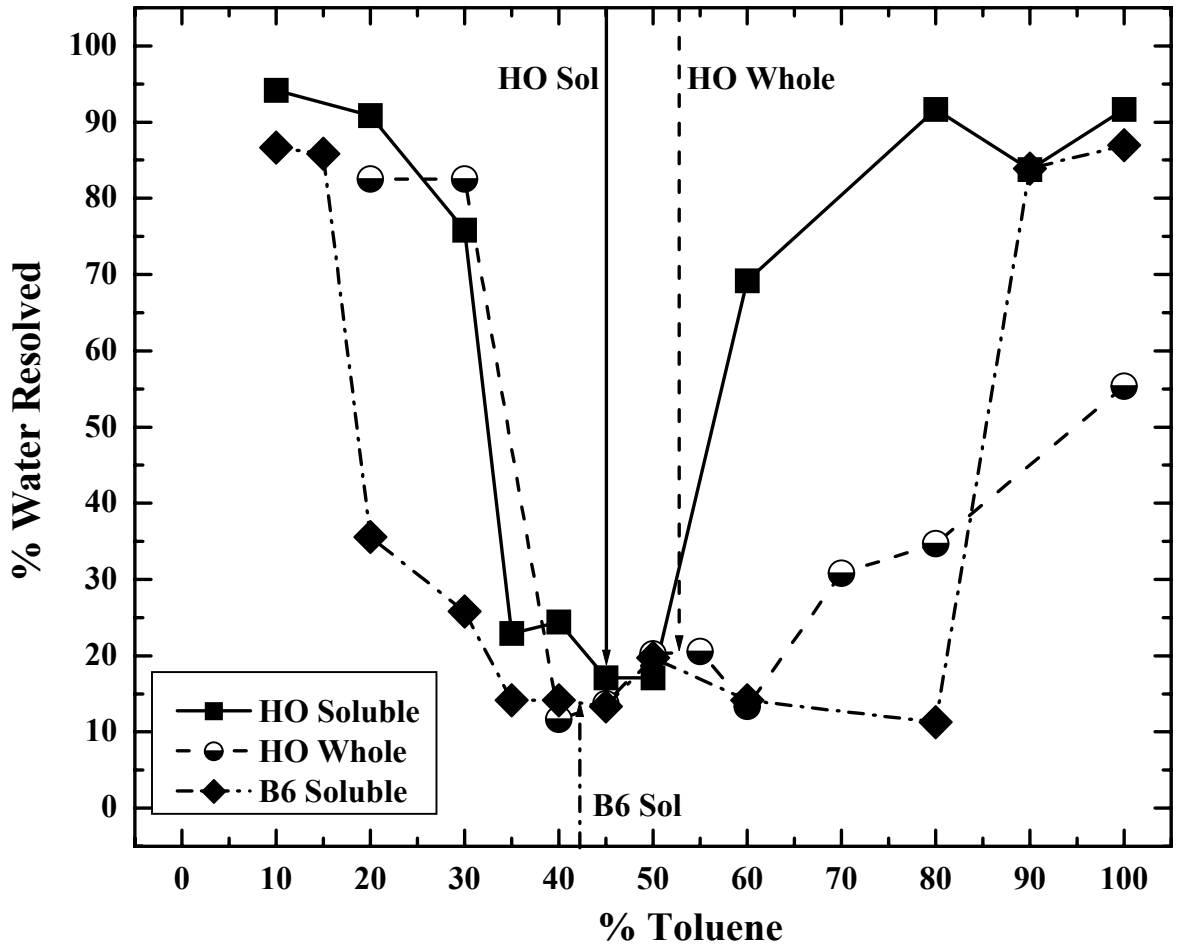

Figure 3.10 Class 2 emulsion behavior. Emulsion conditions identical to previous figures. Vertical lines represent solubility limits of asphaltenes to which they point.

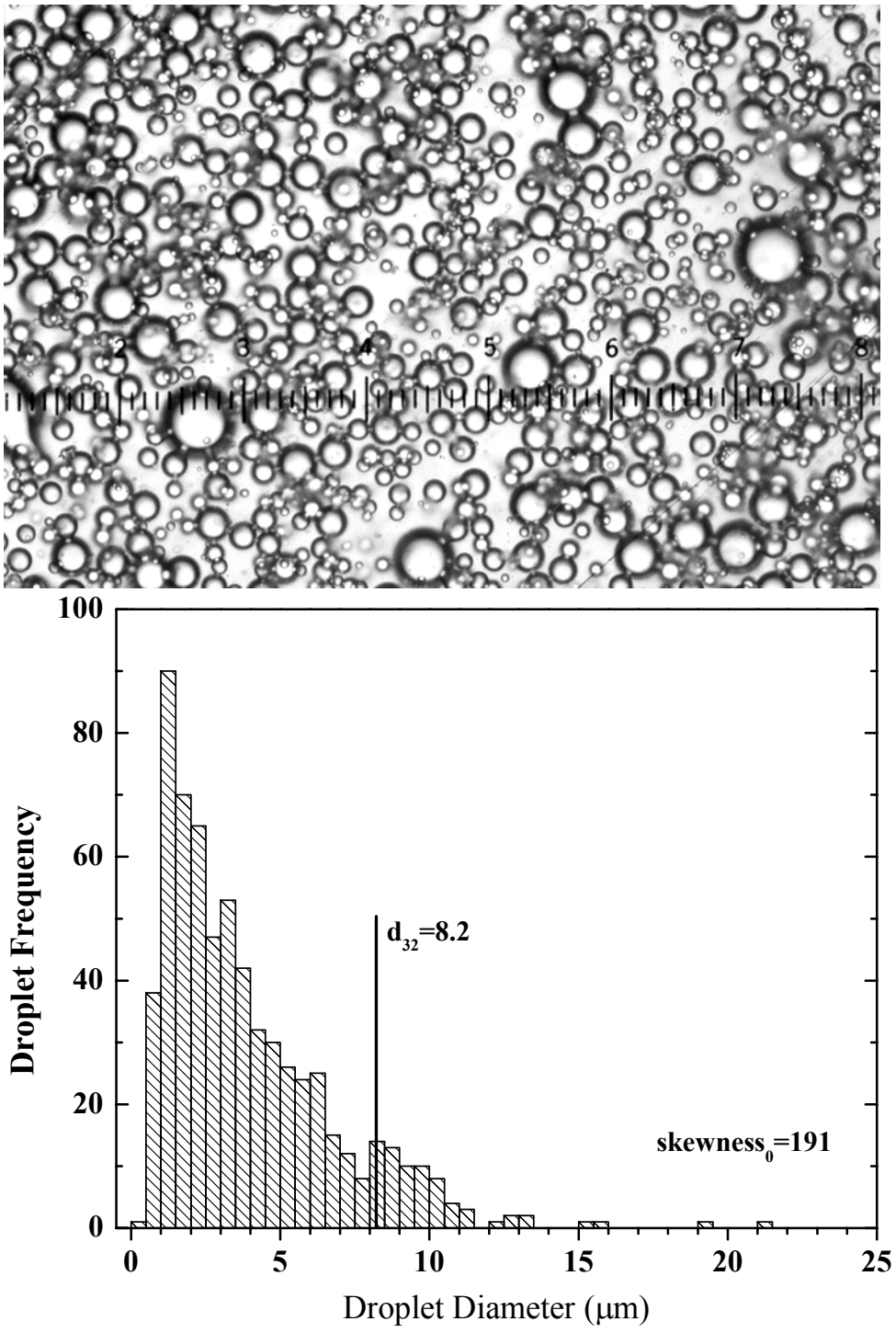

Figure 3.11 Class 2 emulsion former B6 Soluble in heptol (60 % toluene). Emulsion diluted in five parts mineral oil. 40 % water resolved.

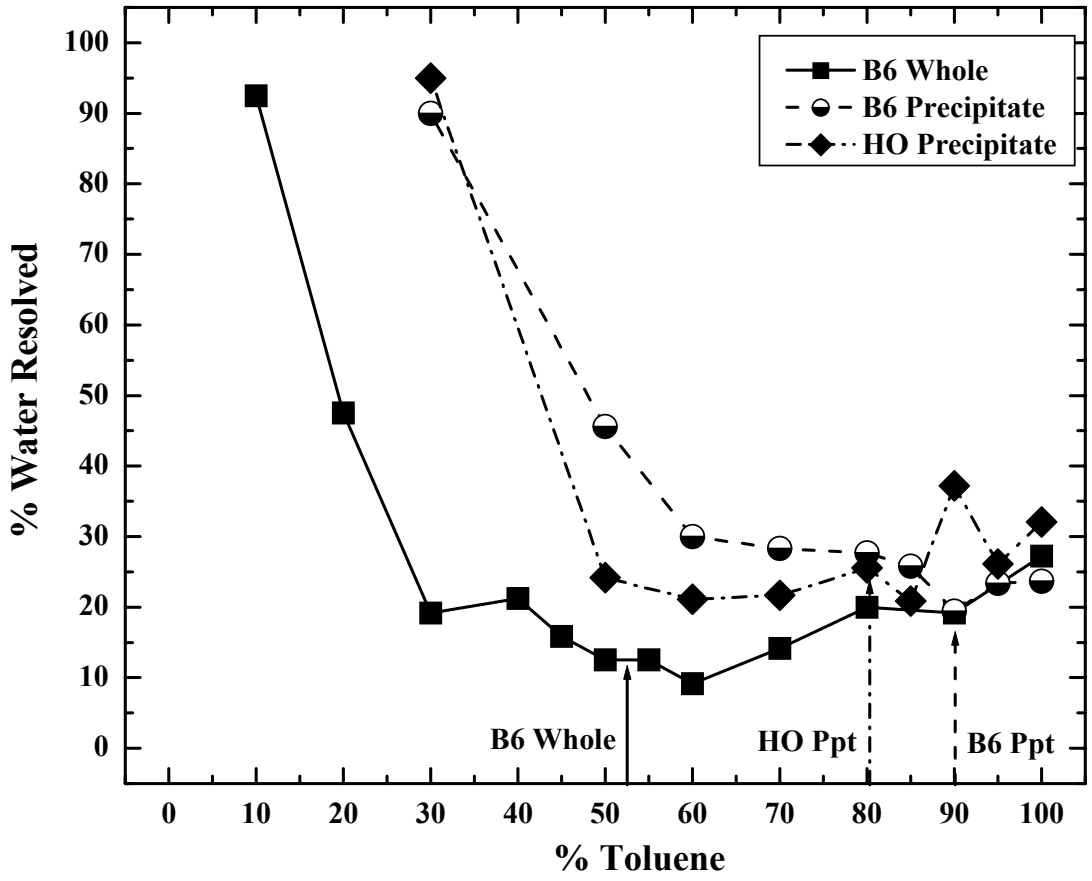

Figure 3.12 Class 3 emulsion behavior. Emulsion conditions identical to previous figures. Vertical lines represent solubility limits of asphaltenes to which they point.

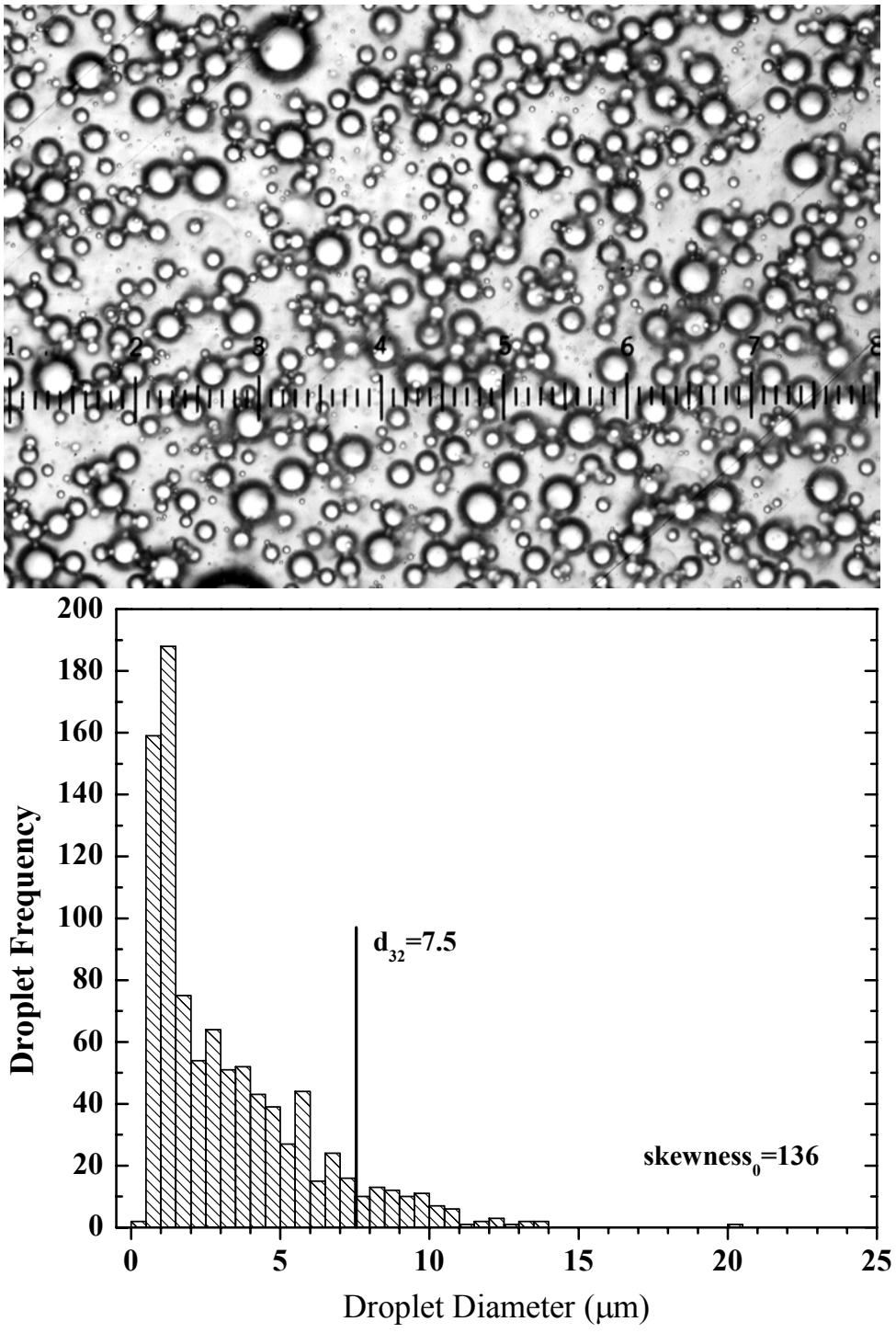

Figure 3.13 Class 3 emulsion former B6 Precipitate in toluene. Emulsion diluted in five parts mineral oil. 18 % water resolved.

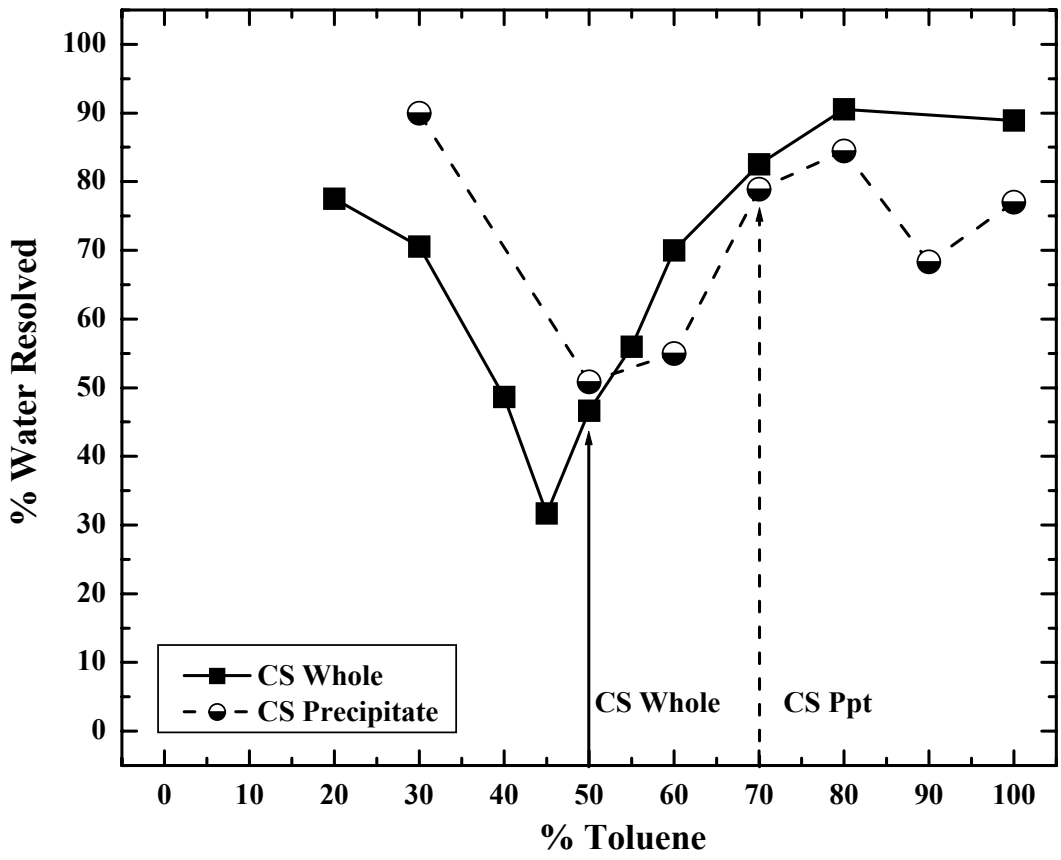

Figure 3.14 Class 4 emulsion behavior. Emulsion conditions identical to previous figures. Vertical lines represent solubility limits of asphaltenes to which they point.

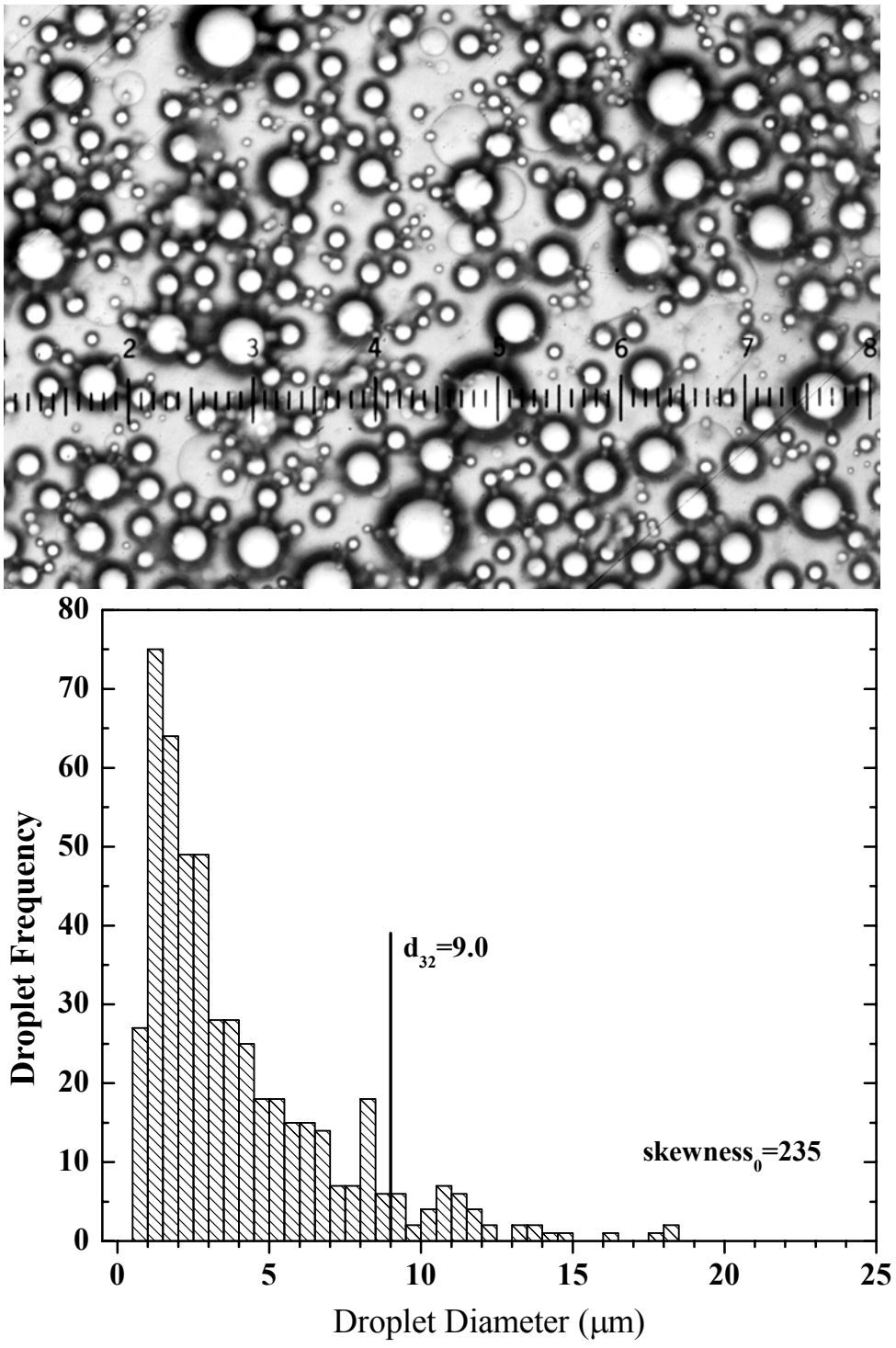

Figure 3.15 Class 4 emulsion former CS Precipitate in heptol (50 % toluene). Emulsion diluted in five parts mineral oil. 43 % water resolved.

Effects of Resins on Asphaltene Aggregation and Water-in-Oil Emulsion Formation

P. Matthew Spiecker, Chad B. Trail, and Peter K. Kilpatrick

ABSTRACT

Asphaltenes from four crude oils were fractionated by differential solubility in mixtures of heptane and toluene. Solubility profiles generated in the presence of resins (1:1 mass ratio) indicated the onset of asphaltene precipitation occurred at lower toluene volume fractions (0.1-0.2) than without resins. Small angle neutron scattering was performed on asphaltenes and their more and less soluble fractions at 80°C resin-asphaltene ratios from 0.5-10:1. Non-linear least squares regression of scattering intensities using Ornstein-Zernike formalism indicate that unfractionated asphaltenes reach a minimum sized aggregate with correlation length of ~20 Å. This aggregate dimension was achieved in pure toluene and heptane-toluene mixtures with a toluene volume fraction of 0.6. Resins likely solvate asphaltene aggregates by disrupting the π-π and polar bonding interactions between asphaltene monomers. Comparisons between the stability of water-in-oil emulsions formed with asphaltenes and resins and the degree of aggregation suggests that aggregates of maximum dimension form the most stable emulsions. In the soluble regime, resins solvate asphaltene aggregates and render them less interfacially active.

Emulsions were prepared with asphaltenes and resins above and below the limit of asphaltene solubility in heptane-toluene mixtures. Emulsions formed with asphaltenes at high aromaticities (depending on asphaltene fraction) were destabilized by resin addition. At low aromaticities (≤ 30 % toluene), asphaltenes were poorly solvated without resins and did not form stable emulsions. Increasing the resin-asphaltene ratio to 5 or 10:1 of the less

soluble asphaltene fractions significantly enhanced emulsion stability (< 20 vol % water resolved). Higher R/A (≥ 20) led to emulsions with partial stability (40-80 % water resolved).

CHAPTER 4

EFFECTS OF RESINS ON ASPHALTENE AGGREGATION AND WATER-IN-OIL EMULSION FORMATION

4.1 Introduction

Emulsion challenges during petroleum recovery have been attributed to colloidal aggregation of asphaltenes and waxes[1-6]. Many early studies were performed on the film forming and emulsifying behavior of crude oil-water systems.[1, 7-15] These and later studies often pointed to the asphaltenic constituents in crude oil as being responsible for film formation and stabilization.[10, 11, 16, 17]

Asphaltenes, or *n*-heptane insolubles and toluene solubles[18, 19], are the most refractory compounds present in crude oil and are generally distinguished by a fused aromatic core with polar heteroatom functionality. Studies indicate the presence of carboxylic acids, carbonyls, phenols, pyrroles and pyridinic functional groups[20-24] capable of accepting or donating protons. Vapor pressure osmometry measurements suggest number average molecular weights range from ca. 800 to 3000 Daltons.[25-32] Lower molecular weights are often measured in hot, polar solvents indicating the presence of aggregates formed through stacking interactions between asphaltene monomers. The most plausible mechanisms of asphaltene aggregation involve π-π overlap between aromatic sheets, hydrogen bonding between functional groups and other charge transfer interactions.

Small angle neutron scattering (SANS) has been applied to probe solvent and temperature effects on asphaltene aggregation.[33-44] Proper analysis of the scattering intensity curves can provide aggregate radius of gyration, shape and dimension. Asphaltenic aggregates are comprised of cofacial stacks of flat, fused aromatic ring monomers with

aliphatic side chains. The most likely shape of these aggregates is a flat disk or cylinder with a large diameter to thickness ratio. To date, mono- and polydisperse spheres [35, 45], flat disks [37, 46, 47], and prolate cylinders [38] have all been suggested as possible asphaltene structures; the degree of polydispersity of asphaltenes makes the precise shape difficult to discriminate. Overfield et al. measured the radius of gyration (R_g) of vacuum resid asphaltenes in deuterated toluene at several temperatures. R_g decreased from 116 Å at 25°C to 55 Å at 100°C and explained this in terms of dissociation rather than a conformational change. Aggregate size changes caused by temperature variation were, however, reversible.[47]

While the effects of temperature, solvent aromaticity, and polarity have received much attention, the solvation of asphaltene aggregates by resins has not been fully explored. Espinat et al. measured the scattered intensity from asphaltenic aggregates in several solvents, at low and high temperatures and with resins.[37] Scattered intensity was fit using a thin disc form factor model. In toluene, 2 wt % Boscan asphaltene solutions formed larger aggregates at room temperature (234 Å diameter) than at 76°C (175 Å). At room temperature, aggregates sizes were 2-4 times smaller in high polarity solvents such as pyridine and tetrahydrofuran than benzene. They also found that resin-asphaltene ratios of 2:1 by mass reduced the scattering intensity at low Q suggesting the formation of smaller aggregates. However, the effect of resin solvation on asphaltene aggregate size was not explicitly reported. Bardon et al. explored the solvating effect of resins on Safaniya asphaltene aggregates by SANS and SAXS.[46] Comparisons of scattering curves for asphaltene-resin systems to pure asphaltene and pure resin systems indicated solvation of

asphaltenes by resins. Weight average molecular weights of 2 wt % asphaltene solutions with R/A ratios of 2, 4, and 8:1 were reduced by factors of 2.6, 4.6, and 7.5 respectively.

In earlier studies [44, 48] we examined the aggregation and emulsion stabilizing behavior of asphaltenes and their more and less soluble fractions in mixtures of heptane and toluene (heptol). Gravimetric solubility measurements indicated that asphaltenes start to precipitate at concentrations between 45 and 52 % (v/v) toluene in heptol. Precipitation concentrated the most polar and aromatic constituents as measured by H/C ratio and nitrogen content. In addition, SANS indicated that the less soluble fraction formed the largest aggregates in heptol and the more soluble fraction formed aggregates considerably smaller. As van der Waarden found in 1958 [49], asphaltenes stabilized emulsions near the point of incipient flocculation. This held for each asphaltene and their fractions. The degree of aggregation and proximity to the solubility limit governed the stability of emulsions prepared in heptol.

In this study, we have taken another step towards understanding the mechanisms of asphaltene aggregation and emulsion formation in petroleum and petroleum-derived systems through the addition of solvating molecules. When characterizing crude oils we often refer to SARA fractionation where asphaltenes are removed by precipitation with a paraffinic solvent and the deasphalted oil (DAO or maltenes) is separated into saturates, aromatics and resins by chromatographic separation.[50-54] After asphaltenes, resins are the most polar and aromatic species in crude oil and, it has been suggested, contribute to the overall solubility of asphaltenes in crude oil by creating a strongly solvating layer on the polar and aromatic portions of the asphaltenic aggregates.[25, 55, 56] The solubility of asphaltenes in crude oil is mediated largely by resin solvation and thus resins play a critical role in

precipitation, and emulsion stabilization phenomena.[37, 40, 57-59] Resins, although quite surface-active, have not been found to stabilize water-in-oil emulsions by themselves in model systems.[60, 61] However, the presence of resins in solution can destabilize emulsions via asphaltene solvation and/or replacement at the oil-water interface.[61-65]

Here we probe the effects of resins on asphaltene aggregation and emulsion formation. Aggregation is likely controlled by the ability of asphaltene monomers to stack through aromatic and polar interactions. By fractionating asphaltenes into solubility classes, the most polar and aromatic species can be concentrated. The effectiveness of solvating resins on these more and less soluble asphaltenes will aid in elucidating the mechanisms of colloid formation and emulsion stabilization in petroleum derived fluids.

4.2 Experimental

4.2.1 Asphaltene Precipitation and Fractionation

Asphaltenes were precipitated from four crude oils in a 40:1 excess of *n*-heptane. The crude oils were obtained from several locations around the world: B6 and Hondo (off-shore California), Arab Heavy (Safaniya), and Canadon Seco (Argentina). These crude oils are asphaltene rich and vary in viscosity, resin content and asphaltene H/C ratio. Basic crude oil and asphaltene properties can be found in Table 4.1. Resin content was determined by sequential elution chromatography (discussed in the next section), H/C ratios were calculated from combustion elemental analysis (Perkin Elmer Series II CHNSO), and viscosity measurements were performed on a Rheometrics Dynamic Stress Rheometer with concentric cylinder geometry. Asphaltenes precipitated from the crude oils were then separated into more and less soluble fractions by dissolving in toluene and inducing partial precipitation

through heptane addition. (See Table 4.2) The heptane:toluene ratio (v/v) was chosen to generate approximately 33 % (w/w) insoluble asphaltenes from a 0.75 % (w/v) asphaltene solution. All solvents were HPLC grade and obtained from Fisher Scientific. Details of the precipitation and fractionation procedures can be found in a previous publication.[44]

4.2.2 SARA Fractionation

Petroleum resins were isolated via the SARA technique where DAO, or the so-called maltenes fraction, is charged to silica gel or clay and extracted with solvents of increasing polarity.[50-52, 66] After a two stage asphaltene filtration to ensure complete removal, the heptane-diluted crude oil was rotary evaporated until dry. The DAO was dissolved in methylene chloride (Fisher-HPLC grade) and adsorbed to activated silica gel (Chromatographic silica gel, 35-60 mesh, Fisher). Silica gel activation proceeded under vacuum at 120°C for 48 hours. The silica gel-DAO slurry was shaken for 24 hours then rotary evaporated until dry and placed in a nitrogen flushed vacuum oven at 50°C for 24 hours.

Chromatography columns (2 cm x 100 cm with 250 mL solvent reservoir) were initially filled with a mixture of 68:32 heptane-toluene (v/v). Then, clean activated silica gel was added until the depth reached ~20 cm. Finally, silica gel with adsorbed DAO was transferred to the column until full. A solvent mixture containing 68 % (v/v) heptane and 32 % (v/v) toluene eluted saturates, mono-, di-, and triaromatics from the silica gel. Once the saturates and aromatics were extracted a more polar solvent (40:30:30 acetone-toluene-methylene chloride) was eluted to obtain the resins. The resin-solvent mixture was filtered to remove any silica gel fines and rotary evaporated until dry. The resins were transferred to

jars and placed in a nitrogen flushed vacuum oven at 60°C for 48 hours until completely dry. Combustion elemental analyses of the resins appear in Table 4.3.

4.2.3 Asphaltene and Resin Solubility

The solubility of asphaltenes and their subfractions were determined in heptol with resins. Resins from the crude oil were only added to their complementary asphaltenes. Solubility profiles of the asphaltenes without resins were obtained previously [44] and will be used for comparison. Resin-asphaltene solutions were prepared in heptol at varying heptane-toluene ratios. The asphaltene concentration was 0.75 % w/v (~1 wt %) in 15 mL solvent and the resin-asphaltene ratio was 1:1 by mass. Resins and asphaltenes were dissolved toluene in the same jar for 12 hours followed by heptane addition. After an additional 12 hours, the solutions were vacuum filtered through 1.5 μm Whatman 934 AH filter paper to collect precipitates and rinsed with 7.5 mL of heptol at the same toluene volume fraction. To ensure all of the resins were removed, the precipitate was rinsed with neat heptane prior to dissolution in methylene chloride. The % precipitated was determined from the mass ratio of precipitated asphaltenes to the original asphaltene mass.

4.2.4 Small Angle Neutron Scattering

Neutron scattering of asphaltenic aggregates solvated by resins and other dopants was performed at NIST in Gaithersburg, MD on the NG7 (30 m) beam line. Mixtures of asphaltenes and resins were prepared at resin:asphaltene (R/A) ratios between 0.25 and 10:1. Asphaltene solutions (1 wt %) were prepared in perdeuterated heptane and toluene solutions (CDN Isotopes, Canada) and studied at 25 and 80°C. Scattering intensity versus scattering

angle (I(Q) vs. Q) data were fit to Lorentzian line shapes using a non-linear least squares regression to determine the aggregate correlation lengths. Following Ornstein-Zernicke formalism the scattering intensity, *I*, can be related to the scattering vector, *Q*, by:

$$I(Q) = \frac{I_0}{1+(Q\xi)^2} + A \tag{1.1}$$

where ξ is the correlation length and *A* is a background correction factor.[42, 67] This Lorentzian line shape form was applied to systems with characteristic scattering curves that plateaued at low Q. In the other systems scattering intensity increased monotonically with decreasing Q. A power law term was necessary to account for these large agglomerates in solution. Also, the natural logarithm of the scattering intensity expression was taken to reduce the bias towards the Q regions containing a high density of data points. The functional form of this equation is:

$$\ln\left[I(Q)\right] = \ln\left[\frac{I_1}{Q^4} + \frac{I_0}{1+(Q\xi)^2} + A\right] \tag{1.2}$$

Further details are described elsewhere.[44]

4.2.5 Resin-Asphaltene Emulsions

Water-in-oil emulsions were prepared by homogenizing water and model oil solutions containing asphaltenes and resins. Asphaltenes and resins were dissolved together in toluene for approximately 12 hours followed by heptane addition. 4 mL of this solution with an asphaltene concentration of 0.37 % w/v (~0.5 % w/w), were homogenized with 6 mL of deionized water. A Virtis Virtishear Cyclone I.Q. homogenizer with a 6 mm rotor-stator

emulsion generator assembly was lowered into the oil-water system and run at 15,000 rpm for 3 minutes.

After 24 hours, the emulsions were centrifuged for 1 hour at 15,000 rpm. The stability of the emulsions was calculated from the volume of water resolved:

$$\%\ Water\ resolved = \frac{Volume\ resolved}{6\ ml}\ X\ 100$$

Complete details on solution preparation and homogenization can be found elsewhere.[48]

4.3 Results and Discussion

4.3.1 Asphaltene-Resin Solubility:

The effect of adding resins (1:1 mass ratio) on asphaltene solubility is shown in Figures 4.1 a-d. The half filled markers represent solubility data determined for asphaltenes in neat heptol while the filled markers represent asphaltene solubility with resins. As mentioned before, the Whole asphaltene solubility limits were approximately 50 % toluene. Soluble asphaltenes precipitated at volume fractions between 0.3-0.4 while Precipitate asphaltenes precipitated at considerably higher aromaticity (0.6-0.8). This suggests that the Soluble fraction cooperatively solvates the Precipitate fraction in solution.

The process of fractionation generated unique asphaltene classes distinguished by their solubility behavior. We found that the Precipitate fractions were characterized by higher aromaticity, polarity, molecular weight, and aggregate size than the Whole or Soluble asphaltenes. Their behavior in the presence of resins should help elucidate the mechanisms of aggregation and solvation.

The asphaltene solubility limit, after resin addition, was reduced as much as 10 % (v/v) toluene. In the precipitated regime, resins were capable of enhancing asphaltene solubility (reducing the percentage of precipitates) between 10 and 50 %. Resins appear to enhance the solubility of the Precipitate asphaltenes more so than the Soluble. The solvating interactions between the polar, aromatic resins and highly polar aromatic Precipitate asphaltenes are quite strong. Soluble asphaltenes are less polar and aromatic and do not respond as favorably to resin addition in highly aliphatic solvents. Of note is the considerable solvating effect of CS Whole and Precipitate by CS resins. These interactions suggest CS resins possibly play a greater role in asphaltene solvation in the crude oil.

In solution asphaltenes form aggregates through intermolecular π- and hydrogen bonds between asphaltene monomers. Resins reduce the tendency for asphaltenes to aggregate by disrupting these intermolecular interactions. From Table 4.3 we see that resins contain polar heteroatoms within a mixed aromatic-aliphatic carbon matrix. Like asphaltenes, resins are polydisperse and chemical properties are measured as an average. Polar functional groups give resins the capacity to disrupt the electron donor-acceptor interactions partly responsible for asphaltene aggregation. Resins, however, are less aromatic than asphaltenes as gauged by H/C ratios between 1.31 and 1.51. Due to decreased aromaticity, their solubility in more aliphatic solvents is considerably higher than asphaltenes. Aromatic moieties in resins likely solvate the fused ring portion of the asphaltenes, producing a solvated, stabilized, resin-asphaltene aggregate. The ability of resins to dissociate intermolecular asphaltene bonds facilitates aggregate size reduction.

4.3.2 SANS: Asphaltenes and Resins in Heptol

Small angle neutron scattering (SANS) allows us to probe the effects of resins on asphaltene aggregation. In a previous SANS study, we found that asphaltene Precipitate fractions formed larger aggregates, than the unfractionated or more soluble fractions.[44]

Aggregate correlation lengths were fit by non-linear least squares regression of ln[I(Q)] vs. Q scattering data (Figure 4.2). The fitting procedure is described elsewhere.[44] Aggregate correlation lengths of B6 Whole and Precipitate, CS Whole and HO Whole asphaltenes in pure toluene with B6 resins are presented in Figure 4.3. B6 resins were dissolved in each asphaltene solution and heated to 80°C prior to neutron scattering. At elevated temperatures, asphaltenes have been shown to form smaller aggregates than at room temperature.[35, 37, 38, 44, 47] Precipitate asphaltenes formed considerably smaller aggregates at elevated temperatures while Whole asphaltenes were less affected by heat. Solubles formed aggregates at 80°C only slightly smaller than at room temperature.

SANS was not performed on CS Whole in pure toluene, however, it was assumed that the correlation length was slightly greater than of B6 Whole (> 42.4 Å) based on the trends of the other unfractionated asphaltenes in pure toluene and in 60 % (v/v) (Figure 4.4). Resin-asphaltene mass ratios as low as 0.5:1 and as high as 10:1 were investigated. In the absence of resins, Whole asphaltene correlation lengths followed the trend: CS > B6 > HO. Resin addition was effective at disrupting the intermolecular bonding and aggregation of each asphaltene to a similar extent. The greatest decrease in aggregate size occurred between 0.5 and 2:1 R/A suggesting resins strongly solvate asphaltenes at ratios close to those found in crude oil (Table 4.1). As the R/A ratio approached 10 the Whole asphaltene correlation lengths neared a common value of approximately 20 Å. In toluene, B6 Precipitate

asphaltenes in the absence of resins formed 69.7 Å aggregates, while at a 10:1 R/A ratio, these asphaltenes formed aggregates with a correlation length of 31.4 Å. The higher initial state of Precipitate aggregation could require much higher R/A ratios to reduce aggregate size. In addition, the average monomer dimension likely affects aggregate size and higher R/A ratios may not solvate the asphaltenes beyond a minimum aggregate size or number of monomers.

In less aromatic solvents, asphaltenes form larger aggregates due to solvent-solute incompatibility. Heptane-toluene mixtures of increasingly aliphatic solvent possess a lower degree of π-bond solvating capability and polarity than a pure toluene solvent. As a result, asphaltenes without resins in 60 % (v/v) toluene have larger correlation lengths than in pure toluene. For example, B6 Whole asphaltenic aggregates have correlation lengths of 56.7 Å at a toluene volume fraction of 0.6 as compared to 42.4 Å in pure toluene. In the presence of resins, CS forms the largest aggregates followed by B6 then HO at the R/A ratios examined (Figure 4.4). The plateau values to which each system approaches (HO: 16 Å, CS: 24 Å) are quite close to the values in pure toluene. High resin concentrations are equally effective in different heptol mixtures and are apparently more effective in reducing aggregate size than solvent alone. This comes as no surprise since resins are more chemically similar to asphaltenes and have been linked to asphaltene solubility in a variety of systems including crude oil.

For reference, the aggregation behavior of B6 Whole at 25°C is displayed. At room temperature B6 Whole asphaltenic aggregates have a correlation length of 77.2 Å as compared to 56.7 Å at 80°C. Resins were nonetheless still able to reduce the aggregate size substantially.

The effect of resins from different crude oils on asphaltene aggregation is shown in Figure 4.5. B6 Whole asphaltenes in pure toluene and 60 % (v/v) toluene in heptol were combined with AH and B6 resins at 80°C. At R/A ratios of 1 and 10 in pure toluene, B6 Whole correlation lengths were identical with either AH or B6 resin addition. In the mixed solvent, AH appears to solubilize B6 asphaltenes more effectively at a 2:1 ratio, although the addition of B6 resins at 2:1 is somewhat less effective than would be predicted based on trend from the other B6 resin data points. Above a 4:1 ratio, the asphaltene-resin systems form aggregates of similar dimension in both pure toluene and the mixed solvent. These results suggest that resins from different sources are approximately equal in effectiveness at solvating asphaltenic aggregates. At the highest R/A ratios, the correlation lengths of asphaltenic aggregates are 18 and 22 Å, regardless of solvent aromaticity and resin type.

4.3.3 Asphaltene-Resin Emulsion Stability: Effect of Varied R/A ratio

Asphaltene emulsions were prepared in the presence of resins at R/A ratios from 0.5 to 10 and their stabilities were gauged by measuring % water resolved. These stabilities were compared to aggregate correlation lengths measured at elevated temperature (see Figure 4.6). Without resins, B6 Whole asphaltenes formed emulsions in pure toluene that resolved slightly less than 30 % of the emulsified water. In heptol containing 60 % toluene, the emulsions were somewhat stronger with less than 10 % resolved water. Since asphaltenes in 60 % toluene were very near their solubility limit, correlation length and emulsion stability approached a maximum. In pure toluene, B6 Whole forms smaller, better solvated aggregates and thus, weaker emulsions.

In solvents where asphaltenes were soluble (>0.52 toluene volume fraction), resins decreased asphaltene aggregate size as well their ability to form emulsion-stabilizing films. While resins were effective at destabilizing emulsions in pure toluene and mixed solvents, the initial state of solvation played an important role. In pure toluene, emulsion stability was more sensitive to resin addition the asphaltenes were more soluble and less surface-active than in partially aliphatic solvents. A R/A ratio of 10 was required to completely destabilize emulsion at 60 % toluene while compared to 5:1 R/A in pure toluene. CS Whole asphaltenes formed much weaker emulsions than B6 and were rapidly destabilized in the presence of resins at concentrations less than 2:1 R/A (Figure 4.7). HO Whole formed emulsions in 60 % toluene of equal stability to B6 Whole but resin addition appeared to be more effective at destabilizing HO emulsions (Figure 4.8). Nearly all of the emulsified water was resolved at a resin:asphaltene ratio of 2:1.

The emulsion stability of B6 Whole asphaltenes at 60 % toluene even at high R/A was quite remarkable. HO Whole asphaltenes formed emulsions of comparable stability to B6 Whole in the absence of resins over a wide range of heptol conditions.[48] CS Whole, however, was a considerably weaker emulsion former. In each of these systems, resin solvation reduced the degree of aggregation and decreased the emulsion stability. CS asphaltenic aggregates were the largest, most aromatic and least aromatic of the Whole asphaltenes studied. The lack of polarity and possible inability to form a network of hydrogen bonds likely reduced interfacial activity. Resins rather easily solvated the aggregates and further reduced their emulsion stabilizing ability. The results suggest that even highly solvated B6 Whole aggregates were still surface-active enough (due to high polarity) to adsorb to oil-water interfaces and form emulsion stabilizing films. HO Whole

asphaltenes were also rich in polarity but lacked the surface activity to maintain a cohesive oil-water interfacial film at the highest R/A ratios.

B6 Precipitate emulsions remained very stable in systems containing up to 2:1 resins (Figure 4.9). This was due primarily to the high proportion of film forming species in B6 Precipitate. The fractionation process concentrated the most aromatic and polar material in the Precipitate and as a result, it tended to aggregate, adsorb and consolidate into an elastic film at oil-water interfaces. As the R/A ratio approached 2, the film forming portion of Precipitate asphaltenes were in sufficient supply to maintain nearly complete emulsion stability. The slight increase in stability from 0 to 0.25:1 R/A may be attributed to enhanced asphaltene solubility and lability of the aggregates. In the absence of resins, the aggregate correlation length may be too large to reach a maximum in emulsion stability. As the large aggregates are solvated by resins, they may become more interfacially active and can form a cohesive film. Beyond 2:1 R/A the asphaltenic aggregates become increasingly soluble, less surface-active, and consequently form weaker emulsions.

4.3.4 Asphaltene (Soluble, Whole, Precipitate)-Resin Emulsion Stability:

The stability of emulsions prepared with AH Whole and its fractions at several heptol ratios are shown in Figures 4.10 a-c. As before, the asphaltene concentration was 0.37 % (w/v), or equivalently 0.5 % (w/w), and the resin-asphaltene ratio was varied. The volume fractions of toluene were chosen such that the asphaltenes were either above or below their solubility limits. At the highest toluene concentrations chosen (55 %: AH Whole, 60 %: AH Soluble and Precipitate) asphaltenes were completely soluble. At the lower toluene concentration (30 %), the asphaltenes were partially insoluble.

At 60 % toluene, AH Soluble asphaltenes formed weak emulsions that became increasingly unstable as resin concentration was increased (Figure 4.10a). The asphaltenes were very soluble at these conditions and could not form interfacial films capable of withstanding rupture. At 30 % toluene, AH Soluble asphaltenes were partially precipitated. Resin addition initially solvated the flocculated aggregates at R/A ratios of 0.25 and 0.5 resulting in enhanced emulsion stability. Further solvation by resins completely destabilized the emulsions at a R/A ratio of 2.

AH Whole asphaltenes formed emulsions in 55 % toluene with close to 50 % water resolved (Figure 4.10b). In the insoluble regime, (30 % toluene) the emulsions were considerably weaker due to non-surface-active, flocculated asphaltenic aggregates. Resin addition, though, reversed this behavior. At higher R/A ratios, the 30 % toluene system became highly solvated and emulsions were destabilized. Much the same effect was seen with AH Precipitate asphaltenes where the emulsions containing the most soluble asphaltenes became unstable while partially insoluble systems actually formed stronger emulsions.

The emulsions formed by CS Whole asphaltene and its fractions were often unstable. Above the solubility limit, the ability of each asphaltene to form stabile emulsions decreased with resin addition (Figures 4.11 a-c). The emulsion stability of CS Soluble at 40 % toluene appeared to increase slightly up to an R/A of 0.5 then decrease. CS Whole asphaltenes formed unstable emulsions beyond an R/A of 1 due to resin solvation. The results of partially insoluble CS Precipitate at 50 % toluene suggest that resins were capable of a modest enhancement of emulsion stability. Even when the systems were rendered more soluble with resins, emulsion stability did not increase appreciably. High aromaticity, as suggested by low H/C ratios, likely caused large aggregate formation through strong π-π

interactions between asphaltene monomers and reduced aggregate lability. These properties suggest that CS asphaltenes are inherently weak emulsifiers due possibly to large aggregate formation, low polarity and an inability to form hydrogen bonds.

Unlike the weak emulsions formed by AH and CS asphaltenes over a wide range of solvent conditions, B6 and HO asphaltene stabilized emulsions were considerably stronger. The effects of resins on emulsion stability in the soluble and insoluble regimes are quite apparent. In Figure 4.12a, resins are shown to destabilize emulsions in the soluble regime of B6 Soluble. In the insoluble regime (30 % toluene), emulsion stability is reduced only after reaching a 5:1 R/A ratio. Resins initially redissolve precipitated asphaltenes and render them interfacially active until the system becomes too soluble and the driving force for film formation disappears. In a highly aliphatic solvent (10 % toluene) B6 Soluble did not form a stable emulsion even with an R/A of 5. At these conditions the asphaltenes are nearly insoluble because of limited solvent-solute π-π interactions. B6 Whole asphaltenes were studied three concentrations of toluene in the presence of resins (Figure 4.12b). Both 60 % and 100 % toluene were within the soluble regime of B6 Whole where 60 % was very near the solubility limit. In pure toluene, B6 Whole was very soluble but still formed stable emulsions until the addition of 0.25:1 resins. At this point the emulsion stability rapidly decreased as a result of enhanced solubility. At 60 % toluene, B6 Whole formed its largest soluble aggregates and were stronger emulsion formers in the presence of resins than in pure toluene. Its emulsions eventually became unstable at a 10:1 R/A ratio. Systems containing a fraction of insoluble asphaltenes (40 % toluene) were able to form very stable emulsions up to a R/A ratio of 5. The gradual redissolution of this insoluble material supported interfacial

film formation until the asphaltenes became too soluble and unable to adsorb and consolidate at the oil-water interface (R/A > 10).

B6 Precipitate asphaltenes were insoluble to some degree at both 30 and 60 % toluene but soluble in pure toluene. At 60 and 100 % toluene B6 Precipitate formed stable emulsions, however, 30 % toluene was not sufficient for emulsion stabilization (Figure 4.12c). In this highly aliphatic system, the majority of B6 Precipitate was insoluble and unable to form a cohesive interfacial film. The effect of resin addition on insoluble asphaltenes at 30 % toluene was dramatic redissolution and formation of completely stable emulsions above a R/A of 5. Even at 20:1 R/A, there still existed a sufficient supply of film forming material. This level of solubility is quite high and suggests that B6 Precipitate has unique chemistry that allows it to stabilize emulsions in the most soluble systems. In particular, a balance between aromaticity and hydrogen bonding capacity must exist to allow stability in both pure toluene with no resins (high aromaticity, low polarity) and in highly aliphatic solvents with substantial resin content (low aromaticity, high polarity).

The solubility profiles of B6 Whole and Precipitate at 40 and 30 % toluene, respectively, are shown in Figure 4.12d. The effectiveness of resins on asphaltene solubility depends on asphaltene chemistry and state of initial solubility. B6 Whole asphaltenes formed stable emulsions without resins but were only 60 % soluble. The amount of precipitated material fell below 10 % at an R/A of 1. Above this resin content, the asphaltenes were soluble and formed stable emulsions up to R/A of 5. Further solvation eventually destabilized the emulsions. At 30 % toluene, B6 Precipitate asphaltenes did not form stable emulsions. Emulsion stability increased marginally by adding resins of equal mass ratio to asphaltenes. Solubility measurements indicated that the asphaltenes were nearly insoluble at

these conditions. However, at an R/A of 5, B6 Precipitate solubility increased markedly and emulsion stability reached a maximum. Further solvation with resins did not enhance gravimetric solubility, but emulsion stability decreased substantially.

HO Whole and its more and less soluble fractions behaved in a very similar fashion to B6 asphaltenes (Figures 4.13a-c). HO Soluble asphaltenes formed stable emulsions at 60 % toluene that became unstable above 2:1 R/A (Figure 4.13a). At conditions that generated insoluble material (30 % toluene), resin addition did not facilitate emulsion formation. HO Whole asphaltenes were completely soluble at 60 % toluene and formed unstable emulsions due to resin solvation at a R/A of 2 (Figure 4.13b). At 40 % toluene, HO Whole asphaltenes were partially precipitated yet still formed stable emulsions with the remaining surface-active species. The effect of resins was delayed in this case as interfacially activity persisted until a R/A of 5. HO Precipitate, however, could be resolubilized with resins at 30 % toluene and form stable emulsions. Again, in the soluble regime resin addition led to immediate (100 % toluene) or delayed (60 % toluene) emulsion destabilization.

The power of resins to solvate asphaltenes of all chemistries is evident from SANS, solubility, and emulsion stability measurements. In addition, the ability to redissolve insoluble asphaltenes and render them capable of emulsion stabilization is remarkable. However, this resin-asphaltene interaction appears to act primarily with HO and B6 Precipitate, and CS to a lesser degree, and must be linked to their unique compositions. Both asphaltene fractions have the highest polarity of any Whole asphaltene or fraction. Their H/C ratio is also lower than B6 or HO Whole but not as low as AH or CS asphaltenes indicating a moderate level of aromaticity. These chemical properties suggest that aggregation and film formation may be driven more so by polar heteroatom interactions such

as hydrogen bonding than π-π bonding between asphaltene aromatic cores. AH and CS asphaltene contain low concentrations of polar nitrogen and likely aggregate via aromatic stacking. Without sufficient proton donor-acceptor sites, the asphaltenes cannot adsorb and form a cohesive film at the oil-water interface.

4.4 Conclusions

In this study, SARA fractionated resins had a dramatic solvating effect on asphaltenes and their more and less soluble subfractions. At an R/A ratio of 1:1, the toluene concentration at which asphaltenes began to precipitate in heptol was reduced by as much as 10 %. Similar behavior was supported by reductions in asphaltenic aggregate correlation lengths from neutron scattering. At elevated temperature, the correlation lengths of Whole asphaltenes approached a value of approximately 20 Å at high resin concentrations (R/A of 10:1) regardless of asphaltene, resin added, or % toluene (in the soluble regime). However, room temperature studies also showed that aggregate sizes were reduced at higher R/A ratios. While B6 Precipitate formed aggregates with correlation lengths 30 Å larger than B6 Whole, high R/A ratios still solvated aggregates to less than half their original dimension. It is not known to what extent the aggregates can be dissociated by resin addition. The presumable minimum would be a system of asphaltene monomers surrounded by solvating resins with a dimension determined by the monomer molecular weight.

Asphaltene stabilized emulsions were susceptible to the effects of resin solvation. Soluble asphaltenes typically formed the weakest emulsions due to small, well solvated, low aromaticity and low polarity aggregates. Soluble and Whole asphaltenes at toluene concentrations below their solubility limit could be solvated to produce slightly more stable

emulsions than without resins. Above the solubility limit, resins completely destabilized emulsions at a R/A of 2:1 except in the case of B6 Whole, which formed stable emulsions up to a R/A of 10:1.

AH and CS Precipitate asphaltenes, poor emulsion formers without resins, were only modestly better emulsion formers with resins. Their lack of polarity, even when solvated to become more labile, prevented them from interacting strongly with oil-water interfaces. B6 and HO Precipitate, however, formed very stable emulsions in their soluble regime that were resistant to the solvating effects of resins. Both approached complete instability at a R/A of 10:1. At 60 % toluene B6 and HO were partially insoluble but formed very stable emulsions due to their highly polar and H-bonding nature. Resins added to these systems solvated the insoluble asphaltenic flocs, rendering them surface-active, and did not destabilize B6 even at a R/A of 20:1. In non-dispersive solvents containing just 30 % toluene, B6 and HO Precipitate asphaltenes were largely insoluble and did not form stable emulsions. Resins were able to solvate these systems to a considerable extent and led to stable emulsions at R/A ratios of 10:1 (HO) and 20:1 (B6).

These results show that the solvating effects of resins can be attributed to the polar and dispersive nature of the resin molecules. In solvents of high aromaticity, where π-π interactions between asphaltenic aggregates are largely mitigated, resins must solvate aggregates through additional polar, hydrogen bond disruption. At low solvent aromaticity, resin solvation proceeds via disruption of dispersion and hydrogen bonding interactions between aggregates. Systems containing asphaltenes with high polarity and surface activity (B6 and HO Whole and Precipitate), resin solvation is sometimes insufficient to induce

emulsion destabilization. Weak emulsion formers and Soluble asphaltenes with lower polarity and aromaticity are easily destabilized in the presence of resins.

4.5 Acknowledgements

This work was supported by grants from the National Science Foundation (CTS-981727), PERF (97-07), and shared consortium funding from ExxonMobil, Ondeo-Nalco Energy Systems, Shell Oil Company and Texaco. Special thanks go to George Blankenship and Semaj McIver who assisted with the experimental work.

4.6 References

1. Berridge, S.A., M.T. Thew and A.G. Loriston-Clarke, "The Formation and Stability of Emulsions of Water in Crude Petroleum and Similar Stocks," *Journal of the Institute of Petroleum*, 1968, **54** (539): p. 333-357.

2. Blair, C.M., "Interfacial Films Affecting the Stability of Petroleum Emulsions," *Chemistry and Industry*, 1960: p. 538-544.

3. Nellensteyn, F.J., "The Constitution of Asphalt," *Journal of the Institute of Petroleum Technologists*, 1924, **10**: p. 311-325.

4. Pfeiffer, J.P. and R.N.J. Saal, "Asphaltic Bitumen as Colloid System," *Journal of Physical Chemistry*, 1940, **44**: p. 139-149.

5. Lawrence, A.S.C. and W. Killner, "Emulsions of Seawater in Admiralty Fuel Oil with Special Reference to their Demulsification," *Journal of the Institute of Petroleum*, 1948, **34**: p. 281.

6. Denekas, M.O., et al., "Material Adsorbed at Crude Petroleum-Water Interfaces," *Ind. and Eng. Chem.*, 1951, **43** (5): p. 1165-1169.

7. Dodd, C.G., "The Rheological Properties of Films at Crude Petroleum-Water Interfaces," *Journal of Physical Chemistry*, 1960, **64** (5): p. 544-550.

8. Neumann, H., "Investigations Regarding the Separation of Crude Oil Emulsions," *Petrochemie*, 1965, **18**: p. 776-779.

9. Kimbler, O.K., R.L. Reed and I.H. Silberberg, "Physical Characteristics of Natural Films Formed at Crude Oil-Water Interfaces," *Society of Petroleum Engineers Journal*, 1966 (6): p. 153-165.

10. Strassner, J.E., "Effect of pH on Interfacial Films and Stability of Crude Oil-Water Emulsions," *Journal of Petroleum Technology*, 1968, **20**: p. 303-312.

11. Mackay, G.D.M., et al., "The Formation of Water-in-Oil Emulsions Subsequent to an Oil Spill," *Journal of the Institute of Petroleum*, 1973, **59** (568): p. 164-172.

12. Cairns, R.J.R., D.M. Grist and E.L. Neustadter. *The Effect of Crude Oil-Water Interfacial Properties on Water-Crude Oil Emulsion Stability*. in *Theory and Practice of Emulsion Technology*. 1974. Brunel University: Academic Press.

13. Oren, J.J. and G.D.M. MacKay, "Electrolyte and pH Effect on Emulsion Stability of Water-in-Petroleum Oils," *Fuel*, 1977, **56** (10): p. 382-384.

14. Jones, T.J., E.L. Neustadter and K.P. Whittingham, "Water-in-Crude Oil Emulsion Stability and Emulsion Destabilization by Chemical Demulsifiers," *Journal of Canadian Petroleum Technology*, 1978, **17** (2): p. 100-108.

15. Bridie, A.L., et al., "Formation, Prevention and Breaking of Sea Water in Crude Oil Emulsions 'Chocolate Mousses'," *Mar. Pollut. Bull.*, 1980, **11**: p. 343-348.

16. Taylor, S.E., "Resolving Crude Oil Emulsions," *Chemistry and Industry*, 1992, **20**: p. 770-773.

17. Shetty, C.S., A.D. Nikolov and D.T. Wasan, "Demulsification of Water in Oil Emulsions Using Water Soluble Demulsifiers," *Journal of Dispersion Science and Technology*, 1992, **13** (2): p. 121-133.

18. Mitchell, D.L. and J.G. Speight, "The Solubility of Asphaltenes in Hydrocarbon Solvents," *Fuel*, 1973, **52** (4): p. 149-152.

19. Yen, T.F., J.G. Erdman and S.S. Pollack, "Investigation of Structure of Petroleum Asphaltenes By X-Ray Diffraction," *Analytical Chemistry*, 1961, **33** (11): p. 1587-&.

20. Barbour, R.V. and J.C. Petersen, "Molecular Interactions of Asphalt: An Infrared Study of the Hydrogen-Bonding Basicity of Asphalt," *Analytical Chemistry*, 1974, **46** (2): p. 273-277.

21. Boduszynski, M.M., J.F. McKay and D.R. Latham, "Asphaltenes, Where Are You?," *Proceedings of the Association of Asphalt Paving Technologists*, 1980, **49**: p. 123-143.

22. Ignasiak, T., O.P. Strausz and D.S. Montgomery, "Oxygen Distribution and Hydrogen Bonding in Athabasca Asphaltene," *Fuel*, 1977, **56**: p. 359-365.

23. Moschopedis, S.E. and J.G. Speight, "Investigation of Hydrogen Bonding by Oxygen Functions in Athabasca Bitumen," *Fuel*, 1976, **55**: p. 187-192.

24. Petersen, J.C., "An Infra-red Study of Hydrogen Bonding in Asphalt," 1967: p. 295-305.

25. Al-Jarrah, M.M.H. and A.H. Al-Dujaili, "Characterization of Some Iraqi Asphalts II. New Findings on the Physical Nature of Asphaltenes," *Fuel Science and Technology International*, 1989, **7** (1): p. 69-88.

26. Acevedo, S., et al., "Asphaltenes and Resins From the Orinoco Basin," *Fuel*, 1985, **64**: p. 1741-1747.

27. Boduszynski, M.M., "Composition of Heavy Petroleums. 2. Molecular Characterization," *Energy & Fuels*, 1988, **2** (5): p. 597-613.

28. Wiehe, I.A. and K.S. Liang, "Asphaltenes, Resins, and other petroleum macromolecules," *Fluid Phase Equilibria*, 1996, **117** (1-2): p. 201-210.

29. McKay, J.F., et al., "Petroleum Asphaltenes: Chemistry and Composition," *Analytical Chemistry of Liquid Fuel Sources, Advances in Chemistry Series*, 1978, **170**: p. 128-142.

30. Andersen, S.I., A. Keul and E. Stenby, "Variation in composition of subfractions of petroleum asphaltenes," *Petroleum Science and Technology*, 1997, **15** (7-8): p. 611-645.

31. Yarranton, H.W. and J.H. Masliyah, "Molar Mass Distribution and Solubility Modeling of Asphaltenes," *AICHE Journal*, 1996, **42** (12): p. 3533-3543.

32. Yarranton, H.W., H. Alboudwarej and R. Jakher, "Investigation of asphaltene association with vapor pressure osmometry and interfacial tension measurements," *Industrial & Engineering Chemistry Research*, 2000, **39** (8): p. 2916-2924.

33. Herzog, P., D. Tchoubar and D. Espinat, "Macrostructure of Asphaltene Dispersions by Small-angle X-ray Scattering," *Fuel*, 1988, **67**: p. 245-250.

34. Ravey, J.C., G. Ducouret and D. Espinat, "Asphaltene Macrostructure by Small Angle Neutron Scattering," *Fuel*, 1988, **67** (11): p. 1560-1567.

35. Overfield, R.E., et al., "SANS Study of Asphaltene Aggregation," *Fuel Science & Technology International*, 1989, **7** (5-6): p. 611-624.

36. Sheu, E.Y., D.A. Storm and M.M.D. Tar, "Asphaltenes in Polar Solvents," *Journal of Non-Crystalline Solids*, 1991, **131-133**: p. 341-347.

37. Espinat, D., et al., "Colloidal Macrostructure of Crude-Oil Studied By Neutron and X- Ray Small-Angle Scattering Techniques," *Journal De Physique Iv*, 1993, **3** (C8): p. 181-184.

38. Thiyagarajan, P., et al., "Temperature-Dependent Structural-Changes of Asphaltenes in 1- Methylnaphthalene," *Energy & Fuels*, 1995, **9** (5): p. 829-833.

39. Rassamdana, H. and M. Sahimi, "Asphalt Flocculation and Deposition: II. Formation and Growth of Fractal Aggregates," *AICHE Journal*, 1996, **42** (12): p. 3318-3332.

40. Barre, L., et al., "Colloidal structure of heavy crudes and asphaltene solutions," *Revue De L Institut Francais Du Petrole*, 1997, **52** (2): p. 161-175.

41. Lin, M.Y., E.B. Sirota and H. Gang, "Neutron scattering characterization of asphaltene particles," *Abstracts of Papers of the American Chemical Society*, 1997, **213**: p. 66-FUEL.

42. Sirota, E.B., "Swelling of asphaltenes," *Petroleum Science and Technology*, 1998, **16** (3-4): p. 415-431.

43. Fenistein, D. and L. Barre, "Experimental measurement of the mass distribution of petroleum asphaltene aggregates using ultracentrifugation and small-angle X-ray scattering," *Fuel*, 2001, **80** (2): p. 283-287.

44. Spiecker, P.M. and P.K. Kilpatrick, "Aggregation and solubility behavior of petroleum asphaltenes and their subfractions," *Langmuir, to be submitted*, 2001.

45. Sheu, E.Y., et al., "Polydispersity Analysis of Asphaltene Solutions in Toluene," *Journal of Colloid and Interface Science*, 1992, **153** (2): p. 399-410.

46. Bardon, C., et al., "The colloidal structure of crude oils and suspensions of asphaltenes and resins," *Fuel Science & Technology International*, 1996, **14** (1-2): p. 203-242.

47. Ravey, J.C. and D. Espinat, "Macrostructure of Petroleum Asphaltenes by Small Angle Neutron Scattering," *Progress in Colloid and Polymer Science*, 1990, **81**: p. 127-130.

48. Spiecker, P.M. and P.K. Kilpatrick, "The Role of Asphaltene Solubility and Chemistry on the Stability of Water-in-Oil Emulsions," *Journal of Colloid and Interface Science, to be submitted*, 2001.

49. van der Waarden, M., "Stability of Emulsions of Water in Mineral Oils Containing Asphaltenes," *Kolloid Z. Z. Polymer*, 1958, **156** (2): p. 116-122.

50. Miller, R., "Hydrocarbon Class Fractionation with Bonded-Phase Liquid Chromatography," *Analytical Chemistry*, 1982, **54** (11): p. 1742-1746.

51. Reynolds, J.G., "Characterization of Heavy Residua by Application of a Modified D 2007 and Asphaltene Separation: Effect of Solvents on Physical and Chemical Properties of Fractions Derived From Hondo 850^{O}F Residuum," *Fuel Science and Technology International*, 1987, **5** (5): p. 593-620.

52. Ali, M.F., A. Bukhari and M.U. Hasan, "Structural Characterization of Arabian Heavy Crude Oil Residue," *Fuel Science and Technology International*, 1989, **7** (8): p. 1179-1208.

53. Alula, M., et al., "Efficiency of Sequential Elution Solvent Chromatography-Extrography Technique for the Characterization of Hydroliquefaction and Pyrolysis Products," *Fuel*, 1989, **68** (10): p. 1330-1335.

54. Middleton, W.R., "Gradient Elution Chromatography Using Ultraviolet Monitors in the Analytical Fractionation of Heavy Petroleums," *Analytical Chemistry*, 1967, **39** (14): p. 1839-1846.

55. Reynolds, J.G. and W.R. Biggs, "Effects of Asphaltene Precipitation and a Modified D 2007 Separation on the Molecular Size of Vanadium- and Nickel-Containing Compounds in Heavy Residua," *Fuel Science and Technology International*, 1986, **4** (6): p. 749-777.

56. Nghiem, L.X., et al., "Efficient Modelling of Asphaltene Precipitation," *Society of Petroleum Engineers*, 1993, **5**: p. 375-384.

57. Andersen, S.I. and K.S. Birdi, "Aggregation of Asphaltenes as Determined by Calorimetry," *Journal of Colloid and Interface Science*, 1991, **142** (2): p. 497-502.

58. Murgich, J., J.A. Abanero and O.P. Strausz, "Molecular recognition in aggregates formed by asphaltene and resin molecules from the Athabasca oil sand," *Energy & Fuels*, 1999, **13** (2): p. 278-286.

59. Murgich, J. and O.P. Strausz, "Molecular mechanics of aggregates of asphaltenes and resins of the Athabasca oil," *Petroleum Science and Technology*, 2001, **19** (1-2): p. 231-243.

60. McLean, J.D. and P.K. Kilpatrick, "Effects of asphaltene aggregation in model heptane-toluene mixtures on stability of water-in-oil emulsions," *Journal of Colloid and Interface Science*, 1997, **196** (1): p. 23-34.

61. Fordedal, H., et al., "Crude Oil Emulsions in High Electric Fields as Studied by Dielectric Spectroscopy. Influence of Interaction Between Commercial and Indigenous Surfactants," *Colloids and Surfaces A: Physicochemical and Engineering Aspects*, 1996, **106**: p. 33-47.

62. Mohammed, R.A., et al., "Dewatering of Crude Oil Emulsions 2. Interfacial Properties of the Asphaltic Constituents of Crude Oil," *Colloids and Surfaces A: Physicochemical and Engineering Aspects*, 1993, **80**: p. 237-242.

63. Fordedal, H., et al., "A Multivariate Screening Analysis of W/O Emulsions in High External Electric Fields as Studied by Means of Dielectric Time Domain Spectroscopy, II," *Journal of Colloid and Interface Science*, 1996, **182**: p. 117-125.

64. McLean, J.D. and P.K. Kilpatrick, "Effects of Asphaltene Solvency on Stability of Water-in-Crude Oil Emulsions," *Journal of Colloid and Interface Science*, 1997, **189**: p. 242-253.

65. Gafonova, O.V. and H.W. Yarranton, "The stabilization of water-in-hydrocarbon emulsions by asphaltenes and resins," *Journal of Colloid and Interface Science*, 2001, **241** (2): p. 469-478.

66. McLean, J.D. and P.K. Kilpatrick, "Comparison of Precipitation and Extrography in the Fractionation of Crude Oil Residua," *Energy and Fuels*, 1997, **11**: p. 570-585.

67. de Gennes, P.-G., *Scaling Concepts in Polymer Physics*. 1979, Ithaca, NY: Cornell University Press.

Table 4.1 Crude Oil Properties

Crude	Wt % Asph	R/A Ratio	H/C Asph	Viscosity (cP) 100°F
AH	6.7	1.12	1.14	33.8
B6	13.1	0.92	1.22	2030
CS	7.5	1.19	1.11	70
HO	14.8	1.39	1.29	363

Table 4.2 Asphaltene Fractionation Results (wt %)

	H/C		Nitrogen		Sulfur	
Asphaltene	Whole	Ppt	Whole	Ppt	Whole	Ppt
AH	1.14	1.13	1.02	1.08	8.32	7.66
B6	1.24	1.22	1.87	1.93	6.68	6.33
CS	1.11	1.09	1.32	1.39	0.52	0.48
HO	1.29	1.24	1.99	2.11	8.53	8.48

Table 4.3 Resin Composition in wt %, except H/C (O by difference)

Resin source	H/C	N	S	O
AH	1.31	0.81	6.49	1.53
B6	1.51	1.48	6.91	1.98
CS	1.39	1.52	0.88	2.77
HO	1.51			

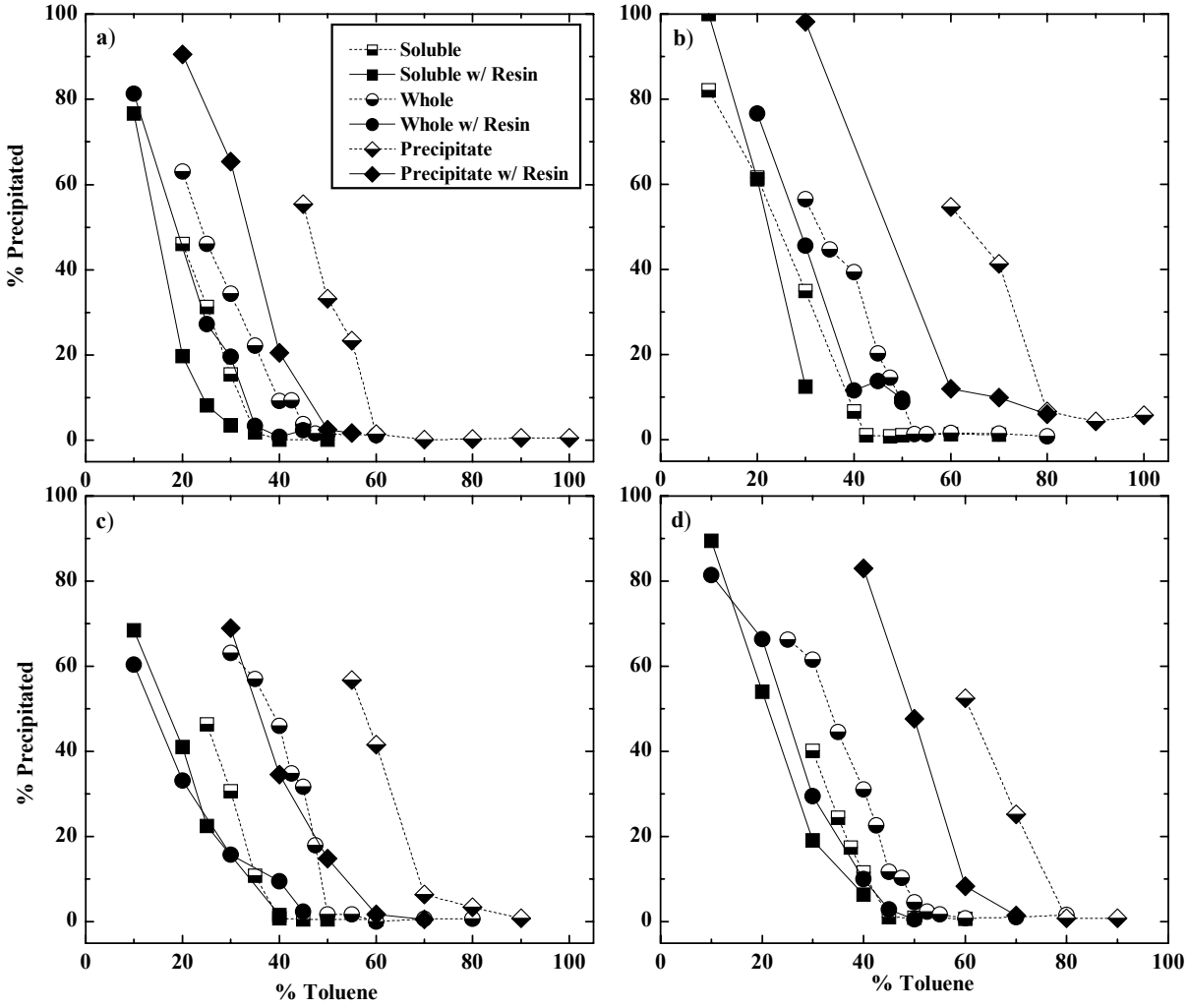

Figure 4.1 Solubility of 0.75 % (w/v) Whole asphaltenes and their more and less soluble subfractions in heptol with and without resins. Half filled markers denote systems without resins. R/A ratio was fixed at 1:1 by mass.

a) AH
b) B6
c) CS
d) HO

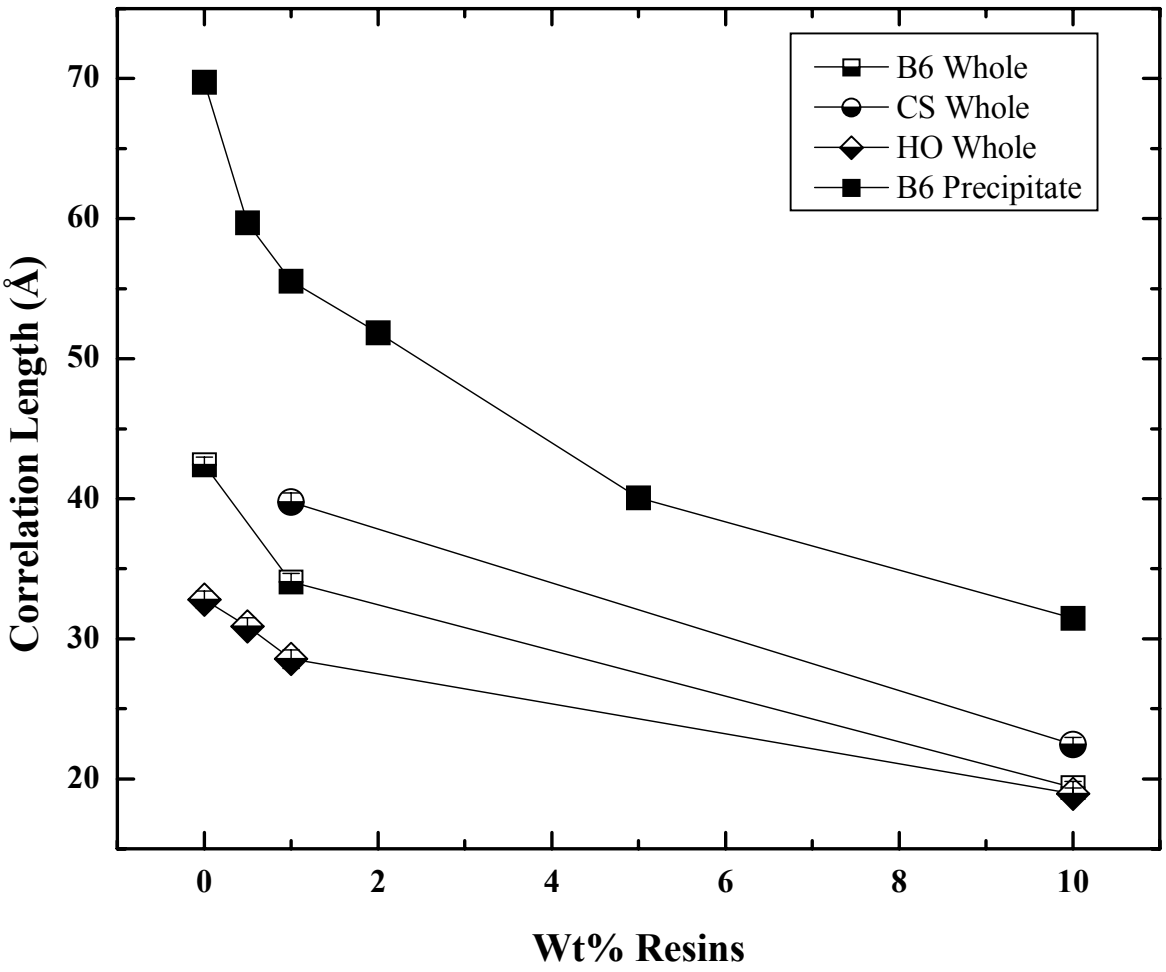

Figure 4.2 Correlation lengths (ξ) in Å of asphaltenic aggregates with B6 Resins in 100 % toluene at 80°C determined from SANS.

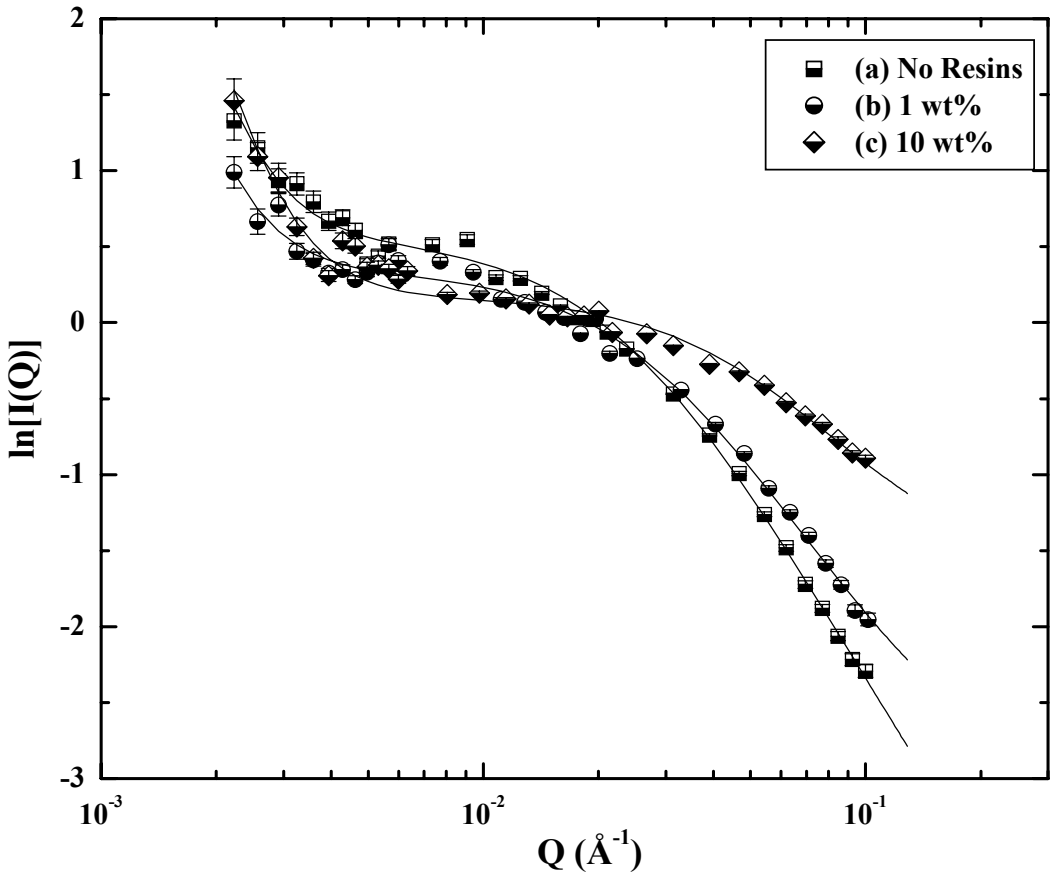

Figure 4.3 SANS fits using Lorentzian line shapes: B6 Whole asphaltenes at 80°C in toluene with:

a) No Resins:
   Background: 0.0054 ± 0.0027, I_0: 1.73 ± 0.02, I_1: 5.91E-11 ± 3.20E-12
   ξ: 42.4 ± 0.5
b) 1 wt% B6 Resins:
   Background: 0.038 ± 0.005, I_0: 1.36 ± 0.01, I_1: 3.17E-11 ± 2.65E-12
   ξ: 34.0 ± 0.6
c) 10 wt% B6 Resins:
   Background: 0.19 ± 0.01, I_0: 1.00 ± 0.01, I_1: 8.42E-11 ± 4.05E-12
   ξ: 19.4 ± 0.4

Note: Every 5th data point plotted above Q = 0.006

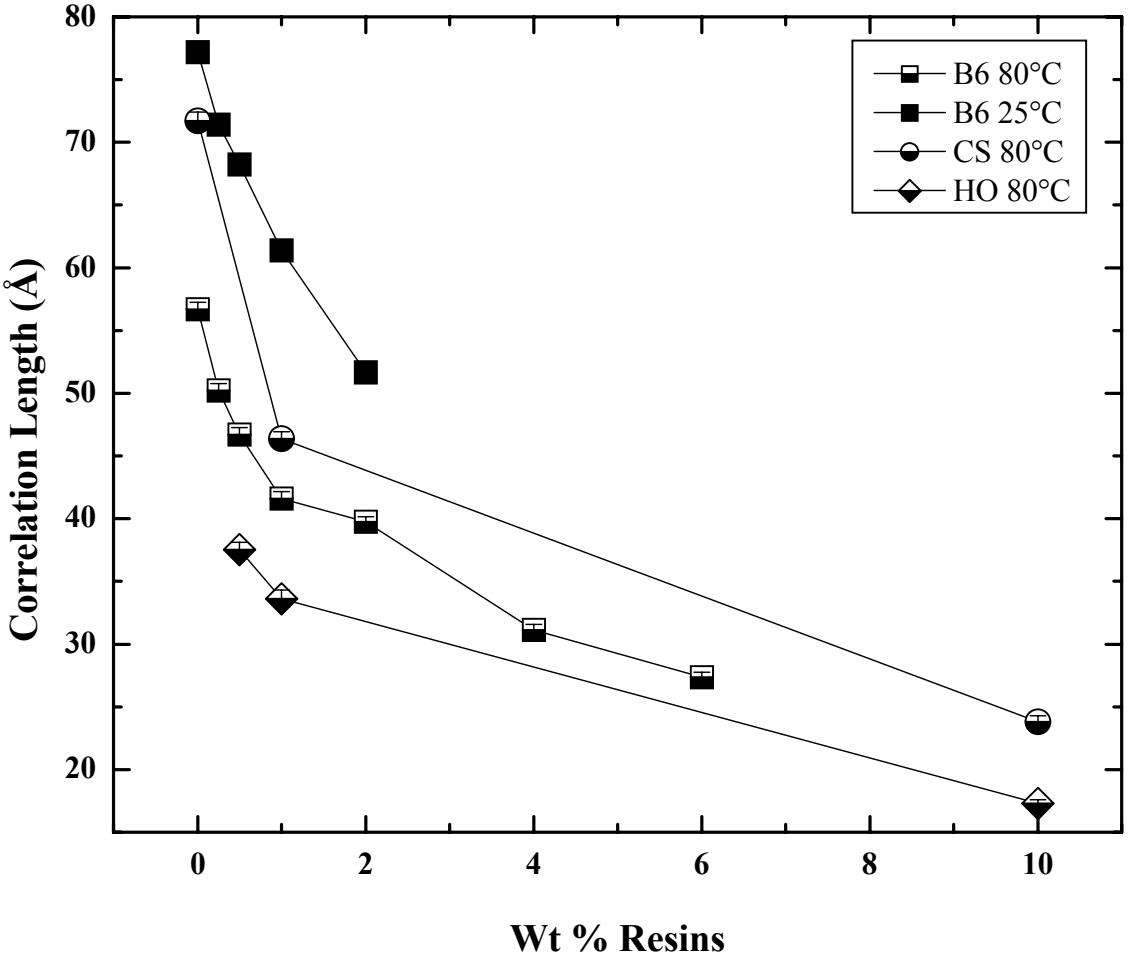

Figure 4.4 ξ of B6, CS, and HO Whole asphaltenic aggregates with B6 Resins in 40 % heptane - 60 % toluene at 25 and 80°C determined from SANS.

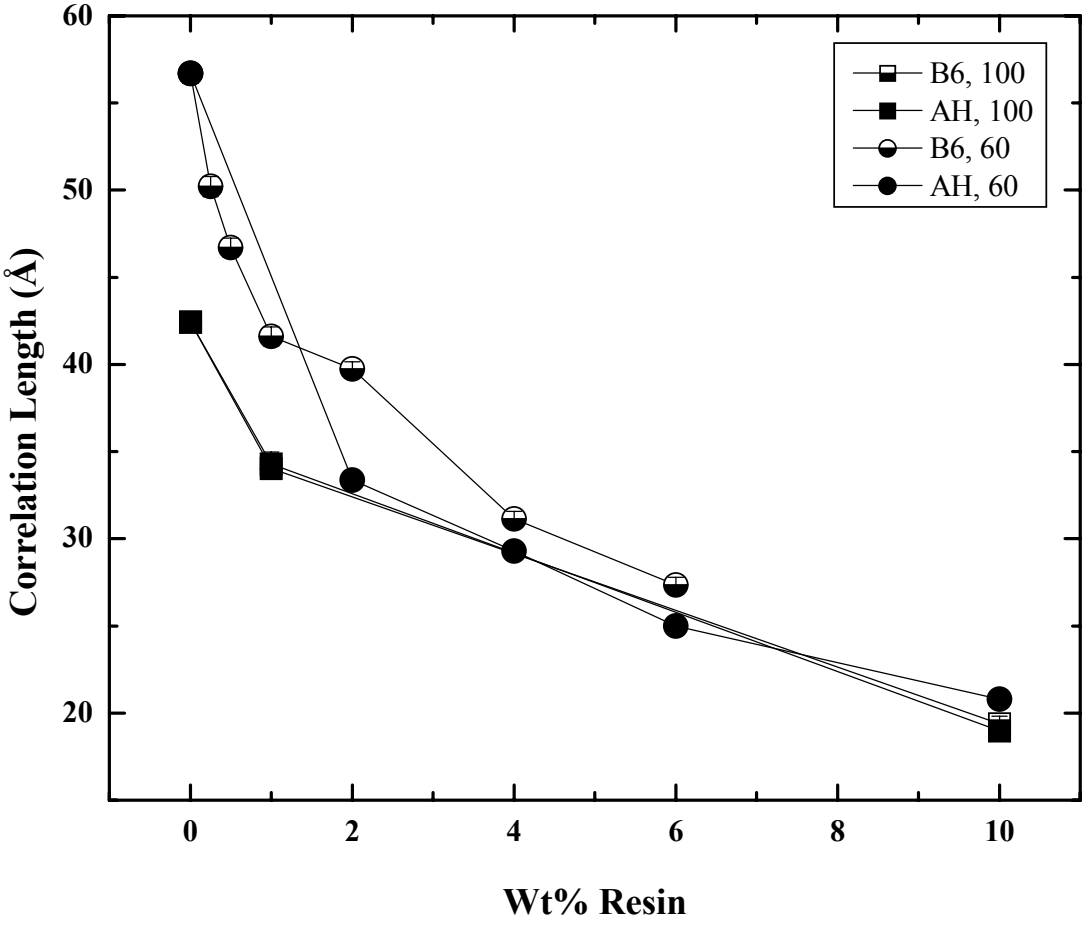

Figure 4.5 ξ of 1 wt % B6 Whole asphaltenic aggregates with AH and B6 Resins in pure toluene and 60 % toluene at 80°C determined from SANS. Legend displayed as (resin type, % toluene).

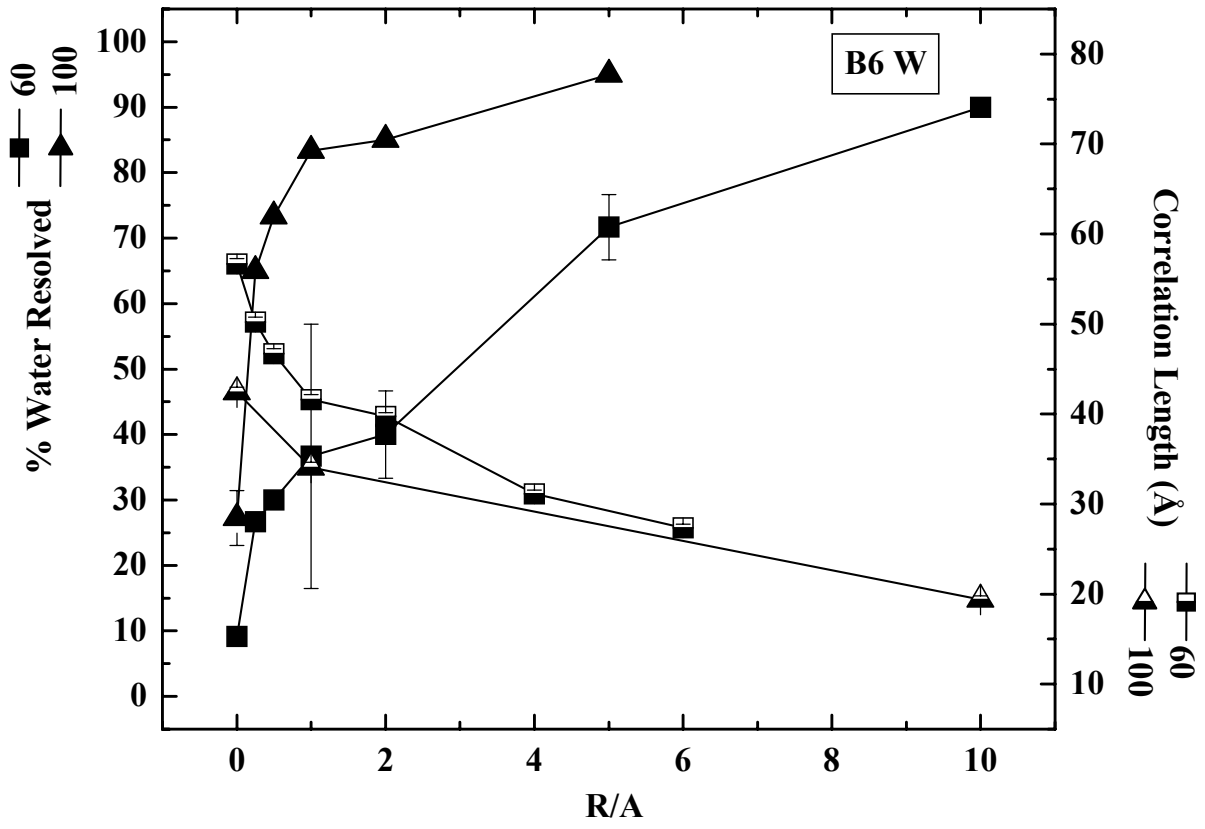

Figure 4.6 Emulsion stability (% water resolved) and aggregate ξ of B6 Whole asphaltenes in 60 and 100 % toluene with B6 resins. R/A represents mass ratio of resins to asphaltenes. Emulsions tested at 0.5 wt %, 25°C and ξ determined by SANS at 80°C, 1 wt %.

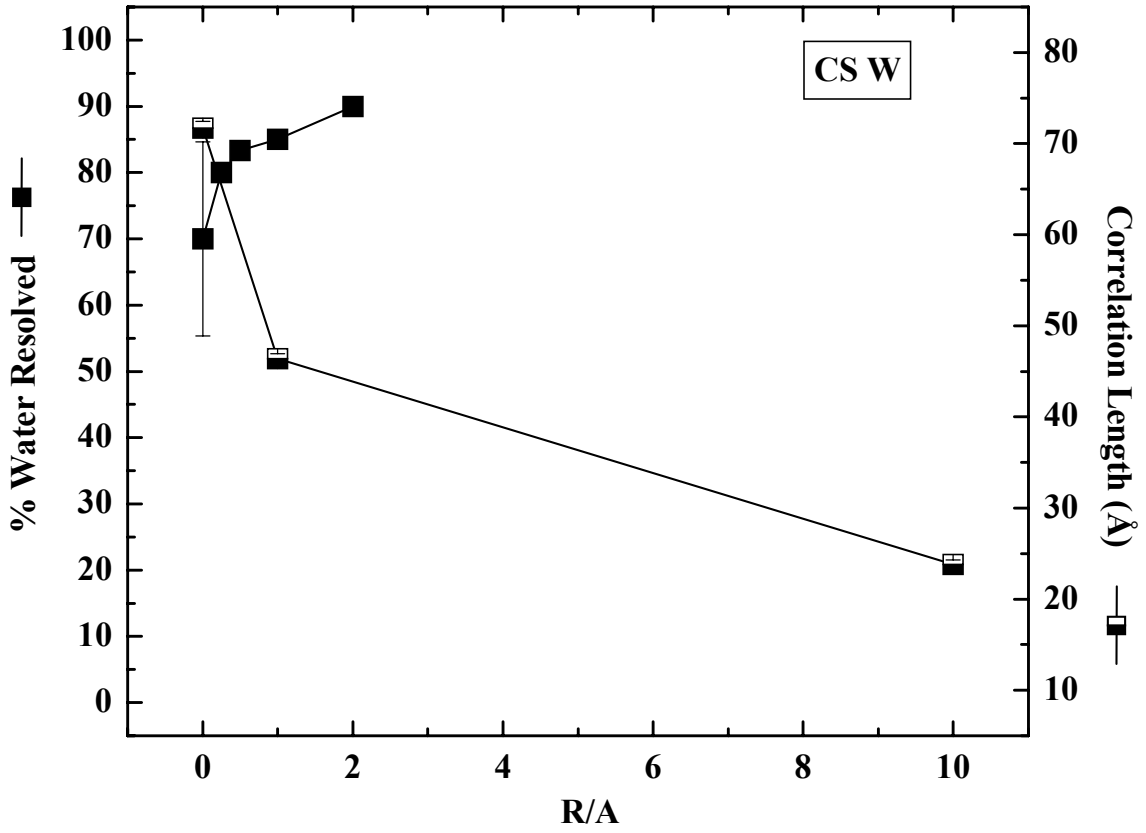

Figure 4.7 Emulsion stability (% water resolved) and aggregate ξ of CS Whole asphaltenes in 60 % toluene with CS resins. R/A represents mass ratio of resins to asphaltenes. Emulsions tested at 0.5 wt %, 25°C and ξ determined by SANS at 80°C, 1 wt %.

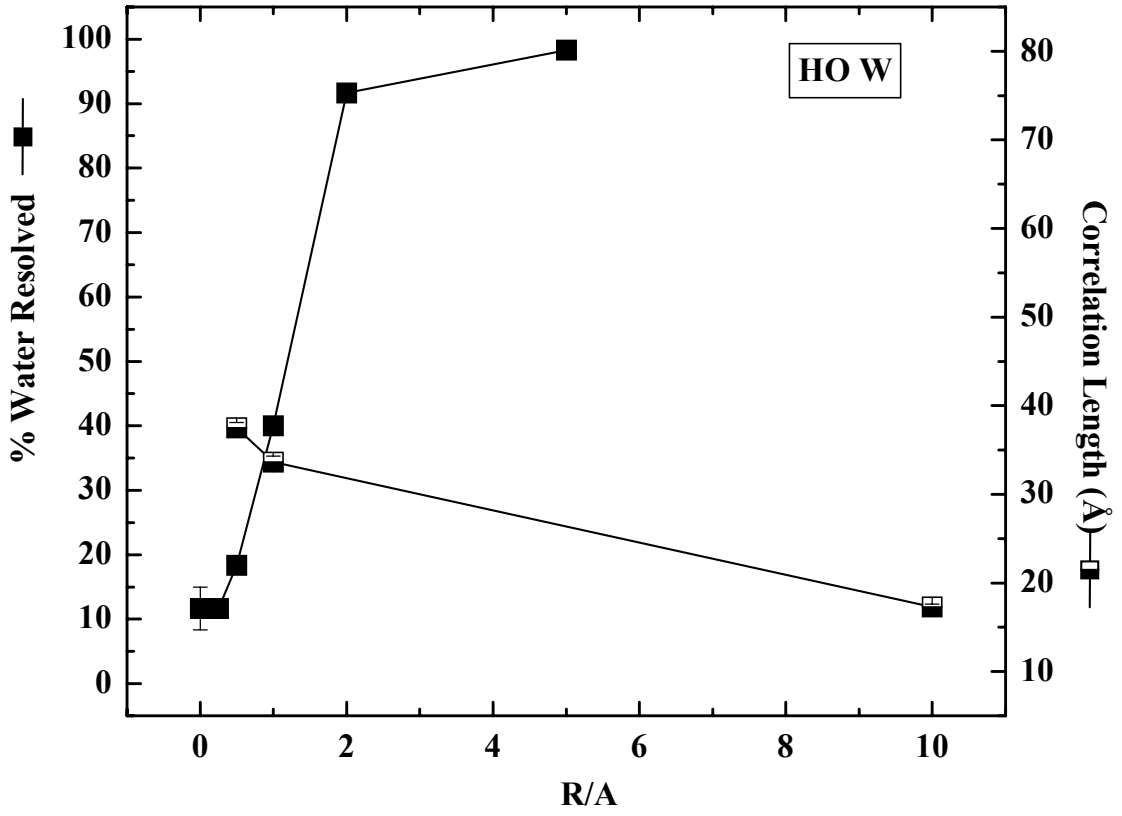

Figure 4.8 Emulsion stability (% water resolved) and aggregate ξ of HO Whole asphaltenes in 60 % toluene with HO resins. R/A represents mass ratio of resins to asphaltenes. Emulsions tested at 0.5 wt %, 25°C and ξ determined by SANS at 80°C, 1 wt %.

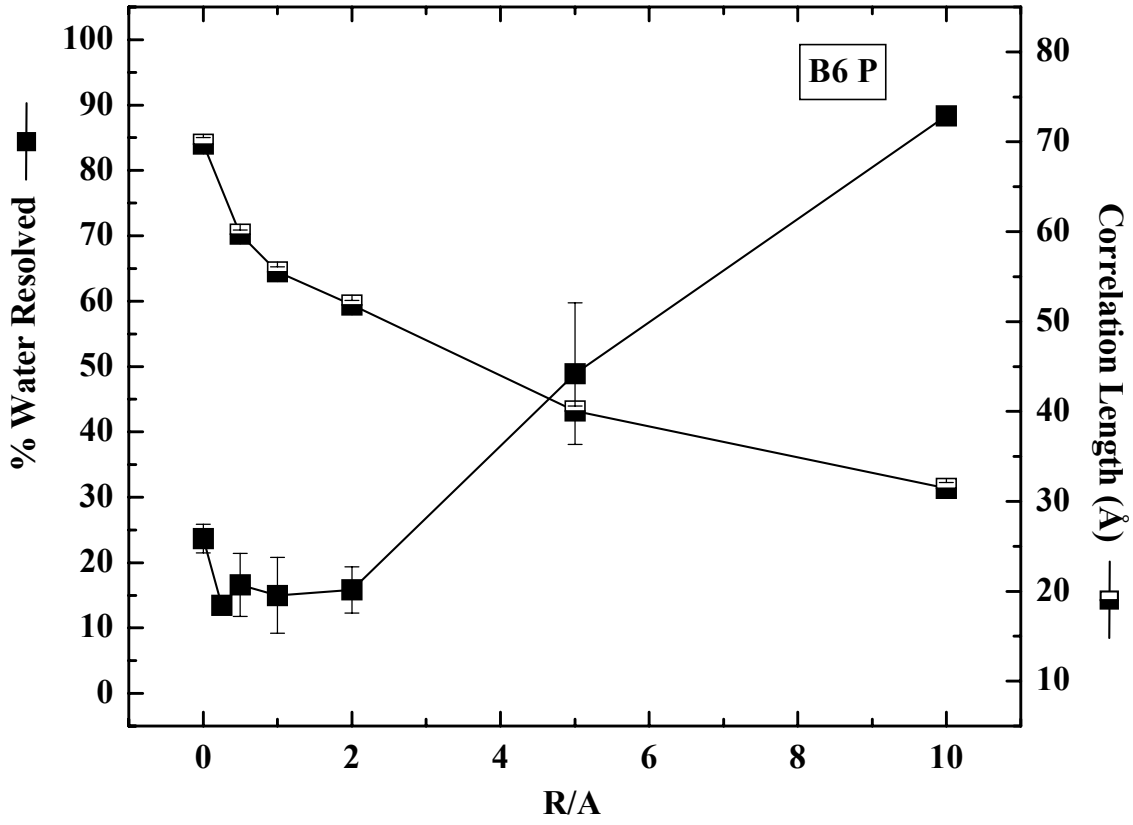

Figure 4.9 Emulsion stability (% water resolved) and aggregate ξ of B6 Precipitate asphaltenes in toluene with B6 resins. R/A represents mass ratio of resins to asphaltenes. Emulsions tested at 0.5 wt %, 25°C and ξ determined by SANS at 80°C, 1 wt %.

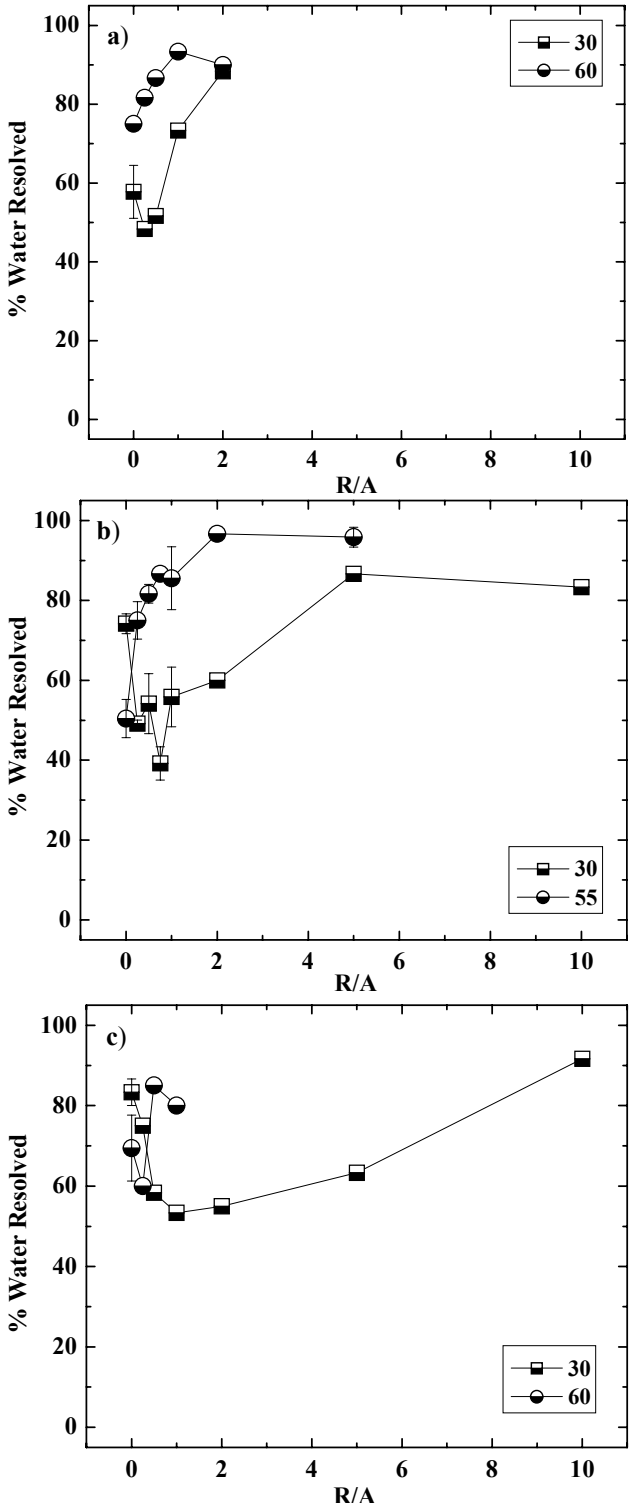

Figure 4.10 a-c Emulsion stability (% water resolved) of AH asphaltenes in heptol with AH resins. Emulsions tested at 0.5 wt %, 25°C.

a) Soluble: 30, 60 % toluene
b) Whole: 30, 55 % toluene
c) Precipitate: 30, 60 % toluene

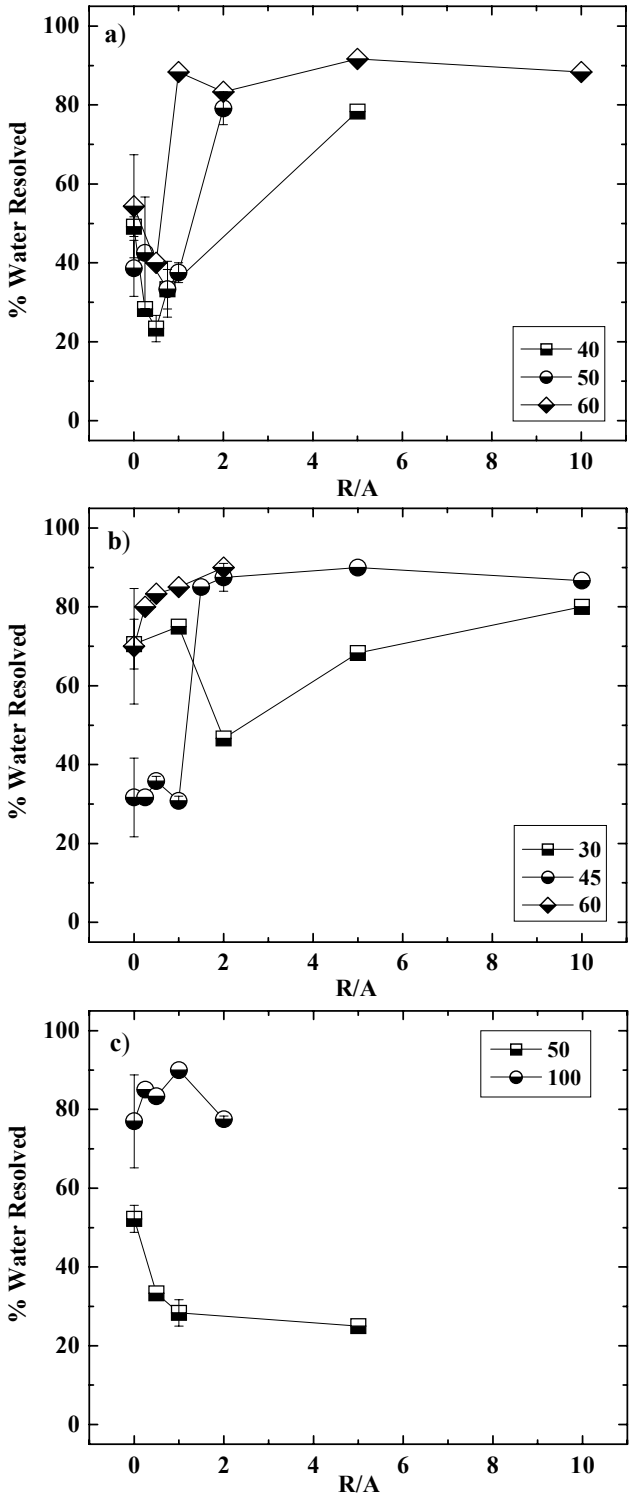

Figure 4.11 a-c Emulsion stability (% water resolved) of CS asphaltenes in heptol with CS resins. Emulsions tested at 0.5 wt %, 25°C.

a) Soluble: 40, 50, 60 % toluene
b) Whole: 30, 45, 60 % toluene
c) Precipitate: 50, 100 % toluene

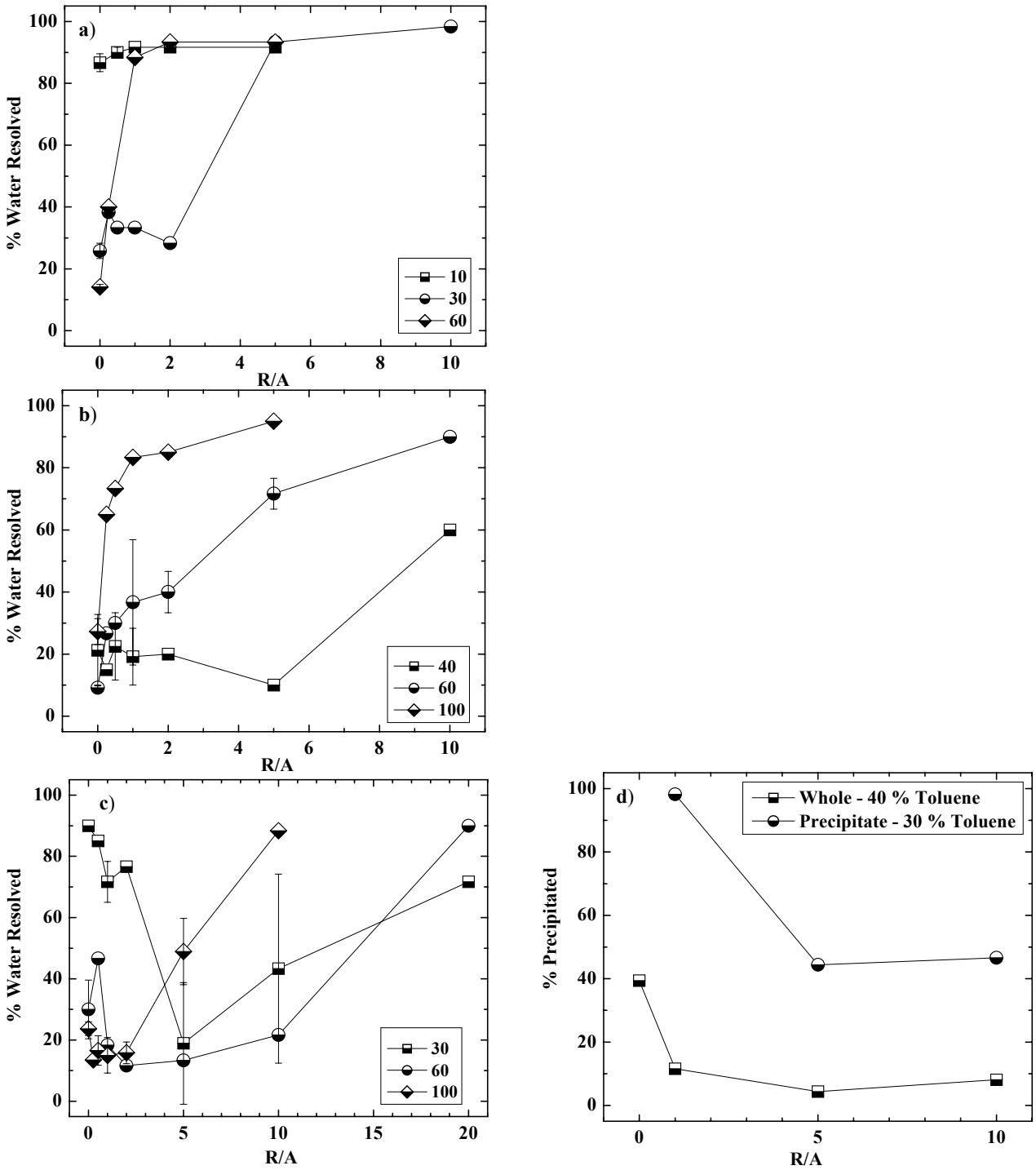

Figure 4.12 a-d Emulsion stability (vol % water resolved) and solubility (wt % precipitated) of B6 asphaltenes in heptol with B6 resins. Emulsions tested at 0.5 wt %, 25°C.

a) Soluble: 30, 60 % toluene
b) Whole: 40, 60, 100 % toluene
c) Precipitate: 30, 60, 100 % toluene
d) Whole and Precipitate solubility with resins

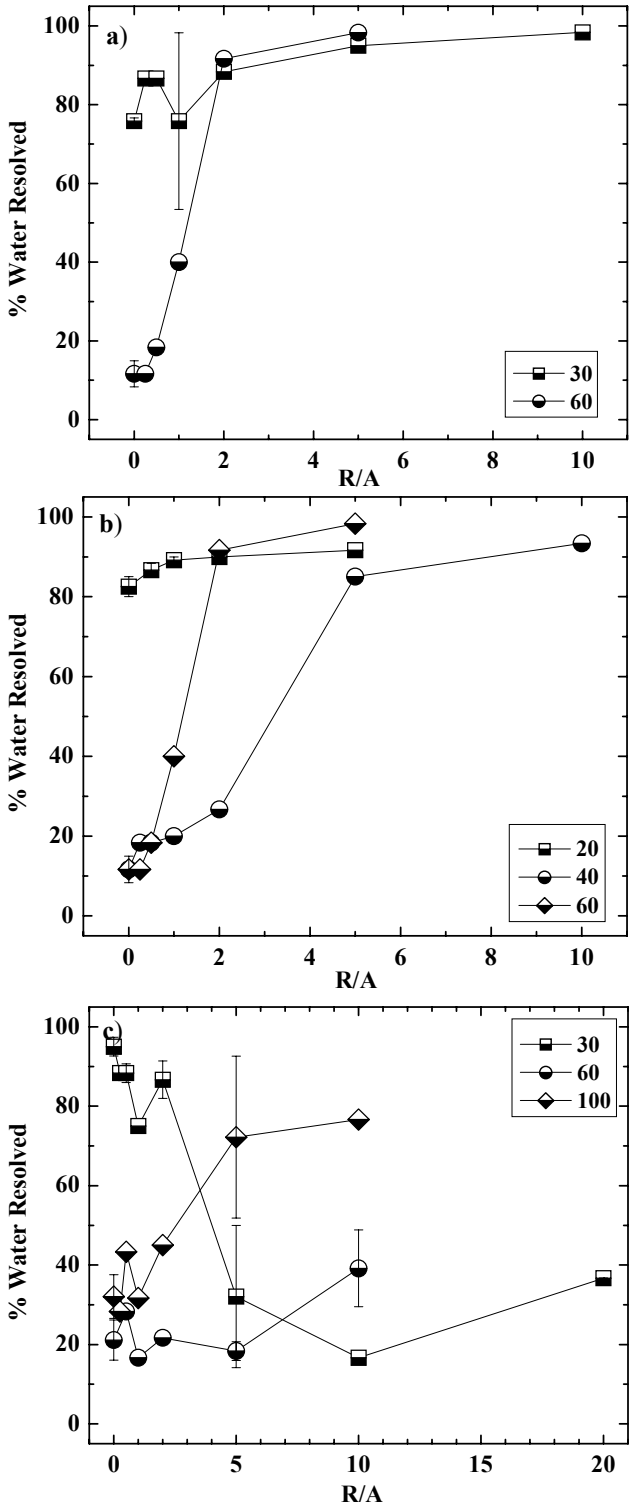

Figure 4.13 a-c Emulsion stability (% water resolved) of HO asphaltenes in heptol with HO resins. Emulsions tested at 0.5 wt %, 25°C.

a) Soluble: 30, 60 % toluene
b) Whole: 40, 60 % toluene
c) Precipitate: 30, 60, 100 % toluene

Interfacial Rheology of Petroleum Asphaltenes at the Oil-Water Interface

P. Matthew Spiecker and Peter K. Kilpatrick

ABSTRACT

A biconical bob interfacial shear rheometer was used to study the properties of asphaltene films. Solutions of asphaltenes from four crude oils dissolved in a model oil of heptane and toluene were allowed to age in contact with water. Film elasticities (G′) were measured over a period of several days and yield stresses and film masses were determined at the end of testing. The degree of film consolidation was determined from ratios of G′/film mass and yield stress/G′. Asphaltenes with higher concentrations of heavy metals (Ni: 330-360 ppm, V: 950-1000 ppm), lower aromaticity (H/C: 1.24-1.29), and higher polarity (N: 1.87-1.99) formed films of high elasticity, yield stress and consolidation. Asphaltenes with lower metals content (Ni: 21-160 ppm, V: 48-490 ppm), higher aromaticity (H/C: 1.11-1.14), and lower polarity (N: 1.02-1.32) formed films with low elasticity, yield stress and consolidation. Rapid adsorption kinetics and G′ increases were seen when asphaltenes were near their solubility limit in heptane-toluene mixtures (~48-52 % (v/v) toluene). At these conditions, asphaltene aggregation reached a maximum. For example at 60 % toluene G′ of a B6 asphaltene film after 72 hours aging was 17.2 Pa. G′/Mass and yield stress/G′ values were 421 Pa/g and 4.46e-2, respectively. In solvents of greater aromaticity, adsorption kinetics and film masses were reduced at comparable aging times. Poor film forming asphaltenes had yield stress/G′ values (1.01-1.21e-2) more than four fold lower than good film forming asphaltenes.

Asphaltenes fractionated by filtering solutions at low aromaticity (~40 % toluene in mixtures of heptane and toluene) possessed higher concentrations of heavy metals, nitrogen, and higher aromaticity. The less soluble fractions of good film forming asphaltenes exhibited enhanced adsorption kinetics and higher G′ (28.4 Pa) and yield stress (0.834 Pa) in pure toluene. Replacing the asphaltene solutions with neat heptane-toluene highlighted the ability of films to consolidate and become more elastic over several hours. After 8-12 hours, consolidation ceased and elasticity reached equilibrium. Adding resins in solution to a partially consolidated film caused a rapid reduction in elasticity followed by gradual but modest consolidation.

CHAPTER 5

INTERFACIAL RHEOLOGY OF PETROLEUM ASPHALTENES AT THE OIL-WATER INTERFACE

5.1 Introduction

Interfacial phenomena control the properties of emulsions and foams in the pharmaceutical, food products, cosmetics, and petroleum industries. Studying the rheology of emulsions and foams can provides valuable information concerning bulk viscosity, shear properties, and other end use issues. The knowledge gained by investigating interfacial properties, however, is considerably more revealing than the information available from bulk emulsions. From interfacial studies one can determine the fundamental mechanisms and kinetics of film formation, surfactant adsorption, and film rupture that ultimately govern emulsion behavior.

The types of interfaces studied are typically air-water, where the surfactant resides in the aqueous phase or water-oil, where the surfactant resides in the aqueous or oleic phase. Various techniques exist for the study of adsorption of surface-active agents to air-water and oil-water interfaces.[1-5] Benjamins et al. have non-destructively measured the viscoelastic modulus in compression and expansion of protein films at air-water and oil-water interfaces using a dynamic drop tensiometer and barrier-plate apparatus.[2] They found that increased protein adsorption time leads to an enhanced dilatational elastic modulus for both interfacial tensiometers. Inokuchi investigated the elastic and viscoelastic films formed by 6-nylon at an air-water interface with a trough device.[6] The films were characterized according to the degree of compression: Hookian elasticity at large areas and viscoelasticity at small areas with instantaneous elasticity, delayed elasticity, and stationary flow under constant applied

stress. These studies highlight the robustness of interfacial rheometric techniques for studying the adsorption of various adsorbates to different types of interfaces.

Of extreme importance in the petroleum industry is the formation of highly viscous water-in-oil emulsions. Crude oil is found in reservoirs along with water or brine and during oil removal, water is often coproduced. Water is also injected into the crude to remove salts or as steam to improve fractionation.[7] Petroleum emulsions (typically water-in-oil[8-11]) readily form with water in the highly turbulent nozzles and piping used for oil production. These emulsions increase pumping and transportation expenses, corrode of pipes, pumps, production equipment and distillation columns, and the poison downstream refinery catalysts.[12] It is well recognized that emulsion stability arises from the formation of an elastic interfacial film.[12-18] Soluble aggregates from the oleic phase adsorb to the oil-water interface and present a physical barrier to flocculation and coagulation of the dispersed phase droplets. Researchers have linked interfacial film and emulsion forming behavior to petroleum asphaltenes and their interplay with resins as a solubilizing agent.[10-12, 14-16, 19-31]

Asphaltenes are a solubility class of molecules found in the low-volatility portion of crude oil that form aggregates in crude oil solvated by resins.[32-35] Asphaltenes are defined as the portion of crude oil insoluble in n-alkanes such as n-heptane or n-pentane yet soluble in benzene or toluene.[36, 37] Asphaltenes are characterized by fused ring aromaticity, small aliphatic side chains, and polar heteroatom-containing functional groups. Number average molecular weights by vapor pressure osmometry range from ca. 800 to 3000 g/mol.[33, 38-44] Many studies have indicated the presence of carboxylic acids, carbonyl, phenol, pyrroles, and pyridine functionality.[45-49] These heteroatom containing groups are

capable of donating or accepting protons inter- and intra-molecularly. The most plausible mechanisms of asphaltene aggregation involve π-π overlap between aromatic sheets, hydrogen bonding between functional groups and other charge transfer interactions. The degree to which aggregate sizes vary is controlled by the polydispersity and chemistry of the single asphaltenic sheets.

Miller and coworkers provide a comprehensive review of both tested and novel methods for probing interfacial dilatational and shear properties of adsorption layers at liquid interfaces.[50] They describe devices that measure surface velocity profiles (indirect methods) or determine torsional stress values (direct methods). Indirect techniques such as canal surface viscometers, deep-channel surface viscometers and rotating wall knife-edge surface viscometers require measurements of fluid flow using easily visible inert particles from which surface viscosities can be determined. In direct methods, however, a pendulum is placed at the interface containing surfactant and measures the torque generated after the application of an oscillatory stress.[51] The biconical disc or bob interfacial viscometer is a modification of the flat disk viscometer. In each case a stress is applied to the interface by oscillating the cylindrical cup containing the fluids. This stress in turn confers motion to the bob that is generally monitored through deflection of incident light on the torsion wire. Wibberly employed biconical bob viscometery to the study of aqueous potassium arabate-air and liquid paraffin interfaces.[52] The apparatus consisted of a biconical brass bob 5.621cm in diameter and with and included angle of 20°. The bob was suspended by a copper beryllium wire with known torsion constant and moment of inertia. An optical lever of 2.7 meters measured the torsional displacement of the bob when subjected to an oscillation. They found the films were pseudo-plastic in nature and became more rigid with time.

Recently, liquid-liquid interfaces containing various polymers were studied with the biconical bob technique and a deep channel rheometer.[53] Comparable measurements of interfacial viscoelasticity were achieved using both rheometers demonstrating instrument independence. Enhanced sensitivity when working with very elastic interfaces further supported the use of biconical bob rheometry.

The rheological properties of asphaltene films, like their protein and polymer counterparts, can be probed by a variety of techniques.[16, 22, 54-59] Biconical bob rheometry has been applied to both crude oil-water and model oil-water interfaces.[57, 60-62] Cairns et al. employed a biconical bob rheometer to study the interfacial viscosities of crude oil-water films.[60] They found that viscosity increased with aging time of the interface several fold from 2 to 6 hours and suggested the presence of a viscous "interphase". Gradual increases over several days were attributed to changes in solvent character while multilayer formation caused the larger increases at short times. Acevedo et al. examined the shear viscoelasticity and creep compliance of Cerro Negro crude oil and asphaltenes diluted in xylene using the biconical bob rheometer of Cairns.[57] High interfacial elasticities, rather than viscosities, were purported to correlate with strong emulsions. It was again suggested that mechanically strong films result from the adsorption of aggregated asphaltenes. Mohammed and coworkers found that aging times approaching eight hours yield films with viscosities four hundred times greater than films aged for six hours. Beyond eight hours the films were too rigid to deform when subjected to any applied stress.[62]

In this study we have utilized a commercially available dynamic stress rheometer with stainless steel biconical bob to probe interfacial film viscoelasticity. As we will show, the film properties compare well with measures of emulsion stability on systems with

comparable composition. Thus, this technique provides useful insight into the mechanisms of emulsion stability in asphaltenic films and the effects of asphaltene solvency and chemistry.

5.2 Experimental

5.2.1 Asphaltene Precipitation and Fractionation

All organic solvents were HPLC grade and were obtained from Fisher Scientific. Petroleum asphaltenes were precipitated from four crude oils with a 40:1 excess of n-heptane. The crude oils, B6 and Hondo (off-shore California), Arab Heavy (Safaniya), and Canadon Seco (Argentina), were chosen for their high asphaltene content. Heptane precipitated asphaltenes were divided into more- and less-soluble fractions by dissolving in toluene and inducing partial precipitation with heptane. Asphaltene solubilities (pre- and post-fractionation) were determined in mixtures of heptane and toluene by filtration. Fractionation and solubility measurements were performed at a solute concentration of 0.75 % w/v. Details of these procedures can be found elsewhere.[63]

5.2.2 Interfacial Film Formation: Asphaltenes

The oil-water interfacial film studies were performed using a TA Instruments AR-1000 stress rheometer. Two sample cups were developed for holding the oil and water phases. A glass sample cell with exterior water circulation was fashioned from precision bore Pyrex tubing with an interior diameter of 8 cm and a depth of 2 cm (Figure 5.1). The temperature was maintained at 25°C by circulating water from a Fisher Scientific Isotemp 1016P programmable water bath. The second cup was machined from an ingot of Teflon to

the same interior dimensions. This cup version did not have water circulation and was temperature controlled by the rheometer's water-cooled Peltier plate. Both sample cells were designed to sit on top of the Peltier plate assembly and were held in place during the course of the experiment. A biconical bob similar in design to Shotton et al.[64] and Cairns et al.[60] for measuring interfacial rheological properties was machined from 316 stainless steel. The lower part of the bob immersed in the two phases was designed to be as thin as practically possible to reduce inertia. The upper part had recessed threads to mate properly with the instrument's stress head (Figure 5.1). The bob was tapered from the narrow center shaft (0.5 cm diameter) out to a "knife"-edge at the perimeter (4 cm diameter). The edge was serrated around the circumference (30°, 3 mm deep) to maintain adhesion to the film at higher applied stresses.

Before each experiment, the bob was cleaned with methylene chloride followed by water and detergent, and then rinsed with deionized water. The interior of each cup was cleaned with a 7:3 (v/v) mixture of concentrated sulfuric acid and 30% hydrogen peroxide (Technical grade, Fisher), so-called "piranha" solution. (Piranha solution is extremely corrosive and highly exothermic. Prepare only as much as necessary.) This step ensured that the cup walls were free of the most stubborn organics.

Films were formed by adding a solution of asphaltenes dissolved in heptane and toluene to deionized water (HCl and NaOH adjusted to pH 6). The water phase (40 ml) was added to the sample cell first. This volume of water was chosen to provide a sufficient distance between the bob and the bottom of the glass cup (>1 cm). The bob was then lowered onto the surface of the water. Upon initial contact, the water was drawn upwards towards the edge of the bob due to the high surface energy of stainless steel. As the bob was

lowered, the meniscus formed between the bob edge and water gradually diminished. The final vertical position of the bob was set when this meniscus was eliminated. Precise control of the vertical movement of the bob ensured an accurate and reproducible means of locating the position of the interface regardless of aqueous phase volume. At this point, angular rotation of the bob was stopped mechanically. The oil phase (35ml) was pipetted slowly onto the bob and flowed outwards to minimize interfacial disturbance.

To reduce solvent evaporation, a Teflon solvent cap split into two halves was placed over the cup. A thin layer of silicon grease was applied to the edge of the glass to help seal the system. Additionally, two solvent troughs were affixed to the underside of the cap into which heptane and toluene were transferred throughout the experiment. A small gap, however, was maintained around the bob shaft to allow frictionless oscillation during testing.

Appropriate correction factors were used to control and monitor the response of the film to an applied stress. We used the approximation of Shotton *et al*. in which the interphase region is treated as a slice through a concentric cylinder system.[64] The instrument stress and rate factors were determined from bob and cup dimensions and the expressions for a generic concentric cylinder geometry. These expressions appear as follows:

$$F_{stress} = \frac{R_i^2 + R_o^2}{4\pi R_i^2 R_o^2} \tag{1.1}$$

$$F_{rate} = \frac{R_i^2 + R_o^2}{R_o^2 - R_i^2} \tag{1.2}$$

where R_i and R_o are the bob radius (2 cm) and cup radius (4 cm) respectively.

In the presence of a mechanically rigid film and under low amplitude oscillatory motion, the contribution of the two nearly Newtonian fluids on top and bottom of the bob was neglected. Thus, the resistance to applied oscillation resulted from the asphaltenic film and was gauged by the magnitudes of elastic and viscous moduli. These moduli represented as G′ (storage modulus) and G″ (loss modulus) are either in-phase or out-of-phase with the strain, respectively. Relating the moduli to the sinusoidally varying stress is the following expression

$$\sigma(t) = \gamma_o \left[G'(\omega)\sin(\omega t) + G''(\omega)\cos(\omega t) \right] \qquad (1.3)$$

where σ is the shear stress, γ_o is the applied strain amplitude and ω is the frequency of oscillation.[65] Low loss tangents (tan δ = G″/G′ 1) imply solid-like behavior while high loss tangents imply liquid-like behavior. Since Newtonian liquids such as water and heptane-toluene mixtures have no inherent elasticity their loss tangents are accordingly high. The rigid asphaltene films, however, have much lower loss tangents.

Frequency sweeps were performed on the interface to probe the kinetics of film formation. The film was allowed to develop for at least 1 to 2 hours before the initial testing. Even though there was evidence of asphaltene adsorption within minutes of the oil phase addition, there was not sufficient coverage or consolidation to impart a measurable signal when probed by the rheometer. Sheu found that dynamic toluene-water interfacial tension values measured at lower bulk asphaltene concentrations (<0.1 wt%) via Wilhelmy plate approached equilibrium within 100 minutes.[66] Beyond two hours, the interfacial tensions reached a plateau due to film formation and provided no additional information. The bulk concentration of our systems is 7.5-fold greater and less aromatic which will enhance

adsorption and decrease the time to reach an equilibium dynamic interfacial tension. At this point, the emergence of measurable film elasticity allows us to follow adsorption and film consolidation. The highly elastic film precludes the measurement of interfacial tension since the asphaltenes will have adsorbed to the plate or du Nouy ring apparatus.

Some slow adsorbing systems, however, required substantially more aging time before testing. Film growth was monitored in some cases for as long as several days. Exploratory film experiments provided the optimum stress and frequency ranges that would yield a smooth and timely response to the applied stress. These sweeps were performed at an applied stress of 0.01 Pa (within the linear viscoelastic regime) from 0.1 to 3 rad/s. Very low applied stresses (<0.001 Pa) often produced weak signals and scattered data. An applied stress too high often exceeded the yield stress of the premature film and cause rupture. Operating at low frequencies (<0.1 rad/s) required testing times minutes that may have approached or exceeded the aging times. At high frequencies (>3 rad/s), high bob inertia caused erroneous data. After the final frequency sweep, a stress sweep at 1 rad/s was used to determine the film yield stress.

The stress sweep was performed until the film ruptured (at either the bob edge or at the cup wall). Upon completion, the PTFE cap was removed, the oil was extracted via pipette and the bob was raised and detached from the rheometer. The remaining oil and water were both extracted to expose the film (if present). Alternating methylene chloride and acetone rinsing helped to dissolve the film from the glass. Finally, the redissolved/dispersed film material was transferred to a small vial for drying and weighing.

5.3 Results and Discussion

5.3.1 Rheological Behavior of a Rigid Interfacial Film

A solution of B6 asphaltenes in 35 mL of heptol (55 % v/v toluene) was transferred onto the water surface and the interface aged for 24 hours. Frequency and stress sweeps were performed to obtain representative data of a rigid film. When using the transparent glass sample cup, the oil-water interface showed the signs of asphaltene adsorption after just a few minutes of aging. The interface, initially black colored due to the opacity of the asphaltene solution, rapidly became light brown as asphaltenes adsorbed. Adsorption quickly covered the entire interface from the biconical bob edge to the glass wall. The adsorbed asphaltenes clearly adsorbed within the gaps of the bob serrations designed to maximize adhesion to the bob edge. Initial experimentation established that the degree of adsorption and consolidation was insufficient for rheological testing until at least 1-2 hours of aging due to instrument sensitivity. At short aging times, the applied stress necessary to generate the minimum torque (0.1 μNm) was greater than the film yield stress.

Upon aging for 24 hours, an oscillatory frequency sweep (Figure 5.2) was performed at an applied stress of 0.01 Pa from 0.1 to 3 rad/s and revealed elastic solid-like behavior in which G′ increased slightly and was about one order of magnitude greater than G″. Since tan $\delta < 1$ the film was solid-like throughout the frequency range tested. At higher frequencies, the response to the applied oscillation became clouded by the effects of bob inertia; however, inertial effects were minimized as the film became more rigid and developed. Frequency sweeps at very short aging times (less than 1 hour) occasionally showed G′-G″ crossover where tan $\delta = 1$ indicating a weakly cross linked film.

The 24-hour frequency sweep was followed by a stress sweep (Figure 5.3) at 1.0 rad/s from the minimum applied stress to the yield stress. We saw that the linear viscoelastic regime extended over two decades of applied stress. As the applied stress approached the rupture point, the film began to break down as witnessed by the sharp decrease in elastic modulus. At the same time, the viscous modulus rose to a maximum during film rupture. This peak in G″ arose as the solid film began to rupture and introduced many defects with entrained liquid. The liquid conferred a greater viscous nature as the film began to yield. When the applied stress exceeded the rupture stress the bob ultimately spun free from the resisting film and G′ and G″ reduced to values associated with a non-viscoelastic, asphaltene free oil-water interface. The film separated from either the edge of the bob or the glass cylinder wall in all experiments. In most cases the film ruptured along the bob edge. The yield stress measured for this process could be considered a lower bound on the actual yield stress due to limitations on the adsorptive behavior between asphaltenes and glass/stainless steel.

After the film was sheared beyond its rupture point, further rheological experimentation was discontinued and the sample cell was cleaned. The oil phase was pipetted from the cell exposing the light-brown film. The film had considerable resistance to probing with a pipette tip and a thickness on the order of microns (by visual inspection). Measurements of the film mass appear later and are presented to elucidate possible differences in the ratio between elastic modulus and mass according to aging time, aromatic solvent content, or asphaltene concentration.

The effect of interface aging on film elasticity is shown in Figure 5.4. Interfacial aging allows enhanced asphaltene adsorption and consolidation that contribute to film

rigidity. Only G′ appears on this plot to improve clarity and since we found the magnitude of the elastic modulus to be a better measure of film growth. To further aid comparison of asphaltene films growth, the magnitude of G′ at 1 rad/s was selected from each frequency sweep and plotted as a function of time. A plot of G′ versus time for this system (half-filled squares) is shown in Figure 5.4 (inset). Below 2 hours no frequency sweeps were performed due to insufficient film modulus. Between 2 and 8 hours the rate of film growth as measured by its elastic modulus was nearly constant. G′ continued to increase to 24 hours, whereupon, the rate of growth slowly decreased. This growth process can be explained by a combination of asphaltene adsorption and consolidation. The available supply of asphaltenes in solution provided a driving force for adsorption from the bulk. The interface may behave like an infinite sink capable of adsorbing all asphaltenes in solution. This is unlikely, however, as the region above the film will become a region of high asphaltene concentration and remain in dynamic equilibrium with adsorbed asphaltenes. We will investigate the degree of film consolidation and asphaltene adsorption shortly.

It appears that by extrapolating to zero time, G′ passes through the origin. Also, films with G′ < 1 Pa were typically not consolidated enough to withstand the applied stress and the measured strain was high. The minimum time required to age the film therefore was approximately at the intersection of a horizontal line through G′ = 1 Pa and the extrapolated G′ versus time line to the origin. We found that high strains resulted when films were probed at short times due to insufficient asphaltene adsorption and consolidation.

5.3.2 Asphaltene Solubility and its Effects on Film Rheology

The limits of asphaltene solubility in heptol were determined by filtration experiments and have been reported in a previous publication [63]; all four asphaltenes studied were completely soluble above toluene volume fractions ranging from 0.48 to 0.52. Below this toluene concentration, the fraction of precipitate increased as the ratio of heptane to toluene increased. SANS of asphaltene aggregates in heptol solution showed that aggregate correlation lengths reached their maximum at the solubility limit. Higher toluene volume fractions reduced the degree of aggregation by disrupting intermolecular π-bonding between asphaltene monomers. At the solubility limit, enhanced aggregation produced a large driving force for adsorption to oil-water interfaces. This effect was seen in the stability of water-in-oil emulsions formed with asphaltenes near their solubility limit.[67] Well-solvated asphaltenic aggregates create much weaker emulsions than larger, interfacially active aggregates. This phenomenon also translates to the growth of films probed using interfacial rheology.

Figure 5.5 shows the effect of solvency on film elasticity as a function of aging time. At 55 % toluene the asphaltenes formed sizeable aggregates and were driven to adsorb strongly. As a result, elasticity grew at a rate higher at 55 % than at 60 or 80 % toluene, where the aggregates were better solvated slower to adsorb to the oil-water interface. More than 5 hours of aging was required at 80 % toluene to ensure a well-formed film existed before testing. It is clear that the films had not reached their equilibrium elasticity even after 24 hours and that adsorption and consolidation were still proceeding.

In contrast to the films formed by well-solvated asphaltenes, systems containing a large fraction of precipitated asphaltenes behave quite differently. In heptol with a toluene

volume fraction of 0.4, approximately 33 % (w/w) of the asphaltenes are insoluble and form large (> 1 μm) flocs. The quiescent lower density oil phase will naturally rest on top of the aqueous phase. Since the large flocs are not soluble, they settle onto the oil-water interface. Previous studies found that emulsions formed by the isolated insoluble material, when redissolved in toluene and mixtures of heptane and toluene, were as stable as those formed by the unfractionated asphaltenes.[67] This less-soluble or "Precipitate" fraction was also shown to possess a higher level of aromaticity (lower H/C), polarity (higher N), and heavy metals (Ni and V) than the more-soluble, or "Soluble" or unfractionated "Whole" asphaltenes (Table 5.1).[63] Thus, by inducing the flocculation of the most aromatic and polar asphaltene fraction, film formation was hindered by both a reduced amount of soluble interfacially active material and an oil-water interface covered by large flocs.

The effects of asphaltene precipitation on film formation and elasticity are shown in Figure 5.6. There is a considerable time lag with the 40 % toluene solution and can be attributed to precipitates at the interface. After 24 hours enough soluble material had adsorbed and consolidated into an elastic film. Certainly, the heavy accumulation of precipitated asphaltenes conferred some resistance to the applied stress and contributed to interfacial elasticity. Prior to 38 hours, film elasticity may have resulted from accumulated precipitates. The jump in G′ from 36 to 38 hours may be due to the formation of a partially consolidated film comprised of some soluble asphaltenes and many precipitated asphaltenes.

Challenges arise when comparing films at different solvencies and aging times. Two standard measures used to aid comparison were G′/film mass (or G′/Mass) and yield stress/G′ (or YS/G′). The ratio G′/Mass differentiates films by their elasticity per unit mass or their degree of consolidation. Two films with comparable elasticity but different film masses will

have different G′/Mass ratios. Low ratios suggest low consolidation and accumulated material that is not well integrated into a coherent film. High ratios suggest higher consolidation and film comprised of soluble and highly surface active asphaltene aggregates. YS/G′ provides another measure of film consolidation and becomes valuable when the film is not recoverable. The yield stress per unit elasticity is the ratio of film strength to film elasticity and describes the brittleness of the film.

Stress sweeps performed on each film immediately following the final frequency sweep are shown in Figure 5.7. G′ is plotted as a function of applied stress at a frequency of 1 rad/s. These films were aged between 24 (55 % toluene) and 72 hours (60 % toluene) making direct comparison difficult. However, G′/Mass and YS/G′ for the 40 % toluene film suggest lower consolidation compared to the films formed under more soluble conditions (see Table 5.2). At 40 % toluene, there was a heavy accumulation of unconsolidated asphaltenes on the interface and a correspondingly high film mass. The film elasticity in this low solubility regime was the lowest of the four systems and resulted in the lowest ratio of elasticity to film mass. The second measure of film consolidation (YS/G′) indicated the 40 % toluene film was the weakest and most brittle of all B6 Whole systems studied. The precipitated material likely conferred some degree of elasticity to the interface but its lack of consolidation led to a low yield stress and low YS/G′. A highly consolidated film is characterized by high G′/Mass and YS/G′. These occur in the soluble regime with B6 Whole asphaltenes. The specific gravities of heptol (~0.75), asphaltenes (~1.2) and water (1), lead to flocculate accumulation on the interface. At solvency conditions in the soluble regime but near the solubility limit and in the insoluble regime, a large accumulation of asphaltenes was observed on the bob and interface. Asphaltene adsorption and precipitation was often

noticed on the bob due to the high surface energy of stainless steel and on the interface. Since it was often difficult to discriminate between asphaltenes adsorbed to the interface and those precipitated or accumulated on top, G′/Mass values may be inflated. The next section discusses films formed by AH, CS, and HO asphaltenes. In some cases, the films were not cohesive enough to recover at the conclusion of an experiment. In addition, precise sampling procedures are required to recover the film after experimentation. Some film material may inadvertently be removed with the oil phase by pipette. Incomplete oil phase removal will cause some soluble asphaltenes to report to the film mass. We estimate the uncertainty on the film masses to be ± 5-10%. For these reasons YS/G′ may be a better discriminator of film consolidation.

In spite of the challenges associated with measuring film mass, we can infer from film mass the polarity of adsorbed asphaltenes. Near the solubility limit asphaltene aggregation is mediated by dispersive interactions between aromatic rings, and polar and hydrogen bonding between functional groups. At these solvent conditions, asphaltenes form aggregates of the largest dimension [63] and are most prone to adsorb. The limited state of solubility drives a large percentage of asphaltenes to the interface, film mass rises and G′/Mass decreases. As the solvent becomes more aromatic, its ability to disrupt π bonding between asphaltene aggregates is reduced. Here, aggregation and adsorption are governed by polar and hydrogen bonding interactions. Thus, aggregates capable of adsorbing to the oil-water interface are the most polar.

Film formed in the soluble regime, above ~50 % toluene, have YS/G′ values more than double those in the insoluble regime. It appears that B6 Whole asphaltenes form films with comparable consolidation from measurements of YS/G′ even though the kinetics of

formation is different. When operating in the soluble regime and near the solubility limit, (e.g. 50-55 % toluene for B6) a high degree of adsorption We found from the analysis of emulsions formed with asphaltenes at these solvency conditions (> 50 % toluene) that their stabilities were quite high. 80 % toluene produced emulsions slightly weaker than at 55 or 60 % toluene due to enhanced solubility. This can be attributed to the longer time scale required for minimum adsorption and consolidation of rigid films.

Diffusion length scales allow comparison between emulsion and interfacial rheology asphaltene adsorption. Emulsions are formed by the high energy mixing of oil and water with dissolved asphaltenes and are stable after just a few seconds of mixing. In a previous study minimum droplet diameters of a few microns were generated after 3 minutes of homogenization.[67] Sufficient adsorption times prior to rheological testing, however, were on the order of hours. In an emulsion, 6 mL of water were completely dispersed as micron sized droplets within 4 mL of oil containing dissolved asphaltenes. The distances between droplets were equally short, on the order of a few microns. Thus, the characteristic diffusion time follows:

$$t_D \cong L^2 / D \tag{2.1}$$

where L is the diffusion length and D is the asphaltene self-diffusion coefficient (~ 1 X 10^{-6} cm^2/s in toluene[68]). In an emulsion $t_D \cong 0.04$ sec, assuming a 2 μm diffusion length. In the case of a large reservoir of asphaltene solution above water and choosing a diffusion length between 0.1 and 0.2 cm, the characteristic diffusion time approaches 10 hours. The induction time of several hours before rheological measurements thus becomes more understandable.

5.3.3 Asphaltene Chemistry and Film Formation

In the previous section, we saw that B6 asphaltenes formed films of highest elasticity near the solubility limit and the kinetics of film formation reduced as their solvency increased. AH, CS, and HO asphaltene solutions (0.75 % w/v) were prepared at solvency conditions near their solubility limit to study film elasticity. Films of HO and CS asphaltene were probed from 10 to 48 hours while AH was tested once at 96 hours (Figure 5.8). By studying the properties of films formed with asphaltenes precipitated from different crude oils we gained a better understanding of adsorption and consolidation mechanisms. The chemical properties of all four asphaltenes and their more and less soluble fractions appear in Table 5.1. AH asphaltenes were the most soluble, formed the smallest aggregates in solution, had high aromaticity, and low nitrogen polarity and metals content. CS asphaltenes formed the largest aggregates, were the most aromatic and also had low polarity and metals content. B6 and HO were both offshore California crude oils and had chemically similar asphaltenes. They had similar aromaticity and higher nitrogen and metals contents than AH or CS. Emulsion stability tests indicated that B6 and HO asphaltene formed the strongest emulsions while AH and CS asphaltenes formed emulsions considerably weaker at all conditions of solvency.

The behavior of HO asphaltene films at 55 and 60 % toluene suggest they were similar in many respects to B6 asphaltene films. Both HO and B6 films were light brown colored and quite resistant to applied stresses. However, HO required nearly five times longer before testing was initiated and G′ at 24 or 48 hours was less than half that of B6 at comparable aging time. The effect of asphaltene solvency was apparent on HO where solutions prepared in 60 % toluene were not as elastic as 55 % toluene solutions.

While the film elasticities of CS asphaltenes were shown to increase with aging time and had a 10+-hour induction period before testing, there were significant differences between CS and films of B6 and HO asphaltenes. At the conclusion of the 55 and 60 % toluene experiments, the oil phases were removed via pipette to reveal a film layer of minimal consolidation. There was no rigid film as found with B6 and HO and the film material appeared to be easily removed through pipette induced convection. Even after attempts to extract the oil phase with minimal convection, the adsorbed asphaltenes were very mobile on the interface. Even though CS at 55 % toluene showed a substantial rise in G′ between 24 and 48 hours, this may be attributed to accumulated, adsorbed asphaltenes that were driven from solution after extended interfacial contact with water. This material, being confined by the glass wall and serrated edge bob, conferred a degree of elasticity with very little consolidation. The asphaltenic aggregates were likely quite large (>250 Å), as measured by SANS in heptol [63] and thus were not able to form a defect-free, cohesive interfacial film.

AH asphaltenes were nearly incapable of forming a rigid-cohesive interfacial film even after 96 hours of interfacial aging. SANS measurements performed on solutions at comparable bulk concentration indicated that AH asphaltenes formed the smallest aggregates of the asphaltenes examined and were very well solvated in heptol.

In Tables 5.2 and 5.3 we find film properties AH, CS, HO and B6 asphaltene that shed light on the differences seen between cohesive film formers (B6 and HO) and unconsolidated film formers (AH and CS). High G′/Mass and YS/G′ were the trademarks of well-consolidated B6 films. HO films actually had higher G′/Mass and YS/G′ than B6 asphaltene films but lower G′ values at comparable aging times. HO asphaltenes formed

smaller aggregates (73 Å) than B6 (98 Å) near the solubility limit as measured by SANS and were slightly less surface active and weaker emulsion formers. Reduced surface activity prevented a larger accumulation of unconsolidated asphaltenes onto the film. As a result the film mass of HO asphaltenes was lower than B6 and G′/Mass was correspondingly higher. Lower film masses and kinetics of formation also indicate that HO asphaltenes are well solvated even near the solubility limit and imply that HO is less polar than B6.

Another interesting byproduct of high surface activity and film adsorption was the tendency of B6 films to expand in the direction of the meniscus formed between oil-water and the cup wall. The contact angle between pure water and clean glass is near 0°. The oil phase pipetted on top at the beginning of the experiment naturally followed the shape of this meniscus. At times greater than 8 to 10 hours the film-glass interface appeared to slowly wrinkle, deform and extend upwards into the oil phase. At 48 hours this process changed the appearance of the film edge noticeably (see Figure 5.9). Decreased adhesion of the film to the glass surface at this stage of film aging may have reduced the yield stress and led to lower YS/G′ values than HO. HO was slower to form and did not appear to exhibit the same degree of edge effects.

In contrast to B6 and HO films, CS films had YS/G′ values nearly five fold lower. Stress sweeps of CS and HO asphaltene systems after aging for 48 hours are shown in Figure 5.10. While CS films had higher elasticities than HO at comparable solvencies and aging times, their yield stresses were nearly three fold lower. The lower yield stresses of CS translated to YS/G′ values close to 10 while HO had values greater than 50. Loose connections between adjacent CS asphaltenic aggregates conferred interfacial elasticity but under stress, the weak fabric holding the film together broke down more easily. As a result,

CS films were quite brittle compared to HO and B6 films. The poor film formation of AH and CS suggests even lower polarity than B6 and HO asphaltenes. B6 asphaltenes, however, were less effective film formers in the insoluble regime and YS/G′ was much closer (18.3) to that of CS (10.1-12.1). The same convective forces applied successfully to pipette the oil phase from B6 and HO films apparently loosened and dispersed the CS film structure. Subsequently, no CS films were recovered. AH asphaltene aggregates were too soluble to create elastic films or measurable film masses.

5.3.4 Asphaltene Fraction Rheology

Film properties of B6, HO and CS Precipitate asphaltenes are presented in Table 5.4. Limited solubility of the asphaltenes at intermediate toluene fractions precluded testing at these conditions. The elasticities of B6 and HO Precipitate films at such high toluene volume fractions (0.8-1.0) were remarkable. This asphaltene fraction, though only slightly more aromatic and polar than the Whole asphaltenes, was significantly more surface active. Clearly fractionation by heptol solubility, has isolated a group of asphaltenes capable of forming very rigid films and strong emulsions [67] in highly aromatic solvents. HO Precipitate formed films of particularly high consolidation, where G′/Mass exceeded 1000 Pa/g and YS/G′ was indicative of cohesion. B6 Precipitate was more prone to interfacial adsorption as suggested by the high film mass and lower G′/mass than HO. CS Precipitate was nearly incapable of elastic film formation even after 100 hours of aging. Very large aggregates and poor solubility led to very weak consolidation and no cohesive, recoverable film.

5.3.5 Quantifying Film Consolidation and Adsorption

Several processes of interfacial film formation were buried within the G′ versus time trend, namely adsorption, desorption and consolidation. To determine how these processes impact film elasticity, we allowed the asphaltene solutions to remain above the interface for discrete time periods then carefully removed them via pipette. The interface was rinsed with toluene to remove any remaining asphaltene solution and prevent further adsorption. Asphaltene-free solutions of heptol at the same toluene volume fraction were then transferred to the interface. This procedure was performed at several time intervals on identical B6 Whole asphaltene, 60 % (v/v) toluene systems as well as B6 Precipitate in 100 % toluene. The results of oil replacement are shown in Figures 5.11 and 5.12. The control system showed some positive and negative elasticity deviation at the longest times as a result of the aforementioned tendency of well-formed films in the presence of an asphaltene solution to wrinkle at the cup wall.

The first oil replacement occurred after 4 hours of interface aging where the first three points represent film elasticities at 2, 3, and 4 hours in the presence of asphaltenes. Following the frequency sweep at 4 hours, the oil phase was replaced and film left undisturbed for approximately 35 minutes until the 5-hour frequency sweep. G′ at 5 hours was only slightly higher (0.1 Pa) than the control experiment. The increase in elasticity from 5 to 6 hours was substantial and nearly 1 Pa higher than the control. Film elasticity continued to rise in the absence of adsorbing asphaltenes until 12 hours and varied little for the next 36 hours. Between 4 and 12 hours, G′ was higher than the control possibly due to the applied convective forces during oil transfer. Molecular ordering and the process of

interfacial consolidation continued for 12 hours. Beyond 12 hours, the asphaltene aggregates were likely in their final state of molecular ordering.

Two additional oil replacements were performed after the 8 and 12-hour frequency sweeps. Before oil replacement these two films formed slightly slower than the control film therefore the 8 and 12-hour G′ values were slightly lower than the control. After replacement, each film's elasticity surpassed the control film within 4 to 6 hours. The 8 and 12-hour replacement experiments reached their plateau G′ values after 8 additional hours of aging (G′ of the 12-hour film at the 16^{th} and 48^{th} hours were equivalent). The overturn in G′ of the 12-hour film between the 16^{th} and 42^{nd} hour was likely caused by a small degree of asphaltene desorption or molecular arrangement within the film. In all cases, very little asphaltene desorption was evident and the films were quite rigid after 48 hours of aging. The affinity of the asphaltenes for the oil-water interface clearly exceeded the solvating power of heptol and adsorption appears to be irreversible in this case.

A fourth replacement experiment was performed in an attempt to desorb asphaltenes from the interface with a known asphaltene solvent. A 0.75 % w/v resin solution was prepared in 35 mL of 40:60 heptol. This solution was added to the film after an identical oil removal procedure. The solvating power of resins is evident as G′ fell significantly between the fourth and fifth hours. However, further desorption was not witnessed and the film began to consolidate under the new solvency conditions.

The final replacement experiment showed the degree of Precipitate asphaltene film consolidation (Figure 5.12). After 4 hours of aging, the B6 Precipitate solution was removed from the cell and replaced with pure toluene. At the 8^{th} hour, consolidation had ceased and

G′ was more than twice the magnitude 4 hours prior. Further testing revealed a very slight decrease in film elasticity over the next 40 hours.

G′/Mass and YS/G′ values for each film are listed in Table 5.5. The films subjected to rinsing had lower masses than the control film and correspondingly higher G′/Mass values. This suggests that some of the additional asphaltenes adsorbed after 72 hours of asphaltene solution contact did not necessarily contribute to film elasticity and resulted in lower overall consolidation. G′/Mass of the resin experiment was noticeably lower than the resin-free films. It is likely that the resin solution was ineffective at removing asphaltenes from the interface but was able to disrupt the degree of film cohesion. Comparable YS/G′ values suggested that the films were ostensibly similar in form and degree of consolidation.

5.4 Conclusions

Asphaltene films formed at oil-water interfaces were successfully probed by interfacial shear rheometry with a serrated edge biconical bob. The films exhibited linear viscoelasticity and yield stresses. Elasticity and yield stress of the films increased with aging time and did not appear to reach equilibrium after several days due to an abundant asphaltene supply. Many factors influenced the degree of interfacial adsorption, elasticity, and yield stress. B6 and HO asphaltenes were the least aromatic, most polar (by nitrogen content) and had the highest concentrations of heavy metals (Ni and V). They formed films with a distinctive light-brown color, high elasticity and yield stress. Near the solubility limit, asphaltenes were highly aggregated, films formed rapidly and had considerable mass. In more aromatic solvents, interfacial adsorption was likely dominated by polar asphaltenes due to the high degree of solvent dispersion forces. These films did not form as quickly and

elasticity and yield stress at comparable aging times was lower. In the insoluble regime, precipitation hindered the adsorption process and measurable elasticities were obtained after much longer aging times. G′/film mass and yield stress/G′ were developed to measure the degree of asphaltene consolidation. Films at high solvent aromaticity had higher G′/Mass since the film masses were considerably lower than solvents near the asphaltene solubility limit. B6 and HO films also had high values of yield stress/G′ indicating substantial consolidation and film strength.

AH and CS asphaltenes were more aromatic, less polar and had low concentrations of heavy metals. AH films were often too weak to measure. CS films were measurable but weaker than B6 or HO films. They did not possess the light-brown color and high degree of consolidation indicative of B6 or HO films either. CS films had such low consolidation that the adsorbed asphaltenes dispersed under convective forces during oil phase removal. In these cases, G′/film mass comparisons were not possible. Yield stress/G′ indicated CS and AH films were more than four times "weaker" than B6 of HO.

Film elasticities and yield stresses were also measured on fractionated asphaltenes. The fractionation concentrated the less soluble, more polar and aromatic asphaltenes with a greater propensity to adsorb at the oil-water interface. B6 and HO fractions formed film faster than unfractionated asphaltenes with higher elasticities at comparable aging times in highly aromatic solvents. Adsorption at high solvent aromaticity was likely dominated by asphaltenes with considerable polarity and ability to form hydrogen bonds. Film consolidation exceeded that of the unfractionated asphaltenes as well.

Oil replacement experiments demonstrated the dual film formation processes of asphaltene adsorption and aggregate consolidation. After the asphaltene solution was

removed and further adsorption was eliminated, film elasticity increased for several hours then reached equilibrium. Films aged longer after solution replacement, had higher ratios of yield stress to G′ indicating enhanced consolidation. Replacing the oil phase with resins in heptol rapidly reduced film elasticity due to film solvation.

The long time film elasticities and yield stresses of the asphaltenes correlate with the stability of emulsions formed at similar asphaltene concentrations and heptol ratios. Asphaltenes are well solvated in highly aromatic solvents, form films of lower elasticity, and yield stress and weaker emulsions. Enhanced aggregation near the solubility limit, contributes to strong film and emulsion formation. B6 and HO asphaltenes have higher polarity and form well consolidated films and strong emulsions. AH and CS have lower polarity and are poor film and emulsion formers. B6 and HO fractions of enhanced polarity form very strong films and emulsions even in highly aromatic solvents. These results strongly suggest that asphaltene chemistry dictates the properties of adsorbed films and that film shear elasticity and yield stress determine the strength of asphaltene stabilized water-in-oil emulsions.

5.5 Acknowledgements

This research was supported by funding from PERF (97-07), the National Science Foundation (CTS-981727), ExxonMobil, Ondeo-Nalco Energy Systems, Shell, and Texaco.

5.6 References

1. Benjamins, J. and F.V. Vader, "The Determination of the Surface Shear Properties of Adsorbed Protein Layers," *Colloids and Surfaces*, 1992, **65** (2-3): p. 161-174.

2. Benjamins, J., A. Cagna and E.H. LucassenReynders, "Viscoelastic properties of triacylglycerol/water interfaces covered by proteins," *Colloids and Surfaces a-Physicochemical and Engineering Aspects*, 1996, **114**: p. 245-254.

3. Nino, M.R.R., et al., "Surface dilational properties of protein and lipid films at the air-water interface," *Langmuir*, 1998, **14** (8): p. 2160-2166.

4. Dufour, E., M. Dalgalarrondo and L. Adam, "Conformation of beta-lactoglobulin at an oil/water interface as determined from proteolysis and spectroscopic methods," *Journal of Colloid and Interface Science*, 1998, **207** (2): p. 264-272.

5. Ybert, C. and J.M. di Meglio, "Study of protein adsorption by dynamic surface tension measurements: Diffusive regime," *Langmuir*, 1998, **14** (2): p. 471-475.

6. Inokuchi, K., "Rheology of Surface Films IV. Viscoelastic Properties of 6-Nylon Films at Air/Water Interface," *Bulletin of the Chemical Society of Japan*, 1955, **28** (7): p. 453-465.

7. Grace, R., *Commercial Emulsion Breaking*, in *Emulsions: Fundamentals and Applications in the Petroleum Industry*, L.L. Schramm, Editor. 1992, American Chemical Society: Washington, D.C. p. 313-339.

8. Obah, B., "The Chemical Demulsification of Crude Oil Emulsion: Problem in a Niger Delta Oil Terminal," *Erdohl, Kohle, Erdgas Petrochemie*, 1988, **41** (2): p. 71-74.

9. Neumann, H., "Investigations Regarding the Separation of Crude Oil Emulsions," *Petrochemie*, 1965, **18**: p. 776-779.

10. Eley, D.D., et al., "Electron Micrography of Emulsions of Water in Crude Petroleum," *Journal of Colloid and Interface Science*, 1976, **54** (3): p. 462-466.

11. Taylor, S.E., "Resolving Crude Oil Emulsions," *Chemistry and Industry*, 1992, **20**: p. 770-773.

12. Shetty, C.S., A.D. Nikolov and D.T. Wasan, "Demulsification of Water in Oil Emulsions Using Water Soluble Demulsifiers," *Journal of Dispersion Science and Technology*, 1992, **13** (2): p. 121-133.

13. Blair, C.M., "Interfacial Films Affecting the Stability of Petroleum Emulsions," *Chemistry and Industry*, 1960: p. 538-544.

14. Little, R.C., "Breaking Emulsions of Water in Navy Fuel Oils," *Fuel*, 1974, **53** (10): p. 246-252.

15. Mackay, G.D.M., et al., "The Formation of Water-in-Oil Emulsions Subsequent to an Oil Spill," *Journal of the Institute of Petroleum*, 1973, **59** (568): p. 164-172.

16. Strassner, J.E., "Effect of pH on Interfacial Films and Stability of Crude Oil-Water Emulsions," *Journal of Petroleum Technology*, 1968, **20**: p. 303-312.

17. Dodd, C.G., "The Rheological Properties of Films at Crude Petroleum-Water Interfaces," *Journal of Physical Chemistry*, 1960, **64** (5): p. 544-550.

18. Graham, D.E., A. Stockwell and D.G. Thompson, *Chemical Demulsification of Produced Crude Oil Emulsions*, in *Chemicals in the Oil Industry*, P.H. Ogden, Editor. 1983, Royal Society of Chemistry: Sunbury-on-Thames, Middlesex, U. K. p. 73-91.

19. Johansen, E.J., et al., "Water-in-Crude Oil Emulsions from the Norwegian Continental Shelf Part I. Formation, Characterization and Stability Correlations," *Colloids and Surfaces*, 1989, **34**: p. 353-370.

20. Cratin, P.D., "A Quantitative Characterization of pH-Dependent Systems," *Industrial and Engineering Chemistry*, 1969, **61** (2): p. 35-45.

21. Oren, J.J. and G.D.M. MacKay, "Electrolyte and pH Effect on Emulsion Stability of Water-in-Petroleum Oils," *Fuel*, 1977, **56** (10): p. 382-384.

22. Mansurov, I.R., E.Z. Il'yasova and V.P. Vygovskoi, "Shear Strength of Interfacial Films of Asphaltenes," *Chemistry and Technology of Fuels and Oils*, 1987, **23** (1-2): p. 96-98.

23. Siffert, B., C. Bourgeois and E. Papirer, "Structure and Water-Oil Emulsifying Properties of Asphaltenes," *Fuel*, 1984, **63** (6): p. 834-837.

24. Menon, V.B. and D.T. Wasan, "Coalescence of Water-in-Shale Oil Emulsions," *Separation Science and Technology*, 1984, **19** (8 & 9): p. 555-574.

25. Mukherjee, S. and A.P. Kushnick. *Effect of Demulsifiers on Interfacial Properties Governing Crude Oil Demulsification*. in *Symposium On Advances in Oil Field Chemistry Presented Before the Division of Petroleum Chemistry, Inc.* 1988. Toronto: American Chemical Society.

26. Isaacs, E.E., et al., "Electroacoustic Method for Monitoring the Coalescence of Water-in-Oil Emulsions," *Colloids and Surfaces*, 1990, **46**: p. 177-192.

27. van der Waarden, M., "Stability of Emulsions of Water in Mineral Oils Containing Asphaltenes," *Kolloid Z. Z. Polymer*, 1958, **156** (2): p. 116-122.

28. Hassander, H., B. Johansson and B. Tornell, "The Mechanism of Emulsion Stabilization by Small Silica (Ludox) Particles," *Colloids and Surfaces*, 1989, **40**: p. 93-105.

29. Papirer, E., et al., "Chemical Nature of Water/oil Emulsifying Properties of Asphaltenes," *Fuel*, 1982, **61**: p. 732-734.

30. Aveyard, R., et al., "The Resolution of Water-in-Crude Oil Emulsions by the Addition of Low Molar Mass Demulsifiers," *Journal of Colloid and Interface Science*, 1990, **139** (1): p. 128-138.

31. Lawrence, A.S.C. and W. Killner, "Emulsions of Seawater in Admiralty Fuel Oil with Special Reference to their Demulsification," *Journal of the Institute of Petroleum*, 1948, **34**: p. 281.

32. McLean, J.D. and P.K. Kilpatrick, "Effects of Asphaltene Solvency on Stability of Water-in-Crude Oil Emulsions," *Journal of Colloid and Interface Science*, 1997, **189**: p. 242-253.

33. Al-Jarrah, M.M.H. and A.H. Al-Dujaili, "Characterization of Some Iraqi Asphalts II. New Findings on the Physical Nature of Asphaltenes," *Fuel Science and Technology International*, 1989, **7** (1): p. 69-88.

34. Reynolds, J.G. and W.R. Biggs, "Effects of Asphaltene Precipitation and a Modified D 2007 Separation on the Molecular Size of Vanadium- and Nickel-Containing Compounds in Heavy Residua," *Fuel Science and Technology International*, 1986, **4** (6): p. 749-777.

35. Nghiem, L.X., et al., "Efficient Modelling of Asphaltene Precipitation," *Society of Petroleum Engineers*, 1993, **5**: p. 375-384.

36. Mitchell, D.L. and J.G. Speight, "The Solubility of Asphaltenes in Hydrocarbon Solvents," *Fuel*, 1973, **52** (4): p. 149-152.

37. Yen, T.F., J.G. Erdman and S.S. Pollack, "Investigation of Structure of Petroleum Asphaltenes By X-Ray Diffraction," *Analytical Chemistry*, 1961, **33** (11): p. 1587-&.

38. Acevedo, S., et al., "Asphaltenes and Resins From the Orinoco Basin," *Fuel*, 1985, **64**: p. 1741-1747.

39. Boduszynski, M.M., "Composition of Heavy Petroleums. 2. Molecular Characterization," *Energy & Fuels*, 1988, **2** (5): p. 597-613.

40. Wiehe, I.A. and K.S. Liang, "Asphaltenes, Resins, and other petroleum macromolecules," *Fluid Phase Equilibria*, 1996, **117** (1-2): p. 201-210.

41. McKay, J.F., et al., "Petroleum Asphaltenes: Chemistry and Composition," *Analytical Chemistry of Liquid Fuel Sources, Advances in Chemistry Series*, 1978, **170**: p. 128-142.

42. Andersen, S.I., A. Keul and E. Stenby, "Variation in composition of subfractions of petroleum asphaltenes," *Petroleum Science and Technology*, 1997, **15** (7-8): p. 611-645.

43. Yarranton, H.W. and J.H. Masliyah, "Molar Mass Distribution and Solubility Modeling of Asphaltenes," *AICHE Journal*, 1996, **42** (12): p. 3533-3543.

44. Yarranton, H.W., H. Alboudwarej and R. Jakher, "Investigation of asphaltene association with vapor pressure osmometry and interfacial tension measurements," *Industrial & Engineering Chemistry Research*, 2000, **39** (8): p. 2916-2924.

45. Barbour, R.V. and J.C. Petersen, "Molecular Interactions of Asphalt: An Infrared Study of the Hydrogen-Bonding Basicity of Asphalt," *Analytical Chemistry*, 1974, **46** (2): p. 273-277.

46. Boduszynski, M.M., J.F. McKay and D.R. Latham, "Asphaltenes, Where Are You?," *Proceedings of the Association of Asphalt Paving Technologists*, 1980, **49**: p. 123-143.

47. Ignasiak, T., O.P. Strausz and D.S. Montgomery, "Oxygen Distribution and Hydrogen Bonding in Athabasca Asphaltene," *Fuel*, 1977, **56**: p. 359-365.

48. Moschopedis, S.E. and J.G. Speight, "Investigation of Hydrogen Bonding by Oxygen Functions in Athabasca Bitumen," *Fuel*, 1976, **55**: p. 187-192.

49. Petersen, J.C., "An Infra-red Study of Hydrogen Bonding in Asphalt," 1967: p. 295-305.

50. Miller, R., et al., "Dilational and Shear Rheology of Adsorption Layers at Liquid Interfaces," *Colloids and Surfaces A: Physicochemical and Engineering Aspects*, 1996, **111**: p. 75-118.

51. Langmuir, I., *Science*, 1936, **84**: p. 303.

52. Wibberley, K., "Some Physical Properties of Interfacial Films of Potassium Arabate," *Journal of Pharmacy and Pharmacology*, 1962, **14**: p. 87T.

53. Nagarajan, R., S.I. Chung and D.T. Wasan, "Biconical bob oscillatory interfacial rheometer," *Journal of Colloid and Interface Science*, 1998, **204** (1): p. 53-60.

54. Pasquarelli, C.H. and D.T. Wasan, *The Effect of Film-Forming Materials On the Dynamic Interfacial Properties In Crude Oil-Aqueous Systems*, in *Surface Phenomena in Enhanced Oil Recovery*, D.O. Shah, Editor. 1981, Plenum Press: New York. p. 237-248.

55. Eley, D.D., M.J. Hey and M.A. Lee, "Rheological Studies of Asphaltene Films Adsorbed at the Oil/Water Interface," *Colloids and Surfaces*, 1987, **24**: p. 173-182.

56. Wasan, D.T., *Destabilization of Water-in-Oil Emulsions*, in *Emulsions - A Fundamental and Practical Approach*, J. Sjöblom, Editor. 1992, Kluwer Academic Publishers: Netherlands. p. 283-295.

57. Acevedo, S., et al., "Interfacial Rheological Studies of Extra-Heavy Crude Oils and Asphaltenes: Role of the Dispersion Effect of Resins in the Adsorption of Asphaltenes at the Interface of Water-in-Crude Oil Emulsions," *Colloids and Surfaces A: Physicochemical and Engineering Aspects*, 1993, **71**: p. 65-71.

58. Mohammed, R.A., et al., "Dewatering of Crude Oil Emulsions 2. Interfacial Properties of the Asphaltic Constituents of Crude Oil," *Colloids and Surfaces A: Physicochemical and Engineering Aspects*, 1993, **80**: p. 237-242.

59. Khristov, K., et al., "Thin liquid film technique - application to water-oil-water bitumen emulsion films," *Colloids and Surfaces a-Physicochemical and Engineering Aspects*, 2000, **174** (1-2): p. 183-196.

60. Cairns, R.J.R., D.M. Grist and E.L. Neustadter. *The Effect of Crude Oil-Water Interfacial Properties on Water-Crude Oil Emulsion Stability*. in *Theory and Practice of Emulsion Technology*. 1974. Brunel University: Academic Press.

61. Neustadter, E.L., K.P. Whittingham and D.E. Graham, *Interfacial Rheological Properties of Crude Oil/Water Systems*, in *Surface Phenomena in Enhanced Oil Recovery*, D.O. Shah, Editor. 1981, Plenum Press: New York. p. 307-326.

62. Mohammed, R.A., et al., "Dewatering of Crude Oil Emulsions 1. Rheological Behavior of the Crude OIl-Water Interface," *Colloids and Surfaces A: Physicochemical and Engineering Aspects*, 1993, **80**: p. 223-235.

63. Spiecker, P.M. and P.K. Kilpatrick, "Aggregation and solubility behavior of petroleum asphaltenes and their subfractions," *Langmuir, to be submitted*, 2001.

64. Shotton, E., et al., "A Versatile Surface Rheometer," *Rheological Acta*, 1971, **10**: p. 142-152.

65. Larson, R.G., *The structure and rheology of complex fluids*. Topics in Chemical Engineering, ed. K.E. Gubbins. 1999, New York: Oxford University Press.

66. Sheu, E.Y., M.M. Detar and D.A. Storm, "Interfacial Properties of Asphaltenes," *Fuel*, 1992, **71** (11): p. 1277-1281.

67. Spiecker, P.M. and P.K. Kilpatrick, "The Role of Asphaltene Solubility and Chemistry on the Stability of Water-in-Oil Emulsions," *Journal of Colloid and Interface Science, to be submitted*, 2001.

68. Ostlund, J.A., S.I. Andersson and M. Nyden, "Studies of asphaltenes by the use of pulsed-field gradient spin echo NMR," *Fuel*, 2001, **80** (11): p. 1529-1533.

Table 5.1 Asphaltene Chemistry

Asph	Fraction	Solubility Limit (% Toluene)	ξ (Å)	H/C	N (wt%)	Ni (ppm)	V (ppm)
AH	Sol	38	34.5	1.17	0.92	84	350
	Whole	48	67.3	1.14	1.02	160	490
	Ppt	60	130	1.13	1.08	160	540
HO	Sol	45	52.3	1.30	1.95	340	930
	Whole	52	72.8	1.29	1.99	360	950
	Ppt	80	200	1.24	2.11	410	1100
B6	Sol	42	62.7	1.30	1.81	350	1000
	Whole	52	97.6	1.24	1.87	330	1000
	Ppt	90	262	1.22	1.93	410	1200
CS	Sol	40	138	1.12	1.32	19	42
	Whole	50	246	1.11	1.32	21	48
	Ppt	70	520	1.09	1.39	28	48

Table 5.2 B6 Whole Asphaltene Film Properties: 0.75 % w/v in Heptol, Frequency – 1 rad/s

% Tol	Aging Time (hrs)	G′ (Pa)	Yield Stress (Pa)	Film Mass (g)	G′/Mass (Pa/g)	YS/G′ (x 10^3)
40	48	7.91	0.145	0.0850	93.1	18.3
55	24	12.82	0.497	0.0532	241	38.8
60	72	17.22	0.770	0.0409	421	44.6
80	48	9.18	0.365	0.0200	459	39.8

Table 5.3 Whole Asphaltene Film Properties in the Soluble Regime: 0.75 % w/v in Heptol, Frequency – 1 rad/s

Asph	% Tol	Aging Time (hrs)	G′ (Pa)	Yield Stress (Pa)	Film Mass (g)	G′/Mass (Pa/g)	YS/G′ (x 10^{-3})
HO	55	48	5.55	0.297	0.0097	572	53.4
	60	48	3.64	0.218	0.0068	536	59.9
CS	55	48	10.51	0.106	-	-	10.1
	60	48	5.25	0.0636	-	-	12.1
AH	55	96	0.64	-	-	-	-

Table 5.4 Precipitate Asphaltene Film Properties in the Soluble Regime: 0.75 % w/v in Heptol, Frequency – 1 rad/s

Asph	% Tol	Aging Time (hrs)	G′ (Pa)	Yield Stress (Pa)	Film Mass (g)	G′/Mass (Pa/g)	YS/G′ (x 10^{-3})
B6	100	48	28.37	0.834	0.0492	577	29.4
HO	80	48	17.36	0.750	0.0148	1170	43.3
	90	24	6.62	0.405	0.0066	1000	61.0
CS	90	144	2.525	0.0252	-	-	10.0

Table 5.5 Film Properties of B6 Whole and Precipitate Asphaltenes after Replacing Oil Phase with Neat Heptol: 0.75 % w/v in Heptol, Frequency – 1 rad/s

Fraction	Replacement Time (hrs)	G′ (Pa)	Yield Stress (Pa)	Film Mass (g)	G′/Mass (Pa/g)	YS/G′ (x 10^{-3})
Whole	None (72 hr test)	17.22	0.770	0.0409	421	44.6
	12	6.78	0.405	0.0120	565	59.5
	8	5.73	0.405	0.0093	616	70.4
	4	4.78	0.365	0.0100	478	76.3
	4 w/ Resins	2.20	0.106	0.0152	145	48.3
Ppt	None (48 hr test)	28.37	0.834	0.0492	577	29.4
	4	8.95	0.448	0.0187	479	50.0

First rows of B6 Whole and B6 Precipitate data in table refer to films aged in contact with asphaltene solution for 72 hours and 48 hours, respectively, and no oil phase replacement. All replacement experiments aged for a total of 48 hours.

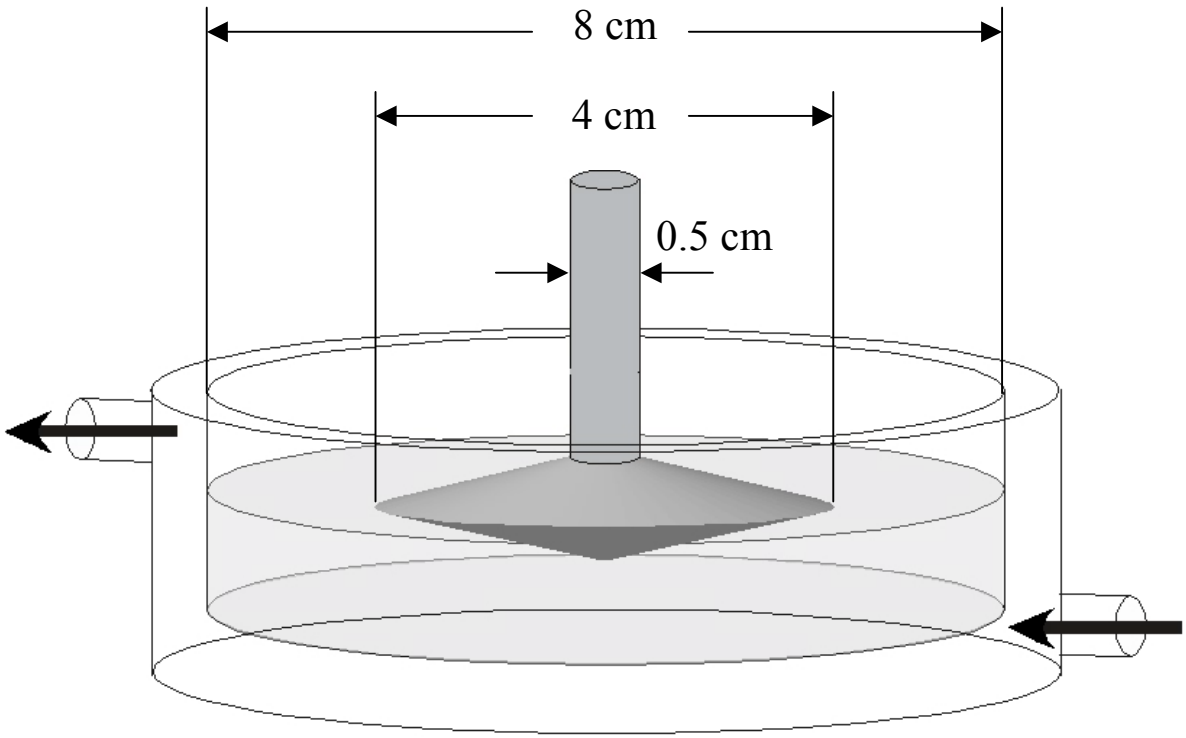

Figure 5.1 Biconical bob and cup rheometer cell

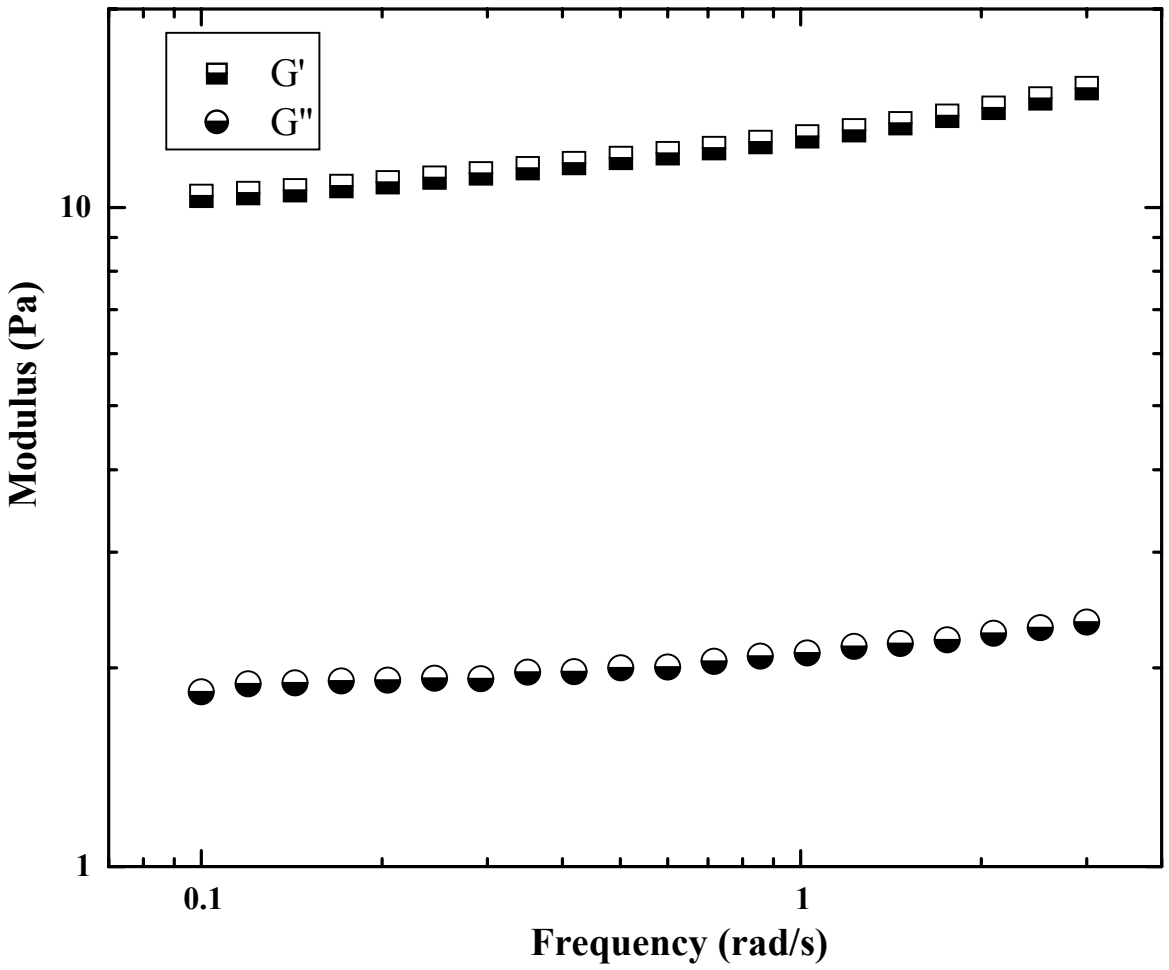

Figure 5.2 B6 Whole asphaltene film frequency sweep: 0.75 % w/v, 55 % toluene, 0.01 Pa, 24 hours.

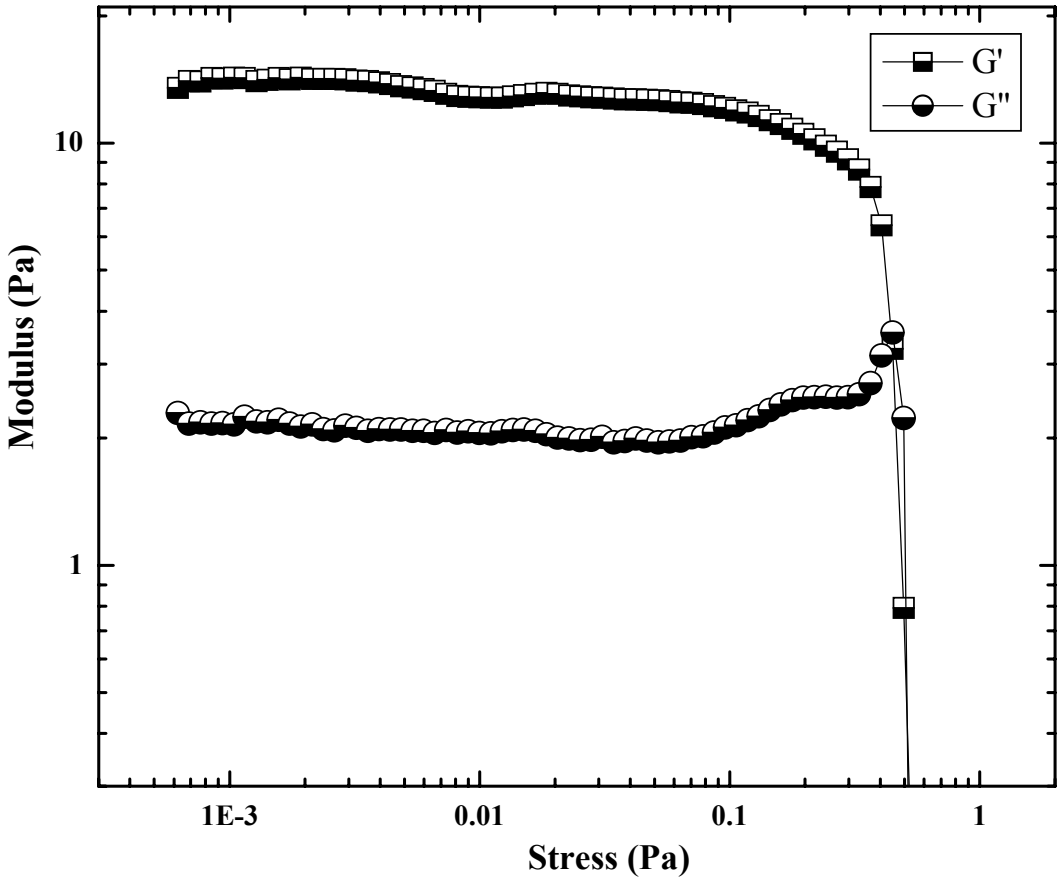

Figure 5.3 B6 Whole asphaltene film stress sweep: 0.75 % w/v, 55 % toluene, 1 rad/s, 24 hours.

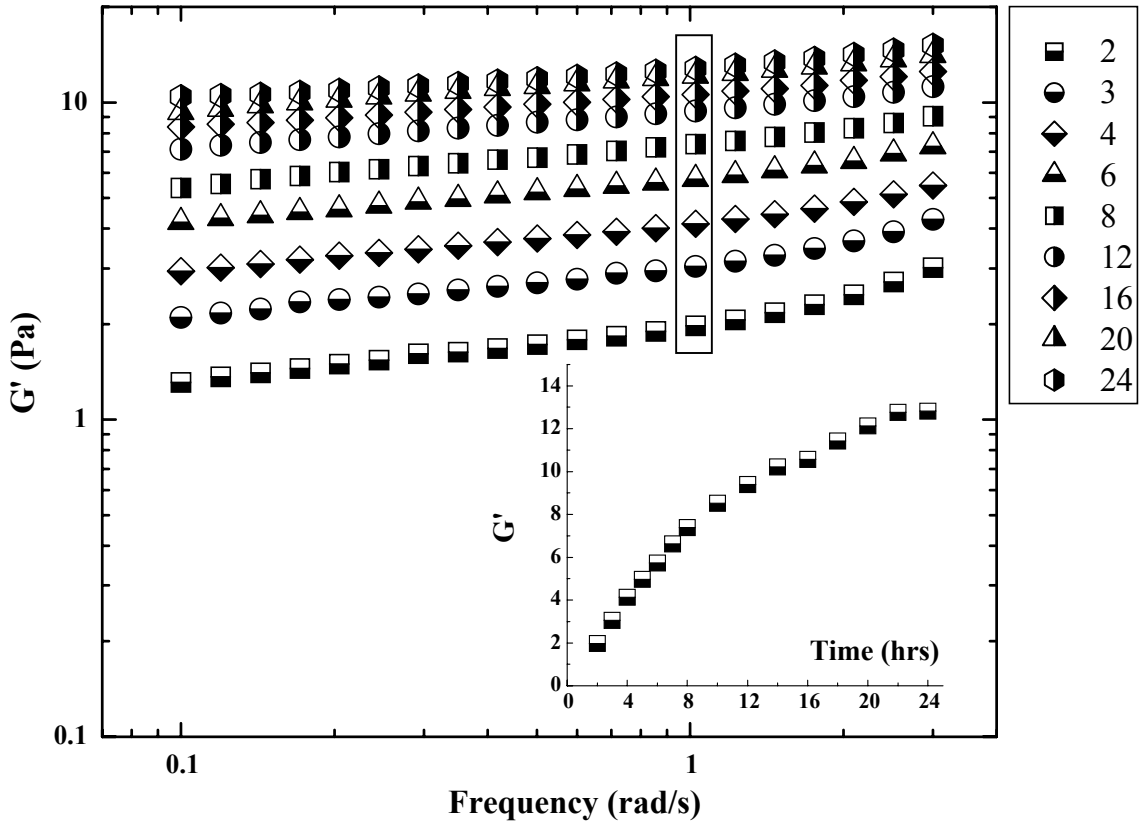

Figure 5.4 B6 Whole asphaltene film frequency sweeps (adsorption time in hours): 0.75 % w/v, 55 % toluene, 0.01 Pa.

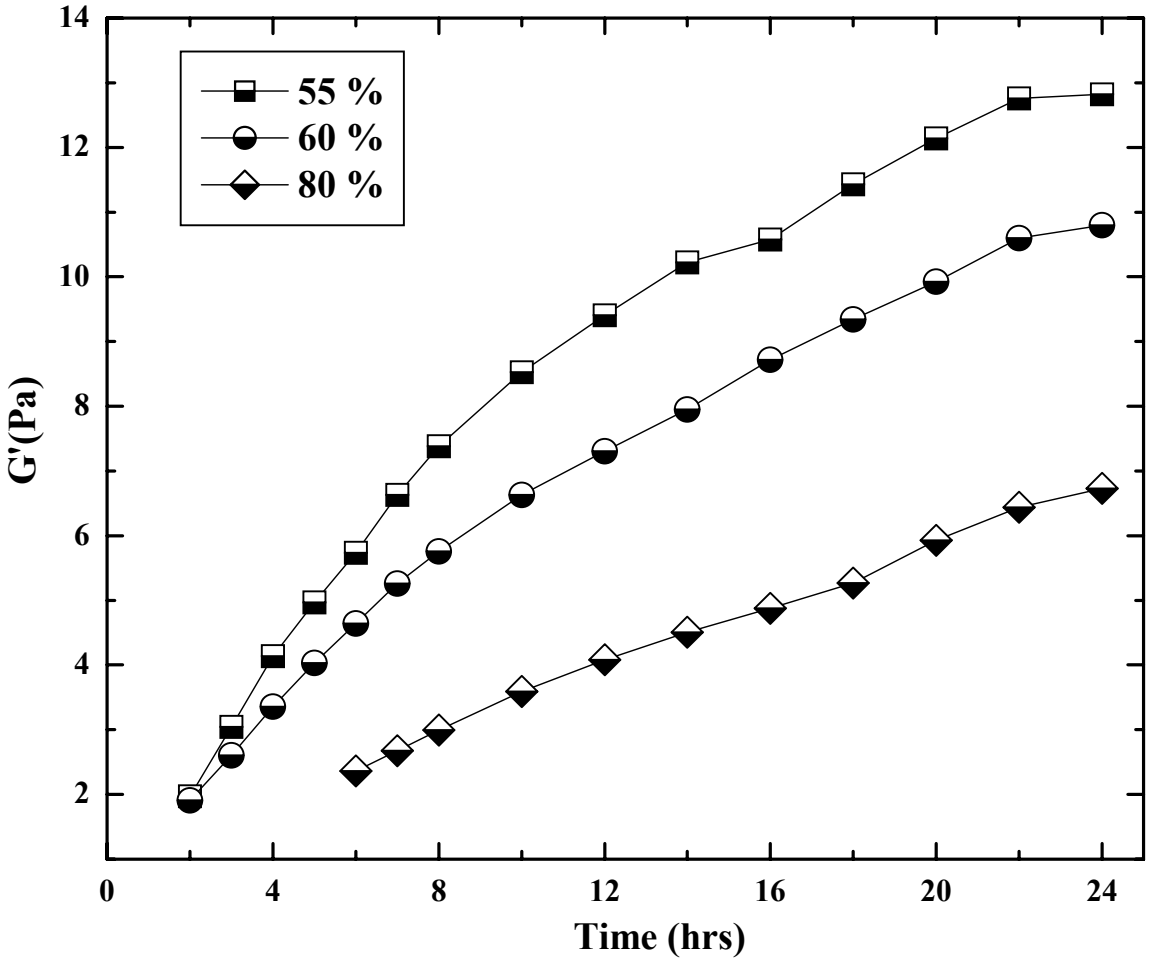

Figure 5.5 B6 Whole asphaltene film kinetics: 0.75 % w/v, 0.01 Pa, 1 rad/s, 55-80 % toluene.

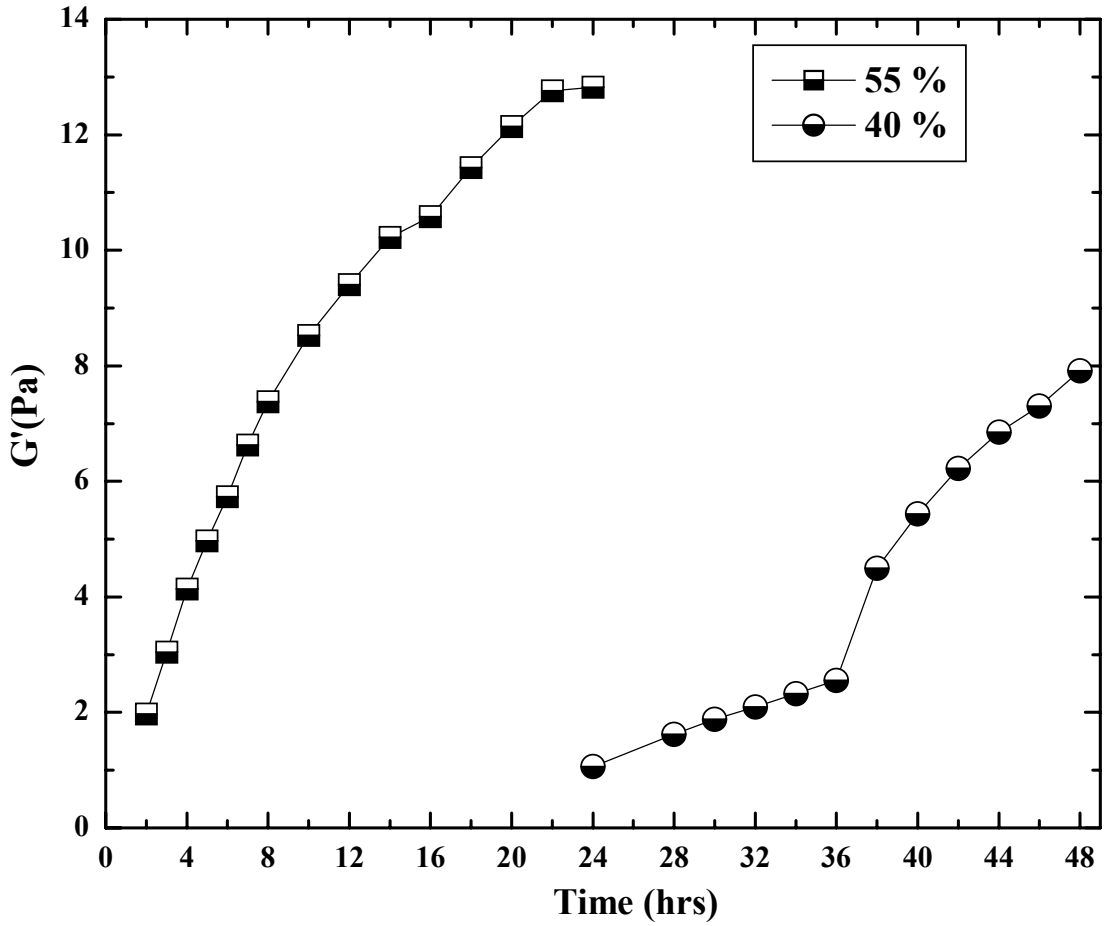

Figure 5.6 B6 Whole asphaltene film kinetics: 0.75 % w/v, 0.01 Pa, 1 rad/s, 40 and 55 % toluene.

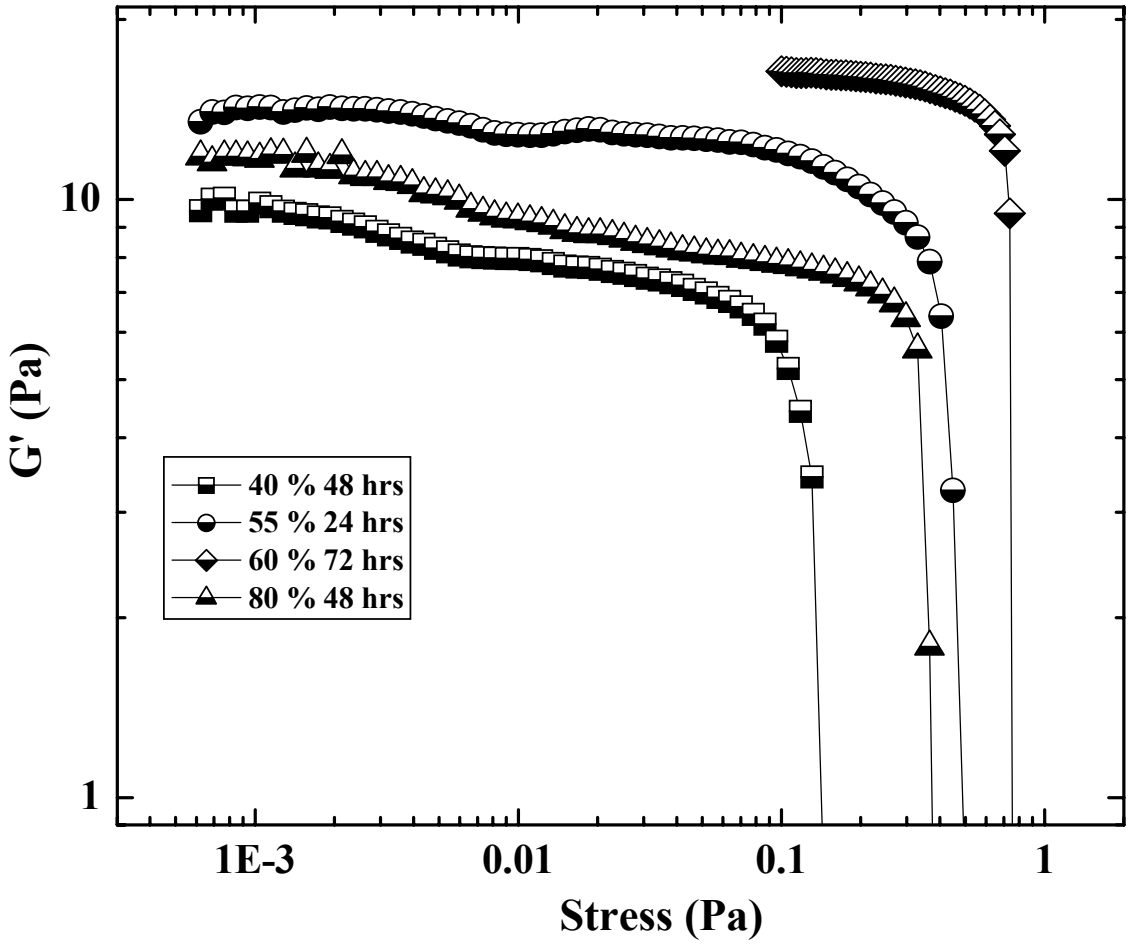

Figure 5.7 B6 Whole asphaltene film stress sweeps at different toluene vol % and aging times: 0.75 % w/v, 1 rad/s.

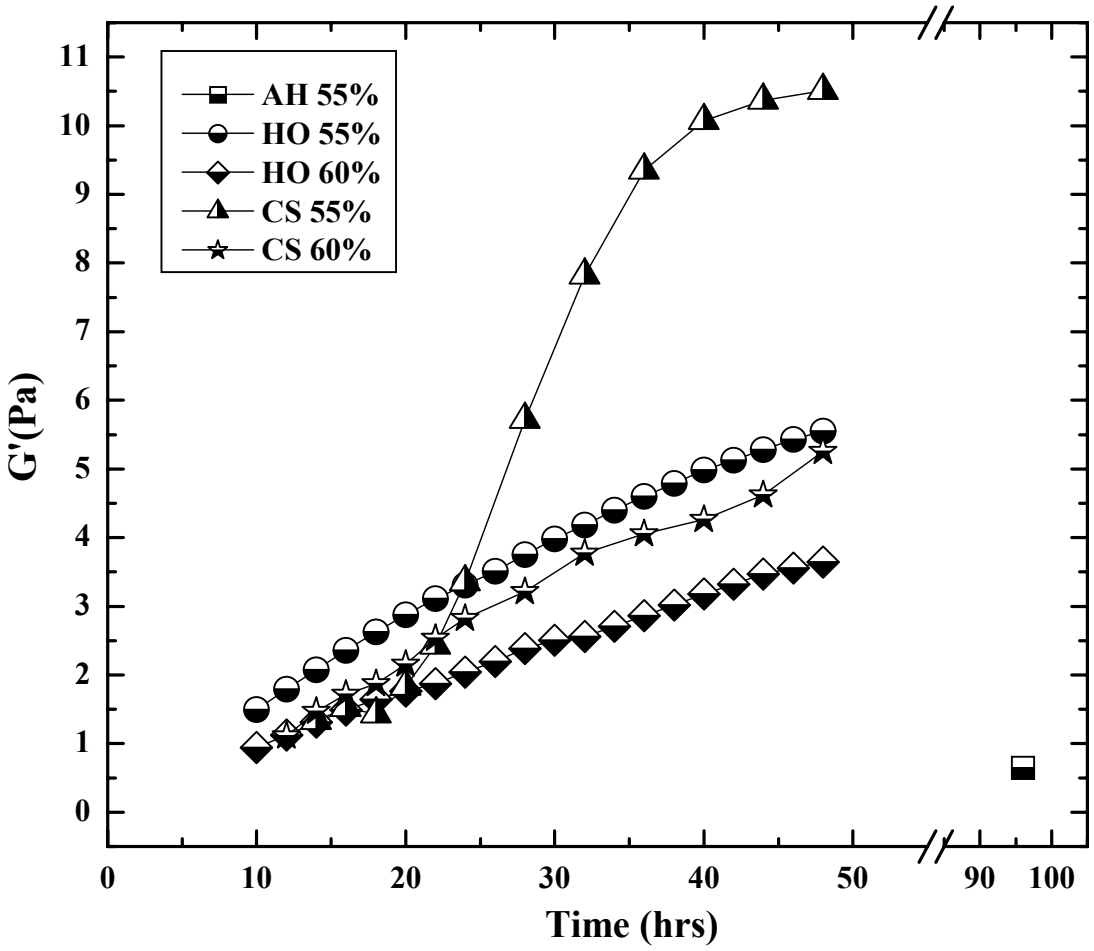

Figure 5.8 AH, CS, HO Whole asphaltene film kinetics: 0.75 % w/v, 0.01 Pa, 1 rad/s, 55 and 60 % toluene in heptol.

Figure 5.9
Top: View of wrinkled film edge between water and oil phases. Edge has extended into oil phase and has fragmented.
Bottom: Film after oil removal. Large fragments resting on top of film originated from film edge extending upwards into the oil phase then fracturing and falling off. Small triangular film pieces floating on top of water phase were sheared off bulk film by serrated bob edge.

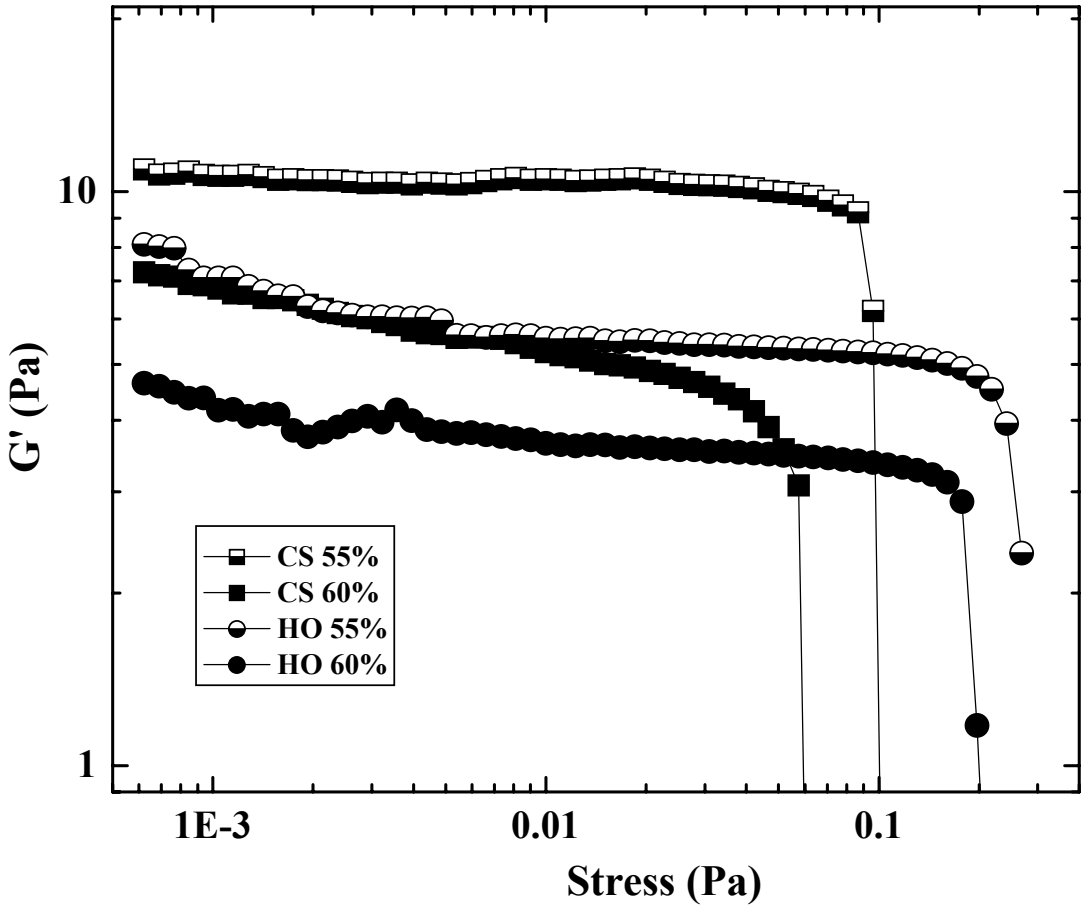

Figure 5.10 CS and HO Whole asphaltene film stress sweeps: 0.75 % w/v, 1 rad/s, 48 hours aging.

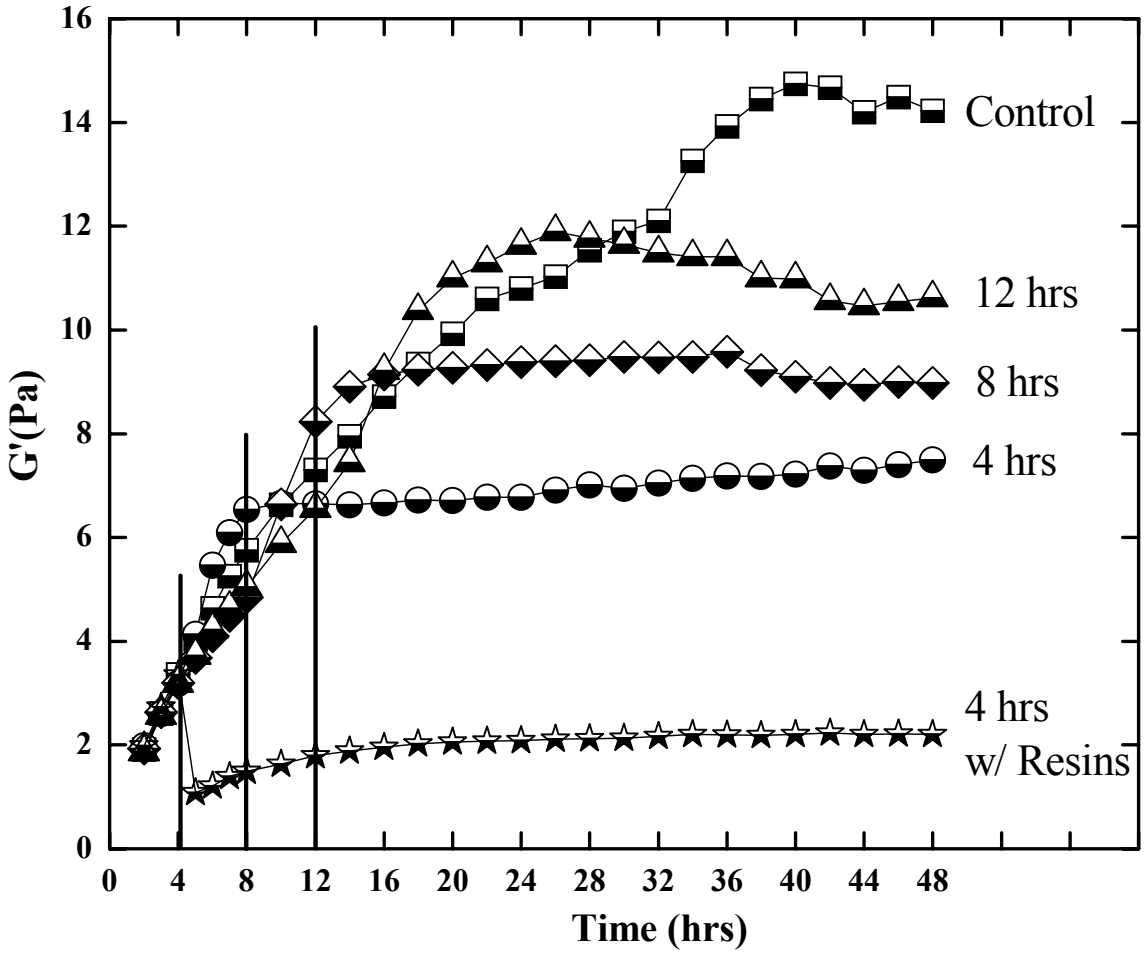

Figure 5.11 B6 Whole asphaltene film kinetics-oil replacement: 0.75 % w/v, 60 % toluene, 0.01 Pa, 1 rad/s. Graph labels refer to contact time between asphaltene solution and water before replacing oil phase with neat heptol (or heptol with resins).

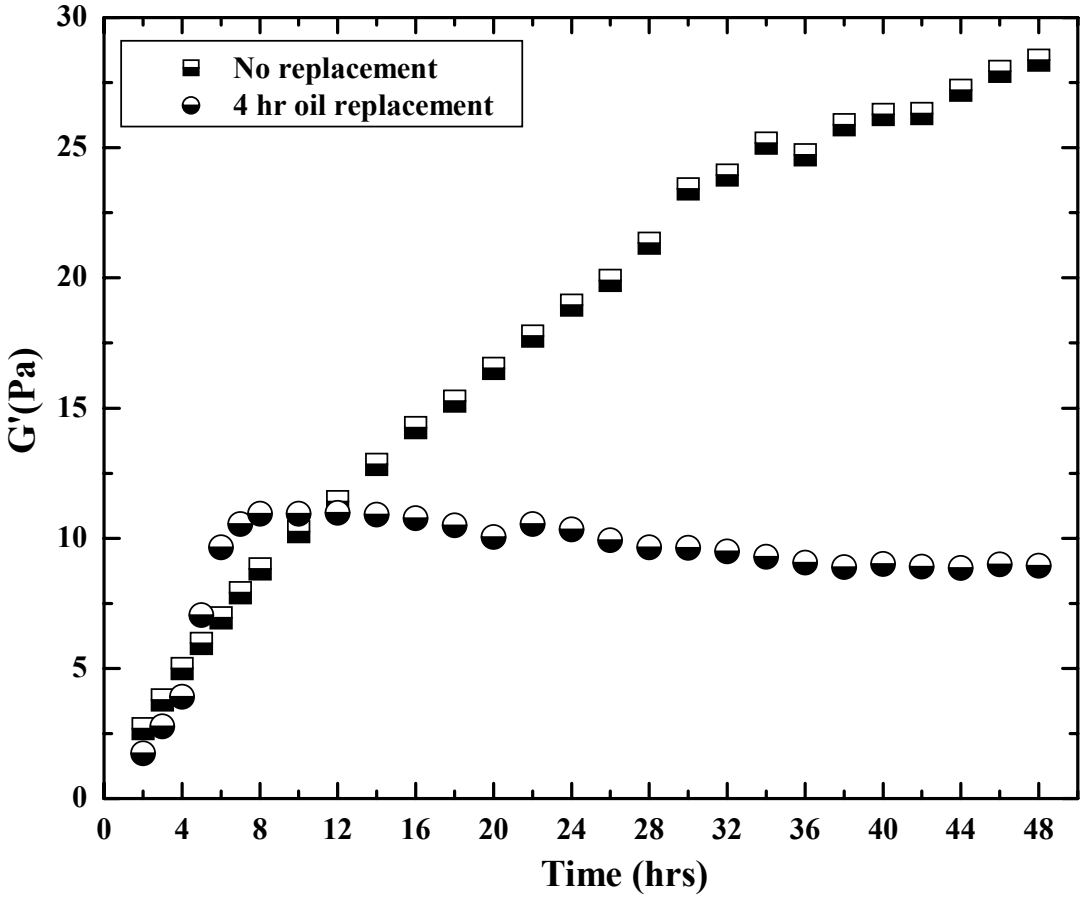

Figure 5.12 B6 Precipitate asphaltene film kinetics-oil replacement: 0.75 % w/v, 100 % toluene, 0.01 Pa, 1 rad/s. Control experiment: asphaltene solution remained in contact with water for 48 hours. Replacement experiment: asphaltene solution removed after 4 hours and replaced with pure toluene.

CHAPTER 6

CONCLUSIONS AND FUTURE WORK

6.1 Conclusions

We have studied the effect of asphaltene chemistry on solubility, aggregation, interfacial film formation and emulsion stabilization. Petroleum asphaltenes were fractionated in mixtures of aromatic (solvent) and aliphatic (anti-solvent) liquids into more soluble and less soluble classes. Chemical analyses indicated that the less soluble asphaltenes were slightly more aromatic, polar and contained higher concentrations of metals (Ni and V) than the more soluble asphaltenes. The more aromatic and polar fraction was found to be considerably less soluble in mixtures of aliphatic and aromatic solvents than the unfractionated asphaltenes. These results suggest that cooperative interactions exist between the various fractions that encompass the broadly defined asphaltene class.

For the first time, the aggregation of asphaltene fractions was probed by small angle neutron scattering. The less soluble asphaltene fractions formed the largest aggregates with the highest degree of temperature sensitivity indicating strong intermolecular associations. The more soluble fractions formed much smaller aggregates at all temperatures. The extent of aggregation was very sensitive to the degree of asphaltene solvation. In highly aromatic solvents (pure toluene), asphaltenes were well solvated and formed very small aggregates. As the aromaticity of the solvent was decreased, asphaltene aggregation increased to a maximum at the solubility limit. Aliphatic solvents induced asphaltene aggregate flocculation and the precipitation of insolubles.

Asphaltene aggregation is mediated by polar and aromatic interactions between monomers in solution. Highly aromatic solvents can favorably solvate π bonds between adjacent aromatic asphaltene cores but are less effective at disrupting intermolecular hydrogen bonding. Petroleum resins are less refractory than asphaltenes yet have similar chemistry. Their higher degree of polarity and heteroatom content enables enhanced asphaltene solvation through the disruption of hydrogen and π bonds. This effect was observed through reduced aggregation and increased solubility even in highly aromatic solvents.

Water-in-oil emulsions were prepared with asphaltenes, their more and less soluble fraction in solvent mixtures from aliphatic to aromatic. Asphaltene solvency and chemistry were the major factors in emulsion stability as measured by the water resolved after centrifugation. Highly aromatic solvents where asphaltene aggregation was minimized resulted in the weakest emulsions. In addition, poorly solvated and partially insoluble asphaltenes (highly aliphatic solvents) formed unstable emulsions. The strongest emulsions were formed by asphaltenes near their solubility limit with the largest, **soluble** aggregates. Aggregates near the point of incipient flocculation have the highest affinity for oil-water interfaces and thus adsorb to form the thickest and strongest films. The formation of a cohesive-elastic interfacial film is the key to generating a stable emulsion. Asphaltenes with intermediate aromaticity, higher polarity and metals content were found to form the strongest emulsions. The less soluble fractions of these good emulsion forming asphaltenes were the most effective at stabilizing emulsions in highly aromatic solvents. The more soluble fractions were poor emulsion formers in aromatic solvents due to low interfacial affinity and small aggregate formation.

The addition of resins to asphaltene systems that formed strong emulsions always led to emulsion destabilization. Enhanced asphaltene solubility reduced the interfacial affinity and resins (interfacially active but poor emulsion formers) likely competed with asphaltenes for available oil-water interfacial area. Resins did display a remarkable ability to solvate the less soluble asphaltene fraction at very low aromaticity. In a low aromaticity solvent the less soluble fraction was very insoluble and not capable of stabilizing emulsions. At a resin-asphaltene ratio of 5:1, the most polar asphaltenes formed very stable emulsions. However, R/A greater than 10 or 20 typically destabilized all asphaltenes and their fractions.

A novel application of biconical bob interfacial rheometry successfully probed asphaltene films formed at oil-water interfaces. The films exhibited linear viscoelasticity and yield stresses. Elasticity and yield stress of the films increased with aging time and did not appear to reach equilibrium after several days due to an abundant asphaltene supply. Many factors influenced the degree of interfacial adsorption, elasticity, and yield stress. The asphaltenes that formed the most stable emulsions (lower aromaticity, higher polarity and heavy metals—Ni, V—content) also formed interfacial films with high elasticity and yield stress. Near the solubility limit, asphaltenes were highly aggregated, films formed rapidly and had considerable mass. In solvents of higher aromaticity, interfacial adsorption was likely dominated by polar asphaltenes due to the high degree of solvent dispersion forces. These films did not form as quickly and elasticity and yield stress at comparable aging times was lower. In the insoluble regime, precipitation hindered the adsorption process and measurable elasticities were obtained after much longer aging times. G′/film mass and yield stress/G′ were developed to measure the degree of asphaltene consolidation. Films at high solvent aromaticity had higher G′/Mass since the film masses were considerably lower than

solvents near the asphaltene solubility limit. Film elasticities and yield stresses were also measured on fractionated asphaltenes. The fractionation concentrated the less soluble, more polar and aromatic asphaltenes with a greater propensity to adsorb at the oil-water interface.

Oil replacement experiments demonstrated the dual film formation processes of asphaltene adsorption and aggregate consolidation. After the asphaltene solution was removed and further adsorption was eliminated, film elasticity increased for several hours then reached equilibrium. Films aged longer after solution replacement, had higher ratios of yield stress to elasticity indicating enhanced consolidation. Replacing the oil phase with resins in heptol rapidly reduced film elasticity due to film solvation.

The long time film elasticities and yield stresses of the asphaltenes correlate with the stability of emulsions formed at similar asphaltene concentrations and heptol ratios. Asphaltenes are well solvated in highly aromatic solvents, form films of lower elasticity, and yield stress and weaker emulsions. Enhanced aggregation near the solubility limit, contributes to strong film and emulsion formation. B6 and Hondo asphaltenes have higher polarity and form well consolidated films and strong emulsions. Arab Heavy and Canadon Seco have lower polarity and are poor film and emulsion formers. B6 and Hondo fractions of enhanced polarity form very strong films and emulsions even in highly aromatic solvents. These results strongly suggest that asphaltene chemistry dictates the properties of adsorbed films and that film shear elasticity and yield stress determine the strength of asphaltene stabilized water-in-oil emulsions.

6.2 Future Work

Several areas of this research can serve as stepping-stones for further study in the petroleum field as well as other surface sciences. While the asphaltenes chosen for this study encompassed a broad range of chemistry and film forming characteristics, including more asphaltenes will help to universalize the findings. We found that B6 and Hondo asphaltenes were very strong film and emulsion formers while Arab Heavy and Canadon Seco were not. B6 and Hondo were both obtained from offshore California oil reservoirs and the asphaltenes that adsorbed to oil-water interfaces were considerably more cohesive film formers.

The solubility profiles determined for the asphaltenes and their subfractions were performed gravimetrically. This study probed the solubility of asphaltenes at one mass concentration of interest. It would be beneficial to compare the gravimetric results to solubility determined using UV-Vis spectroscopy. Beer's Law calibration curves of asphaltenes can then be used to measure the mass concentration solubility limit at each heptane-toluene ratio.

One goal of this study was to correlate asphaltene chemistry to aggregation and film forming behavior. Asphaltenes are polydisperse molecules and inherently difficult to characterize. Exploring the aggregation and film forming behavior of known compounds with chemistry similar to asphaltenes would better reveal the mechanisms of asphaltene aggregation. Blending several well-characterized molecules with appropriate aromaticity, polarity, and hydrogen bonding capacity will yield a suitable asphaltene mimic. Some of these simple molecules can also be doped with asphaltenes to investigate their ability to disrupt or enhance intermolecular bonding. These effects would be evident with small angle neutron scattering, interfacial rheology and emulsion formation.

Asphaltene aggregate correlation lengths were determined by fitting lorentian lines shapes to neutron scattering curves. Another fitting technique involves using particle form and structure factors. Assuming low solute concentration, the intraparticle structure factor is equal to 1. The form factor can provide estimates of aggregate shape (spheres, cylinders, ellipsoids) and polydispersity. We expect asphaltenes to best follow a polydisperse ellipsoid model due to the planar nature of individual asphaltene molecules. A stack of 4-5 asphaltene monomers will likely have a low thickness to diameter ratio. Initial form factor analysis assuming monodispersity failed to accurately fit the scattering curves.

Emulsion stability was determined by measuring the % water resolved after centrifuging an aged emulsion. Often, the emulsions are too stable and very little water is resolved over a range of solvent conditions. Another technique involves applying a DC voltage across an emulsion of saline water and oil. The strongest emulsions require the highest applied voltage to induce water droplet bridging and electrode continuity. Previous attempts suffered from poor water droplet distribution after removing a small sample of emulsion for testing. Droplet settling during aging causes the largest droplets to migrate to the bottom of the container that houses the aged emulsion. An *in situ* apparatus may help avoid the problems associated with emulsion sampling.

Water droplet distributions were obtained for several asphaltene emulsions immediately after emulsification. This analysis can also be expanded to resin-asphaltene systems and over time to monitor the degree of droplet coalescence.

Another area of asphaltene research that could be enhanced involves asphaltene film elasticity. In this investigation, we examined the shear elasticity and yield stress of asphaltene films at oil-water interfaces. Dilational elasticities have been probed by other

researchers using several techniques including oscillating an oil droplet in water. Interfacial properties are determined from drop shape and pressure measurements. This analysis would complement the current shear rheology very nicely.

APPENDIX A

FRACTIONATION OF CRUDE OIL RESIDUA INTO ACID, BASE AND NEUTRAL COMPONENTS BY ION EXCHANGE CHROMATOGRAPHY

A.1 Introduction

A.1.1 Emulsions in the Petroleum Industry

The petroleum industry has sought to improve their production and refining crude oil into marketable materials. Reducing the volume of generated waste and increasing efficiency from the oil well to the refinery helps the conversion of crude to out-the-door product. Many problems arise along the way, however, which stem from certain components found in the heavier fractions of crude oil, namely higher molecular weight asphaltenes and resins. These components can lead to the formation of catalyst and equipment fouling emulsions, sludge, and coke.

The mixing of immiscible liquids such as oil and water, in the presence of a surface active agent, can often lead to the formation of an emulsion. One phase will form small droplets in the other phase leading to emulsions of the oil-in-water (oil droplets dispersed in the aqueous phase, o/w), water-in-oil (w/o), or a complex oil-water-oil (o/w/o) or water-oil-water (w/o/w) type. These small, dispersed droplets will naturally flocculate and coalesce without surfactant. The surfactant migrates to the oil-water interface and inhibits droplet rupture by steric, electrostatic, or other stabilizing mechanisms. Several factors govern the type of emulsion that forms. If the ratio of phase volumes is quite small or large, the phase having the smaller volume usually forms the dispersed phase.[1] The dispersed droplets gradually settle (dispersed water) or cream (dispersed oil) under the force of gravity and form

a clusters or flocs. Without surfactant or other stabilizing mechanisms, droplet approach will result in thinning continuous phase films, droplet contact and coalescence.

Emulsions are formed quite often in industrial processes and can be both desirable and undesirable. Emulsions occur in foods (milk and mayonnaise), cosmetics (creams and lotions), pharmaceuticals (vitamins and hormones), agricultural products (insecticides and herbicides) and in the petroleum industry. [1] Crude oil is found in reservoirs along with water or brine, and as oil is removed, water will eventually be coproduced. Water is also injected into the crude to wash out contaminants or as steam to improve fractionation. Petroleum emulsions (often water-in-oil, or w/o) readily form with water in the highly turbulent nozzles and piping used for oil production. This vigorous mixing of crude oil and water can form highly viscous emulsions of higher viscosity than either separate phase. These emulsions increase pumping and transportation expenses (owing to the higher viscosity and additional water present), corrosion of pipes, pumps, production equipment and distillation columns, and the poisoning of downstream refinery catalysts. [1]

Many processes are currently employed to separate oil and water emulsions at the refinery. These include large gravity settling tanks, plate separators that allow dispersed droplets to adhere and coalesce, and hydrocyclones that create high velocity vortexes and thus a larger gravitational field. Other methods include heat-treating, chemical demulsification, and electric field separation. The application of heat tends to lower the density of oil faster than that of water and thus induces rapid separation. Heat also reduces the continuous (oleic) phase and droplet film viscosities that result in enhanced film drainage and emulsion destabilization. Demulsifiers act by disrupting the interfacial properties of the stable emulsion and promote droplet coalescence. Electric fields are effective when crude

oils with high levels of salt (above 10 lb. salt/1000 bbl present in emulsified water) are washed with additional water in an electrostatic desalter.[2]

A.1.2 Crude Oil Chemistry

To help improve the conversion of crude oil into useful products by reducing losses to sludge and emulsions, it is necessary to better understand the factors that affect their formation. Paramount to this understanding is an in-depth knowledge of the structures and interactions of the components in question. By studying these properties, we hope to develop predictive models for crude oil behavior and emulsion forming tendencies.

To deduce the mechanisms by which emulsions are stabilized requires an intimate knowledge of crude oil composition. Currently we have compiled an extensive set chemical characterization data for many crude oils.[3] Crude oils have been fractionated with sequential elution chromatography termed extrography (extractive chromatography). Prior to extrography, asphaltenes are precipitated out of crude oil with *n*-heptane. The asphaltene class is defined by its insolubility in a particular solvent, namely n-heptane and solubility in toluene. Asphaltenes driven from solution with heptane have higher average molecular weights and polarities within a more narrow distribution than crude oil. The deasphalted crude is then charged to silica gel and various fractions are eluted with increasing polarity solvents. Extrographic separation has elucidated the amounts of saturates, aromatics, resins and asphaltenes present in these crude oils. Analyses of these fractions by elemental analysis, Fourier transform infrared (FTIR) spectroscopy, and nuclear magnetic resonance (NMR) spectroscopy have further described their chemical compositions.

Each of these analyses, coupled with model oil-water emulsion studies, has provided much information regarding the propensity for crude oils and their resins and asphaltenes to form and stabilize emulsions. Understanding that resins and asphaltenes play the greatest role in emulsion formation and stability logically leads us to probe these fractions for even more compositional data.[3]

Our current knowledge of resins and asphaltenes is detailed in some respects, yet certainly not comprehensive. We have analyzed these two fractions using elemental analysis, FTIR spectroscopy, ^{1}H and ^{13}C NMR, and vapor pressure osmometry. From these data, generalized structures have been developed. Both resins and asphaltenes have varied distributions of heteroatom functionality. Many studies have indicated the presence of carboxylic acids, carbonyl, phenol, pyrroles, and pyridine functionality.[4-8] These groups are capable of donating or accepting protons inter- and intra-molecularly. The most plausible mechanisms of asphaltene aggregation involve π-π overlap between aromatic sheets, hydrogen bonding between functional groups and other charge transfer interactions. The degree of aggregation is controlled by the polydispersity and chemistry of asphaltene monomers.

Resins have similar heteroatom functionality compared to asphaltenes, but with a lower molecular weight.[9] Structurally, resins have two distinct regions. One region consists of aliphatic hydrocarbons, while the other contains polar functional groups interspersed amongst aromatic hydrocarbons. Asphaltenes, on the other hand, appear more planar and have a distinct center and periphery. The center contains aromatic carbons and polar heteroatoms, while the exterior is primarily aliphatic. Asphaltenes present in crude oil are thought to be solubilized by resins.[10-13] The asphaltenes also tend to stack into

aggregates like discotic liquid crystal formers solvated on the edges by resins. [11] [13, 14] The aliphatic periphery of these micelles sterically inhibit flocculation and precipitation unless the crude oil aromaticity is reduced by addition of an *n*-alkane such as *n*-heptane.

A.1.3 Ion Exchange Chromatography

To understand the role of the various chemical asphaltene and resin functionalities in emulsion stability, it is necessary to create chemically distinct subfractions. The structures of these new fractions may look vastly different from their parent blend. One method to further separate these resin and asphaltene fractions involves non-aqueous ion exchange chromatography (IEC). Munday and Eaves first suggested the removal of acids and bases from petroleum fractions in 1959.[15] Since then, many researchers have applied this chromatographic technique for separating crude oil derivatives. Jewell et al. devised a separation scheme that removed the polar non-hydrocarbon compounds from heavy-end petroleum distillates as acid, base, and neutral-nitrogen fractions.[16] The acids were removed on anion exchange resins and the bases on cation resins. This method required a recycling arrangement and nearly a day to obtain one fraction. The entire distillation cut was applied to the anion column after dissolution in pentane or cyclohexane and washed for two days to remove non-reactive substituents. Three acid fractions were removed by 24-hour elution with benzene, methanol, and finally CO_2 saturated methanol. The acid-free sample was applied to the cation column and bases eluted with benzene, methanol and then isopropylamine/methanol. Neutral-nitrogens were obtained by coordination-complex formation with ferric chloride on Attapulgus clay. The remaining non-polars were separated

by elution chromatography using silica gel. This method could obtain nearly nine fractions but required several days to complete.

McKay *et al.* have separated high-boiling petroleum distillates into acids and bases, according to Jewell's procedure, and analyzed them to determine their chemical constituents.[17, 18] McKay successfully separated n-pentane precipitated asphaltenes, from a Wilmington crude oil, into distinct fractions according to the same procedure.[19] He found for this particular crude, the acids and bases constituted 81% and 12% of the total, respectively, with neutral nitrogens, saturates and aromatics constituting the remainder. Hasan *et al.* fractionated asphaltenes from two Saudi Arabian crudes (Arab Heavy and Arab Berri) using similar methods and analyzed them by elemental analysis, ^{1}H and ^{13}C NMR, and infrared spectroscopy.[20] In each case, the acid fraction constituted nearly half of the original sample (AH-45%, AB-49%) followed by bases (AH-20%, AB-27%) and residues (AH-34%, AB-20%). In each case, the H/C ratios for both increased from acid (AH-1.04, AB-0.91) to base (AH-1.14, AB-0.96) to neutral residue (AH-1.27, AB-1.24). The acid fractions contained the most sulfur followed by the bases and residues. The highest values of nitrogen were found in the AH bases and AB residues. Both acids and bases had considerably more aromatic carbon (two to four times) than aliphatic carbon. These results demonstrate the types of differences that can exist between fractions of generic asphaltenes.

Green *et al.* pioneered the next major advance in ion exchange chromatography of liquid fossil fuels.[21] They separated various crude boiling fractions into acids, bases, and neutrals by eluting the sample through anion and then cation resins in connected columns. They optimized both the resin preparation procedure to obtain highly active resins and the elution procedure to save time yet obtain distinct fractions. Based on Green's procedures,

Branthaver *et al.* separated and analyzed several asphalts from the Strategic Highway Research Program (SHRP).[22] They found neutrals comprised 50-60% by weight and total acids:total bases ranged from 1.22-2.55. The neutrals tended to be quite viscous in nature, relatively aliphatic, contained little polar group functionality, and were low in nitrogen and oxygen concentration. The other fractions were very much the opposite.

By employing ion exchange techniques others have developed, we will fractionate resins and asphaltenes for further study. The initial goals of the separation are to achieve acceptable yields and reproducibility and to obtain chemically distinct fractions. These fractions should follow a general trend where neutrals are more aliphatic and have less polar group functionality than acids or bases. After perfecting the fractionation technique on the more plentiful crude oil resins, we will move on to asphaltenes. Once acid, base, and neutral fractions are obtained and scrutinized analytically, model emulsions using these fractions will be prepared. In general, the acid and base fractions (with more plentiful and reactive functional groups) should stabilize water-in-oil emulsions better than the neutrals. Adding fractionated resins to the model emulsions will certainly reveal valuable insight about the stability process. These tests should help clarify the mechanisms by which emulsions are stabilized.

The following pages will describe the methods used to separate various resins obtained previously by extrography into neutrals, acids, and bases. In addition, detailed fractionation results are presented along with elemental analysis, FTIR and NMR results. Some initial emulsion stability results using fractionated asphaltenes and resins are also included.

A.2 Experimental

A.2.1 Crude Oil Fractionation

Asphaltenes were precipitated from crude oil with a 40/1 (v/w) excess of n-heptane (all solvents: Fisher Scientific HPLC grade). The mixture was shaken for 24 hrs and then double vacuum filtered through Whatman 934-AH filter paper and rinsed with heptane. The asphaltenes were redissolved in methylene chloride, transferred to glass jars and dried under nitrogen vacuum at 70°C until a constant weight is reached. The remaining heptane/crude oil mixture (maltenes) was rotary evaporated at 65°C to remove heptane. Once dry, the maltenes were redissolved in methylene chloride and mixed with activated silica gel (Fisher Scientific, Chromatographic grade, Davisil 35-60 mesh, heated to 120°C in a nitrogen flushed vacuum oven for 24 hrs). After 24 hours of contact, the methylene chloride was rotary evaporated under vacuum at 50°C and the silica gel with adsorbed maltenes were placed in a nitrogen flushed vacuum oven for 24 hours at 50°C.

Saturates, aromatics and resins were fractionated by sequential elution chromatography. After packing the columns with fresh activated silica gel and then the pre-adsorbed silica gel, saturates and aromatics were eluted with a 68-32 (v/v) heptane-toluene mixture. Resins were eluted with a mixture of 30-30-40 (v/v) toluene-methylene chloride-acetone. The two fractions were rotary evaporated and dried under nitrogen in a vacuum oven to constant weight.

A.2.2 Resin and Asphaltene Ion Exchange Chromatography

Fractionation of resins and asphaltenes into acids, bases, and neutrals required a pump (LMI hazardous duty metering pump-300 psi), two water-jacketed columns (Omnifit

1.5 cm X 1000 cm) plumbed to a water bath, and sample loop injector (Omnifit) (Figure 1). The adsorbed asphaltenes were removed from the ion exchange resins using Soxhlet extractors with coarse filter thimbles (<75 μm retention). The ion exchange resins used were macroporous styrene-divinylbenzene copolymers (BioRad 100-200 mesh (75-150 μm)). The AG MP-1 and AG MP-50 resins are surface functionalized with strong base (quaternary ammonium) and strong acid (sulfonic acid) groups, respectively.

We activated the resins according to Green's procedure.[21] The resins must be rinsed with several solvents in order to properly activate them for petroleum samples. To prepare the MP-1 resins, 1.5 kg were placed in a large Büchner funnel and rinsed under vacuum with 25 L of 1 N HCl, 4 L DI water, 25 L 1 N NaOH, 12 L water, 25 L 1:1 2-propanol-water, 25 L 2-propanol, 24 hrs Soxhlet extraction with ethyl ether, and 24 hrs Soxhlet extraction with *n*-pentane. These steps were performed consecutively. The procedure for cation resins was the same except the acid and base wash steps were reversed. Once prepared, the resins were stored in amber bottles with cyclohexane under an argon atmosphere. All solvents were supplied by Fischer Scientific and of the highest purity (HPLC or Certified ACS) available.

To pack the resins, two columns of equal size were connected with a sleeve. The resins stored in jars with cyclohexane were slurried, transferred to large separatory funnels, and poured into the double column arrangement. The solvent drained out the bottom of the columns through Teflon tubing connected to a column end piece. When the slurry filled the bottom column, 20-psi nitrogen gas was supplied to the top of the column to force most of the cyclohexane from the slurry. This process continued until the bottom column was almost full of resins. The upper packing column was disconnected and a column end piece was

attached. The resins were then packed by flowing approximately 20 ml/min of cyclohexane through the column. After 200 ml of solvent elution, the resins settled overnight and the adjustable plungers were lowered to remove any void volume.

The petroleum samples were dissolved in the elution solvent, either cyclohexane (resins) or an aromatic solvent (asphaltenes). If the elution solvent was not cyclohexane, a sufficient volume of aromatic solvent was pumped through both columns to flush out the cyclohexane. When adsorbing samples, the columns were arranged so that the sample passes through the strongly basic column (to adsorb acids) and then the strongly acidic column (to adsorb bases). The approximate flow rate was 5 mL/min. Those species passing through both columns were collected as neutrals.

If the anion column was left in series too long, weakly held acids may be pulled from the anion column with excessive solvent elution.[21] To prevent this from occurring, the anion column was removed from the flow system after approximately 2.5 void volumes of solvent had eluted. The void volume was estimated from calculations based on column and resin particle volumes as well as tracer experiments with toluene and a UV spectrometer scanning between 200 and 300 nm. Once the adsorption was complete (no appreciable solute elution), the column resins were emptied into Soxhlet extraction thimbles. One column end cap was removed and solvent was pumped from the other end, which forced resins from the column.

After resin transfer, approximately 600 ml of toluene or benzene are added to the boiling pots along with 35 ml of propylamine (MP-50 resins with adsorbed bases) or 35 ml of formic acid (MP-1 resins with adsorbed acids). The propylamine was added in small amounts over a period of about a day to avoid rapid and violent sample desorption. Since

formic acid forms an azeotrope with benzene, the entire volume can be added at the beginning. After a day, 60 ml of acetone may be added to break the azeotrope and extract more acids. All extractions were performed under an argon atmosphere.

Upon separation and extraction, the samples were rotary evaporated to remove solvent and then dried in a vacuum oven at 75^{o}C for two to three days in the presence of nitrogen. After weighing the samples to determine yields, they are analyzed by FTIR, ^{13}C NMR and elemental analysis.

A.2.3 Subfraction Analyses

The newly generated fractions underwent careful examination to determine elemental composition and functional group and aromatic/aliphatic carbon concentration. Elemental analyses (C, H, N, and S) were obtained with a Perkin-Elmer 2400 Series II CHNS/O Analyzer operating in combustion mode. These data provided H/C ratios and mass ratios of nitrogen and sulfur. Oxygen values may be determined by pyrolysis in a helium/hydrogen mixture. In general, highly aliphatic species with long alkyl chains will have H/C ratios around 2 while aromatic species with highly substituted rings will be closer to 1. A Nicolet Magna IR 750 Spectrometer with a TGS detector was used in the Fourier-transform infrared (FTIR) studies. This method obtains qualitative information about the relative amounts of functional groups such as pyrrolic nitrogen, saturate, aromatic, carbonyl carbon, and sulfoxides. Aromatic carbon content was also determined by ^{13}C NMR with a General Electric GC 300 Omega NMR spectrometer.

A.2.4 Emulsion Preparation and Stability Testing

We examined how the compositional differences between acids, bases and neutrals affects the stability of model emulsions formed by high energy mixing in the presence of water. We will also show, by varying the resin to asphaltene ratio using acid, base, and neutral components, that the interaction between resins and asphaltenes plays a major role in stabilizing emulsions. First, whole asphaltenes and then asphaltene subfractions will be dissolved in a mixture of heptane and toluene to simulate the aromaticity of crude oil.

High-energy emulsification of the oil and aqueous phases was performed with a homogenizer. The homogenizer can create a high shear field employing a rotor-stator apparatus. Since the emulsifying surfactants have such a low solubility in water, they will be primarily oil wet and remain in the bulk oil phase. The aqueous phase will therefore disperse into the oil phase in the form of small droplets. Sub-fractionated asphaltenes (0.5 wt% weighed on a Mettler AE166 balance accurate to 0.0001 g) were dissolved in varying amounts of toluene then mixed with heptane to bring the total volume to 4 mL. The oil aromaticity ranged from 20-100 % (v/v). 6 mL of deionized water (Barnstead ROPure LP and NANOPure 4 module systems), pH adjusted to 6 in most cases (unbuffered), was added to the oil phase. The system is emulsified with a Virtis Virtishear Cyclone IQ Homogenizer and rotor-stator apparatus (a 6-mm internal shaft diameter and a gap width of 127 μm) at 15,000 rpm for two minutes at the oil-water interface and one minute at the bottom of the sample vial. The generated dispersed water droplets were typical of those found in refinery emulsions (5-50 μm).[23] The emulsion were then transferred to a polypropylene centrifuge tube and sat for 24 hrs before centrifugation in a Dupont Sorvall RC-5C centrifuge with a fixed angle SS-34 rotor at 15,000 rpm for 30 minutes. Upon centrifugation, the resolved

water phase were pipetted into graduated vials to determine the resolved volumes. In addition, fractionated resins were dissolved in heptane and added to the asphaltenes dissolved in toluene at resin-asphaltene ratios from 0-4.

A.3 Results

A.3.1 Resin/Asphaltene Fractionation

Table 1 shows the procedures implemented to fractionate asphaltenes and resins into acids, bases, and neutrals. Figure 2 shows the mass of solute charged to the columns and the mass recovered after Soxhlet extraction. Yields steadily improved as the experimental procedures were refined. Volatile crude oil components and irreversible adsorption may attribute to the low yield in the first run. During the extraction of AH 167 basic resins, the Soxhlet boil up-drain down cycle created rapid volatilization that ruptured the pot, ejecting the sample. The separation of SJV resin S-#3, yielded poor results when the acid sample boiled over in the vacuum oven. After scraping off and then weighing the acidic material that baked to the top of the oven, though, the yield increased to 98%. Several reasons could account recoveries in excess of 100%. (1) Excess formic acid present in the acid sample may not have been driven off during the vacuum oven drying even though the samples were placed back in the ovens without much improvement. (2) Excess formic acid may have reacted with the sample to form oxygen-containing compounds, thus adding to the final weight.

As samples were eluted through the columns, a common color pattern formed on the resins. The MP-1 resin column had a gradually decreasing dark brown color beginning at the top and ending at the bottom of the packed resin. The MP-50 resins had a visibly different

color pattern. A black color spread down about 15 cm (proportional to the amount of sample injected) that constituted nearly the entire base fraction. Neutrals first eluted from the columns with 200-300 ml of cyclohexane (resin fractions), beginning yellow-green in color and slowly progressing to solid yellow. There was a very slow moving band on the MP-50 column that required the most time to elute. This yellow-brown material eluted soon after the anion column was taken off-line. Increasing the temperature from 25 to 40° seemed to have increased the efficiency of the resins to retain organic compounds as predicted by Lee and Hoffman.[24]

As expected, the SJV crude experiment yielded nearly 50% neutral species. These neutrals probably contained hydrocarbons very low in polar functional groups. Following the same procedure, SJV resins 145-149 yielded much lower amounts of neutrals. Each of the SJV S1-4 fractionations yielded between 45% and 52% acid, 33% to 38% base and 15% to 18% neutral. The total amount recovered for three of the experiments exceeded the amount injected by approximately 1-3%. As explained before, excess formic acid may have been present and oxidized the samples.

Arab Heavy asphaltene fractionation varied according to the polarity of the solvent. Toluene was used to elute AH 16 and is less aromatic and less polar than benzene, THF, and ethanol. The neutral fraction is considerably greater when using the stronger solvent since the asphaltenes were better solvated and less prone to adsorb to the ion exchange resins. The mixture also stripped more acidic solute from the MP-1 column than in previous runs. A stronger solvent will elute a greater amount of the slow moving neutrals as well as weakly bound acids and bases. In addition, the amphoteric nature of the compounds making up asphaltenes may have allowed the anionic column to be depleted.

A.3.2 Elemental Analysis

Elemental analysis data is reported for several chromatographic separations in Figures 3-14. In each figure, results from the unfractionated sample, or "Whole" are compared to values from each separate fraction and the sum of all fractions weighted by their mass percentage. General trends arise after careful inspection of the data. The neutrals had the highest H/C ratio, followed by bases and then acids. The H/C ratio of the neutral resins fell close to 1.55 in most cases. The AH#16 asphaltenes had a neutral H/C ratio of 1.18 and an acid and base ratio of 1.08 and 1.09, respectively. Similarly, AH#4997 asphaltenes had a high neutral H/C ratio (1.15) and low acid and base H/C ratios (1.09 in each case). With asphaltenes, it was more difficult to discern acids and bases based on H/C ratio suggesting they may have similar aromatic structures.

As mentioned before, sulfur and nitrogen can be found in such compounds as thiophenes, sulfoxides, pyridines, and pyrroles. Sulfur and nitrogen analysis showed a drastic difference between the amounts present in SJV and AH resins. SJV resins were high in nitrogen and low in sulfur whereas the opposite was true for AH resins. In each case, acids had the least amounts of sulfur, then bases and neutrals. Neutrals were lowest in nitrogen for both SJV and AH. AH and SJV 145-149 acids had more nitrogen than bases and the remaining SJV bases had more nitrogen than acids. Nitrogen is often in the form of basic pyrroles. A high concentration of these compounds in an acidic fraction must mean that the nitrogen is not basic or is outweighed by the presence of compounds such as carboxylic acid.

The similarity between S and N results of the SJV Resins S 1-4 show that fractions of reproducible contents can be obtained. The sulfur and nitrogen contents of the two AH

asphaltene fractionations showed similar trends. In each case, the nitrogen content increased from neutral to acid then base and the sulfur content increased from acid to neutral then base. The two HO asphaltenes also displayed this trend.

The oxygen data was calculated by subtracting the sum of the other elements from 100. Since the samples are quite susceptible to oxidation, care was taken at all points during handling to avoid contact with oxygen. Overall, more oxygen was present in the acid samples than any other fraction by a factor of 1.5 to 6. Much of the acid character originated from carboxylic groups. This high amount of oxygen, especially in the last resin runs, might also be explained by the presence of formic acid or oxidized species. Formic acid, on the other hand, has an H/C ratio of 2 which would inflate the acid fraction H/C and hence the overall H/C. None of the summed totals, though, had overall H/C ratios higher than the original sample.

A.3.3 FTIR Analysis

Figure 15 is a typical FTIR plot, with the most important peaks located. The CH_2-CH_3 peak is generally the largest of all the peaks since it comprises the bulk of the sample. The other important peaks include pyrrolic nitrogen, carbonyl carbon and aromatic carbon. Functional group concentrations in terms of weight percent determined by FTIR are presented in Table 2. Included are the molar absorptivities used for each discernible peak on the FTIR plots.[3] Aldehyde percentages are given when a clear peak near 1660 cm^{-1} existed. In almost all cases, neutrals contained the highest percentage of saturates, followed by bases then acids. As expected, carbonyl content of the acidic fractions (most likely present as carboxylic acid derivatives) outweighed the amounts found in the basic fraction.

Pyrrolic nitrogen concentrations varied between 0.1 and 1.56% with most falling between 0.2 and 0.4%. One would expect to see a greater concentration of pyrroles in the basic fractions than in the acidic fractions. In the experiments where the opposite was true, the ratio of pyrrolic to carbonyl content still left the acids with a greater relative acidity.

A.3.4 ^{13}C NMR Analysis

NMR analysis was performed on selected fractions to obtain the relative proportions of aromatic and aliphatic carbon. The spectra were divided into two regions for analysis: the aromatic region (110-160 ppm) and the aliphatic region (5-60 ppm) (see Figure 16). A sharp peak appeared at 76.6 ppm corresponding to the sample solvent deuterated chloroform. The aromatic region is characterized as relatively smooth and broad whereas the aliphatic region has many more distinct peaks. The percentage of aromatic and aliphatic carbon in each sample was calculated from the ratio of the two areas over the total area excluding the solvent peak.

The aromatic carbon content of the asphaltenes and a representative resin fraction is presented in Table 3. The acidic asphaltenes were highest in aromatic carbon followed by the neutrals and bases. The acidic resins again were highest in aromatic carbon followed by the bases and neutrals. In terms of aromatic carbon, the asphaltene fractions were quite similar. They all contained a substantial proportion of aromatic to aliphatic carbon, supporting the notion that asphaltenes consist primarily of fused aromatics with an aliphatic periphery. The resins, however, contained much more aliphatic carbon, corresponding to large alkyl chains and limited fused aromatic ring presence. The neutrals had the least amount of aromatic carbon and would probably solubilize asphaltenes in a very limited

capacity. Acidic resins would most likely interact very well with, and readily solubilize asphaltenes.

A.3.5 Emulsion Stability

Figure 17 shows how emulsion stability, as gauged by percent water resolved, varied with solvent aromaticity and AH#16 asphaltene fraction. Each data point represents an average of three to five duplicated tests with error bars in terms of standard deviation. The asphaltenes were dissolved at 0.5 wt% and emulsified with pH 6 deionized water. The stability of both the whole asphaltene and base fraction tended to decrease with increasing aromaticity. The acid fraction was the most stable overall and had a clear maximum in stability between 40 to 50% toluene. After the maximum stability regime, greater aromaticity destabilized the subsequent emulsions. The asphaltene aggregates that migrated to the interface were solubilized to such an extent that they were no longer as interfacially active. Below 40% toluene, the acid fraction became increasingly unstable. As the aromaticity of the solvent decreased, the acidic asphaltenes became less soluble and probably began to precipitate to some extent. From ^{13}C NMR analysis, the basic fraction contained more aliphatic carbon than the acidic fraction and so, may still have been soluble in the oil. Experiments performed at lower toluene:heptane ratios may reveal a minimum in emulsion stability. Homogenization of the neutral fraction did not produce stable emulsions and usually separated completely under the influence of gravity. This result has never been seen before and shows that "asphaltenes" may be too broad a term when describing emulsion stabilizers. By focusing in on the subfractions of asphaltenes, we have narrowed the important emulsion stabilizing species to acids and bases.

The stabilizing effects of the fractions tended to be additive at the extremes of aromaticity with the whole asphaltene stability lying between those of the acid and base. In the intermediate range, the whole and base fractions followed each other closely, while the water resolved in the acid fraction was lower by about 20% in each case.

Resolved water pH's for the asphaltene subfractions are plotted in Figure 18. The base and whole fraction have similar pH's over the entire range of aromaticities. The acid fraction tends to impart its acidic nature on the water by reducing the pH to as low as 4. The maximum in acidic pH falls in line with the maximum in stability. In the strong emulsions, most of the water is dispersed as fine droplets with adsorbed asphaltenes. Any acidic constituents that are water soluble would be trapped in these droplets. On the other hand, the weak emulsions allow the asphaltenes to interact with the water phase and then separate. The water soluble acids could more easily reach the bulk water phase and not remain sealed within dispersed phase droplets.

The emulsion stability of the second set of fractionated AH asphaltenes is presented in Figure 19. Even though the subfraction yield compositions, as compared to AH#16, were more heavily weighted towards the bases, the percent water resolved followed similar trends. The acidic fraction had a maximum stability at 40% toluene, but the overall maximum occurred with the base fraction at 30% toluene. As with the previous stability tests, increased aromaticity solubilized the asphaltenes and reduced their interface stabilization properties. The base fraction may have reached a point of incipient precipitation at 30% toluene and the further reduction in aromatic solvent content created portions of undissolved asphaltenes that could not stabilize an oil-water interface.

The effects of SJV resin addition on AH#16 asphaltene (acid and base fractions) emulsion stability at 30% toluene are represented in Figure 20. Before resin addition, the asphaltenes had already begun to lose their stabilizing propensity. Resin addition to the acidic asphaltenes began the solvation process and overcame the oil phase's low aromaticity to create more stable emulsions at the lowest R/A ratio. Increasing the amount of resins would tend to solubilize the asphaltenes and rob them of their interface stabilizing properties. The acidic and basic resin fractions decreased stability to nearly pre-resin addition levels; whereas neutral resins stabilized the emulsions equally well throughout the R/A range.

Resin addition to the basic asphaltenes had a more dramatic destabilization effect, most notably with basic resins (see Fig 21). The asphaltenes had probably reached their maximum stability in the heptane-toluene mixture and any further perturbation would result in destabilization.

A.4 Conclusions

As shown through analysis of the fractions obtained, ion exchange chromatography can be used as an effective method to produce chemically distinct fractions with acidic, basic, and neutral character. The methods developed have also demonstrated a high degree of reproducibility and yield a "closed" material balance. Maintaining an elevated elution temperature using water jackets improves column efficiency and leads to a more visibly distinct separation. In all cases, the H/C ratio decreased from acid to base to neutral. Each of the fractions had different nitrogen and sulfur levels. FTIR provided useful information on the content of the fractions in terms of carbonyl, saturate, and pyrrolic concentrations.

13C NMR spectra showed that acids and bases have higher levels of aromatic carbon than do neutrals.

The most interesting results emanated from the emulsion stability testing, which showed that neutral asphaltenes do not stabilize emulsions whereas their acidic and basic counterparts do. The addition of resins in varying amounts to asphaltenes in the model oil emulsions had very profound effects. Interfacial rheology and dielectric spectroscopy studies will certainly complement our current techniques for studying emulsions. By continuing to fractionate asphaltenes from various crude oils, we will be able to run a full array of stability tests and make great leaps towards a further understanding of the stability mechanism.

A.5 References

1. Schramm, L.L., *Petroleum Emulsions: Basic Principles*, in *Emulsions: Fundamentals and Applications in the Petroleum Industry*. 1992, American Chemical Society: Washington, D.C. p. 1-49.
2. Gary, J.H. and G.E. Handwerk, *Petroleum Refining: Technology and Economics*. 1994: Marcel Dekker, Inc. 39-42.
3. McLean, J.D. and P.K. Kilpatrick, "Comparison of Precipitation and Extrography in the Fractionation of Crude Oil Residua," *Energy and Fuels*, 1997, **11**: p. 570-585.
4. Barbour, R.V. and J.C. Petersen, "Molecular Interactions of Asphalt: An Infrared Study of the Hydrogen-Bonding Basicity of Asphalt," *Analytical Chemistry*, 1974, **46** (2): p. 273-277.
5. Boduszynski, M.M., J.F. McKay and D.R. Latham, "Asphaltenes, Where Are You?," *Proceedings of the Association of Asphalt Paving Technologists*, 1980, **49**: p. 123-143.
6. Ignasiak, T., O.P. Strausz and D.S. Montgomery, "Oxygen Distribution and Hydrogen Bonding in Athabasca Asphaltene," *Fuel*, 1977, **56**: p. 359-365.
7. Moschopedis, S.E. and J.G. Speight, "Investigation of Hydrogen Bonding by Oxygen Functions in Athabasca Bitumen," *Fuel*, 1976, **55**: p. 187-192.
8. Petersen, J.C., "An Infra-red Study of Hydrogen Bonding in Asphalt," 1967: p. 295-305.

9. Pelet, R., F. Behar and J. Monin, "Resins and Asphaltenes in the Generation and Migration of Petroleum," *Organic Geochemistry*, 1985, **10**: p. 481-498.

10. Swanson, J.M., "A Contribution to the Physical Chemistry of the Asphalts," *Journal of Physical Chemistry*, 1942, **46**: p. 141-150.

11. Al-Jarrah, M.M.H. and A.H. Al-Dujaili, "Characterization of Some Iraqi Asphalts II. New Findings on the Physical Nature of Asphaltenes," *Fuel Science and Technology International*, 1989, **7** (1): p. 69-88.

12. Burke, N.E., R.E. Hobbs and S.F. Kashou, "Measurement and Modeling of Asphaltene Precipitation," *Journal of Petroleum Technology*, 1990, **Nov**: p. 1440-1456.

13. McLean, J.D. and P.K. Kilpatrick, "Effects of asphaltene aggregation in model heptane-toluene mixtures on stability of water-in-oil emulsions," *Journal of Colloid and Interface Science*, 1997, **196** (1): p. 23-34.

14. Nghiem, L.X., et al., "Efficient Modelling of Asphaltene Precipitation," *Society of Petroleum Engineers*, 1993, **5**: p. 375-384.

15. Munday, W.A. and A. Eaves. . in *World Petroleum Congress Proceedings 5th*. 1959. New York.

16. Jewell, D.M., et al., "Ion-Exchange, Coordination, and Adsorption Chromatographic Separation of Heavy-End Petroleum Distillates," *Analytical Chemistry*, 1972, **44** (8): p. 1391-1395.

17. McKay, J.F., et al., "Analysis of Acids in High-Boiling Petroleum Distillates," *Fuel*, 1975, **54** (1): p. 50-61.

18. McKay, J.F., J.H. Weber and D.R. Latham, "Characterization of Nitrogen Bases in High-Boiling Petroleum Distillates," *Analytical Chemistry*, 1976, **48** (6): p. 891-898.

19. McKay, J.F., et al., "Petroleum Asphaltenes: Chemistry and Composition," *Analytical Chemistry of Liquid Fuel Sources, Advances in Chemistry Series*, 1978, **170**: p. 128-142.

20. Hasan, M., M.N. Siddiqui and M. Arab, "Chromatographic Separation and Characterization of Asphaltene Subfractions from Saudi Arabian Crudes," *Fuel*, 1988, **67** (9): p. 1307-1309.

21. Green, J.B., et al., "Separation of Liquid Fossil Fuels into Acid, Base, and Neutral Concentrates," *Fuel*, 1984, **63** (9): p. 1290-1301.

22. Branthaver, J.F., M.W. Catalfomo and J.C. Petersen, "Ion Exchange Chromatography Separation of SHRP Asphalts," *Fuel Science and Technology International*, 1992, **10** (4 - 6): p. 855-885.

23. McLean, J.D. and P.K. Kilpatrick, *Basic Principles and Control of Refinery Emulsions Through Crude Solvency and Resin-Asphaltene Interactions*, . 1996, North Carolina State University.

24. Lee, H.K. and N.E. Hoffman, "Effect of Temperature on the Retention of Simple Organic Compounds in Ion Exchange HPLC.," *Journal of Chromatographic Science.*, 1994, **32** (March): p. 97-101.

Table 1. Ion Exchange Fractionation Conditions and Results

Sample	Solvent	Column Temp (°C)	Neutral (wt %)	Acid (wt %)	Base (wt %)	Unrecovered (wt %)
SJV Whole Crude	1	25	49.04	17.62	15.14	18.20
Resins						
SJV (145-149)	1	25	8.28	39.46	37.96	14.30
SJV (168)	1	25	18.67	36.26	35.70	9.36
AH (167) – (Base sample spilled)	1	25	43.32	29.33	0.99	26.35
AH (S60)	1	25	30.26	34.09	34.81	0.84
SJV #4 (pooled from several S- runs)	1	25	18.23	49.49	34.02	-1.74
SJV S-#3	1	40	15.16	50.04	33.20	1.60
SJV S-#2	1	40	18.10	46.16	38.76	-3.02
SJV S-#1	1	40	15.62	52.35	33.40	-1.37
Asphaltenes						
AH #16	2	40	10.52	39.66	45.89	3.93
AH 4-9-97	3	40	26.50	19.29	52.67	1.54
AH 12-9-97	2	40	4.00	57.15	18.64	20.21
AH 12-9-97#3	4	40	24.25	34.23	39.28	2.24
AH 6-13-98	4	40	21.95	32.17	44.15	1.73
AH 6-13-98#2	5	40	24.43	30.57	45.30	-0.30
HO 12-3-98	5	40	11.83	47.59	30.23	10.35
HO 1-20-99	6	40	12.53	50.17	25.19	12.11
HO 2-25-99	5	40	17.03	41.78	38.59	2.60
HO 5-8-99	5	40	14.00	41.99	39.74	4.27
AH 7-8-99	5	40	24.88	31.74	31.89	11.49
B6 10-1-99	5	40	10.22	40.63	25.47	23.68

Solvent:

1 – Cyclohexane
2 – Toluene
3 – 45% THF, 45% Toluene, 10% Ethanol
4 – 75% Toluene, 25% Ethanol
5 – 90% Toluene, 10% Ethanol
6 – 90% Benzene, 10% Ethanol

Note: All SJV experiments were performed on the same crude (Lot #92-11899-4L). The AH used in expt. #4 was different (Lot #92-36501-10N) from those used in all later experiments (Lot #031996). During the elevated temperature runs (40°C) we allowed the water bath circulation pump to run for an hour to equilibrate the columns.

Table 2. Functional Group Concentrations (wt%) of the Various Fractions from FTIR

		CH_2&CH_3 (Saturate)	C=O (Carbonyl)	RH-C=O (Aldehyde)	N-H (Pyrrole)
Peak Wavenumber	(cm^{-1})	≈2900	≈1700	≈1660	≈3460
Molar Absorp	(l/mol-cm^2)	6,664	27,400	47,000	12,000
Crude Sample	Fraction				
SJV Crude	N1	56.55	0.28		0.02
	N2	46.29	2.64		0.93
	A1	41.49	2.16	1.14	1.24
	A2	42.87	4.26		0.54
	B1	46.12	2.68		0.42
	B2	41.31	3.96		0.09
SJV Resin 145-9	N1	56.33	3.27		0.16
	N2	54.22	3.66		0.80
	A1	41.40	2.02	2.21	1.56
	A2	43.36	2.02	2.98	1.09
	B1	50.98	3.74		0.74
	B2	48.92	1.90	1.02	0.44
SJV Resin 168	N1	53.52	4.32		0.53
	N2	51.42	4.91		0.55
	A	44.57	3.76	1.96	0.80
	B	48.75	1.80	1.07	0.42
AH Resin 167	N1	46.03	1.63		0.13
	N2	50.43	1.98		0.20
	A	38.48	1.80	0.68	0.69
	B	54.76	1.56		0.34
AH Resin S60	N1	52.39	1.17	0.87	0.08
	N2	64.92	2.84		0.22
	A	40.23	2.92	0.69	0.49
	B	47.25	0.64	0.42	0.17

Table 2. Continued

		CH_2&CH_3 (Saturate)	C=O (Carbonyl)	RH-C=O (Aldehyde)	N-H (Pyrrole)
Molar Absorp. (l/mol-cm^2)		6,664	27,400	47,000	12,000
Crude Sample	Fraction				
SJV Resins	N	47.66	3.46		0.29
S-#4	A	39.52	3.91	1.25	0.31
	B	47.73	1.01	0.73	0.31
S-#3	N1	56.97	3.48		0.35
	N2	50.69	3.60		0.44
	A	45.41	5.99		0.35
	B	51.83	1.28	0.67	0.37
S-#2	N1	50.18	3.11		0.33
	N2	49.59	3.65		0.41
	A	37.84	5.84		0.28
	B	46.82	0.97	0.84	0.33
S-#1	N1	50.41	3.74		0.29
	N2	50.10	3.81		0.41
	A	40.07	4.70		0.85
	B	46.59	1.07	0.65	0.29
AH Asph	N	42.43	0.95		0.30
#16	A	36.72	1.30	0.89	0.21
	B	39.38	0.90		0.18
AH Asph	N	36.86	0.44	0.44	0.31
#4997	A	34.33	1.81	0.61	0.25
	B	34.79	0.88		0.19

Table 3. Percentage of Total Carbon that is Aromatic

Fraction	% Aromatic Carbon
Asphaltenes	
AH#16 Neutral	52.4
Acid	52.9
Base	50.1
AH#4997 Neutral	51.7
Acid	53.1
Base	51.3
Resins	
SE51 Neutral#2	15.8
Acid	37.3
Base	26.4

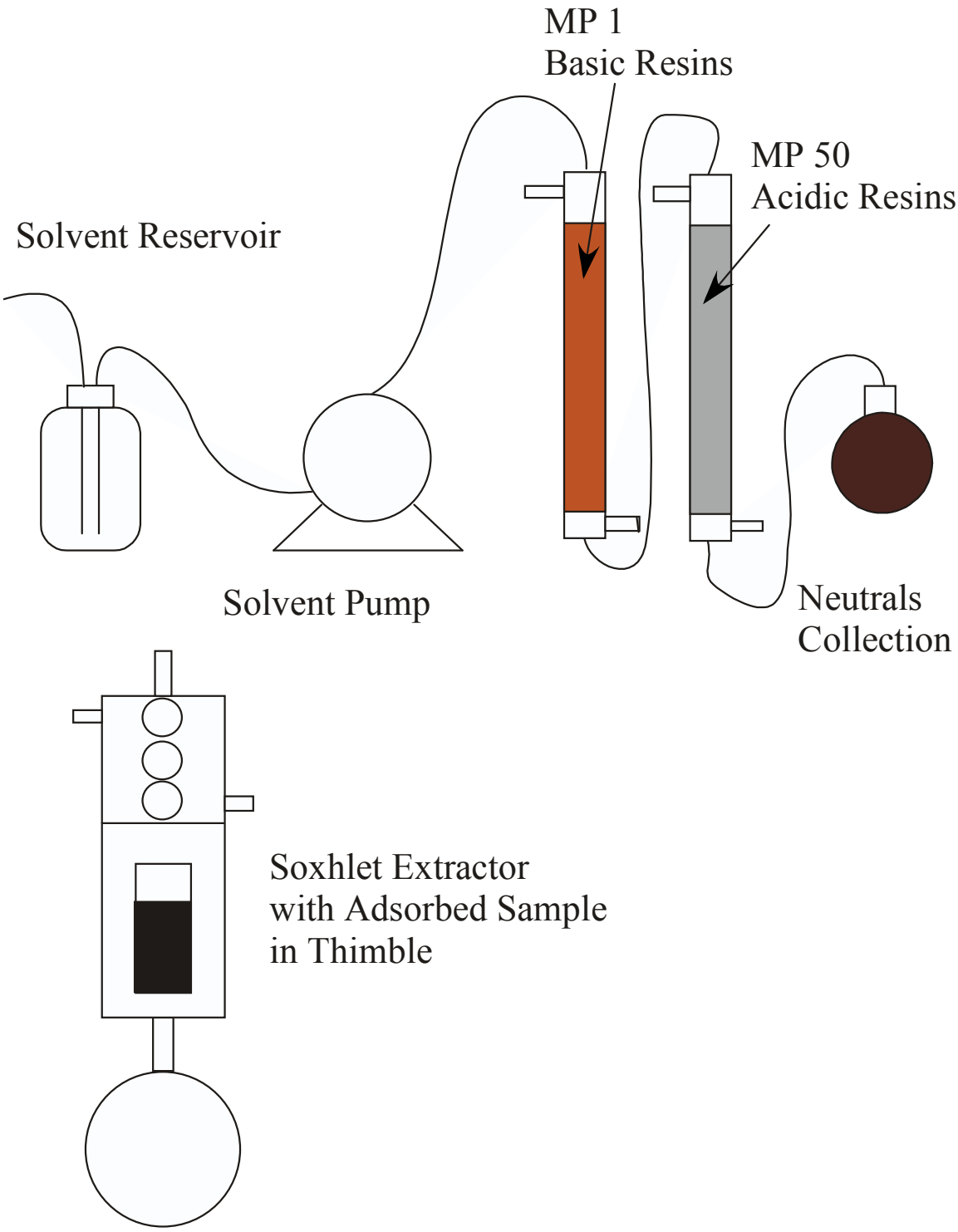

Figure A.1 Ion Exchange Chromatography procedure.

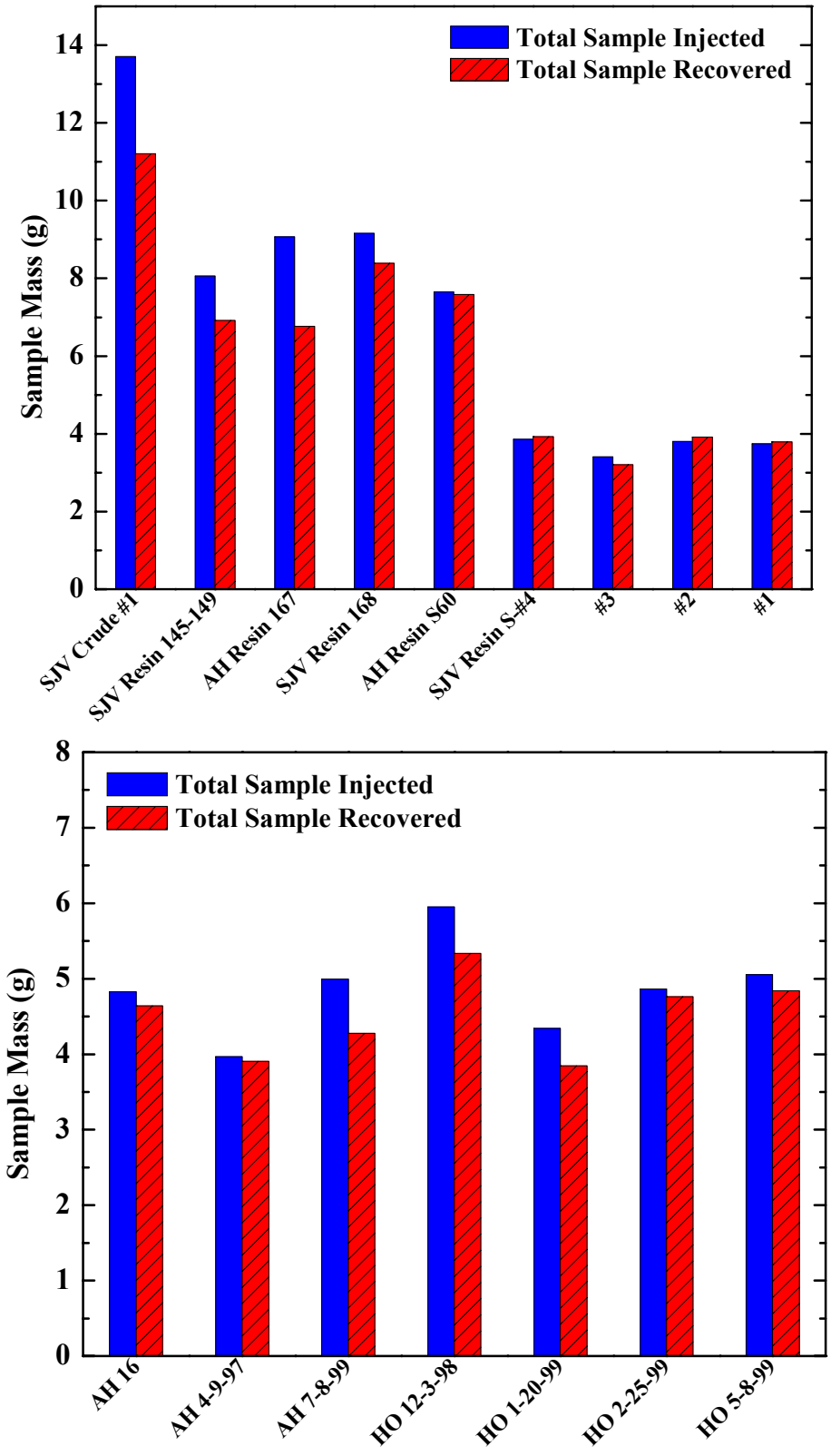

Figure A.2 Total Sample Recovery from Ion Exchange Columns

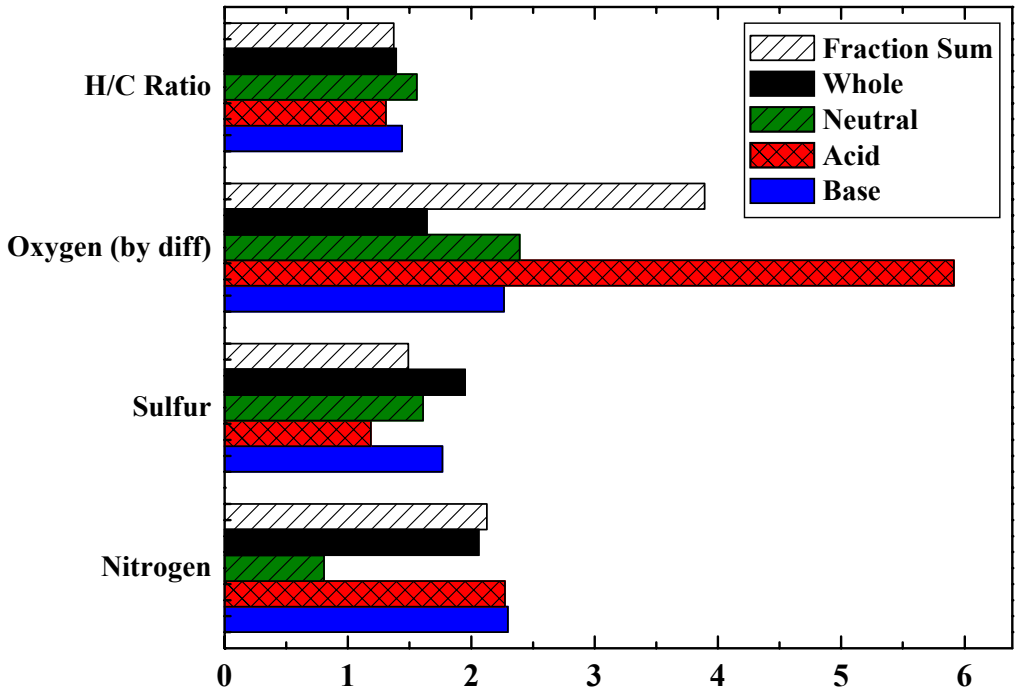

Figure A.3 Elemental Analysis SJV Resins (145-149)

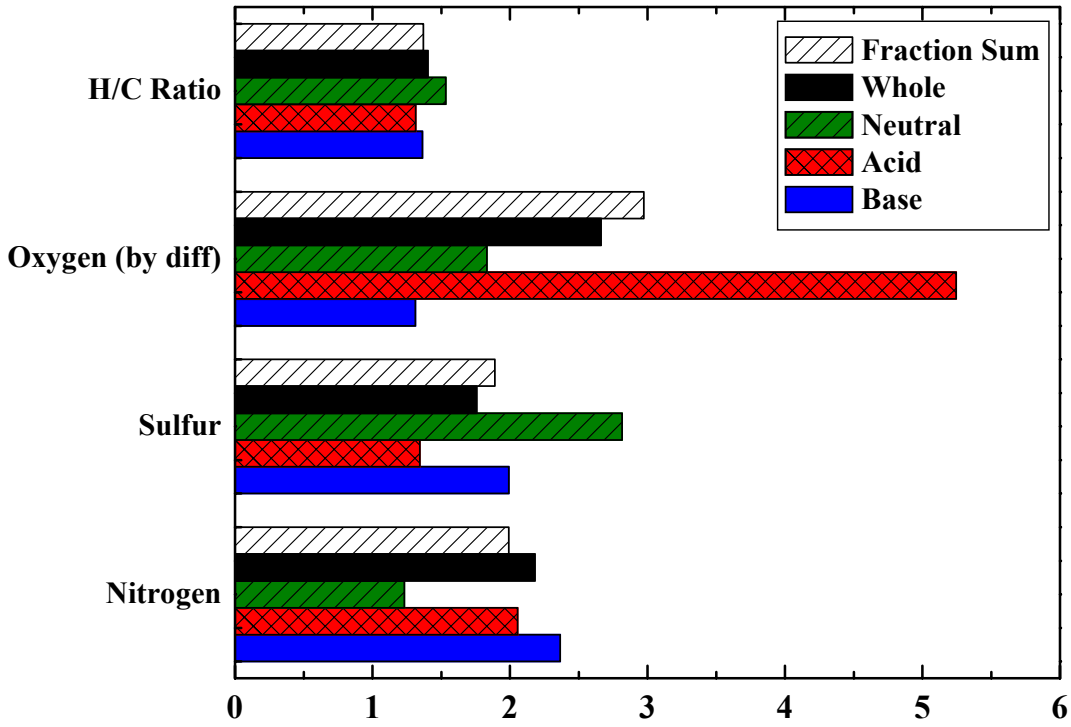

Figure A.4 Elemental Analysis SJV Resins (168)

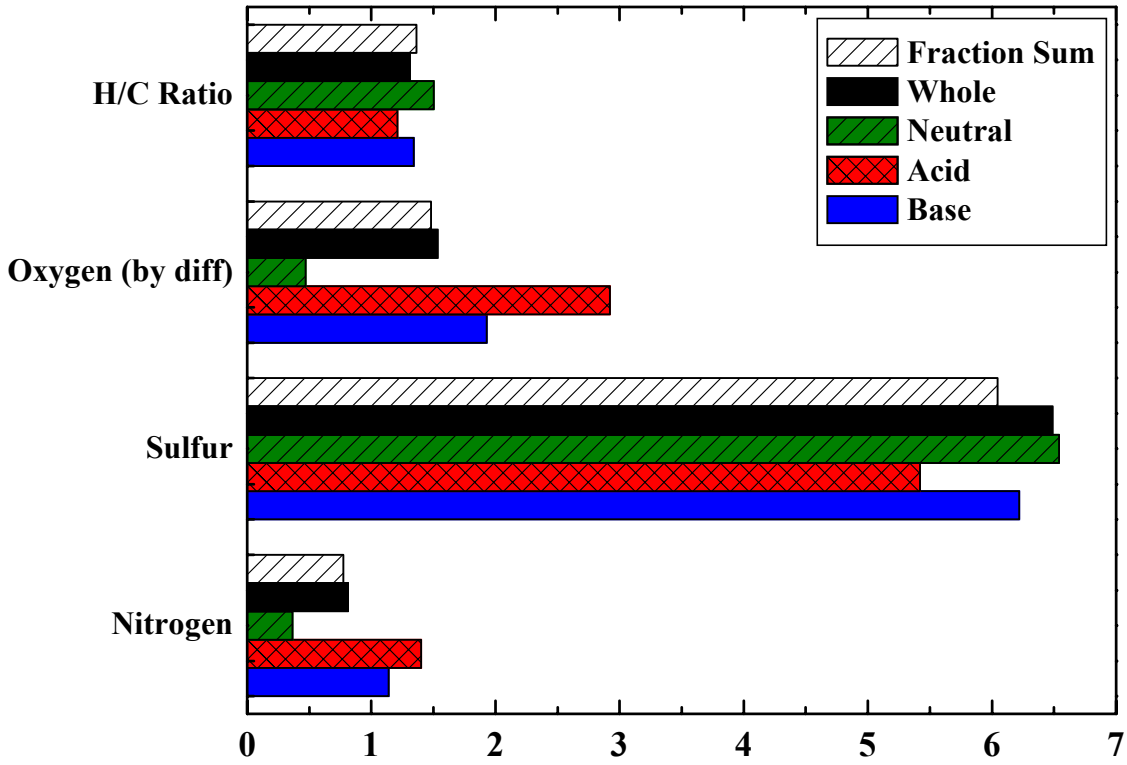

Figure A.5 AH Resins 167

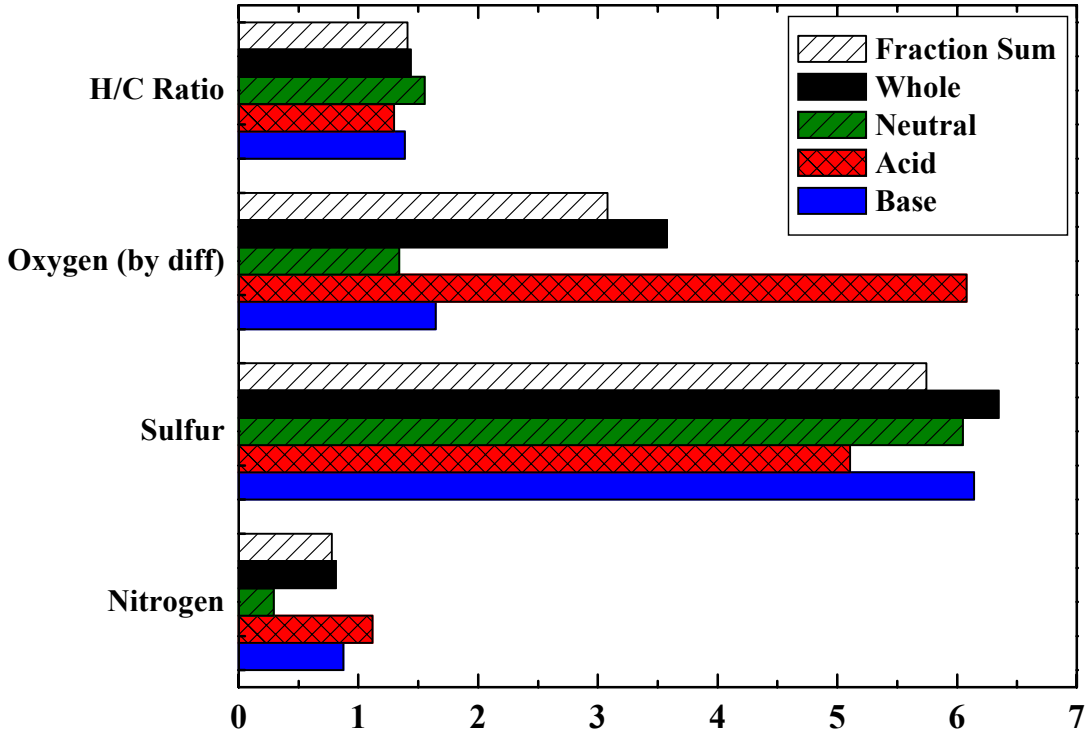

Figure A.6 AH Resins S60

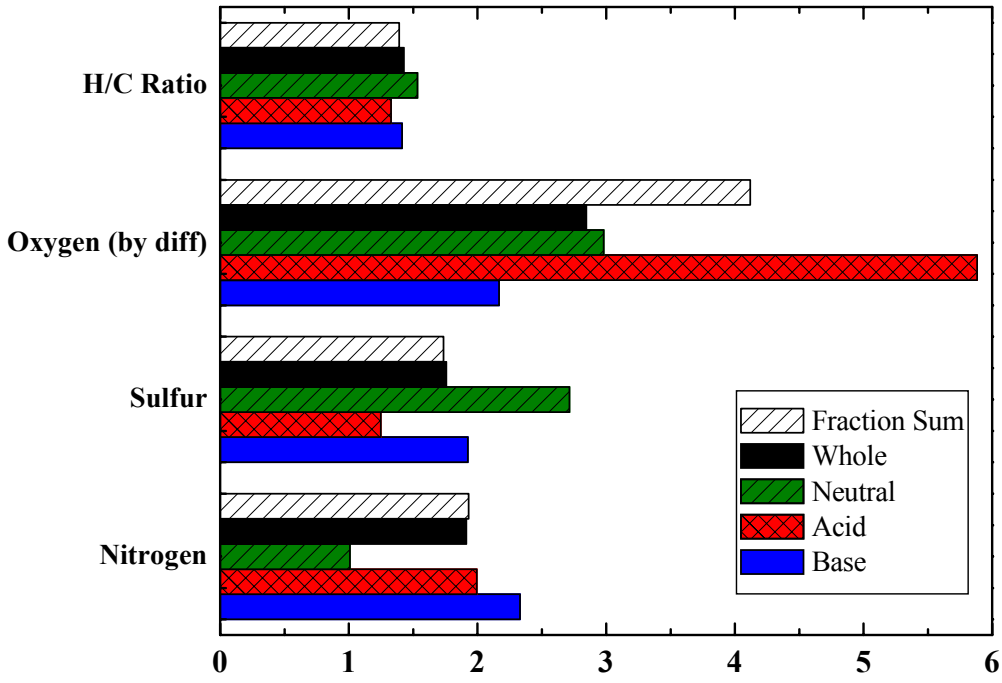

Figure A.7 SJV Resins S-4

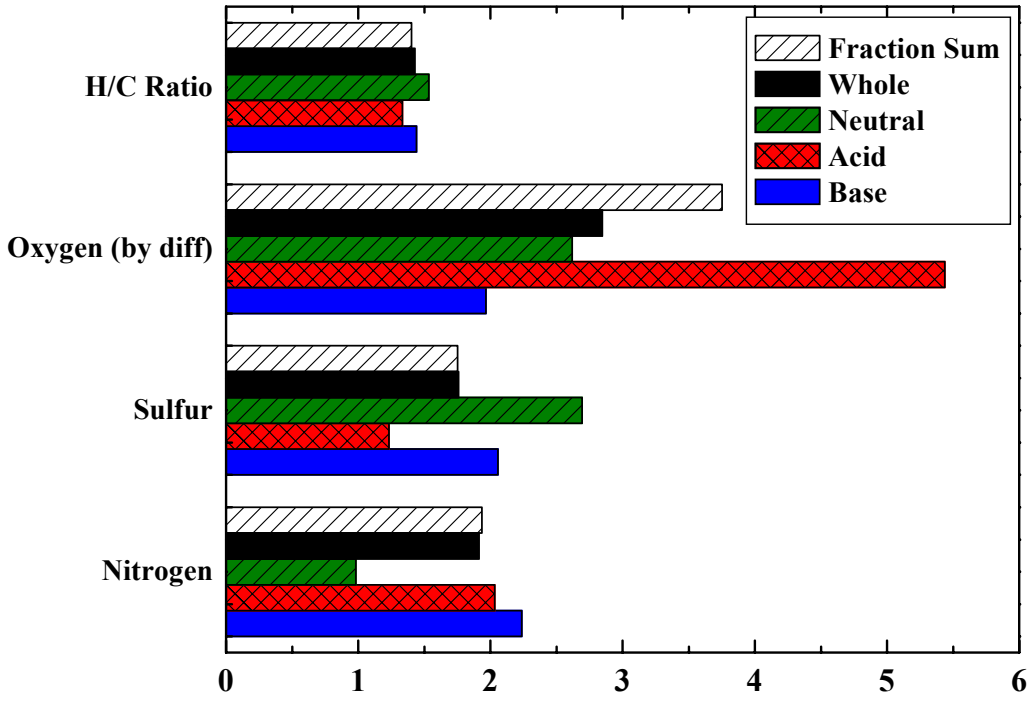

Figure A.8 SJV Resins S-3

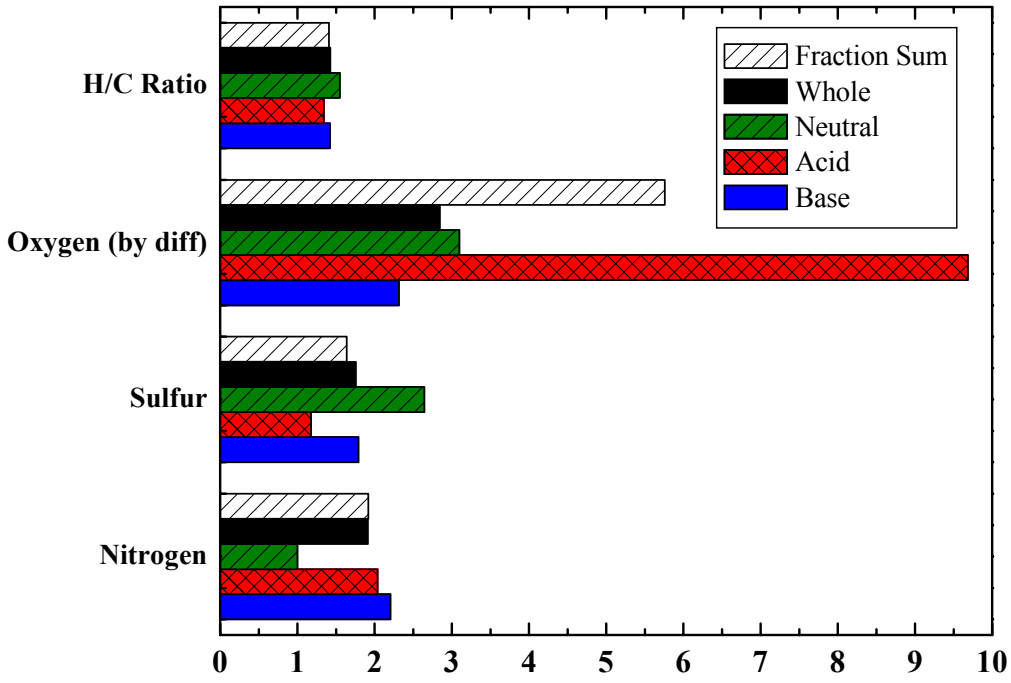

Figure A.9 SJV Resins S-2

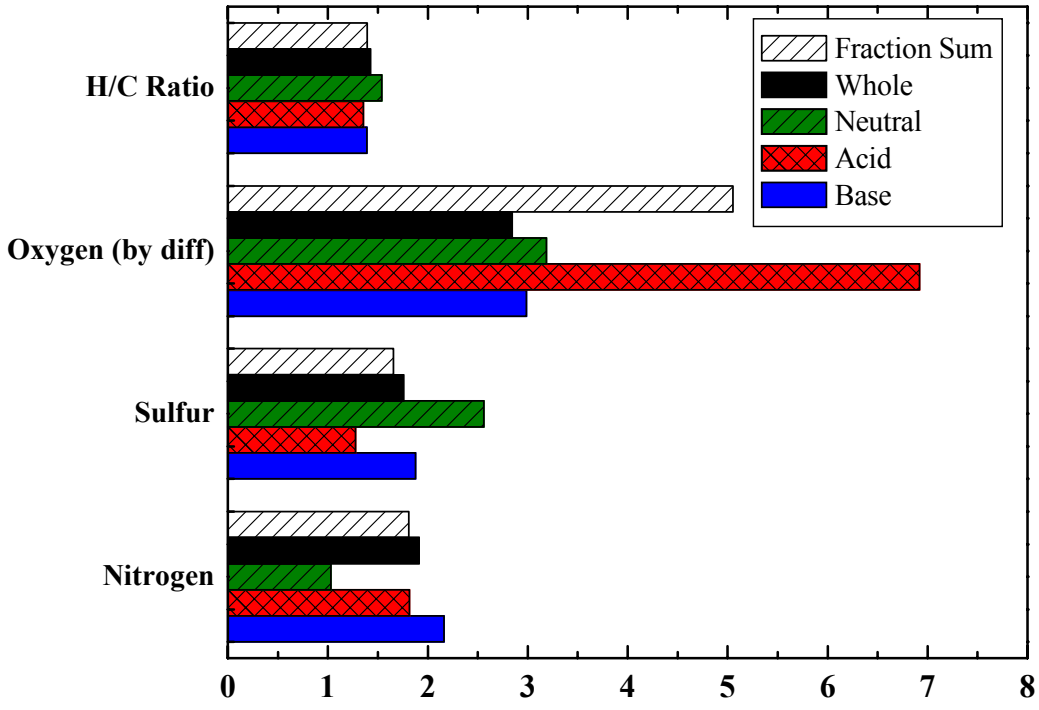

Figure A.10 SJV Resins S-1

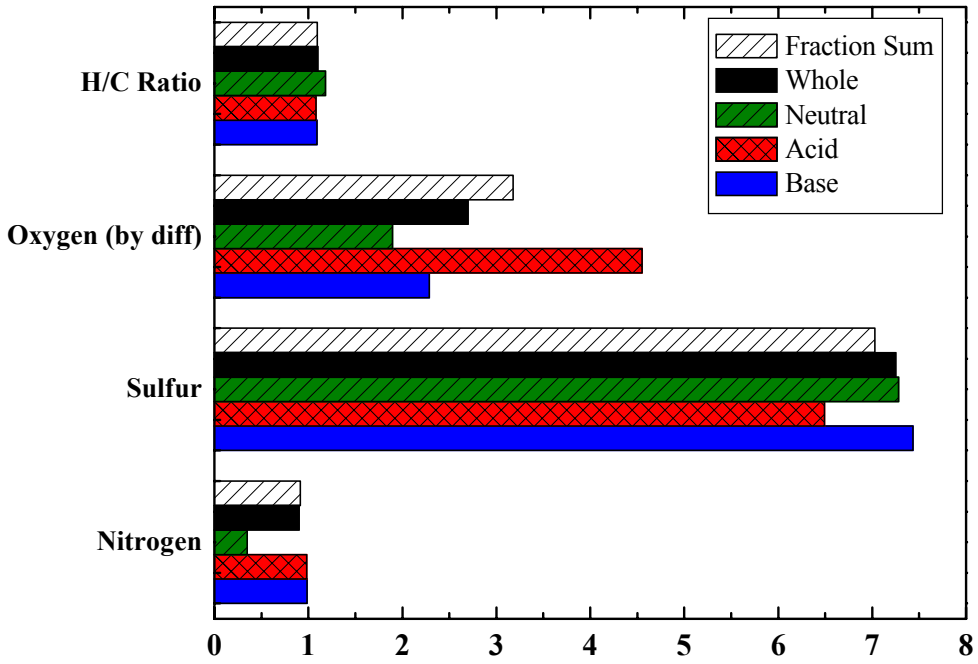

Figure A.11 AH Asphaltenes 16

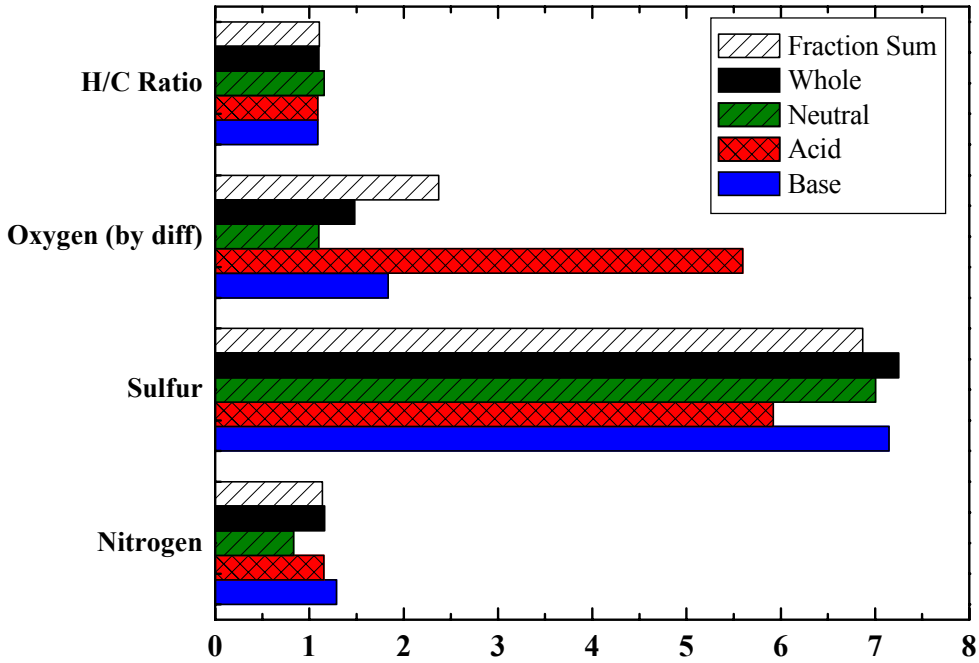

Figure A.12 AH Asphaltenes 4-9-97

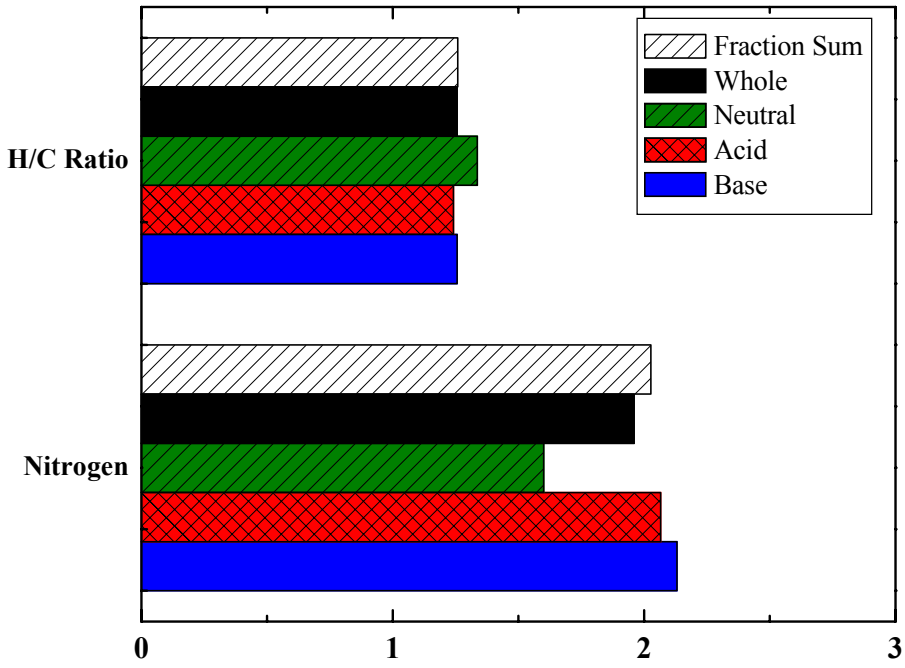

Figure A.13 HO Asphaltenes 12-3-98

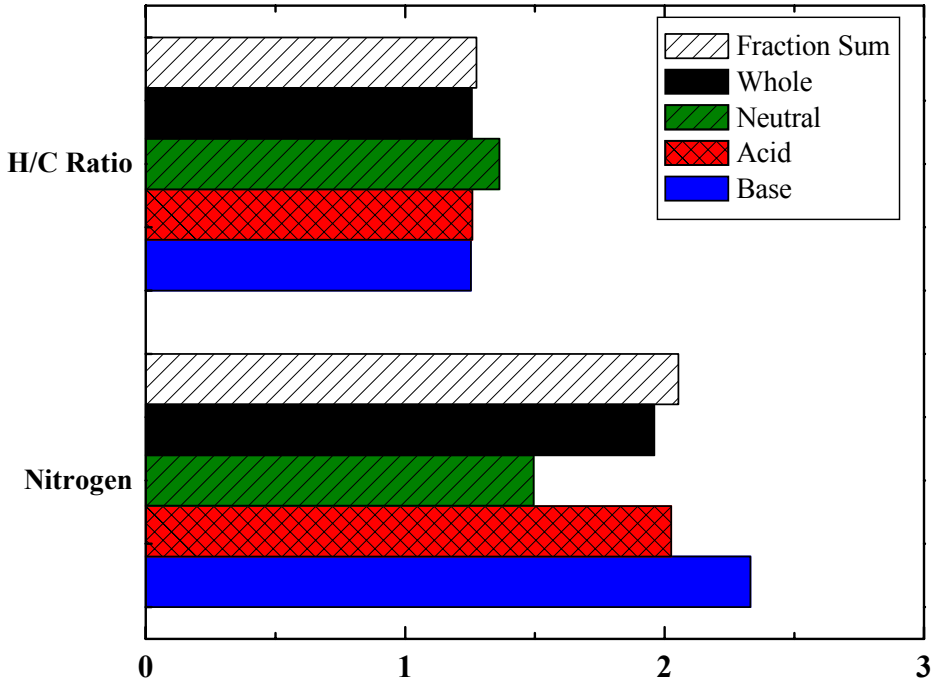

Figure A.14 HO Asphaltenes 2-25-99

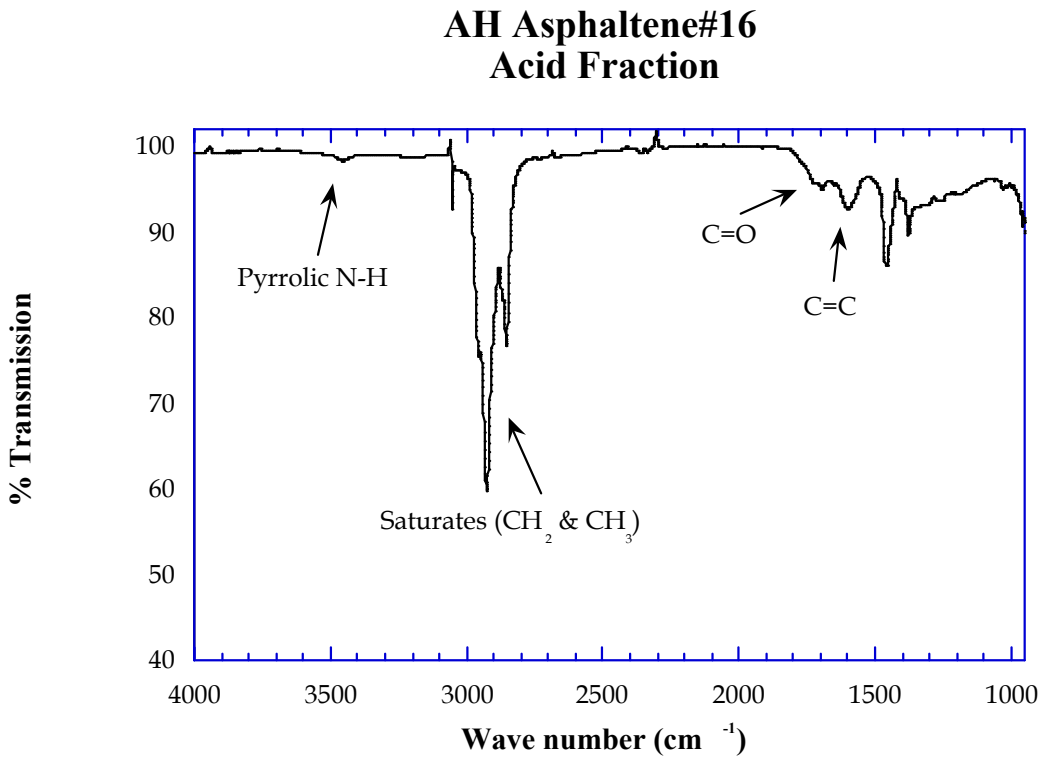

Figure A.15 FTIR Spectrum of Isolated AH#16 Acid Fraction

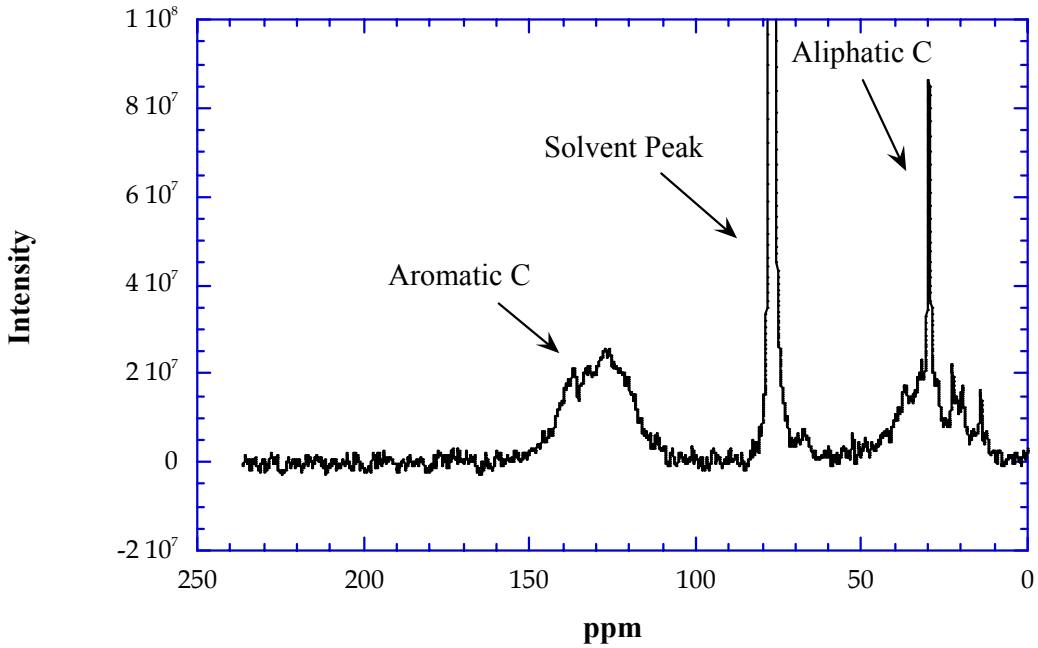

Figure A.16 ^{13}C NMR Spectrum of Isolated AH#16 Acid Fraction

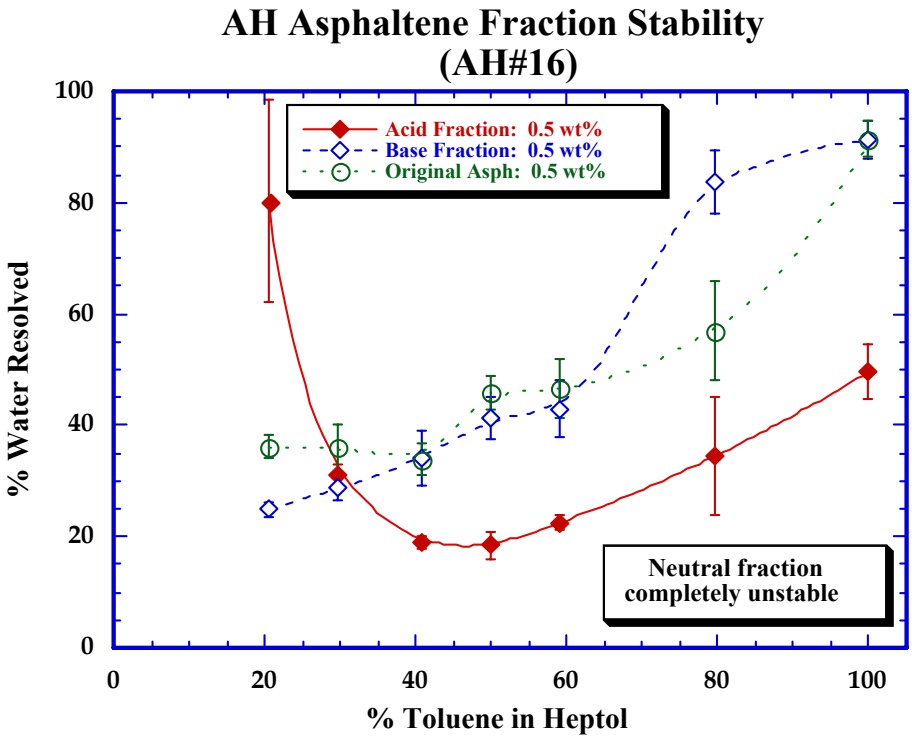

Figure A.17 AH#16 Fraction Emulsion Stability

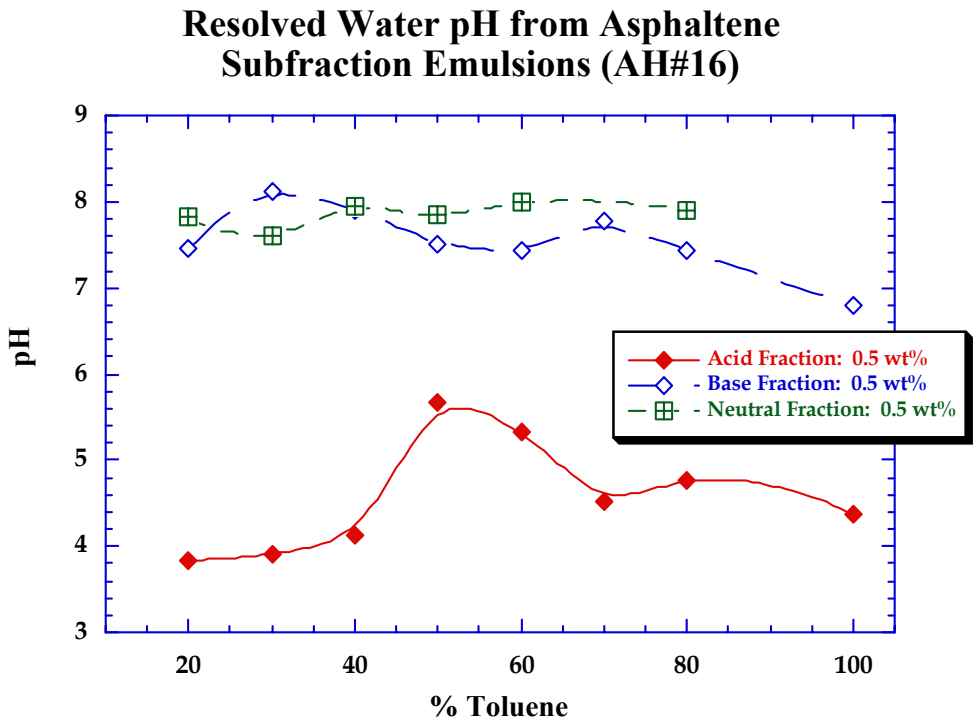

Figure A.18 Resolved Water pH (AH#16 Asphaltene Emulsions).

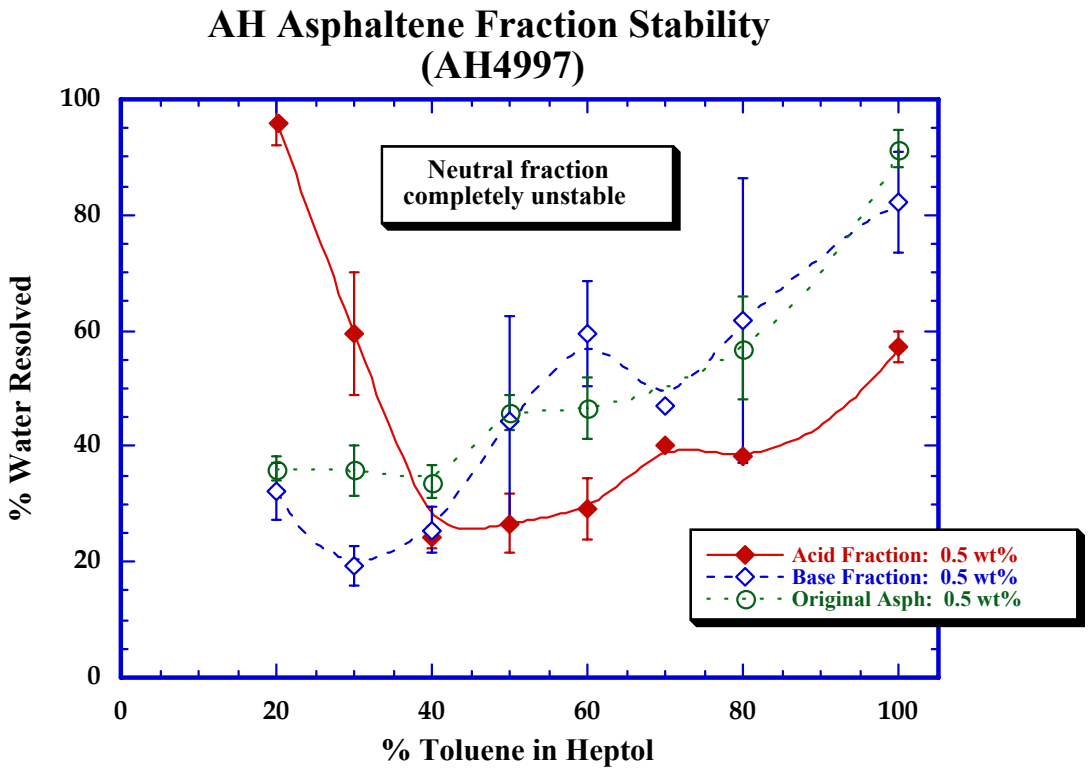

Figure A.19 AH#4997 Fraction Emulsion Stability.

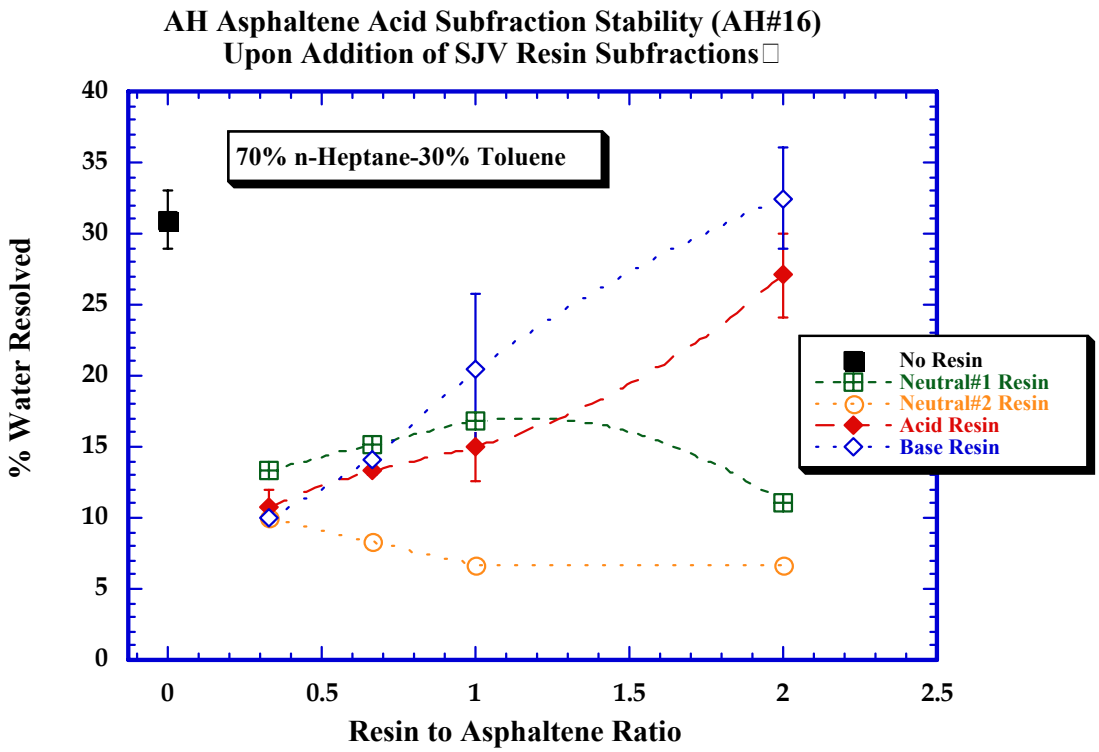

Figure A.20 AH Acid Asphaltene/SJV Resin Emulsion Stability (0.5 wt% Asph).

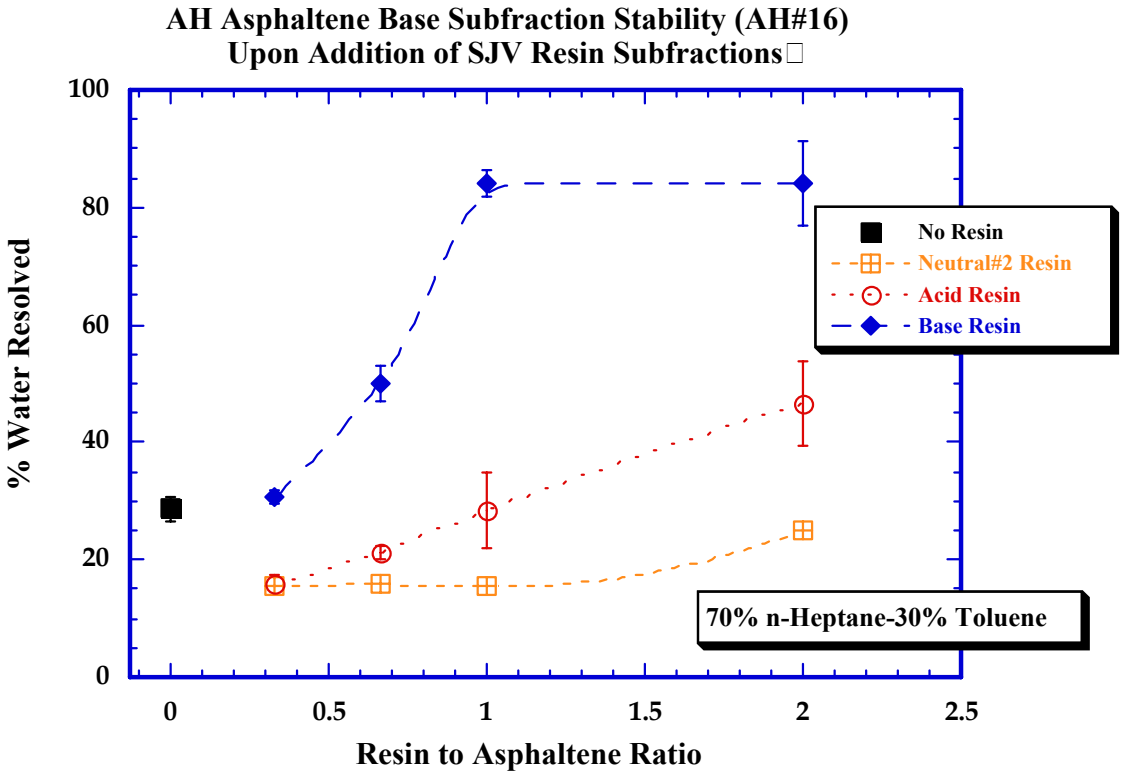

Figure A.21 AH Base Asphaltene/SJV Resin Emulsion Stability (0.5 wt% Asph)

APPENDIX B
ASPHALTENE PRECIPITATION

- All crude oils are stored near 0°C in sealed containers with an argon blanket. These precautions are taken to minimize possible oxidation of the crude oil.
- Remove crude oil can from refrigerator and place in paint can shaker for several three-minute cycles (Crude should be returned to room temperature before sampling).
- Add 15-20 g of crude oil to a 1 L round bottom flask using 25 mL glass pipette and green pipetter.
- Use large balance on bench top and cover the area with plastic-backed laboratory paper.
- Add HPLC grade *n*-heptane to flask in a 40:1 by volume ratio to the crude (approximately 750 mL). Depending on crude oil viscosity, shake flask by hand to completely disperse crude.
- Place on shaker with a cork ring and set to ~4 (moderate). Shake for 24 hours.
- Asphaltenes are removed from solution by vacuum filtration through 15 cm diameter, 1.5 μm Whatman 934-AH glass microfiber filter paper. The filter paper is supported on a ceramic Büchner funnel. The funnel sits on a 1 L vacuum flask.
- Pour the contents of the flask through the filter paper. Rinse the round-bottomed flask with heptane to remove precipitates and transfer to filter.
- Add ~250 mL heptane to the precipitated asphaltenes collected on the filter paper to completely remove remaining soluble material or until the effluent runs clear.
- Transfer the Büchner funnel to a new vacuum flask. Dissolve the asphaltenes with methylene chloride (HPLC grade, Fisher) under a partial vacuum. (Methylene chloride has a high vapor pressure and low boiling point causing it to evaporate quite rapidly and reduce the local temperature. Atmospheric moisture would often condense and freeze on the filter paper hindering the flow of the organic phase.)
- If you have more than one crude oil flask, use a new piece of filter paper. Continue the process with the remaining flasks.

- Refilter the soluble maltenes (deasphalted crude+heptane) to remove any residual asphaltenes. Depending on the volume of maltenes generated they may need to be stored in clean 4 L screw-cap bottles.
- Rotary evaporate the methylene chloride-asphaltene solution under partial vacuum at 50°C. Transfer <300 mL of solution to a 1 L round bottom flask and place on the Rotavap. Pull a relatively low vacuum and submerge only a small portion of the flask in the water bath. This solution will very easily "bump" or boil unexpectedly and launch material into the condenser. Watch the solution very carefully until stabilized and after a portion of the Methylene chloride has evaporated. Once dry, add more solution and continue until finished.
- Add Methylene chloride back into the flask (enough to redissolve the asphaltenes and transfer to 1-2 glass jars with green PTFE lined caps. Dry the slurry under an argon stream until most of the solvent has evaporated. Place aluminum foil over the mouth of the jar and poke a few small holes. Dry the asphaltenes in a nitrogen flushed vacuum oven at 50°C for 24 hours. Excess solvent present in the jars will cause the asphaltenes to rise upwards and may spill out.

APPENDIX C
EXTROGRAPHY TO RECOVER RESINS

Material Preparation

- Pour silica gel into large neck, round, flat-bottomed flasks (~150-200 grams/flask)
- Place flasks in vacuum oven at 120°C for 24 hours at full vacuum (activation)
- Pour ~50 grams of activated silica gel in a 500 mL round bottomed flask already containing deasphalted crude from asphaltene precipitation of 10 grams of crude oil
- Add 200 mL of HPLC methylene chloride
- Shake the flask for at least 24 hours
- Rotavap until dry (looks like dirty sand), low vacuum and 50°C or higher vacuum with very low surface area contact with water
- Place in a vacuum oven at 50°C for 24 hours (full vacuum), watch the oven for the first 8 hours because the cold trap will probably plug

Column Setup

- Rinse column with methylene chloride and n-heptane or first solvent to be used
- Fill the column with 300 mL of *n*-heptane
- Add 30 grams of activated silica gel slowly with occasional tapping of the column to minimize trapped air in the silica and to prevent plug formation
- Drain 50 mL of n-heptane from the column to eliminate super-fine silica particles and to eliminate air trapped in the silica gel matrix
- Add the activated silica with adsorbed deasphalted crude (slowly and with tapping)

Column Operation

- Open the buret tip so that the column drains at 8-10 mL/min (fast drip). Use a 100 mL graduated cylinder to collect the eluted solvent. To prevent splashing place the graduated cylinder so that the solvent runs down the inside wall. When the 100 mL cylinder gets full, switch to another cylider without stopping the solvent flow. Empty the full cylinders into a round bottomed flask and label as E1 (extrography fraction 1).
- When the level of n-heptane approaches the top of the silica gel add more n-heptane in 100 mL increments
- When a pale yellow color gets to the bottom of the buret, switch to a new collection cylinder (now empty the full cylinders into a different round bottomed flask, labeled E2-

4) and begin to add solvent #3 (68 % n-heptane/32 % toluene) the next time the solvent level approaches the top of the silica in the column.

- Continue to collect for E2-4 until the pale yellow color changes to dark orange and then gets significantly lighter in color (use ~ 500 mL solvent #3, may need 100 mL more in some cases).
- When the solvent level approaches the top of the silica gel add solvent #4 (40 % acetone/30 % toluene/30 % methylene chloride) in 100 mL increments (400 mL total, most of the color will come off the column in the first 100-200 mL)
- Switch collection cylinders when dark color reaches the bottom of the plug and from here on add to a round bottomed flask labeled E5.
- When the solvent level reaches the silica, continue to drain into the collection cylinder
- Force additional solvent out by applying pressure to the top of the column with nitrogen
- Allow the columns to dry for a little while, then turn the column over and empty the silica into a round bottomed flask. To aid in this, apply pressure through the buret tip with nitrogen.

Fraction Handling

- Rotavap E1, E2-4, and E5 until dry
- Transfer the samples to weighed, Qorpak, straight walled jars using methylene chloride
- Allow the samples to dry in a fume hood
- Add ~ 300 mL of pyridine to the silica gel from the column and let sit for ~ 20 minutes
- Using the large Buchner funnel and Whatman 934-AH glass microfiber filters, vacuum filtrate the silica gel. Wash the silica gel with pyridine until the filtrate is clear (this will take a couple hundred mL).
- Pour the filtrate and methylene chloride rinsings into a 1000 mL round bottom flask
- Rotavap this at 50°C and at a high vacuum (it takes a while).
- When the sample is dry, add a little methylene chloride to redissolve the material and pour it into a separatory funnel (pre-rinsed with methylene chloride) with a fritted glass disc on the bottom to eliminate any silica particles. Collect this material in the Qorpak jar labeled E5

Fraction Drying

- E1 and E2-4:
    - Apply vacuum until gauge reads 20 or wherever the sample begins to bubble

    - purge with nitrogen three times
    - pull the vacuum down to 15, close the valve to the vacuum and turn the heat on (50°C)
    - After several hours increase the vacuum, and eventually pull the maximum vacuum and keep the vacuum valve open
- E5:
    - full vacuum after purging twice with nitrogen
    - turn heat on to 70°C
- keep samples in oven for at least 24 hours
- weigh samples

APPENDIX D
FTIR PROCEDURES (DR. PARSONS' LAB)

- Dissolve about 0.05g in 5ml methylene chloride. A sample concentration of about 10g/L is desired. Tall glass jars work well but have a tendency to tip over. Use black caps with Teflon lining to reduce solvent evaporation. Since methylene chloride evaporates quickly, avoid condensation which will introduce water in the sample.
- Use CaF_2 IR cell with 0.2mm path length. Rinse and fill with HPLC methylene chloride which will serve as the background.
- If the instrument has not been used for a long time **Align Bench** under **Collect: Collect Bench Setup.** Make sure there is no sample in place, the doors are open (handles face forward) and the system has purged for at least one minute.
- Change resolution from 4 to 2, other parameters should read Happ-Genzel, 64 scans. These setting are in **Collect: Collect Setup**.
- Close laser doors (slide handles to vertical) and place methylene chloride background in slot. **Collect: Collect Sample Background.** Save background file as bkg***.spa under c:\omnic\…\joe.
- Close laser doors and remove sample cell. Lay cell flat, remove pegs and pipette first sample into upward facing hole with Kimwipe under other opening. Fill with enough solution to completely evacuate methylene chloride from previous run. Replace pegs and clean cell window if necessary.
- Place cell in instrument and purge for at least one minute. Open doors and collect sample **Collect: Collect Sample**. Save spectrum in \joe. Subtract background under **Process: Reprocess**: **Browse** Find appropriate bkg***.spa and hit OK. Save this spectrum as the same file name with an additional "2". Finally save the spectrum to a floppy disk as a .csv text file. Be sure to remove the .spa extension and replace with .csv. This file will take a long time to save.
- Close laser doors and remove sample cell. Remove pegs and rinse cell and pegs with methylene chloride. Pipette next solution into cell and replace pegs.
- After collecting spectra, return Resolution from 2 to 4 and close Omnic.

APPENDIX E

OUTLINE PROCEDURE FOR ACTIVATION OF BIORAD MP-50 ION EXCHANGE RESINS

Materials

- fifteen 4L bottles (2 must be clean-the rest are for waste)
- 2 L graduated cylinder
- large source of DI Water
- 600 mL beaker
- 2 L Erlenmeyer flask
- 4 L vacuum filtration flask
- 4 L ceramic filter
- 3 funnels
- metal stir rod
- pellet scoop
- 2 gallon bucket
- giant Soxhlet condenser
- giant Soxhlet extractor
- 12 L round bottom flask
- fiberglass insulation
- 3 rubber hoses (one for argon blanket, two for condenser)
- large exhaust tube (for top of condenser)
- heater for round bottom flask (including two heating controllers)

Procedure

1. **NaOH wash (1 M) 35 L**
    - Weigh out 160 g of NaOH into the 600 mL beaker
    - Pour 2 L of DI water into a clean 4 L bottle
    - Add the 160 g of NaOH
    - Close lid and shake well until all pellets are dissolved

- **Caution! – This will evolve heat!**
- Add another 2 L of DI water to the 4 L bottle
- Close lid and shake well for approx. 30 seconds
- Apply vacuum and pour solution onto the clumps of cation resin slowly until the resin becomes more compact.
- Continue to pour out the rest of the NaOH solution (making sure not to overflow the top of the filter) until all 4 L have been used.
- Once the 4 L flask is full, carefully pull the ceramic filter off of the flask and gently set it into the bucket.
- Then pour the NaOH waste into one of the 4 L bottles
- Place the ceramic filter back on the flask and repeat until the resin has been washed with 35 L of 1 M NaOH.

2. **DI Water wash 4 L**
    - Measure out 2 L of DI water and pour it into the ceramic filter
    - Repeat once
3. **HCl wash (1M) 35 L**
    - Pour out 2 L of HCl into a 2 L erlenmeyer flask
    - After 4 L of HCl have been used remove the ceramic filter and pour the HCl waste into one of the 4 L bottles
    - Repeat until resin has been washed with 35 L of HCl
4. **Acid/Base neutralization**

- In 3 gal bucket empty contents of 4 L acid waste container.
- Add base container while stirring and periodically measure pH until between 5 and 12.
- Once neutralized pour down drain.

5. **DI Water wash 12 L**
    - Measure out 2 L using a 2 L-graduated cylinder and pour it into the ceramic filter.
    - Rinse and empty the effluent water until the resin has been washed with 12 L of DI water.
6. **1:1 2-propanol/DI water rinse 25 L**
    - Measure out 1L of DI water in a graduated cylinder

- Pour 1 L of 2-propanol into an erlenmeyer flask
- Add the 1 L of DI water to the erlenmeyer flask
- Mix the 2 L of 1:1 2-propanol/water with the metal stir rod
- Add the mixed liquid to the to the ceramic filter (caution – mixture drains slowly)
- Repeat until the resin has been rinsed with 25 L of 1:1 2-porpanol/DI water

7. 1-propanol rinse 25 L

- Measure out 2 L of propanol in erlenmeyer flask
- Pour propanol into ceramic filter (caution – propanol drains very slowly)
- Repeat until resin has been washed with 25L of 1-propanol
- Once rinsing is complete, continue to vacuum filter so that the resin will dry completely to a sandy white color

8. Ethyl Ether wash 6 L in Soxhlet apparatus

- **Caution – Ethyl Ether is extremely volatile and flammable! This is a two-man job. (check MSDS of ethyl ether before use)**
- Carefully transfer the resin from the ceramic filter to the thimble
- Inside a hood, pour 6 L of ethyl ether into the 12 L round bottom flask
- Quickly cover the flask with parafilm
- Place flask onto the heater
- Apply two wraps of Teflon tape to ground glass joint of extractor
- Insert the thimble into the extractor (do so by tilting the extractor onto its side)
- Remove the parafilm from the round bottomed flask and quickly place extractor onto the flask
- Quickly place the condenser onto the extractor
- Add argon blanket from the top of the condenser
- Turn on water feed to the condenser
- Attach exhaust tube to the top of condenser and place the outlet of the tube into the hood
- Adjust the two heating controllers to a setting of approximately 25
- Wait about an hour and fine tune the setting so that the heat is just enough to obtain a steady dripping of ethyl ether off the bottom of the condenser

- Allow the process to continue for about 24 hours
- After 24 hours has passed wait for the part of the cycle where the condensed ethyl ether drains back into the round-bottomed flask.
- Once all the ethyl ether starts to drain turn off power to the heating controllers
- Remove all insulation from the extractor and round bottomed flask
- Wait until boiling flask returns to room temperature
- Take the exhaust tube off of the condenser
- Remove the argon tube
- Turn off the water feed to the condenser
- Between one arm and your chest, cautiously pull upward on the condenser to remove the it from the extractor (there may be significant resistance)
- Remove the thimble from the extractor using gloves and put the thimble in the hood on a glass tray (there may be some residual ethyl ether in the thimble)
- Obtain one of the spent containers of ethyl ether inside the hood and put a funnel on its opening and label it waste ethyl ether
- Remove the extractor from the round bottomed flask.
- Quickly cover the round bottomed flask with parafilm
- Pour any residual ethyl ether in the extractor into the waste container (make sure to raise funnel from top of waste container to improve drainage)
- Slowly pour the remaining ethyl ether in the round bottomed flask into the waste container until almost full
- Then pour the remaining solution into a brown glass container
- Leave the round bottomed flask in the hood to dispel any remaining ethyl ether

9. **Pentane wash 6 L in Soxhlet apparatus**

- Inside a hood, pour 6 L of pentane into the 12 L round bottom flask
- Follow same procedures as with ethyl ether
- Obtain a bottle of cyclohexane which has been degassed with argon
- Put a funnel on top of a 1 L brown bottle
- Use the metal stir rod to scrape out some resin in the thimble and allow it to dry
- Carefully pour the dried resin into the funnel

    - Use the cyclohexane squirt bottle to get the resin to flow through the funnel
    - Continue this process until all of the resin is transferred
- Fill remainder of bottle with degassed cyclohexane and blanket with argon
- Label bottles

MP-1 Resin preparation: NaOH and HCl steps are switched and only need 25 L/1.5 kg of resin

APPENDIX F
ION EXCHANGE CHROMATOGRAPHY PROCEDURE

Column Packing:

- Two column types: 100 cm x 1.5 cm or 50 cm x 2.5 cm with heating jackets.
- Fit threaded column end fittings in one end of each column as deep as possible. Typically, the adjustable end fittings do not slide into the columns with ease. Try cooling the end pieces in the refrigerator to facilitate insertion. Secure with black threaded piece and white end cap which screws onto exterior column threads. Finally, attach small colored caps and 1/8" tubing with 2 way coupler and plugs.
- Secure column in a diagonal fashion in fume hood with large coupler and additional overflow column above. This will allow a greater volume of liquid and ion exchange resin for more rapid packing.
- Shake cation (MP-50) resin bottle until a slurry is generated then transfer 250 mL to a separatory funnel with stopper. Re-slurry and transfer to columns. Repeat this process until overflow column reaches 1/3 – 1/2 full, remove plug from tube end and apply compressed gas (<20 psi) with fixed length end fitting to the top of the column arrangement. This will help pack column and remove excess solvent. Continue to add resin material until it is within a few inches from the top of the jacketed column. Plug the tube end when the liquid level is just below the junction. Rotate the dual column arrangement to vertical and remove the upper column.
- Insert adjustable column end fitting with attached tubing. The tubing allows the air and solvent above the resin to escape. Lower the end fitting within one inch of the resin and affix.
- Pack column with hazardous duty pump at stroke 30 and speed 45 with degassed cyclohexane until resins no longer compress.
- Repeat process with anion (MP-1) resins (they will compress more than the cation resins).

Column Operation:

- Once columns are packed, connect bottom of anion (MP-1) to top of cation (MP-50) with two pieces of tubing. Flush injection loop with solvent from pump to remove air bubbles then attach to anion column.
- Dissolve about 5 grams of sample in 60-70 mL of solvent of choice (benzene-ethanol or toluene-ethanol mixture). Lower concentrations prevent the injection loop from clogging.
- Change elution solvent and flush until both columns have "changed color". Also, begin circulating 40°C water through column jackets. Allow 1 hour for temperature equilibration.
- Using syringe, inject 15 mL into loop while collecting the overflow. When sample loop is full, pump sample onto columns. Continue until all sample has been injected.
- Elute until eluant from anion column is mostly clear, about 1 liter(could use online / flow-through uv spectrophototmeter). Eluant from both columns are non-binding neutrals. At this point, remove anion column from flow scheme and continue eluting through cation column (approx 250 ml). Combine eluant as neutrals.
- Remove top endpieces and pump solvent up through columns from the bottom to loosen the packing material. Invert columns over soxhlet thimble with an overlap of column end and thimble top. Thimble should be suspended above a funnel and 250 ml collection flask. Pump solvent into columns to force packing resins into funnel. Once liquid fills the column and resins are removed, the remaining liquid will be slowly drawn from the column as the liquid level in the thimble drops. Label solvent from the anion column "Acids" and cation column "Bases".

Soxhlet Extraction:

- When the thimble is full and excess solvent has drained, slide gently into soxhlet recycling apparatus. Connect to 1000 mL boiling flask (2 openings: 24/40 & 29/42) and place condenser on top. Use one ring stand for each soxhlet apparatus. Begin flowing argon in the condenser top and leave the boiling flask open.

- After 15 minutes add 550 mL benzene to each pot. Add 20 mL formic acid to the anion pot and mix 30ml propylamine with 30ml benzene and add 1/4 of mixture to cation pot. Place stoppers in pot openings and hold down with tape.
- Wrap and tape insulation around pot, neck, exterior tube and recycling apparatus.
- Turn on power supply and set to 4.3.
- Turn on condenser water supply at a low rate of flow.
- Recycling should begin within 1 hour.
- Periodically, add propylamine to cation pot after recycling when the boiling rate is the slowest. Add propylamine over 24-48 hours until no more sample is extracted. Do the same for the anion pot to ensure complete extraction.

Filtration:

- When all asphaltenes have been extracted and additional acid/base has no effect, remove heat and insulation. Allow to cool and remove condensers. Using tongs, remove thimble, invert over funnel and white-capped jar and rinse resins out with toluene. First add toluene to fritted end until resin moves down thimble then force toluene into open end until resins slide out.
- Place vacuum filter over 1000 mL flask and filter benzene/asphaltene solution to remove any excess packing resin.
- Add solution from 250 mL flasks generated when emptying columns and rotavap.

APPENDIX G
RHEOMETER START-UP PROCEDURE

- Open gate valve below main pressure gauge (should read 100 psi normally).
- Open ball valve on pressure regulator (outlet pressure to instrument should read 28-30psi).
- Plug in circulating water pump for Peltier plate temperature control.
- Remove bearing lock from rheometer stress head.
- Turn on instrument control unit and computer.
- If air supply has been turned off for an extended period of time determine bearing friction correction by deselecting bearing friction correction and inertia correction. In the main window apply a stress to induce rotation of the shaft of about 15-20 rad/s. After equilibration bearing friction correction equals Torque/Rotational velocity (μN-m / rad/s). Turn on bearing friction correction. Turn on inertia correction.
- Every month calibrate system inertia without geometry in place and then with geometry in place.
- Map the bearing anytime a geometry is attached to the shaft before running an experiment.

RHEOMETER SHUT-DOWN PROCEDURE

- Place bearing lock on shaft.
- Turn off main air supply gate valve.
- When pressure regulator drops to 0 psi close ball valve.
- Unplug water circulator.
- Turn off rheometer control unit.

APPENDIX H
RHEOMETER OPERATION

- In a clean jar weigh out the desired amount of asphaltenes.
- Add the appropriate volume of toluene, place jar on shaker and allow asphaltenes to dissolve completely (at least 2-4 hours).
- Add heptane to toluene and shake overnight.
- Place Teflon cup or water-jacketed glass cell on Peltier plate. PDMS sheet provides high friction to keep cup from sliding around.
- Apply silicon grease to lip of Teflon cap.
- Run Sampleload.nvs macro in Navigator.
- To level bob at water-air interface, find light reflection on water surface and raise or lower bob until meniscus at bob edge disappears.

Running experiment:

- Select long-time macro in Navigator and update time intervals, sample names as necessary.
- Check condition of film prior to first frequency sweep by running 1ptfreq.pr2 at 0.001 Pa. If G′ is greater than about 1 Pa, the film should be durable enough to test at operating stress of 0.01 Pa.
- The test macro will end with a stress sweep until film rupture.

Cleaning up:

- Remove Teflon cap and pipette oil into waste beaker.
- Raise rheometer head and detach bob.
- Rinse bob with methylene chloride, then hand wash with detergent (no scrub brush).
- Pipette remaining oil and water into waste beaker and preserve film.
- Dissolve film with a minimum of methylene chloride and acetone and transfer to tared 15 mL glass jar.
- Wipe cup edge to remove grease, clean cup interior with methylene chloride.
- Hand wash cup (no brush) to remove any remaining grease, rinse with DI water, wipe dry.